Machining Fibre Metal Laminates and Al2024-T3 aluminium alloy

by

KHALED GIASIN

A thesis presented for the degree of

Doctor of Philosophy

in the

Composite Systems Innovation Centre

Department of Mechanical Engineering

September 2016

Declaration of Authorship

I, Khaled Giasin (Yasin), declare that this thesis titled, 'Machining Fibre Metal Laminates and Al2024-T3 aluminium alloy' and the work presented in it are my own. I confirm that:

- This work was done wholly or mainly while in candidature for a research degree at this University.

- Where any part of this thesis has previously been submitted for a degree or any other qualification at this University or any other institution, this has been clearly stated.

- Where I have consulted the published work of others, this is always clearly attributed.

- Where I have quoted from the work of others, the source is always given. With the exception of such quotations, this thesis is entirely my own work.

- I have acknowledged all main sources of help.

- Where the thesis is based on work done by myself jointly with others, I have made clear exactly what was done by others and what I have contributed myself.

Signed:————————————————————

Date:————————————————————

"Engineering is not about perfect solutions;

it is about doing the best you can with limited resources."

By Randy Pausch, The Last Lecture

Professor of computer science, human-computer interaction

October 23, 1960 - July 25, 2008

Abstract

The assembly of aerospace structural parts usually requires applying one or more machining operations to join the mating parts or stacks to form an assembly. Drilling is one of the most common machining processes for making holes and rivets in aerospace structural parts. Poor hole quality related to improper hole tolerances or the presence of drilling-induced damage are some of the major reasons for the part rejection at the assembly stage. The rejection is more likely to occur when drilling stacks of carbon/glass fibre reinforced plastic (CFRP or GFRP) composites and metals such as titanium and aluminium alloys or fibre metal laminates due to the difference in mechanical and thermal properties of both materials. Fibre metal laminates commercially known as GLARE are currently being used in the fuselage of the largest commercial aircraft in the world Airbus A380 due to their superior mechanical properties over monolithic aluminium alloys. The process of drilling GLARE fibre metal laminates in aircraft structures is more complicated than drilling metals or composites alone due to its hybrid structure and abrasive nature which can affect the machined surface quality and tool life. Following an extensive literature review on the machinability of aluminium alloys, composites, composite metal stacks and fibre metal laminates. It was found that the research on the machinability of fibre metal laminates is limited by the work of few researchers. Only one master thesis was openly published since the introduction of fibre metal laminates in 1987 followed by some drilling work carried out by few researchers in the past few years. The published work on machining GLARE was concerned with tool wear and delamination as they are considered two of the main problems faced when machining such structures. Moreover, the studies only investigated the machinability of thin laminates of less than 2 mm, which could probably be due to the high costs of GLARE material. As mentioned earlier, very limited research has been reported on the drilling of GLARE fibre metal laminates since its introduction, while no studies have been reported on drilling operations using modern cooling technologies despite showing promising results on improving surface finish in composites and metals. The lack of information on the machinability of GLARE fibre metal laminates prompted tests to determine the influence of cutting parameters and the application of two modern cooling technologies namely minimum quantity lubrication and cryogenic cooling on the machined hole quality in GLARE. Moreover, the effect of fibre orientation and workpiece thickness were investigated using design of experiments to reduce the overall costs and time of the trials.

The present thesis investigates the machining performance of an aerospace structural material commercially known as GLARE fibre metal laminate and its metal constituent aluminium Al2024-T3 aerospace alloy using commercially available solid carbide twist drills. The objective is to quantify the effects of the cutting parameters and two modern coolant technologies on cutting forces and a number of hole quality parameters. The generated drilling cutting forces, quality of machined hole and drilling-induced damage and defects when drilling GLARE fibre metal laminates were experimentally studied. Drilling-induced defects and damage investigated were surface roughness, burr formation at both sides of the workpiece and interlayer burr, hole size and circularity error, chip formation as well as damage described at the macro level (delamination area) using computerised tomography (CT) scan, and at the micro level (fibre matrix debonding, chipping, adhesions, cracks) using scanning electron microscopy (SEM). The experimental results have been statistically analysed using full factorial and response surface methodology statistical techniques to generate multiple regression models which makes it attractive as an indirect tool predicting the machining outputs prior the start of actual tests. Moreover, the analysis of variance (ANOVA) was employed to determine the percentage contribution of drilling parameters on cutting forces and hole quality outputs. The results indicated that the presence of coolant during the drilling process of GLARE could significantly improve hole quality. The use of cryogenic liquid nitrogen was found to eliminate the formation of waste on the borehole surface and burr formation at the hole exit. Using minimum quantity lubrication coolant was found to reduce the workpeice temperature compared to dry drilling at room temperature. Both coolants reduced the surface roughness compared to dry drilling but increased the cutting forces especially when using cryogenic liquid nitrogen. The cutting parameters results indicated that a maximum operating feed rate of 300 mm/min and a maximum spindle speed of 6000 rpm is recommended for superior hole quality results. Moreover, drilling at or below those levels of cutting parameters did not lead to severe delamination or fibre pull outs in the laminate compared to the higher cutting parameters used in the study. In addition, the fibre orientation and workpiece thickness were found to play a significant role on surface roughness and hole size but did not have a considerable impact on cutting forces due to the small thickness of glass fibre layers in the laminate. Adhesion and built up edge was found to be the main wear mechanism when drilling monolithic aluminium alloy, while adhesion and abrasion of the primary and secondary facets of the drill were identified to be the main wear process that occurs in drilling GLARE laminates.

Acknowledgement

I wish to express my sincere gratitude to my current supervisor Dr Christophe Pinna and to my previous supervisor Professor Alma Hodzic for their support. My appreciation extends to my co-supervisor Dr Sabino Ayvar Soberanis at the Advanced Manufacturing Research Centre (AMRC) for his assistance in conducting the experimental part of this research at the AMRC. I would like to sincerely thank the Advanced Manufacturing Research Centre AMRC with Boeing) in Sheffield for providing access to their machining facilities. I have met many wonderful people there who were always supportive of my research in all aspects. The list is long and I am especially very grateful to the following individuals there who have contributed to my research directly:

- Dr Vaibhav Phadnis.

- Dr Julian Merino Perez.

- Mr Ravi Bilkhu

- Mr Ashley Godbehere

- Mr Matthew Broderick

- Professor Jose Sinke from DELFT university of Science and Technology (Technical support).

- Dr Peter Kortbeek from the Fibre Metal Laminate Centre in Netherlands (Material supply).

- Mr Jacob Hawxwell from Sandvik Coromant (CMM measurements).

- Mr Steve Durand from OSG (Cutting tool CAD model supply).

- Mr Tobby French from X-Tek systems/NIKON metrology (CT scans of GLARE samples).

- Mr Tim Mammat from ired Ltd (help with emissivity and temperature measurement).

I would like to thank the Department of Mechanical Engineering at the University of Sheffield for funding my Ph.D. scholarship. I want to express my love and gratitude and give a special appreciation to my parents, my brother and my two sisters for being there for me and for their support for what has been a challenging few years. Finally, all praise is due to Allah, the Lord of the Worlds. The Beneficent, the Merciful to keep us on the right path to serve humanity for every possible good cause.

Khaled Giasin

Sheffield, September 2016

Contents

List of Figures

List of Tables

Nomenclature

Acronyms

AE	Absolute Energy
$ANOVA$	Analysis of Variance
$ARALL$	Aramid Reinforced Aluminium Laminates
BUE	Built Up Edge
CAA	Chromic Acid Anodising
CAD	Computer Aided Design
CCD	Central Composite Design
$CFRP$	Carbon Fibre Reinforced Plastic
CM	Chemical Machining
CNC	Computer Numerical Control
$CO2$	Carbon Dioxide
CT	Computerized Tomography
CTE	Coefficient of Thermal Expansion
CVD	Chemical Vapour Deposition
DF	Degrees of Freedom
DLC	Diamond Like Carbon
DOE	Design of Experiments
EDX	Energy Dispersive X-ray Spectrometer
FML	Fibre Metal Laminate
FRP	Fibre Reinforced Plastics
$GFRP$	Glass Fibre Reinforced Plastic
$GLARE$	GLass Aluminium Reinforced Epoxy
HAZ	Heat Affected Zone
HPC	High Pressure Coolant
HSS	High Speed Steel
IR	Infra Red
$LN2$	Liquid Nitrogen
$LSQC$	Least SQuare Circle
MCC	Minimum Circumscribed Circle

MIC	Maximum Inscribed Circle	
$MQCL$	Minimum Quantity Cryogenic Lubrication	
MQL	Minimum Quantity Lubrication	
MSS	Mean Sum of Squares	
MVF	Metal Volume Fraction	
MZC	Minimum Zone Circle	
PAA	Phosphoric Acid Anodising	
PC	Personal Computer	
PCD	Poly Crystalline Diamond	
PVD	Physical Vapour Deposition	
rev	Revolution	
ROI	Region of Interest	
rpm	Round Per Minute	
RSM	Response Surface Methodology	
SAA	Sulphuric Acid Anodising	
SS	Sum of Squares	

Superscripts

°	degrees	

Greek Symbols

α	Thermal Expansion Coefficient	
μ	Microns	
ν	Poissons Ratio	
Φ	Angular position of the cutting tool with respect to fibre orientation	
ρ	Density	Kg/m^3
σ	Stress	MPa
θ	Fibre Orientation	Degrees
ε	Strain	

Italics

f	Feed rate	mm/rev
n	Spindle speed	rpm

Roman Symbols

A_{max}	Maximum area of delamination	mm^2
A_{max}	Maximum delamination area around the hole	mm^2
A_{nom}	Nominal hole area	mm^2
D_{max}	Maximum diameter damage around the hole	mm
D_{nom}	Nominal hole diameter	mm
E	Emissivity	

E	Young modulus of Elasticity	GPa
F_A	Area delamination factor	
F_D	Diameter delamination factor	
G	Shear Modulus	GPa
HV	Vickers Hardness	
K	Thermal Conductivity	W/m-K
N	Force	N
R_a	Average surface roughness (μm)	
R_t	Valley Height (μm)	
R_y	Valley Depth (μm)	
T_g	Glass transition temperature	°C
V_c	Cutting Speed	m/min
V_f	Feed Speed	mm/min
V_f	Fibre Volume Fraction	

Subscripts

al	aluminium
lam	laminate
ult	ultimate

Chapter 1

Introduction

Fibre metal laminates (FMLs) are hybrid materials made up of alternating layers of thin metallic sheets and composite layers bonded together using adhesive epoxy. FMLs were mainly developed for aerospace applications as an alternative for monolithic aluminium alloys in aircraft structures as they provided better fatigue crack growth resistance and damage tolerance. The recent member of the FML family commercially known as GLARE is currently installed in the upper fuselage of the largest commercial aircraft in the world Airbus A380. GLARE is made of alternating layers of thin aluminium sheets and S2 glass fibre prepregs bonded together using FM94 adhesive epoxy. In addition to the advantages of FMLs mentioned previously, GLARE offered significant weight reductions and impact resistance compared to monolithic aluminium alloys, which makes it even more attractive for other aerospace applications were weight combined with performance is necessary.

There has been much research on milling and drilling of composites and composite metal stacks in the available literature. However, only a limited number of experimental studies were reported on the machinability of fibre metal laminates. The machinability of FMLs and GLARE in particular has been previously tested for their applicability for a variety of conventional machining processes such as drilling and milling, and non-conventional machining processes such as water jet and laser cutting [1]. The manufacturing and installation of GLARE fuselage structures usually require machining processes to shape them to the right dimensions using milling operations or drilling holes for riveting and assembly purposes. The tests on GLARE laminate indicated that three phenomena proved to be important during machining operations necessary to fulfil requirements related to tolerances or assembly needs, which were the the cutting tool wear, delamination in glass fibre layers and the heat affected zone at the edges of the laminate. Nevertheless, there is a limited information on their machinability in the published literature. Improving the machinability of FMLs requires a thorough understanding of the behaviour of its constituents; metal and composite, and the way they interact and affect each other. Metals and composites react differently to

the drilling process and therefore, require different machining considerations. Some areas on the machinability of GLARE still remains to be further verified by more detailed testing and analysis. Therefore, there is an urgent need for new research to understand experimentally how those FMLs behave under various machining conditions. Hence, this thesis carries out a comprehensive machinability study of conventional drilling of GLARE fibre metal laminates and its metallic constituent using twist drilling operation.

The aim of the research is to explore the influence of machining parameters on the hole quality of the aerospace structural material GLARE and its metal constituent Al2024-T3 aluminium alloy using experimental analysis. Moreover, the research will experimentally investigate the impact of using two cooling technologies known as minimum quantity lubrication (MQL) and cryogenic cooling using liquid nitrogen (LN2) on the machinability of the FML. The research will conduct an in-depth analysis of surface quality of machined holes, which includes investigating the surface roughness, burr formation, delamination and variation in drilled hole size and circularity error. In addition, the effect of cutting parameters, cooling condition, workpiece thickness and fibre orientation on cutting forces, cutting temperatures and post machining tool condition will be analysed. The need to optimise the drilling parameters is essential to obtain a high quality of drilled holes and to minimise any defects that may adversely affect the long-term structural durability of the A380 structure. The research presented in this thesis was undertaken within the Composite Systems Innovation Centre in the Department of Mechanical Engineering at the University of Sheffield. The project was carried out in collaboration with the Advanced Manufacturing Research Centre (AMRC) and the support of several industrial collaborators and academic institutions which are fully acknowledged for their contribution in the acknowledgement section.

1.1 Aim of the research

The aim of the research is to investigate the machinability of GLARE fibre metal laminates through the assessment of the following objectives:

- To perform a comprehensive literature review on previous research and published work on the drilling of aluminium alloys, composite metal stacks and fibre metal laminates.

- To perform a comprehensive literature review on previous research and published work on the performance of MQL and cryogenic coolants in machining metals and composites.

- To investigate the generic parameters of drilling GLARE laminates, such as stacking

sequence, hole quality including (Surface roughness, Delamination, Burr formation, deviation of hole size and circularity error), machining temperatures and the influence of ductile/brittle interface zone.

- To evaluate the performance of minimum quantity lubrication and cryogenic cooling using liquid nitrogen in conventional twist drilling of GLARE fibre metal laminates, and compare their effect against dry drilling at room temperature.

- To determine the preferred cutting parameters and conditions of drilling holes in different GLARE grades and thicknesses using carbide TiAlN coated twist drills.

1.2   Novelty of the research

Interest from the aerospace sector on fibre metal laminates is rapidly increasing as they combine outstanding properties of their constituent; metal and composite. GLARE offers the opportunity to study the effect of cutting parameters and two modern cooling technologies on the hole quality in the main families of aircraft materials, i.e. aluminium and composites. The experimental work carried out in this research will help the scientific community to use optimal machining parameters for best hole quality during drilling operation of GLARE. Regarding metal and composite machining, the challenges in producing a good quality hole and the need for an automated inspection/detection of quality problems have been acknowledged by researchers in the manufacturing community. However, as evidenced by the conducted literature review, the machinability of fibre metal laminates can be considered as a new-born research in all machining processes. Among those machining processes, drilling is one of the most frequently used for the production of holes for riveting and bolting applications. This research aims to address some of the influential parameters in the production of a good quality hole when drilling GLARE fibre metal laminates through hole damage and defect examination, and the performance of two modern cooling technologies. The work in this Ph.D. is relevant to the industry such that it contributes to the optimisation of two grades of GLARE fibre metal laminates under dry and MQL conditions. Therefore:

- A limited number of publications are available on machining FMLs, specifically drilling GLARE fibre metal laminates and the use of different cooling technologies to evaluate the hole quality for this material is not reported. This research will focus on filling this gap and give a better understanding of GLARE drilling characteristics.

- This research, for the first time, will present a comparison study on the effectiveness of

applying different cooling methods (minimum quantity lubrication and cryogenic liquid nitrogen cooling) when drilling GLARE in order to investigate its effects on cutting force, torque, delamination, surface roughness, burr formation and tool condition.

- Results from the tests, including thrust force, torque, surface roughness, burr formations, chip formations, hole size and circularity error, drilling-induced delamination damage, post machining microhardness of the upper and lower surface of the laminate are presented and compared with previous available literature on drilling fibre metal laminates.

- The objectives intended in this research are to investigate the machinability of different grades and thicknesses of GLARE fibre metal laminates, based on the available knowledge on machining metals, composites and composites metal stacks. The motivation for this PhD work was to select the optimum machining parameters for maximising effectiveness of minimum quantity lubrication and liquid nitrogen cryogenic cooling application in drilling GLARE and compare them to room temperature cutting environment.

- The research will also look into the effect of MQL coolant flow rate and air pressure on machinability improvements in the drilling of fibre metal laminates. The work in this Ph.D. is important to industry such that it contributes to determining the drilling parameters of two grades of GLARE fibre metal laminates under dry and MQL conditions.

- In the first part of the research, drilling experiments are conducted to investigate and understand the effect of cutting parameters on a number of machinability indices. The tested range of cutting parameters are incorporated in statistical design methodologies to investigate a number of hole quality parameters, such as cutting forces, surface roughness, burr formations, hole size and circularity error, chip formation, post machining microhardness of the upper and lower aluminium sheets and post machining condition of the cutting tools.

- The reported literature on machining GLARE laminates have looked into a limited number of machinability indices, while there has been little effort to associate the performance of coolants with machining parameters. Therefore, the second part of this study attempts to establish the relationships between two modern cooling technologies and the cutting parameters used for making hole in GLARE laminates by evaluating the same machinability outputs described in the first part.

1.3   Thesis Outline

This thesis contains nine chapters.

Chapter 1: Introduction

This chapter summarises the thesis background motivation, and importance to aerospace industry, summarising the fundamental knowledge gap that needs to be filled to improve drilling performance of GLARE fibre metal laminates and aluminium alloy, followed by listing the aim and objectives of the work and the layout of the thesis with a brief description of chapter contents.

Chapter 2: Literature review

This chapter gives a brief introduction to the history of fibre metal laminates with emphasis on GLARE, providing details on its grades, manufacturing process and its current and future applications. The chapter also presents a detailed review particularly focused on the machinability of metals, composites and fibre metal laminates with emphasis on the drilling process. Details of some of the most important aspects of the drilling operation and most noticeable published work on drilling those materials are provided. The chapter also focuses on the impact of cutting parameters, workpiece properties and cutting tools on the machining process. The chapter also presents a literature review on the application of MQL and cryogenic cooling in machining operations with a focus on their use in the drilling process for a wide variety of workpiece materials with emphasis on aluminium and composites which make up GLARE constituents. The chapter also summarises the methods used for delivering the MQL and cryogenic cooling to the cutting zone and their impact on the quality of the machined hole in various materials and machining processes.

Chapter 3: Methodology and experimental details

This chapter presents the methods carried out to conduct the machining trials, samples preparation and the equipment used to measure various hole quality parameters in the research. The type of cutting tool utilised and microscopes used is also presented. In addition, a detailed description of using Design of Experiments (DOE) for drilling trials is provided in this chapter. The chapter also describes the methodologies undertaken to measure the cutting forces, surface roughness, hole size and circularity error, burr and chip formations,

optical and scanning electron microscopy, three-dimensional imaging for surface topography analysis and computerised tomography (CT) scan for internal delamination inspection.

Chapter 4: Performance evaluation of drilling Al2024-T3 alloy at room temperature

In this chapter, the application of various cutting parameters (spindle speed and feed rate) was investigated to evaluate their influence on drilling Al2024-T3 aluminium alloy by analysing their effect on cutting forces and hole quality parameters. Design of experiments statistical techniques were used to plan the drilling trials and reduce reduce the size of the experiments hence, saving time and cost. Analysis of Variance (ANOVA was utilised to find the significant factors influencing hole quality, and finally a set of cutting parameters was recommended for dry drilling the aluminium alloy.

Chapter 5: Performance evaluation of drilling GLARE at room temperature

In this chapter, the application of various cutting parameters (spindle speed and feed rate) was investigated to evaluate their influence on drilling two grades of GLARE namely GLARE 2B and GLARE 3. In addition, the influence of workpiece thickness and fibre orientation was investigated by analysing their effect on cutting forces, hole quality parameters and drilling temperatures at the exit side of the hole. Full factorial and response surface methodology (RSM) statistcal techniques were used to design the drilling trials to reduce the machining time and costs. Analysis of Variance (ANOVA) and multiple linear regression analysis was utilised to find the significant factors contributing to the different hole quality parameters and finally a set of cutting parameters was recommended for dry drilling of GLARE laminates.

Chapter 6: Performance evaluation of drilling GLARE using MQL and Cryogenic liquid nitrogen coolants

In this chapter, the effect of MQL and cryogenic cooling was carried out to evaluate their impact on drilling GLARE 2B fibre metal laminate by analysing their effect on cutting forces, hole quality parameters and drilling temperatures at the exit side of the hole using the same cutting parameters previously used in dry drilling trials in Chapter 6. Full factorial and response surface methodology (RSM) approaches were used to design the experiments. Analysis of Variance (ANOVA) and multiple linear regression analysis was utilised to find the significant factors contributing to the different hole quality parameters and finally pro-

posed a recommended condition for dry drilling of GLARE laminates and aluminium alloy on the basis of the range used cutting parameters under each coolant.

Chapter 7: Discussion on drilling Al2024-T3 and GLARE using Dry MQL and Cryogenic liquid nitrogen

This chapter discusses in details the differences between drilling Al2024-T3 alloy and GLARE 2B 11/10-0.4. The chapter also analyses the differences in drilling GLARE 2B 11/10 under dry, cryogenic and MQL conditions. The comparison is carried out by evaluation the previously reported cutting forces and hole quality parameters in chapters 4, 5 and 6.

Chapter 8: Conclusions and recommendation for future work

This chapter summarises the scientific findings from the research conducted in the previous chapters and provides suggestions for possible future work on machining GLARE.

Chapter 2

LITERATURE REVIEW

2.1 Fibre-Metal Laminates: An Overview

Fibre metal laminates (FMLs) are hybrid materials made up of alternating layers of thin metallic sheets and composite prepregs as shown in Figure 2.1. FMLs are composed of metals usually Aluminium with either glass (commercially known as Glare) based on R-glass or S2-glass fibres [2], Aramid (commercially known as ARALL) or carbon (commercially known as CARALL).
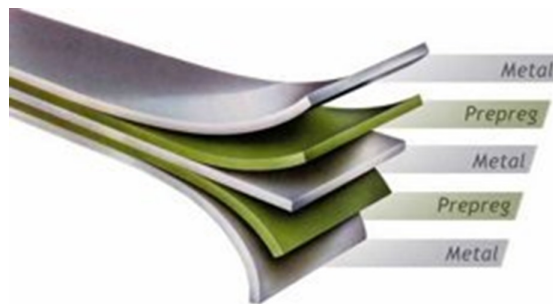
Figure 2.1: A typical fibre metal laminate

Applications of FML are widely used and are consistently growing in aerospace and defence structural applications due their high performance. FMLs which contain aluminium alloys such as GLARE and ARALL as shown in Figure 2.2 were mainly developed for applications in aircraft components where fatigue resistance is required. For example: the lower wing and fuselage skins of a plane. However, these materials are suitable for other areas such as flap skins, cargo bay liners floors and speciality airline containers [3]. Their unique features combine fatigue and impact resistance with relatively low density, flame (high burn-

through) and corrosion resistance. Moreover, they possess excellent damping and insulation properties.
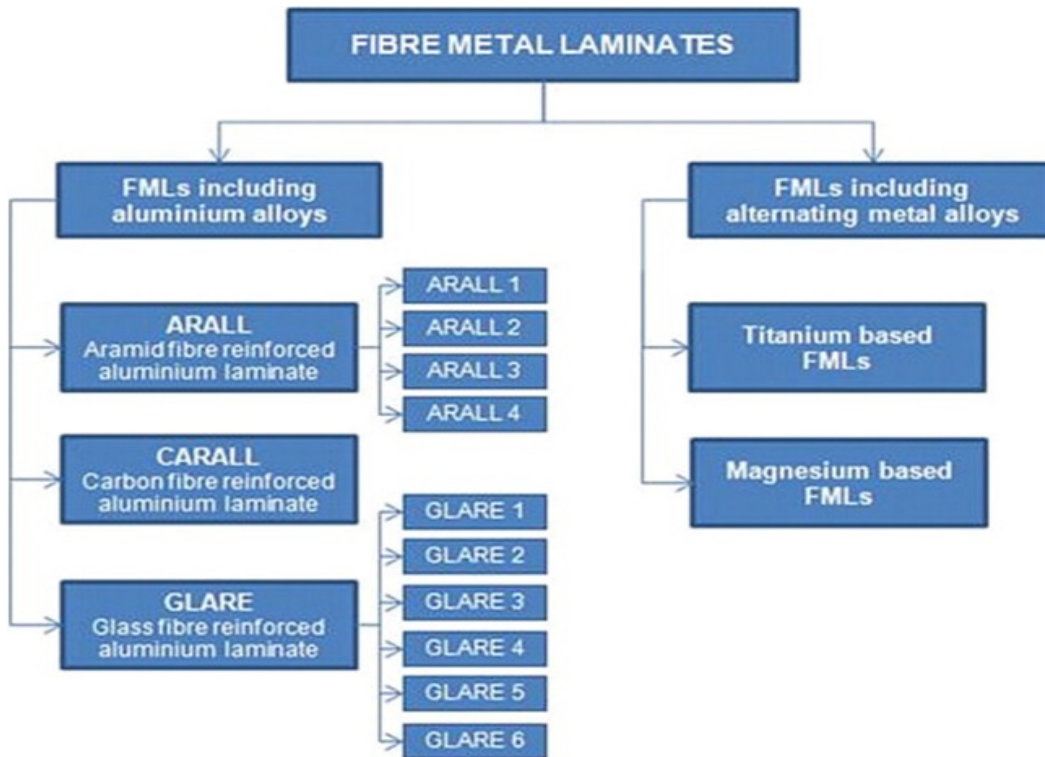
Figure 2.2: Family of fibre metal laminates [4]

The main motivation behind researching and developments in fibre metal laminates (GLARE) was to achieve weight reductions in the aircraft structures [5]. Another motivation was to improve fatigue resistance [6]. It was previously well known that bonded aluminium sheets had better fatigue performance than that in monolithic aluminium with an equivalent thickness. Later on, fibre layers were introduced between the metal sheets to improve further the fatigue performance; the most significant result was crack bridging that is the ability of the fibre to stop the crack from spreading through from the cracked aluminium sheet to the other aluminium sheets in the laminate, although considered to be a composite. Nevertheless, FMLs properties are designed, produced, implemented and inspected similarly to monolithic metal sheets rather than composites [4].

2.1.1   Glare Fibre Metal Laminate

GLARE (GLass Aluminum Reinforce Epoxy) is the second generation of the fibre metal laminates family (FMLs) [1]. GLARE consists of a stack of alternating aluminium sheets and intermediate glass fibre prepregs (usually from 2- 4 prepregs), with a nominal fibre volume

fraction of approximately 59 %. The Aluminium sheets in standard GLARE are aluminium alloy 2024-T3 for GLARE grades (2-6), or aluminium alloy 7475-T761 for GLARE grade 1. Alloys of 7000 grades are stronger and more brittle whereas the 2024 alloy is more ductile and slightly stiffer [7]. The fibre laminates are unidirectional S2-glass fibres (Magnesium alumina silicate glasses) embedded in an adhesive system FM94. The S2 glass fibres and adhesive system were mainly developed for aerospace applications, some of their mechanical properties are shown in Table 2.1.

Table 2.1: Mechanical properties of S2 glass fibre and FM94 adhesive system used in GLARE laminates [1]

Property	S2-glass fibres	FM94 adhesive system
Thickness (µm)	10	-
Strength (MPa)	4000	±50
Stiffness (GPa)	88	±1.7
Strain failure (%)	4.45	5-10

The adhesive system plays a significant role in the bond strength between glass fibre layers and aluminium sheets. The aluminium sheets surfaces are pre-treated either with chromic acid or phosphoric acid anodising process, and then are primed with BR-127 corrosion inhibiting bond primer. The fibres are delivered as a prepreg including the FM94 adhesive system from Cytec in the U.K [1]. The aluminium and glass fibre layers are bonded together with FM94 epoxy adhesive, the thickness of the aluminium sheets varies between 0.2 and 0.5 mm. For each prepreg layer, the nominal thickness of a single layer is 0.127 mm [1]. The glass fibre layers always consist of two or more unidirectional prepreg layers that are related to the aluminium rolling direction, the rolling direction of aluminium defines the fibres direction in the prepreg layer. The longitudinal direction of fibres is either 0° similar to the aluminium rolling direction- or 90° is the transverse rolling direction. The first commercial aircraft to use GLARE in its structure was the Airbus A380 as shown in Figure 2.3. It currently uses GLARE in the upper fuselage skin panel structures of the aircraft [8].

GLARE have six different grades, the standard grades of GLARE and their specifications are summarised in Table 2.2. A laminate coding system is used to define the different GLARE types and lay-ups to be tailored to meet the required performance of various applications (impact, fatigue, shear, off axis properties). The general configuration is represented as shown below [9].

$$Glare - N_{al}/N_{gl} - t_{al} \rightarrow [Al2024/prepreg/Al2024/prepreg/.../Al2024] \qquad (2.1)$$

Where:

- Nal: number of aluminium layers

- Ngl: number of glass fibre prepreg layers

- al: thickness of the aluminium layers (0.2-0.5 mm).

Table 2.2: Standard grades of GLARE [1]

Glare Grade	Sub	Metal Sheet thickness (mm) & alloy	Prepreg[1] in each fibre layer[2]	Main beneficial characteristics
Glare 1	-	0.3-0.4 7475-T761	0/0	Fatigue, strength, yield stress
Glare 2	Glare2A	0.2-0.5 2024-T3	0/0	Fatigue, strength
	Glare 2B	0.2-0.5 2024-T3	90/90	Fatigue, strength
Glare 3	-	0.2-0.5 2024-T3	0/90	Fatigue, impact
Glare 4	Glare 4A	0.2-0.5 2024-T3	0/90/0	Fatigue, strength in 0 direction
	Glare 4B	0.2-0.5 2024-T3	90/0/90	Fatigue, strength in 90 direction
Glare 5	-	0.2-0.5 2024-T3	0/90/90/0	impact
Glare 6	Glare 6A	0.2-0.5 2024-T3	+45/-45	Shear, off axis properties
	Glare 6B	0.2-0.5 2024-T3	-45/+45	Shear, off axis properties

1 The Aluminium rolling directions in standard laminates are in the same orientation; the axial rolling direction is defined as 0°, the transverse rolling direction is defined as 90°.

2 The number of orientations and the thickness listed in this column is equal to the number of UD glass fibre epoxy prepregs (each nominally 0.127 mmthick).

Figure 2.3 below illustrates an example of the configuration of a GLARE lay-ups and Table 2.3 depicts some of the mechanical properties of S2 glass fibre prepreg and Al2024-T3 alloy.
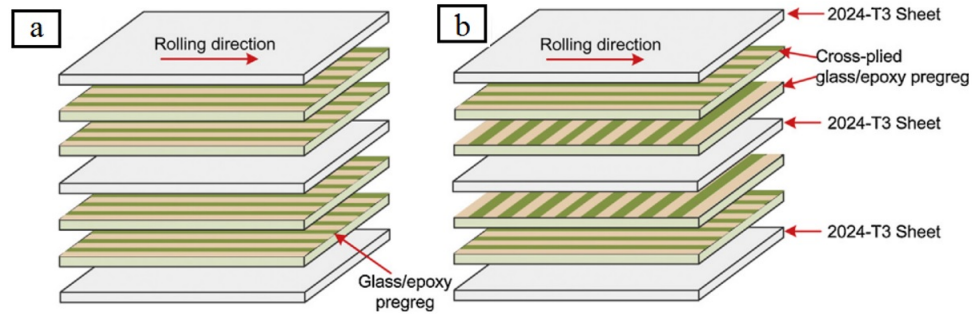
Figure 2.3: Illustrations of GLARE fibre metal laminates [10]: (a) GLARE 2 with unidirectional glass fibre layers ; and (b) GLARE 3 with cross-plied glass fibre layers

Table 2.3: Mechanical Properties of S2-glass fibre prepreg and Al2024-T3 [6, 11–14]

Mechanical property		UD S2 Glass/FM 94 Epoxy Prepreg $V_F = 60\%$	Al2024-T3	Units
Young Modulus (E)	L	54-55	72.2	GPa
	T	9.4-9.5	-	
Ultimate tensile strength (σ_{ult})	L	2640	455	MPa
	T	57	448	
Ultimate strain % (ε_{ult})	L	3.5-4.7	19	-
	T	0.6	-	
Shear Modulus (G)	L	5.55	27.6	GPa
	T	3	-	
Poisson's ratio (ν)	L	0.33	0.33	-
	T	0.0575	-	
Density (ρ)	-	1980	2770	kg/m3
Thermal expansion coefficient(α)	L	3.9-6.1	23.4	$(1/^\circ C) \cdot 10^{-6}$
	T	26.2-55.2	23.4	
Thermal conductivity (K)	L	1.1-1.4	121	W/m-K
	T	0.43-0.53	-	

The symbols L and T stands for longitudinal (the rolling direction for the metal) and transverse directions respectively.

Airbus chose GLARE to be a part of the A380 fuselage skin due to the limited fatigue life of previous aircraft skin structure made up of aluminium, the presence of fatigue requires continuous inspection and maintenance of the aircraft to comply with both the allowable design stresses and airworthiness requirements [15]. 25 % of the Airbus airframe is made of composites, 22 % of which are carbon or glass fibre reinforced plastics CFRPs and 3 % GLARE [16] as shown in Figure 2.4.
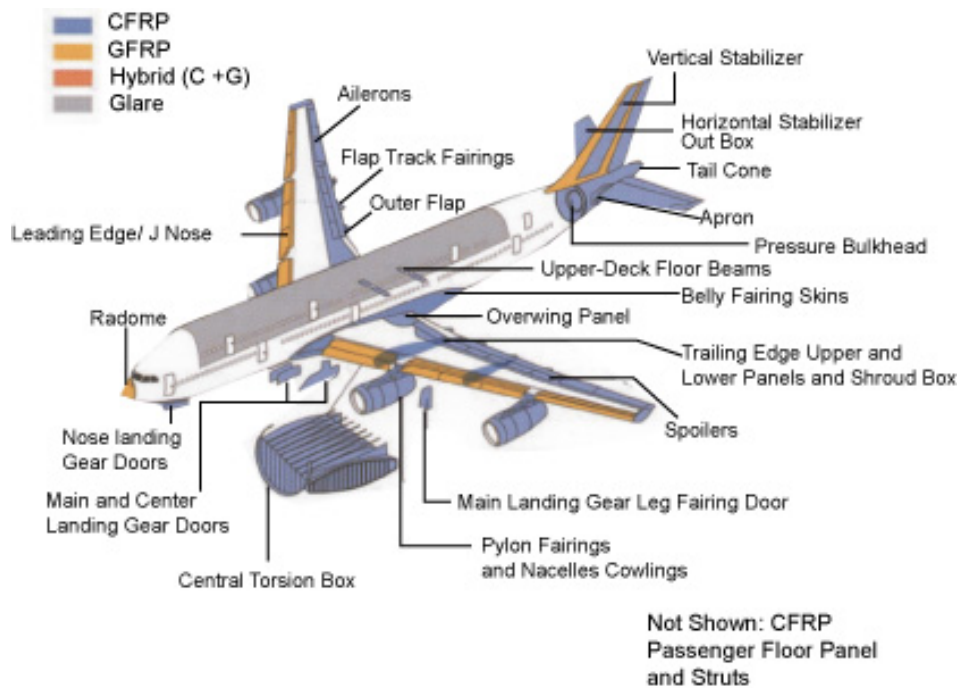
Figure 2.4: Airbus A380 Composite Profile [17]

2.1.2 Manufacturing Process of Glare

Glare is cured in an autoclave for around 300 minutes at elevated temperatures of 120 °C and under a pressure of 6 bars [18] as shown in Figure 2.5. This temperature level guarantees that the resin viscosity will be low enough to allow it to flow easily during the compression process and suppress the voids preventing the damage to occur in Aluminium sheets [19].

The curing process of GLARE causes the bonded aluminium sheets to contract more than the prepreg layers during cooling; this is due to the difference in coefficients of thermal expansion CTE of GLARE constituents. The thermal curing effects cause a mismatch in residual stresses in the FML, which could increase the stress intensity factor at the crack tip [20] while the magnitude of tensile stresses in aluminium sheets depend on the layup. To overcome the problem of contraction mismatch between metals and composites in GLARE, the post stretching process of cured FML is sometimes applied to remove those undesirable tensile residual stresses in aluminium sheets, and compressive residual stresses in prepreg layers. Having compressive stresses in aluminium sheets is desirable to prevent crack initiation and growth [1]. The laminate is stretched in one direction to reverse the stress distributions to a level slightly higher than its yield point and then released. The strains in the aluminium sheets transferred to the plastic region of the stress-strain curve while the fibre layers remain elastic [18].
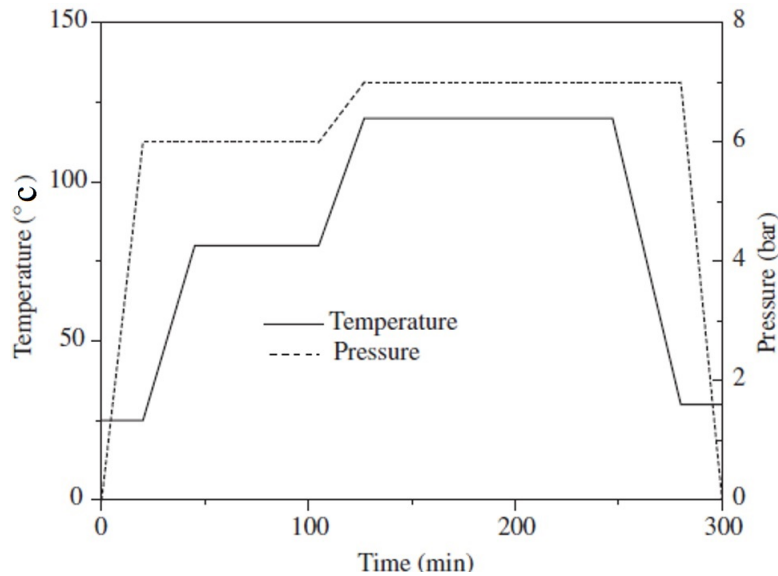
Figure 2.5: Typical autoclave cure cycle for metal/fibre laminates and thermosetting composites [19]

2.1.3   Aluminium Alloys

Aluminium alloys are widely used in aerospace and automotive applications, they are best known for their light weight characteristics, corrosion resistance and average strength. The classification of aluminium alloys can be based on the major alloying element in the following groups and as shown in Table 2.4.

The first digit indicates the principal alloying element and the aluminium alloy series. The second digit indicates the original alloy or the alloy modification if other than 0 (i.e., 1-9). For 2xxx-8xxx Groups, the third and fourth digits have no special significance but serve to identify the alloy in the group [21]. An exception is for 1xxx group where the last two digits provide information on the purity of the alloy above 99 % (the minimum aluminium percentage). For example, alloy Al1050 indicates that it contains a minimum of 99.50 % aluminium in its composition [22]. Aluminium alloys strength and mechanical properties can be either achieved by hardening (cold working) at room temperatures (non-heat treatable alloys). The temper is denoted by letter H, or by aging heat treatment (heat treatable alloys), temper denoted by letter T. Additionally, when the wrought alloys are annealed, the letter O is added in the temper designation, while the letter F is added to the temper designation to indicate that the product has been shaped without any attempt to control the amount of hardening [22]. For example, the Al2024-T351 aluminium alloy used in this research: the first 2 digits indicates the series designation, the 0 indicates that it is mostly pure aluminium with copper being the major alloying element, the T351 indicates that it is

solution heat treated cold worked and naturally aged alloy and relieved by stretching.

Table 2.4: Major alloying element in aluminium alloy series designations [23]

Series designation	Major alloying element	Notes
1xxx	Aluminium > 99%	Commercially pure (contains no alloying elements) low-cost aluminium, used mainly in chemical industries due to its resistance to chemical attack and corrosion, and electrical applications due to its superior conductivity.
2xxx	Copper	Used in aircraft applications, most susceptible to corrosion than other alloy grades, some alloys have superior machinability such as Al2024.
3xxx	Manganese	Non-heat treatable, typically used for anodising and welding applications.
4xxx	Silicon	Used for welding wires and brazing alloy for joining aluminium, mostly used for architectural applications.
5xxx	Magnesium	Good welding characteristics and resistance to corrosion in seawater applications.
6xxx	Magnesium and silicon	Contains equal amounts of Magnesium and silicon as the principal alloying elements, heat treatable and have good formability, machinability and corrosion resistance. Their alloys in this series are widely used for automotive and marine applications.
7xxx	Zinc	Highest strength among all series. Used mainly in airframe structures and mobile equipment and high strength applications.
8xxx	Other elements	Reserved for alloying elements other than those used for series 2xxx to 7xxx. Such as iron and nickel, aluminium-lithium alloy.
9xxx	Unused series	Not currently used. (Reserved for future use).

2.1.4   S2 Glass Fibre And FM94 Adhesive Epoxy

Glass fibre composite materials are made of thin filaments of glass, those filaments can be continuous and coated with an engineered chemical coating or size twisted together (Yarns), gathered without any twist forming (Roving) or chopped individually to uniform length (Chop). Fibreglass is made of glass with the only difference being that glass fibres are cooled slowly rather than rapidly cooled as it is the case in the glass that allows it to have an ordered crystalline structure instead of a random one. S2 glass fibres are made of magnesium alumina-silicate glasses attenuated at higher temperatures into fine fibres ranging from 5 to 24 μm [24]. Some of the mechanical properties of S2 glass fibre are given

in Table 2.5.

Table 2.5: High strength S-2 Glass fibre annealed properties measured at 20 °C [24]

Young's modulus (GPa)	Shear modulus (GPa)	Poisson's ratio	Bulk density (g/cc)
93.8	38.1	0.23	2.488

S2 glass fibres are the strongest regarding strength among other available glass fibres pro-duced because they contain higher levels of silica than standard glass fibre products. Their high compressive and tensile strength, high temperature and impact resistance. They are also resistant to the corrosive environment and suitable for use in high strength applica-tions under extreme temperatures. S2 glass fibres are used as reinforcement in structural composite applications and mainly developed for aerospace applications.

The FM94 is a modified epoxy film adhesive (produced by Cytec) and mainly used for bonding composite metal structures. The adhesive has a service temperature of -55 to 104 °C and some of its unique properties include excellent elongation and toughness, moisture resistance and high-temperature performance making it suitable for aerospace applications. The FM94 adhesive is suitable for bonding purposes in pre-cured and co-cured structural applications. The S2-glass epoxy prepregs in GLARE are delivered in the form of resin-impregnated fibres in a flat form known as a unidirectional tape [25]. The unidirectional tape can be oriented to any direction to give GLARE the desired strength and fatigue properties [25].

2.1.5   Glare Characteristics

GLARE properties combine the advantages of its composite and aluminium alloy. The most noticeable advantage is its light weight compared to monolithic aluminium. The glass fibre has a lower density than Al2024 aluminium, approximately 10 % lower [1] as shown in Table 2.6. Therefore, for a similar thickness of GLARE and monolithic aluminium, the GLARE is lighter for every prepreg layer within its composition which means lighter structures in the aircraft and hence lower fuel consumptions and environmental effects.

The higher melting point of Glass fibre in comparison to monolithic aluminium provides an enhanced fire resistance. The tests performed by Boeing showed that GLARE had a good fire through resistance up to 1200 °C; the skin made of GLARE was able to last for 15 minutes in comparison with monolithic aluminium skin that melts away in 20-30 seconds

Table 2.6: GLARE v.s Aluminium comparison ratio [26]

Property	GLARE	2024-T3 Aluminium
Weight (Density)	0.85-0.9	1
Structural Weight	0.7-0.85	1
Strength	1-2	1
Fatigue	3-100	1
Damage Tolerance	1-2	1
Impact Blast Resistance	1-2	1
Flame Resistance	5-50	1
Lightning Strike	1.5-2.5	1
Thermal Insulation	100-150	1
Corrosion Resistance	1.2-3	1
Reparability	Better	-
Maintenance	Better	-

in case of an outside kerosene fire [2]. GLARE have also proved to last for longer times in the event of a fire. One of the major concerns when using composites in the aircraft is their low impact damage resistance from damage due to taking off and run away debris, hail impact, bird strikes, the impact of dropped tools or cargo and service trucks and engine fragments which require expensive and complicated maintenance procedures. Moreover, the lack of standardisation of composites restrains the aerospace industry in using these materials in new aircraft structures [1]. FML in general and GLARE, in particular, can be easily inspected for plastic deformations caused by impact damages; this can be clearly seen on the exposed aluminium layer. Moreover, the damage caused can be easily repaired using riveted or bonded aluminium patches that have the similar stiffness of the fixed material, hence it does not require any special material to be available in stock for such repairs.

Disadvantages of GLARE is that it has lower stiffness ARALL and Al2024-T3 alloy, especially in biaxial version of GLARE laminates (multidirectional laminate) [27]. Indeed, GLARE usually finds its way in fatigue sensitive tension areas such as the fuselage structures [14]. The price of GLARE is also ten times more expensive than Al2024-T3 per square metre [27]. The compressive yield strength of the GLARE laminates is lower than the tensile yield strength. GLARE can be machined similarly to aluminium, however, further investigation on its machinability is required to elaborate the effects of machining parameters and coolants on the surface finish of machined holes. The manufacturing process of GLARE remains complicated and relatively expensive, developments in Vacuum Assisted Resin Transfer Moulding (VARTM) and out of autoclave manufacturing process is currently investigated to help reduce its manufacturing costs [28].

2.2   Machining metals, composites and fibre metal laminates

2.2.1   Fundamentals of Conventional Machining of Metals and Composites

Nowadays composite structures are stacked with metal structures such as titanium and aluminium alloys. Those stacks can form a hybrid assembly for the purposes of enhancing the performance and strength of the structure, and to reduce the weight of the total structure built. Drilling hybrid stacks is done in the final assembly process to avoid geometry differences in the hole between the mating parts in the stack, and to obtain good alignments and tolerances when assembled; it also improves time and efficiency in the assembly lines hence reducing machining costs. The need to optimise and control the drilling process is desired to obtain a high quality of drilled holes. This is where the problem usually begins, CFRP/GFRP possesses high strength hence they are difficult to cut and abrasive, drilling them requires different machining conditions and parameters than those needed for metals such as titanium and aluminium. Indeed, the machinability of FRPs depends on the physical and mechanical properties of the fibre and matrix, the fibre orientation and fibre content [29]. For example, CFRPs are preferably drilled at low feed rates and high spindle speeds whereas titanium alloys are preferably drilled at high feed rates and low spindle speeds. Thus, hole quality in drilling composite-metal stacks and FML may become a serious problem and drilling the stack might cause damage to the materials if these issues are not taken into consideration.

The properties of the machined material play a significant role in the cutting mechanism and chip formation behaviour during the drilling process. Aluminium alloys are non-ferrous metals while S2/FM94 glass fibre epoxy is a thermoset composite. Drilling GLARE constituents will produce two different types of chips due to the different physical and mechanical properties of its constituents. For example, drilling aluminium sheets produces continuous or discontinuous curling chips due to plastic deformation and elongation with the increase of temperature during the drilling process [30], while drilling the hard yet brittle glass fibre layers will produce fragmented and powdery chips by brittle fracture of the matrix and the fibres [29, 31]. GLARE constituents react differently under different cutting parameters, for example, drilling at high spindle speeds and feed rates causes the glass fibre epoxy matrix to fail earlier than aluminium sheets due to the high strain rates. Aluminium, on the other hand, can undergo considerable deformation under high strain rates even at elevated temperatures. The rise in temperature when machining thick laminates can lead to chip adhesion on the surface of the laminate and the cutting tool.

2.2.2   Chip formation and cutting mechanism in metal cutting

The main mechanisms controlling chip formation in metal cutting is by shearing the metal in three main areas during contact with the cutting tool edge are called: the primary shearing area, the secondary shearing area and the tertiary searing area [32–34] as shown in Figure 2.6.
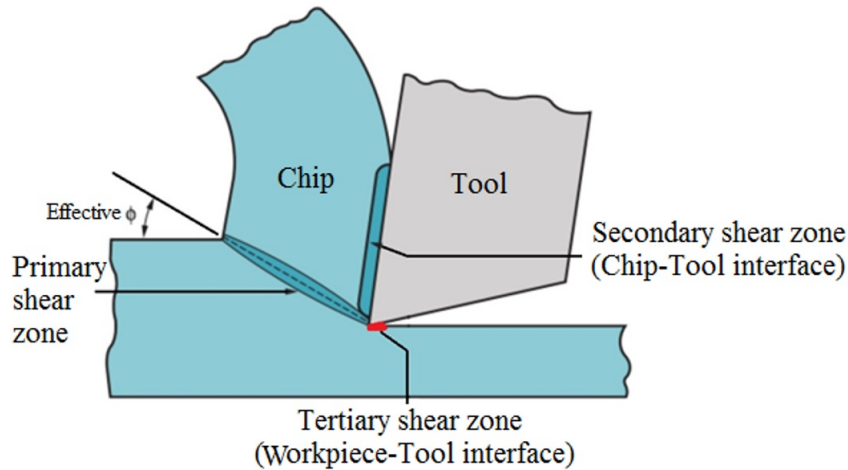
Figure 2.6: Metal cutting mechanism showing the three developed shear zones [32]

The primary shearing area results from the high cutting pressure and shearing of the workpiece material by the cutting tool edge, the cut material undergoes plastic deformation and exhibits rise in temperature. The secondary shearing area occurs in the chip after it has been formed while it slides along the cutting tool rake face and tends to increase with increasing friction between the cutting tool and formed chip. The tertiary shear area between the flank and the machined surface takes place after the cutting tool passes over the workpiece [35]. The tertiary shear depends on the type of the machined material and is responsible for flank wear. The chip formation in metal cutting occurs when the shear force exerted by the cutting tool reaches or exceeds the shear strength of the workpiece material in the primary shear zone. The cut layer (chip) slides over the cutting tool rake face but remains intact to the workpiece and while the cutting tool progress ahead, the chip is subjected to further plastic deformation and shear at the secondary shear zone until the chip can no longer remain intact with the workpiece. The formed chips during metal cutting can be classified into the following types as shown in Figure 2.7.

The type of formed chip depends on the workpiece material and the cutting conditions. For example, continuous chips forms when cutting at high speeds and low feeds and depths [32]. Continuous chips are formed when the workpiece material have high ductilities like steel or aluminium, or when the cutting tool edge is sharp and high cutting speeds with low
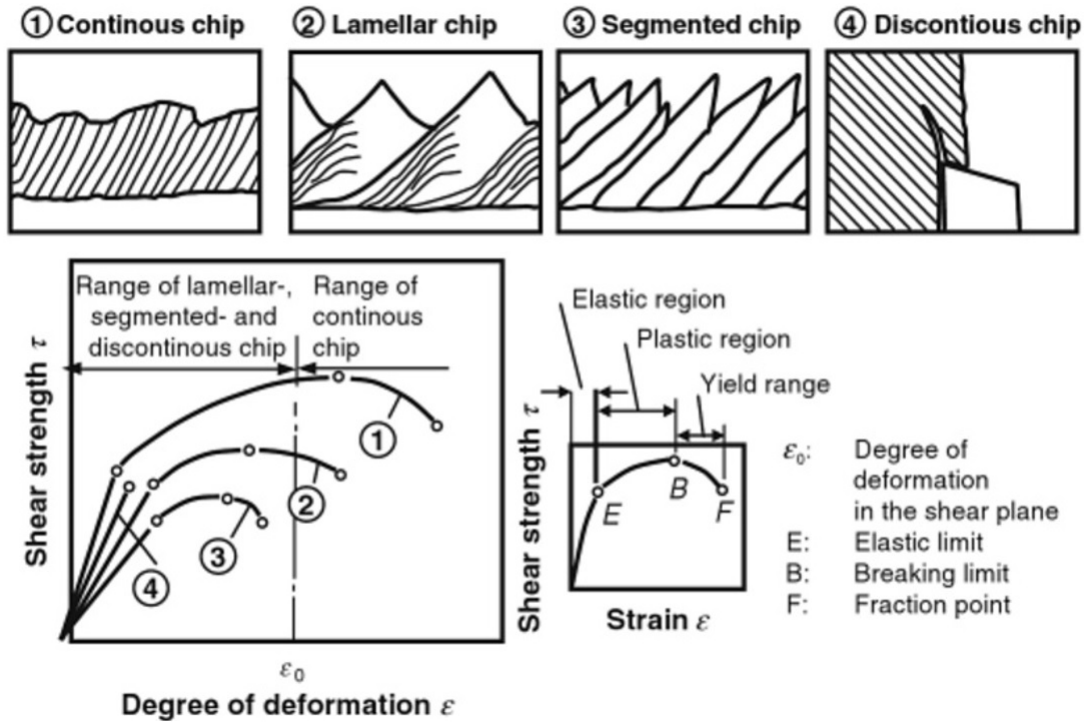
Figure 2.7: Types of chip formation in metal cutting [36]

friction on the rake face are present [32, 37]. Continuous chips indicate a good surface finish. Sometimes the continuous chips undergo high deformations, temperatures and strain hardening in the secondary deformation zone at the chip-tool interface which causes some of the chips to adhere to the rake face of the cutting tool forming what is known as built-up edge formation (BUE). BUE are an undesirable form of adhesion wear which can influence the surface quality of machined parts and the cutting tool life. On the other hand, discontinuous chips are produced when machining hard and brittle materials like cast iron and brass or when cutting ductile metals at very low feeds with small cutting tool rake angle. The formation of discontinues chip when machining hard metals is desirable and indicates a good surface finish [30, 32, 37, 38]. Lamellar chips are a form of continuous chips (semi-continuous) which have variations in the deformation process that form during high cutting speed and feed conditions. The lamellar chips have zones of low and high shear strain bands which form a saw tooth like chip pattern. Lamellar chips are formed due to the thermal or elastomechanical process in the ductile material [37]. The segmented chips are a form of discontinuous chips which occur when cutting at low speeds or when the cutting tool have a negative rake angle. Segmented chips are connected together but have cracks with significant deformations along the flow path [37].

2.2.3 Chip formation and cutting mechanisms in composite machining

The chip formation mechanism in composite machining differs from that in conventional metal machining due to their anisotropic properties, low strength and low susceptibility to plastic deformation [29, 39, 40]. The fibre and the matrix in composites contribute to the cutting mechanism final chip formation. The reinforcement fibres in composites are strong, brittle and have poor thermal conductivity like in aramid and glass fibres while the matrix is less stiff and weak with a low tolerance for high temperatures [29]. An earlier study by Koplev et al. [41] revealed that chip formation when machining CFRPs is produced from a series of intermittent fractures without significant plastic deformations usually found in metal chip formations [40]. The brittle nature of fibre/epoxy matrix in composites produces discontinues chips made up of fragments of fibres and matrix materials [40]. Early work by Wang et al. [42] on machining unidirectional composites indicated that chip formation is highly dependent on the fibre orientation. The type of chip formation in composites primarily depend on the cutting parameters, the physical and mechanical properties of the fibre and the matrix and fibre content and orientation [29, 40]. Other important studies by Arola et al. [43] and Hocheng et al. [31] on machining unidirectional composites indicated that several cutting mechanisms can occur and that the formed chip is highly dependent on fibre orientation. Figure 2.8 shows a schematic diagram of the major types of cutting mechanisms in orthogonal machining of CFRP-based on different angles of fibre orientation relative to the cutting direction.
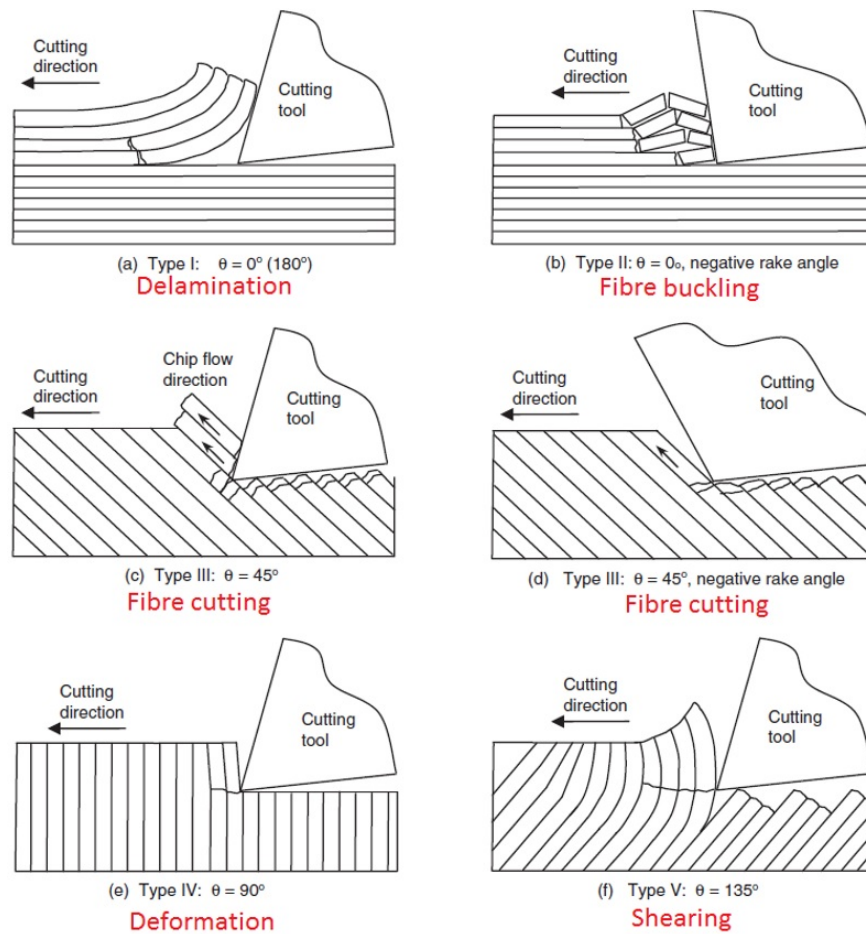
Figure 2.8: Chip formation modes when machining composites using a sharp cutting edge [29, 42]

The formation of chips during machining of unidirectional composites can be classified into the following types based on the fibre orientation and the rake angle of the cutting tool edge [29]:

- Delamination type chip formation (Type I).

- Fibre buckling type of chip (Type II).

- Fibre cutting continuous type chips (Type III)

- Fibre cutting type with discontinuous chips (Type IV).

- Shearing with a discontinuous chip (Type V).

Machining at $\theta = 0°$ fibre orientation with positive rake angle induces Mode I propagation along the fibre/matrix interface. Mode I (peeling) loading and bending induced fracture

occurs as the cutting tool edge advances in the workpiece material perpendicular to the fibre direction which applies pressure in the axial direction of the fibres [44]. A crack initiates at the tool point propagating along the fibre matrix interface [29, 45, 46]. The composite layers peels and slides along the rake face of the cutting tool causing them to bend like cantilever beam [29]. The delamination occurs due to Mode I loading (opening) - which is more dominant when cutting with a positive tool rake angle- or due to mode II (in-plane shearing) [46]. The progression of the cutting tool and the continuous peeling and bending cycles acting upon the fibre/matrix produces small segmented (discontinuous) chips which flatten upon separation and attains its original shape due to the absence of plastic deformation [29]. There is a significant fluctuation in cutting forces in this chip type due to the repeated cycles of delamination, bending and fracture [29]. Fibre ruptures with matrix crack propagation ahead of the tool tip is also common in this type when using positive tool rake angle causing the chip to separate due to brittle fracture [47].

Fibre buckling type of chip (Type II) occurs when zero or negative rake angles are used to machine 0° fibre orientations. The progression of the cutting tool edge in the workpiece material exerts a compressive load on the fibres along their direction and the negative rake angle of the cutting tool prevents them from separating from the machined surface causing them to buckle, and initiate a crack at the fibre matrix/interface [29, 45, 46] as shown in Figure 2.18.b. The in-plane shearing or Mode II loading is the primary mode of delamination which dominates the chip formation producing small discontinuous chips. While cutting force fluctuations are present in this mode, they are much smaller compared to those produced in delamination type I chip formation mode. Additionally, the machined surface in buckling and delamination types are similar, however, the formed chips in the buckling type II tend to be shorter than those produced from delamination type I [29, 46].

The third form of chip occurs with any cutting tool rake angle when the machined fibres are greater than 0° and less than 90°. Figure 2.18 c and d show the cutting mechanism at 45° with positive and negative rake angles. The formed chips may be continuous (Type III) or discontinuous (Type IV) depending on the amount of interlaminar shear when chip slides up the cutting tool rake face [29]. The fibre cutting type chip formation mode is dominated by two distinct fracture modes: First, the fracture occur due to compression-induced shear across the fibres axes which generates cracks in the fibres above (separate from the machined surface) and below (remain on the machined surface and can be seen under microscope) the cutting plane. Second, the interlaminar shear fracture follows next along the fibre/matrix interface as the cutting tool advances in the workpiece material. The chip flows parallel to fibre orientation in a similar way chip passes across the shear plane in metal cutting but with the absence of plastic deformation. The size of the chip here is influenced by fibre

orientation. The interlaminar shear stress at the fibre/matrix interface increase with fibre orientation up to 90° which in return decreases the size of the formed discontinuous chip. The resulting machined surface is irregular and fibres protrude out of the surface in various lengths due to the elastic recovery of the fibres after the progression of the cutting tool away from the machined surface and the continuous stretching-induced fractures of the fibres, the protruded fibres are the cause of flank wear [29, 46].

It was previously reported that when the tool edge radius is small enough it can exert concentrated pressure crushing the individual fibres at the point of contact followed by shear failure in the fibre-matrix interface as described earlier [31, 44]. However, if the cutting tool edge radius is larger than the diameter of the fibre, fibre crushing does not take place and a subsurface interfacial failure occurs causing the fibres to separate from the machined surface due to bending failure [31, 44]. Type V chip formation mode occurs when machining at θ = 135° or 90° < θ < 180° [29, 46]. The formed chips are long and discontinuous due to the compressive stress ahead of the cutting tool point leading to cracks in the fibre and the matrix. In addition, delamination and shear fracture along the fibre/matrix interface is present due to severe bending and compression. The fibres are bent then cut along away from the rake face of the cutting tool while the uncut bent fibres beneath the cutting plane remain intact to the machined surface and tend to recover elastically brushing against the clearance face during their recovery [29]. Though the machining technique of metals and the composite material is similar, their machining behaviour is quite different [48]. The inhomogeneous nature of composite material influence its machinability and quality of the machined surface.

2.3   Drilling and Twist Drills

Drilling can be defined as the process of removing material layers from the workpiece to produce cylindrical holes of various sizes by a combination of the rotary and translational motion of the cutting tool (the drill bit). Twist drills are the most common tools used in drilling operations for joining and assembly operations [48]. Figure 2.9 shows a schematic diagram of a two flute twist drill bit. Twist drills are rotary end cutting tools which have cutting lips extending from a chisel edge with flutes along its length that allow for chip evacuation and coolant delivery [49]. The chisel edge in the drill pushes the workpiece material aside rather than cutting it (indenting mechanism) while the cutting lips clear away the material from the workpiece at a constant thickness to create a hole [50]. The cutting speed in the drill will vary depending on the location of the cutting edges, from zero at the tip of drill and maximum at the outer radius of the major cutting edges [38]. Similar
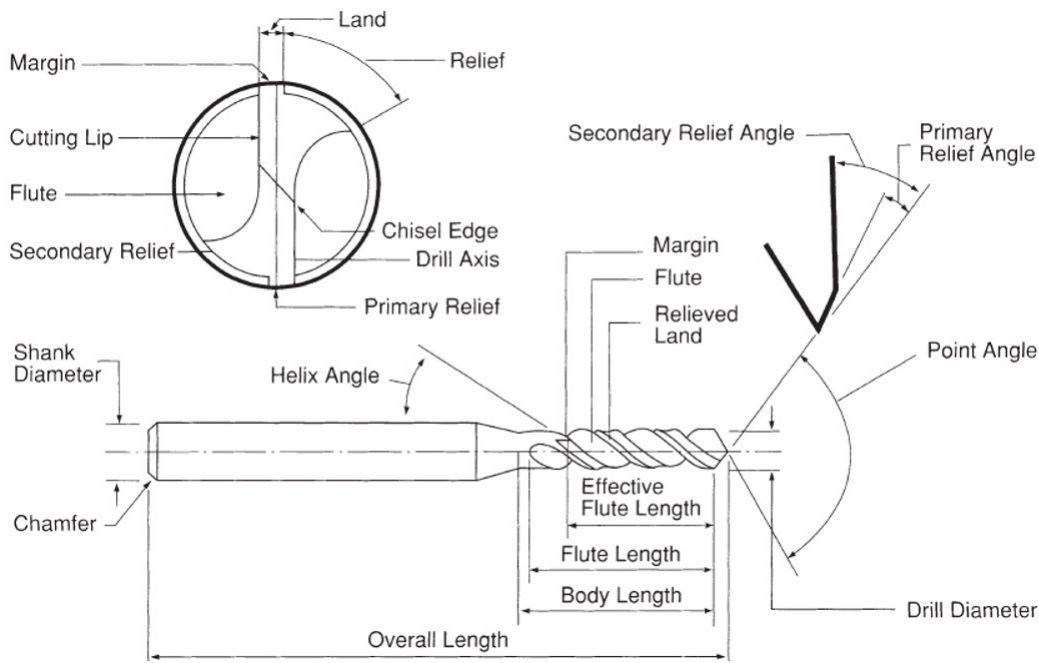
Figure 2.9: Twist drill bit geometry [51]

to orthogonal machining cutting tools, the helix angle in drill bits determines rake angle at the cutting edge of the drill, the rake angle decreases with the decrease of the helix angle which makes the cutting edges stronger [48].

2.4 Hole Quality and Drilling-induced Damage in Metals, Composites and FMLs

The evaluation of machined hole quality in GLARE is a more complex issue than that for composites or metals alone due to its hybrid composite-metal structure. The drilling-induced damage in GLARE can exist in the metallic aluminium sheets, in the glass fibre composite layers or can be transferred from metals to composites and vice versa. Hole quality requirement can vary depending on the material type, drilling conditions and the recommended tolerances desired in each industry. The cutting tools manufacturer SANDVIK reports that the hole quality requirements for metals, composites and composite metal stacks are different as shown in Table 2.7. For example, when drilling composites, there is no significant chip formation while the surface roughness is not of a great importance. While the damage in composites such as delamination, splintering or fraying in addition to tool wear are considered the main indicators of the hole quality.

Table 2.7: Common hole quality requirements by aerospace industry according to SANDVIK Coromant [52]

	CFRP	Stack
Average surface roughness (R$_a$)	Less than 4.8 μm	Less than 3.2 μm in CFRP Less than 1.6 μm in Al or Ti
Maximum delamination diameter	Less than 1 mm	-
Hole tolerance	-	±20 μm to ± 40 μm
Other	No splintering	No delamination or chipping of the CFRP layers at the hole exit No chip erosion on the CFRP from the metallic stack

Regardless of the cutting tool geometry, there will always be a form of damage which would eventually reduce the quality of the machined holes in the workpiece. These hole criteria can give an idea about the quality of the machined part and whether to reject it or not. Also, strict requirements imposed by the aerospace industry demand the production of highly quality machined parts with minimum defects. For example, the presence of waste material pressed in the edges of milled GLARE panels is considered a primary machining defect which leads to immediate rejection of the panel, while some delamination or cracks can be tolerated if they are repairable [1]. The following sections discuss some of the most common drilling-induced damage in metals and composites, and parameters used to determine the surface quality of drilled holes.

2.4.1   Surface roughness

Surface roughness is the measurement of a surface texture or finishes to detect surface irregularities of the workpiece due to manufacturing processes such as machining operations. The quality of surface finish in machined parts can influence their performance and they are usually used as criteria for accepting the finished part [53]. With the advance in drilling technologies and techniques, more attention was attracted to improve the final surface quality of the machined surfaces in composites and metals such as their surface roughness to achieve a damage free surface after machining. Surface roughness is influenced by the cutting parameters, cutting tool geometry and the resulting vibration of the cutting tool on the workpiece material during the machining process. High surface roughness of machined holes in metals or composites might lead to excessive wear, fatigue, lower the material ability to resist corrosion and product performance. The surface roughness can be described in terms of its R$_a$ (average roughness), R$_p$ (maximum peak height), R$_v$ (maximum valley depth) and R$_t$ (peak to valley height) [30]. The average roughness parameters provide a simple value

for accepting and rejecting decisions. Arithmetic average roughness or Ra is the arithmetic average heights of peaks and valleys irregularities measured within the sampling length, L as shown in the following equation. Table 2.8 shows the ideal ranges of surface roughness for selected material removal operations in metal machining.

$$R_a = \frac{1}{L} \int_0^L |y(x)| dx \tag{2.2}$$

Table 2.8: Ideal ranges of surface roughness for selected material removal operations [29]

Machining process	Roughness Ra (µm)
Turning	3-12
Drilling	3-25
Milling	1-10
Grinding	0.25-3

2.4.2 Burr formations

Burr formations are unavoidable protrusions in machining operations, especially in high production environment. Drilling metals can be a challenging task as many defects arise during the machining process when the drilling tool is entering or leaving the workpiece some of the material may plastically deform and not be completely removed which creates sharp edges around the hole which rise above the surface of the works piece. The remaining of the rough edges is called burr or burr formations which usually forms at both sides of the drilled hole. The burr formed at hole entry is usually smaller than that formed at the hole exit. In addition, entry burrs can be easily removed by chamfering the hole [54]. However, the burr formed at the exit side are more difficult to remove and cause more problems if not handled properly [54, 55]. Burr formation is one of the common challenges associated with drilling metals and multilateral stacks since, burrs and rough edges on fastener holes can cause stress concentrations which could initiate fatigue failures, corrosion and reduction in the life of the aircraft [56].

As mentioned earlier, different types of burr are produced during the drilling process with two burrs produced in the drilling of every hole; an entry and an exit burr [55]. Burr formation in drilling mainly depends on the tool geometry and tool-work orientation [57]. The formation of burrs depends on whether the hole axis is orthogonal or not to the plane of

the exit surface of the hole [57]. Burrs are unnecessary material remaining after machining and in order removed it usually requires another machining operation called de-burring. The removal of burrs is an absolute must for high quality, precision parts. Deburring operations account for about 30 % of the total manufacturing cost [58]. It also adds extra time to the machining process, the burrs in the drilling process occupy more than 40 % of total machining time and reduces production efficiency [59]. The deburring process is performed manually due to difficulties in automation [55].

The maximum allowable burr formation on a part may vary depending on the product type application and safety requirements specified by the industry. Some application requires tighter burr tolerances than others. Usually, when there is a limitation on the maximum allowable burr size, the technical drawing should take into consideration any requirements of the state of the edges of the machined part indicating whether the edge should be free from burr or having a sharp edge with limited burr size. Therefore, international standards such as the ISO 13715:2000 are applied to the drawings which required edge treatment aimed at enabling the specification of guidelines for the indication and graphic representation of the states of edges in technical drawings. Table 2.9 shows the reported burr height and thickness from previous studies on drilling GLARE and aluminium alloys.

Measuring the formed burrs is important as it can give an indication of the quality of the drilled hole. Burr is usually classified based on its size and shape but it can also be measured by its height and root thickness. Measuring burr size (burr height and burr root thickness) might sometimes require using accurate devices and software due to their small scale which cannot be seen with naked eye. Optical microscopes [60], surface profile-meters [61], image processing software and by means of a surface roughness profile-meters are some of the methods used to measure burrs size. Even though burr height is the most common measured characteristic when it comes to burr measurements, nevertheless burr thickness contributes more to deburring costs than burr height [62]. The entry burrs are generally smaller and can be removed easily by chamfering the hole, while the exit burrs are larger and are more difficult to remove from the workpiece [54].

2.4.3   Hole size and circularity error (Roundness)

While standard twist drills are commonly used to produce riveted holes for joining aerospace structural parts, Riveting and bolting in aerospace applications typically require tolerances as low as ±0.025 mm [66]. For example, material stacks made up of composites and aluminium or titanium alloys used for aerospace applications requires hole tolerances of 30 µm or lower [67, 68]. Although diametric deviations of drilled holes such as circularity have

Table 2.9: Some of the reported burr height and thickness when drilling GLARE and aluminium alloys [54, 63–65]

	Exit burr height (µm)	Exit burr thickness (µm)	Material	Reference
6.35 mm CVD diamond drill 0.08-0.24 (mm/rev) 50-150 (m/min)	10-60	-	Al2024-T3	[63]
6 mm multifaceted carbide drill 600-1100 (rpm) 0.06-0.1 (mm/rev)	560-1360	-	Al–Si alloy	[54]
2-fluted 3-fluted 4-faceted 6.35 mm	Up to 150 Up to 400 Up to 200	65-70	GLARE 5 GLARE 6	[64]
6.35 mm CVD diamond coated and uncoated drills 20-120 (m/min) 0.05-0.15 (mm/rev)	20-100	-	Al2024 in a CFRP/Al/Ti stack	[65]

a great importance on the performance of machined parts, nevertheless, they have not received much attention as surface integrity [69]. Achieving holes with tight tolerances can be influenced by several factors such as the mechanical properties of the materials and its hardness, coefficient of thermal expansion and conductivity. Other factors include cutting tool rigidity and the actual size of the tool. For example, commercial twist drills used in drilling aerospace structural parts are often smaller than the stated nominal size [70, 71]. Additionally, the machining cutting parameters and the use of coolants can influence the hole size, the workpiece fixture, machine vibrations and stability. Hole circularity (roundness) can be defined as a condition of a surface where all the points of the surface are intersected by any plane that is perpendicular to an axis is equidistant from that axis [72]. Circularity is a unit-less measurement that ranges between zero and one. The error of circularity (roundness error) is used to assess the quality of drilled holes and is usually measured in millimetres. Several methods can be used to determine the error of circularity. The criteria used depends on a reference circle and criteria include the Least Squares Circle (LSQC), Minimum Zone Circle (MZC), Minimum Circumscribed Circle (MCC), Maximum Inscribed Circle (MIC) [73]. The circularity (roundness) can be defined as the geometrical tolerance which indicates how close a section of a cylindrical part is to a true circle [74]. Table 2.10 shows some of the reported ranges of hole size and circularity error when drilling composites and aluminium alloys.

There are several international standards which provide a coordinated system of hole and

Table 2.10: Circularity error range of previous studies on drilling composites and aluminium alloys [63, 68, 75–82]

	Material	Range (µm)	Drill details	Reference
Deviation of hole size from nominal diameter (µm)	Al2024-T3	15-75	6 mm 10°,30° and 40° helix angle 130°, 140° and 180° point angle. Uncoated, TiAlN, TiN, TiN+Ag, Diamond, (Ti, Al)N + WC/C	[75]
	Al2024-T3	35-150	10 and 10.8 mm 24° and 30° helix angle 118°, 130° point angle HSS+TiN, HSS+TiAlN, TiN HSS (uncoated)	[76, 77]
	Al7010	5-35	6.35 mm 34° helix angle 120° point angle CVD diamond	[63]
	AA2024	5-40	6.35 mm 34° helix angle 120° point angle CVD diamond	[63]
Circularity error (µm)	GFRP	4- 41	10 mm HSS	[78]
	GFRP	42.5-312	10 mm HSS 85°, 90° and 95° point angle	[79]
	CFRP	80-250	5 mm Solid carbide u5 118° point angle	[80]
	CFRP/Al2024	6-25	4, 6 and 8 mm solid carbide 118° point angle	[68]
	AlSi3N4 metal matrix composites	136-301	6, 8 and 10 mm	[81]
	Al6061	19-182	8, 10, 12 mm HSS 100°, 110° and 118° point angle	[82]

shaft tolerances used for cutting tools. In the aerospace industry, the rivet or bolt will be a close or interference fit to prevent in-plane movement and maximise the bearing strength [83, 84] by forming compressive residual stresses in the metal surrounding the hole [84]. Both fits require clearances with general requirements for fit accuracy, rigidity and great alignment. The interference fit can provide a significant improvement on the machined part fatigue life but requires accurate hole sizing [85]. Some of the holes drilled into composite metal stack structures for installing fasteners are drilled in clearance fit in the composite structure and interference fit in the metallic structure to enhance the fatigue life. However, this process would require dismantling the composite-metal structure for reaming operation of the holes to provide a clearance fit for the fastener and reassembling process [86], however, this method cannot be applied to GLARE laminates.

Airbus industries comply with AITM 1.0009 standard [83], which requires a hole to have a tolerance of H11 and shaft tolerance of f7, the hole designation is written as 6H11f7 which

are based on 286-2 ISO (System of Limits and Fits is a coordinated system of hole and shaft tolerances). For example, drilling a hole using a 6 mm cutting tool should ideally have an upper hole deviation of 75 μm and a hole lower deviation of 0 μm, which means that the minimum-maximum hole size should be in the range of 6-6.075 mm. Airbus fatigue experts on GLARE machining recommend that achieving a maximum interference fit of 40 microns is required and ideally zero interference fit is desired.

As reported by SANDVIK tool manufacturer, typical hole demands when drilling composite metal stack materials commonly required to achieve an H7 hole tolerance fit based on the ISO 286 standard. This means that the hole should not vary more than ±12 microns but more relaxed tolerances such as H8 ±18 microns or H9 ±30 microns were allowed to be used when drilling composites due to difficulty in achieving H7 tolerances, for example, SANDVIK recommends that drilled hole tolerance in a composite metal stack should be between ±20 and ±40 microns [52].

2.4.4 Drilling-induced damage in composites

In addition to the common drilling-induced damage and hole defects which occur in metals, there are some exclusive forms of drilling-induced damage which might occur in composites. The existence of those defects in composites parts might reduce their durability and long-term performance. Konig et al. [87] described some quantitative assessment which defines the machining quality of drilled holes in composites as shown in Figure 2.10. The defects can be related to the type of cutting tool and workpiece materials, the cutting tool geometry and machining parameters [48]. The type of damage when drilling composites can be classified to a mechanical damage such as, delamination at entry and exit side of the drilled hole, fibre pull out, fibre linting, chipping, matrix cracking, and matrix smearing. Thermal damage such as burn off the matrix, chemical damage such as the water recovery of the matrix [46, 69]. Another classification of drilling-induced damage in composites by Lachaud et al. [88] describes four categories of composite damage when using a twist drill: Hole entry defects which are related to the characteristic of the composite fibres and drill geometry, circular defects due to fibre orientation, thermal damage due to friction between the cutting tool and the workpiece, and delamination at the exit of the hole due to cutting parameters.

2.4.5 Delamination

One of the most critical problems when machining laminated composites is the formation of delaminated zones. Delamination is the separation of the adjacent plies of a laminated
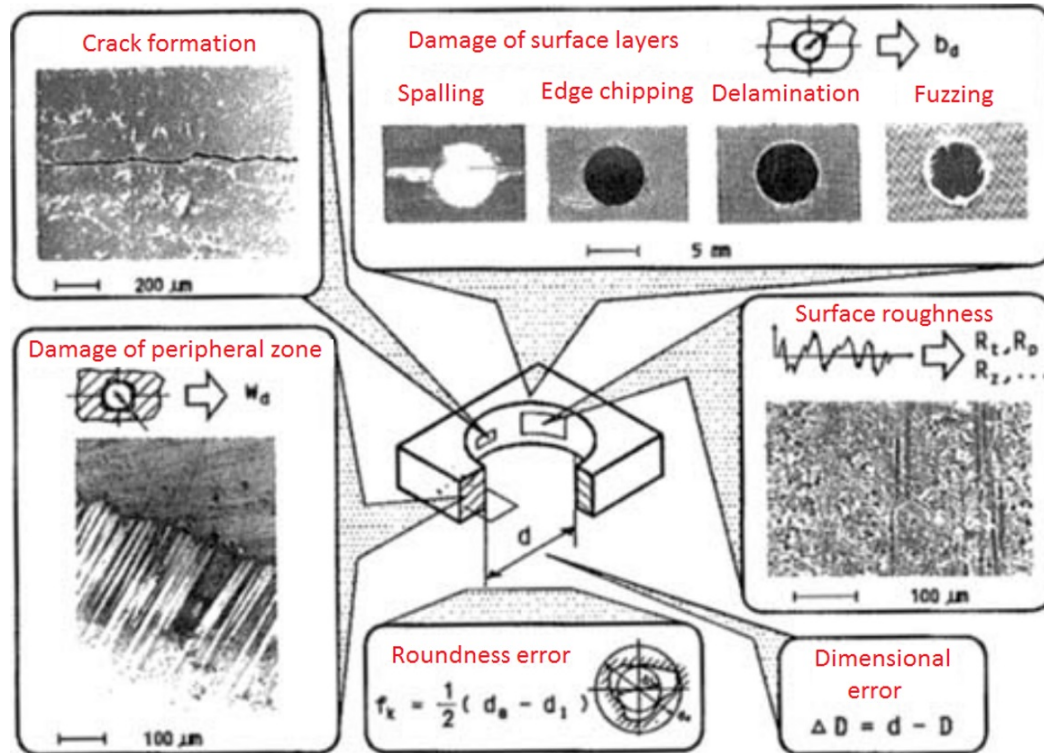
Figure 2.10: Quality criteria for drilling FRPs [87]

composite material. This may be local or may cover a large area of the laminate [89]. Delamination occurs when the last plies of the composite (interlaminar stress level) do not withstand the force exerted by the chisel edge of the drill (the force is greater than the interlaminar strength) [90, 91]. Delamination is generally considered the main reason which leads to a deterioration in the load carrying capacity and reduction in the structural integrity of the laminate [92, 93]. Among the defects caused by drilling composites, delamination appears to be the most critical and most common mode of failure [91, 94]. Delamination is one of the major failure modes that might occur while drilling composite materials due to their suspectiblity to delaminate when experiencing severe mechanical stresses. It has been previously reported that 60 % of all part rejections during the final assembly of an aircraft is related to drilling delamination [95–99]. Boeing reported manufacturing flaws on its first commercial jet built mostly from composites the 787 Dreamliner. Some delamination and separation of baked composite fibers were found in parts of the rear fuselage [100] causing delays in delivering this type of Planes to many airway companies. Therefore, a considerable amount of attention should be given to the factors which might cause delamination in composite materials.

When drilling composites, two types of delamination might occur: Peel up and push-out delamination as shown in Figure 2.11. Peel-up delamination occurs at the upper part of the

laminate. As the drill enters the laminate, a peel force acting opposite to the feed direction tends to lift the upper layers, and the material spirals up the drill flute before it can be cut properly which separates it from lower layers of material being pushed down by the acting thrust force [93, 101, 102]. The peeling force is a function of tool geometry and friction between tool and workpiece [93]. The push-out delamination occurs when the interlaminar bond strength in last few layers in the uncut laminate is unable to resist the compressive thrust force [93, 101]. The push-out delamination depends on the properties of the fibre and the matrix of the composite, and is found to be more severe (critical) than the peel up delamination [101, 102].
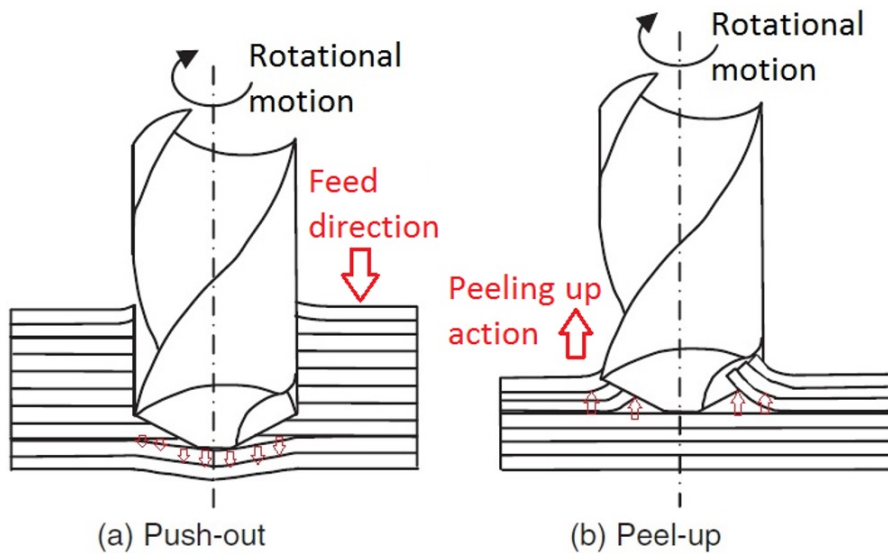
Figure 2.11: Illustration of (a) Push-out delamination at exit and (b) peel-up delamination at entry [29]

Measuring surface delamination

The visualisation of delamination is a difficult process since it can exist externally on the upper and lower surface of a machined hole in composite structure or in its internal layers. Destructive techniques are not common for inspecting delamination since the method takes time and interpretation of results is sometimes difficult since it cannot identify the internal defects. Therefore, visual inspection of delamination using optical microscopy and scanning techniques are more desirable. Previous authors suggested using dimensional and non-dimensional parameters to quantify delamination by measuring the delamination area, the maximum damage radius of drilled hole or sum of the lengths of internal crack [94]. Wong et al. [103] proposed a formula to measure and quantify the extent of delamination in composites. The delamination around the drilled hole can be quantified by measuring

the delamination factor by either one of the following techniques: the first delamination factor Fd is calculated by dividing the maximum diameter of the circle which contains the delamination area over the nominal hole diameter. The second delamination factor Fa is calculated by summing the area of delamination zone and the nominal hole area and divide it by the nominal hole area. Figure 2.12 shows an illustration which explains the two delamination factors. In most of the studies, FD has been used to calculate the delamination factor while FA has been only used in several studies [104–107], this is due to the difficulty in measuring the damaged area surrounding the drilled hole , FA, FD can be calculated using equations shown below:

$$F_D = \frac{D_{nom}}{D_{max}} \tag{2.3}$$

and

$$A_D = \frac{A_{nom}}{A_{max}} \tag{2.4}$$

Where:

- Fd,Fa: delamination factors.

- Dnom:Nominal diameter (hole diameter).

- Dmax: maximum distance of delamination from the centre of the hole.

- Anom:Nominal hole area.

- Amax:Maximum area of delamination.
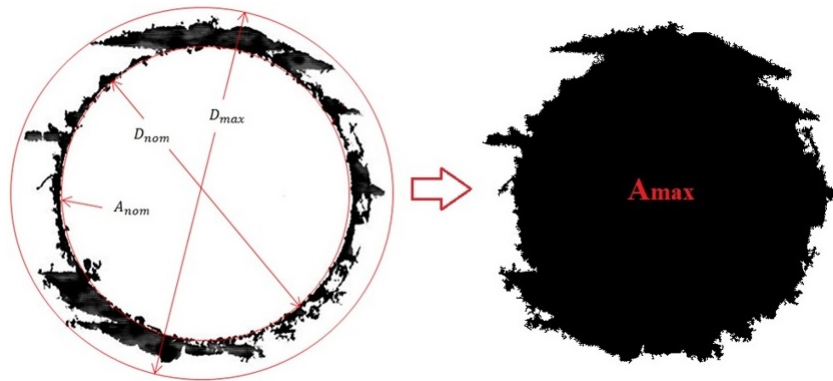
Figure 2.12: Schematic representation of the delamination factors Fa and Fd

2.5   The Effect of Fibre Properties and Orientation on the Machinability of Composites

Composite materials are made from reinforcing plastics with fibres. The strength of the fibres is much higher than the matrix, and indeed it is estimated that 70-90 % of the load applied to composites structures is carried by those fibres [108]. Indeed, when drilling composites the quality of drilled hole depend on more on fibre than the matrix [109]. A critical factor that affects the damage tolerance in composites is the fibre direction. Generally, the energy can be easily passed from one composite layer to the other if they both have same fibre orientation and as a result, the severity of damage is greater than what would be if the fibres in each layer had different orientations, since this will have a transfer of energy between layers and allow it to fail at a higher load. Therefore, from a crack resistance point of view, a [0/90/0/90] stacking sequence is preferred over [0/0/90/90] or [0/90/90/0] [110]. However, from a seperation resistance point of view, the interlaminar interface between laminates with different ply orientations (i.e. cross-ply configuration) are mechanically weak and therefore, local separation of the laminate from one another is a common form of damage in such configurations [111]. The most common types of reinforcing fibre and their properties are given in Table 2.11.

Table 2.11: Typical properties of common reinforcing fibres [112]

Material type	Tensile strength (MPa)	Young modulus (GPa)	Density (Kg/m³)	Cost (£/Kg)
Aramid (Kevlar)	3150-3600	58-160	1390-1470	20
Carbon	2100-7100	220-900	1740-2200	10-200
Glass	3445-4890	72-87	2460-2580	25

As mentioned earlier, the machinability of FRPs depends on the fibre orientation with respect to the direction of the cutting tool motion [29]. Figure 2.13 shows the fibre orientation definition in drilling unidirectional composites. In addition to fibre orientation, there are other factors which govern the fibres contribution to machining composites such as the mechanical properties of the fibre, the interaction between the fibre and the resin and the percentage of fibres in the composite commonly known as fibre volume fraction. These four factors can influence the following parameters when machining composites:

- Cutting forces.

- Cutting temperatures.

- Surface quality (surface roughness).

- Cutting mechanism.
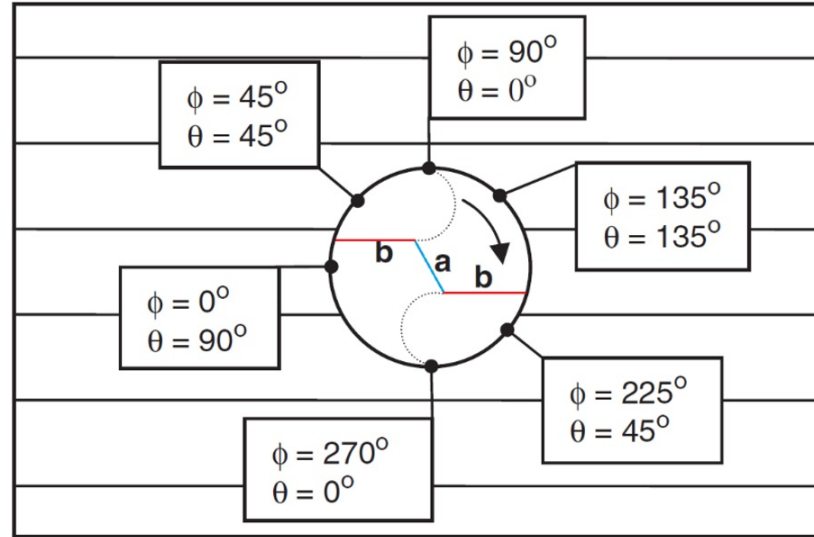
Figure 2.13: Fibre orientation definition in drilling unidirectional composites (a) chisel edge, (b) major cutting (edge $\Phi : angular position, \theta : fibre orientation$) [29]

Cyclic cutting forces are developed when machining composites due to fibre orientation throughout the thickness of the laminate. The material removal in drilling is performed by the two cutting edges (in the case of a two flute twist drill) and the penetration of the chisel edge. The two cutting edges have identical cutting behaviour and relative fibre orientation angle (see Figure 2.10) [29]. The chip thickness is independent of the angular position of the cutting edge. For example, when the cutting tool edge is parallel to the fibres direction, the cutting velocity vector is perpendicular to the fibres which are oriented at 90°. The rotation of the cutting edge clockwise decreases the fibre orientation to zero at 90° angular position [29]. Previous studies on drilling GFRPs indicated that cutting forces were minimum when drilling at 0° or 90° degrees fibre orientations [113]. However, in another study on drilling unidirectional GFRP, Enetyew et al. [114]] reported that lowest thrust force occurs around the rotational angles of 135° and 315°. C.Gao et al. [115]] reported that the cutting force was minimum at 45° fibre orientation and maximum at 90°. Ghafarizadeh et al. [116] also reported that maximum and minimum cutting forces occur at 90° and 0° fibre orientations respectively when milling unidirectional CFRPs. Wang et al. [117] also reported that the surface roughness and cutting forces of machined epoxy reinforced unidirectional carbon fibre were reduced when using positive rake angles 0° and 20°. Drilling at low feed rates and high cutting speeds reduce the cutting forces and delamination, but they could also result in undesirable thermal degradation of the matrix [118]. Previous studies on the effect of fibre orientation on cutting forces when machining epoxy composites reinforced with unidirectional carbon fibre by Wang et al. [117] are shown in Table 2.12. The surface

Table 2.12: Effect of fibre orientation angle on cutting forces [117, 119]

Fibre orientation θ°	Effect on cutting force	Notes
0° ≤ θ ≤ 60°	Increase	-
60° ≤ θ ≤ 120°	Decrease	Increase if depth of cut is large
θ > 120°	Increase	Decrease if depth of cut is large

quality of the drilled hole in unidirectional composites will vary around the circumference due to fibre orientation. For example, the fibres tend to be pulled out when the tool cutting edge is parallel to the fibre orientation. The increase in cutting angle within 20°-45° range causes bending and compression action in addition to fibre pulling and worst surface quality is achieved in this range [108]. Shear and bending is observed when the cutting tool edge is perpendicular to the fibre orientation [108]. Gao et al. [115] reported that the fibre orientation angle, depth of cut, and cutting speed are important factors affecting the cutting force and surface roughness. Wang et al. [117] reported that the surface roughness of machined epoxy reinforced unidirectional carbon fibre was minimum between 0° to 90° fibre orientation and gradually increased with fibre orientations up to 150°, this was also confirmed by Ghafarizadeh et al. [116]. C.Gao et al. [115] also reported that the surface roughness increased with fibre orientation. For example, the surface roughness measured at 45° fibre orientation was smoother than at 135° due to more surface irregularities in the later one. Ghafarizadeh et al. [116] also reported that the minimum surface roughness is achieved for 45° and 90° fibre orientations and maximum at 135° fibre orientation. Palanikumar [120] also reported that the surface roughness increased with the increase of fibre orientation from 15° to 120°, however, the effect of fibre orientation on surface roughness becomes insignificant when increasing the cutting speed beyond 175 m/min.

In another study, H.Gao et al. [121] also reported that drilling damage at the exit of the hole was more likely to occur at fibre orientations in the range of 0° to 90° with damage level increasing with the decrease of the fibre orientation, and less in the range of 90° to 180° with damage increasing with the increase of the fibre orientation when drilling unidirectional epoxy composites. Enetyew et al. [114] reported that when drilling GFRP, the surface roughness is higher at fibre orientations of 135° and 315° along the circumference of the hole, they also indicated that fibre pull-out is likely to occur in the region of 135° to 175° and the region of 315° to 335°. A number of fibres content in the composites plays a significant role on the machined surface quality, chip formation and tool wear, Budan et al. [122] reported that the surface roughness, delamination factor and tool wear increased with the increase in fibre content from 30 % to 60 % when drilling GFRPs. The increase in surface roughness

was due to the increase in the fibre pull-out In addition, the increase in fibre content was reflected by the lack of plasticity deformation and higher brittle fracture which produced small segmented chips while long chips were common with lower fibre content. Having high fibre content in the composite can have a serious impact on health when machined [122].

The surface quality of the machined hole is also influenced by the mechanical properties of the fibres. For example, aramid fibres are weak in compression and tend to bend ahead of the cutting edge which causes them to recede into the matrix during machining and later to be frayed on the surface of the hole [108]. While glass and carbon fibres break in a brittle matter ahead of the cutting edge [29]. The thermal properties of the fibre can also influence the machinability of the composite. For example, the thermal conductivity of carbon fibres is higher than in glass or aramid fibres making it more efficient in dissipating heat away from the cutting zone along its length [29]. Therefore, machining at high cutting speeds forms regions of localised heat zones in the cutting area which could affect the machined surface quality. In addition, the mismatch in thermal expansion properties in the fibre and the matrix could lead to dimensional inaccuracies and thermal stresses which could adversely affect the quality of the hole [29].

The fibre orientation plays a significant role in the developed machining temperatures, Zitoune et al. [123] reported that machining at 90° fibre orientation results in a maximum temperature due to the multiple bending and shearing cutting mechanisms which increase the cutting forces and friction, the rise in friction is due to chip flows up along the rake face due to shear along the fibre matrix interface [29] which was also confirmed by Ghafarizadeh et al. [116] when milling CFRPs . In addition, the failure stress when cutting at 90° can reach up to 1600 MPa compared to 1000 MPa when cutting at 0° fibre orientation. The modulus of elasticity in composites can influence the developed machining temperatures in the workpiece. Merino-Perez et al. [124] reported that the type of fibre reinforcement had an effect on the heat dissipation when drilling a hole in CFRP such that composites with higher modulus dissipate heat more than those with higher strength carbon fibres due to the high degree of crystallinity of the high modulus carbon fibres.

2.6 The Effect of Tool Geometry, Material and Coating on the Machinability of Metals and Composites

The range of materials used in drilling processes can be divided into two general categories, metallic and non-metallic materials. Metallic materials can be further divided into ferrous and nonferrous metals while non-metallic materials include a variety of materials such as

plastics, rubber and wood. The majority of drilling operations for making holes is carried out using twist drills [32] However, other types of cutting tools are also employed for making holes such as brad point, spade or paddle drills for wood, masonry and countersink drills. A common two flute twist drill bit is made up of a drill point, a body and a shank. The shank of the drill is the solid cylindrical part which is attached to the machine tool holder [125]. The land of the drill is the part between the flutes designed to give the cutting tool its torsional strength. The point of the drill has four main features: the cutting edges (cutting lips), the chisel edge, lip relief, and point angles [126]. The cutting process takes place along the cutting lips and at the chisel edge. The majority of the material is removed by the cutting edges while the chisel edges penetrate the workpiece material and is, therefore, the major contributor to the thrust force. It was previously reported that the chisel edge contributes to thrust force range between 40-60 % and up to 80 % at high feed rates [127], hence the chisel edge have a significant influence the delamination in composites. Drill point angle can vary between 80° and 140° depending on the machined material, most common used point angle is 118° [48]. For example, drilling cast iron is recommended with low point angles between 90°-100° while drilling carbon steels with high carbon content requires large point angles between 130°-135° [128]. A general rule of thumb is that soft and ductile materials such soft steels and copper requires smaller point angles while extremely tough, higher alloy content and difficult to cut materials require larger ones [30, 128]. The point angle of the drill has a significant impact on the chip formation, the thrust force and torque as shown in Figure 2.14. Increasing the point angle increases the thrust force and the lower torque [30]. Drills with large point angles produce thinner chips while drills with lower point angles produce wider chips. The lip relief angle can vary between 8° and 24° depending on the size of the drill bit and the hardness of the workpiece material [30]. As a rule of thumb, large diameters and hard materials require smaller relief angles while softer and smaller diameters require higher relief angles.

Another important part of the drill structure is the helix angle, the helix angle is equivalent to the rake angle in other cutting tools. The helix angle can directly influence the cutting forces, the torsional and radial stiffness of the cutting tool. Increasing the helix angle reduces the cutting forces and radial stiffness but and increases the torsional stiffness of the drill [129]. The standard helix angle for most drills is 30° [30], but it can range between 12° to 38° depending on the application. Generally, the helix angle can fall into one of three categories: Slow (12°-22°), regular (28°-32°) and fast (34°-38°) helix angles. The slow helix angles produce broken chips and in vertical drilling without rotation operations. Regular helix angles are the most common and are usually used in various drilling applications of ferrous and non-ferrous materials for making shallow holes because of their limited ability to lift chips. The fast helix angles are an excellent choice for softer materials and usually
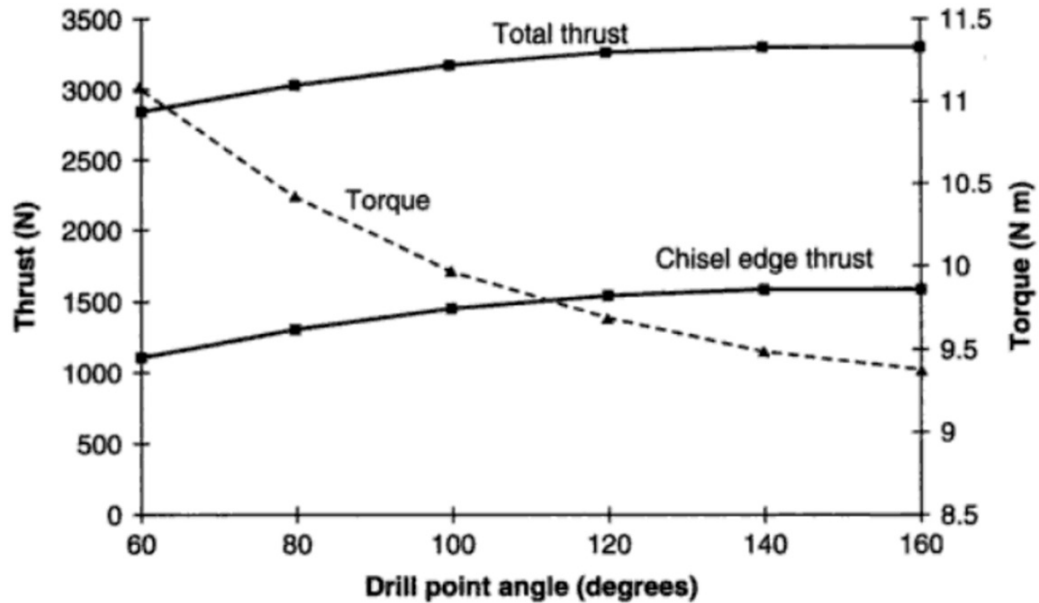
Figure 2.14: The influence of the cutting tool point angle on cutting forces [30]

produces stringy chips, they are used for drilling deep holes because they are excellent in lifting chips. The drill bits can be made of ferrous and non-ferrous materials [130].

Drill bits can be uncoated or coated depending on the application, about 15 to 20 % of all tool steels are coated [131]. The coating is a thin layer (in microns) of a material applied to the surface of the cutting insert. The purposes of the coating is to improve the performance of the cutting tool by extending its life and provide better physical and chemical stability at high temperatures thus allowing for higher cutting speed. Despite the fact that most drills come with an 118° drill point angle, when it comes to drilling FRPs it is recommended to use a drill bit with a 135° point angle [48]. Previous studies on drilling composites showed that increasing the drill point angle improved the hole quality at entrance such entry delamination factor and fibre fraying, however, it increased the exit delamination factor, surface roughness and thrust force [132–135]. Another study showed that increasing the point angle from 90° to 118° also increased delamination factor but reduced the thrust force when drilling GFRPs [136]. El-Sonbaty [137] reported that increasing the drill diameter increases the cutting forces due to the increase in the cross-sectional area of the undeformed chip.

The material type and size of the cutting tool had a significant impact on hole quality when drilling composites. Reddy et al. and Selvan et al. [136, 138] reported that carbide drills had better performance than HSS drills in terms of reducing the thrust force and delamination. In addition increasing the drill bit size and workpiece thickness increased

thrust force. Previous studies also reported that the cutting tool material can influence the type of formed chip due to different tool-chip interaction mechanisms. High cutting speeds are desirable when using PCD drills due to their high hardness which considerably reduce delamination [118]. Madhavan et al. [118] reported that continuous ribbon-like chips were formed using carbide drills while discontinuous chips were formed using HSS drills. Okutan et al. [139] indicated that increasing the feed rate and drill diameter increases cutting forces and the undeformed chip thickness when drilling GFRP. El-Sonbaty [137] also reported that the influence of drill size on surface roughness when drilling glass fibre epoxy composites may vary due to the multiple effects acting on the workpiece such as the cutting forces and the generated machining temperatures. The large rise in cutting temperatures soften the workpiece material and produces a smooth cutting surface finish. Similar trends of the effect of drill bit size on surface roughness were reported by N.S Mohan et al. [140] when drilling GFRPs. While Madhavan et al. [118] reported that using large helix angles can reduce the thrust force and torque when drilling composites.

Similarly for drilling aluminium, the tool geometry plays an important factor in achieving high-quality holes. For instance, a cutting tool with large helix angle- usually larger than 24°, flutes allowing quick chip evacuation [141] and large point angles improve chip removal and reduce burr formation. For most aluminium alloys the drill point angle depends on the silicon content in the workpiece. For aluminium alloys with low or no silicon content a 130°-140° point angle are recommended, while for high silicon content, the recommended point angle is between 115°-120° [128]. In addition, lip clearance angles are usually found to be between 12°-13°. The latter should be increased further to avoid drill breakage or when the alloy is soft, or if the used feed rate is high [141]. The selection of cutting speeds and feed rates depend on the mechanical properties of the workpiece, and the type of material used for the drill bit and its coating. Previous researchers used HSS and carbide cutting tools to drill aluminium and its alloys [76, 142–144], they found that both these were suitable for drilling aluminium. Carbide and coated tools outperformed the non-coated and HSS tools in terms of tool wear and hole quality [143–145].

2.7 Machining metals, composites and fibre metal laminates

Comprehensive reviews of previous research results on the machinability of FRP, aluminium alloys and multi-material stacks using conventional methods were provided in several reports [29, 69, 94, 146–150]. The reviews provide information on the cutting mechanisms, chip formation and theoretical modelling for various machining applications. However, there is a lack of research and interest on the machinability of GLARE fibre metal laminates due

to their limited applications in the past few decades. In addition, the complexity of the machining process of GLARE due to its hybrid layered structure adds more difficulty in analysing the cutting mechanisms involved during the drilling process.

2.7.1   Drilling Aluminium

Aluminium and its alloys are widely used in many applications such as automotive and transport industries. Around 30 % of all aluminium production is consumed in the transportation industry worldwide [151], while drilling accounts for about 40 % of the total material removal process in automotive industries [152]. Aluminium is also one of the key materials used in the aerospace industry. For example, the standard Boeing 747 jumbo jet contains approx. 75,000 kg of aluminium [153]. Aluminium accounts for a large share of the total material used in the modern aircraft, space rockets and satellite structures due to its light weight, corrosion resistant and good strength. Even though there was a great advance in machining metals in general and aluminium, in particular, drilling aluminium still faces a lot of challenges and there is always a need to optimise its machining process. Different machining operations such as turning, drilling milling, boring, tapping, sawing etc. can be easily performed on aluminium and its alloys. Similar to other metals and materials drilling aluminium requires specific machining conditions and parameters to be used together in order to get the best surface finish. The main advantage of aluminium and its alloys is their low density which reduces the intertie forces allowing for higher spindle speeds [154].

Drilling aluminium is usually performed with the assistance of a cutting fluid to help evacuate the formed chips and reduce the temperatures associated with the machining process. The most important mechanisms in machining aluminium alloys are: built up edge (BUE), adherent layer and diffusion on the cutting tool [146]. In comparison to other metals such as steel, aluminium alloys have good machinability due to their mechanical and physical properties which offer better cutting tool life and greater productivity. For example, the high thermal conductivity of aluminium as shown in Figure 2.15 limits the cutting temperature to a maximum of (a maximum of 600 °C compared with 1000 °C for steel and the softening of carbide tools [154]. However, this can sometimes be disadvantageous as a large amount of heat is absorbed during the machining process causing undesirable deformation in the workpiece [155] and adhesions to the tool causing the built up edge effects (BUE). The use of Al2024-T3 can be found in fuselage skin and wing sections of the aircraft [156] due to its high specific strength, stiffness and excellent corrosion resistance. Most of the previous studies on machining Al2024-T3 alloy focused on turning, orthogonal cutting and milling operations while fewer studies were reported on drilling Al2024-T3.
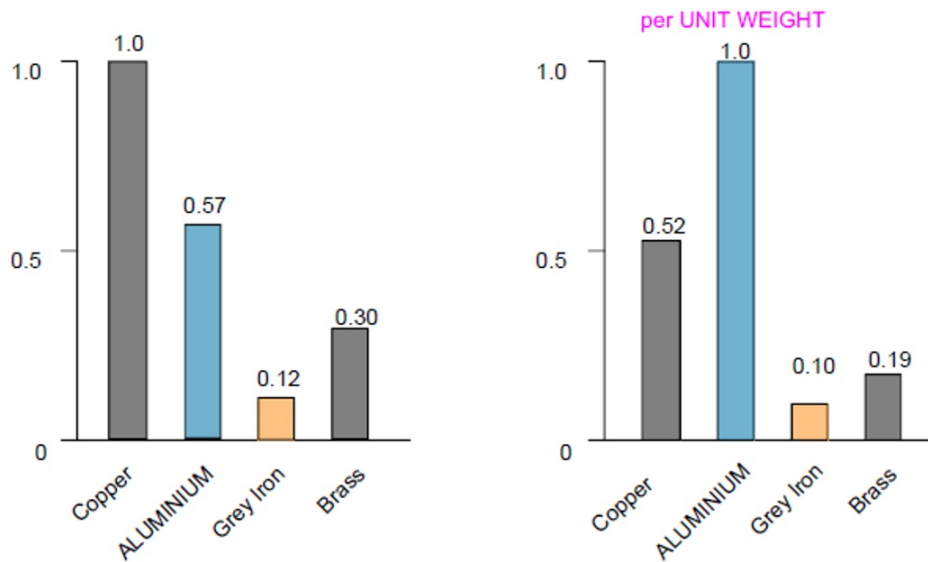
Figure 2.15: Thermal conductivity of Aluminium compared to other metals [157]

Drilling aluminium requires large helix angles and flutes to allow for quick chip evacuation, the drilling speeds and feed rates usually depends on the type of material used for the drill bit and its coating. Aluminium can be machined using HSS, carbide and diamond cutting tools but not silicon nitride based ceramics due to the high solubility of silicon in aluminium [146]. The selection of cutting speeds and feed rates depend on the mechanical properties of the workpiece, the type of material used for the drill bit and its coating. Koklu et al. [158] previously reported that the mechanical properties of drilled aluminium alloy can influence the burr height and surface roughness such that the higher the ductility of the alloy the greater is the amount of burr formed around the drilled hole. In addition, the surface roughness increases with the increase of cutting parameters and drill size [158, 159]. Most Al2024 drilling studied used a tool diameter between 5-10 mm since it is a common range for creating rivets and hole in aerospace structures.

Previous findings also showed that effect of feed rate was more dominant on cutting forces, burr formations and tool life [63, 158].In addition, HSS cutting tools were found unsuitable for drilling aluminium alloys such as Al2024-T3 especially in dry drilling process [144]. While coated carbide tools such as TiAlN coating have excellent wear and oxidation resistance and is suitable for in dry machining applications of alloyed steel and aluminium alloys with 10 % content of silicon due to its low thermal conductivity [75]. Davoudinejad et al. [160] reported that the use of high cutting speeds for drilling Al2024-T3 increased the deviation of hole size and the built-up edge (BUE) formed on the chisel edge and cutting lips, which in return increased the cutting forces. Amini et al. [161] and Barani et al. [162] reported that vibrational drilling of Al2024-T6 alloy could help reduce cutting forces by up to 70 %

compared to conventional drilling. In addition, reduce exit burr formations and increase chip breakability which reduced built edge and dimensional deviation of hole size. The recommended point angles for drilling aluminium alloys with low or no silicon content range between 130°-140°, and between 115°-120° for high silicon content aluminium alloys [128]. Nouari et al. [75] reported that the surface roughness is affected by the point and helix angles such that increasing these two parameters can minimise roughness. In addition, a larger point angle will minimise burr height [75, 163] while a larger helix angle will give minimum diameter deviation compared to the nominal hole diameter which gives good dimensional accuracy [75]. Since large amounts of chips are created during the machining of aluminium, chip morphology and its characteristics were the focus of several studies [164, 165]. These studies looked into the effect of cutting parameters, tools geometry and their coating on chip formation and morphology. Results showed that chip size and length varies with cutting parameters and tool geometry, besides the effect of coolants was considered to be an important factor in controlling chip formation and evacuation.

2.7.2 Drilling Composites and Composite-Metal stacks

Composites are widely used and their applications are consistently growing in aerospace and defence, naval and automotive industries. The global composite materials distribution by market segment in 2017 indicates that electrical and electronic components will account for 17 % of the total composite market, followed by construction, aerospace and transportation with 16 %, 15 % and 14 % respectively [166]. The annual aeroplane demand is projected to increase 35 to 40 percent over the next decade [167] and the composite market is expected to reach a value of 89.4 billion USD by 2020. Major structural components of the modern commercial aircraft such as the fuselage and wings are made of composites. For example, composites account for 9 % of the commercial Boeing 777 aircraft by weight [168], and 50 % of the modern Boeing 787 Dreamliner aircraft by weight [169] as shown in Table 2.13. Composites unique features combine high strength to weight ratio and rigidity; lighter than aluminium, stronger than steel, and with higher elasticity than titanium. Moreover, they possess excellent mechanical and thermal properties making them suitable for use in manufacturing aircraft and spacecraft structural parts such as the aircraft ailerons, race motorcycles frames and formula one race cars, they are even being increasingly used in simpler consumer goods such as bicycles, golf clubs. Therefore, there is an increasing demand to offer an optimised manufacturing and drilling techniques in order to gain defects free composite parts after the machining process. There are several factors which can influence the drilling performance of composites, this includes the machine setup and choice of cutting parameters, cutting tool material and geometry, the presence of coolants and the

mechanical properties of the fibre-matrix such as the matrix softening/cure temperature or the compressive strength, hardness and orientations of the fibres [126].

Table 2.13: Percentage mass of types of materials used in commercial aircraft structures. [169–172]

Aircraft name	Airbus 350 XWB	Airbus A 380	Boeing 747	Boeing 777	Boeing 787
Aluminium	20	61	81	70	20
Titanium	14		4	7	15
Steel	7	10	13	11	10
Composites	52	22	1	11	50
Other	7	3% GLARE	1	1	5

An increasing number of studies have been carried out on drilling composites, some of those studies looked into the effect of drilling parameters [173–176], while other studies investigated the impact of tool geometry [87, 118, 177–181] and material components [182, 183] on the integrity of machined surface and cutting forces. However, a limited number of studies have been carried out on drilling composite-metal stacks and FMLs. Some of the challenges which arise from drilling such configurations of metals and composites are the variation of the cutting behaviour of the materials due to their unique properties across the workpiece. Generally, multi-layer metallic-composite stacks are drilled in two (CFRP/Metal or Metal/CFRP) or three layers (Metal/CFRP/Metal) configurations as shown in Figure 2.16.

Limited research has been reported on the drilling of multilayer stacks, particularly those involving CFRP/Ti, and CFRP/Al. The vast majority of published work has involved coated carbide twist drills in the region of 4-10 mm diameter. They generally looked into cutting forces, tool wear, delamination and hole quality parameters such as surface roughness and chip formation. Previous studies reported that carbide drills produced better hole quality than HSS drills [67, 184, 185]. Other studies also reported that the performance of PCD outperforms carbide drills in terms of reduced hole size difference between the CFRP and metal, better tool life and smaller burrs [186, 187]. Moreover, studies reported that adhesions are more likely to occur on carbide drills than PCD drills which also could suffer from edge chipping [187]. In addition some studies showed that abrasion from the CFRP and adhesions from metals were the primary tool wear mechanisms when drilling composite metal stacks [68, 187, 188]. Generally in composite metal stacks studies, researchers agrees that delamination in CFRP is minimised due the presence of Ti and Al layers above and beneath it [65, 189].
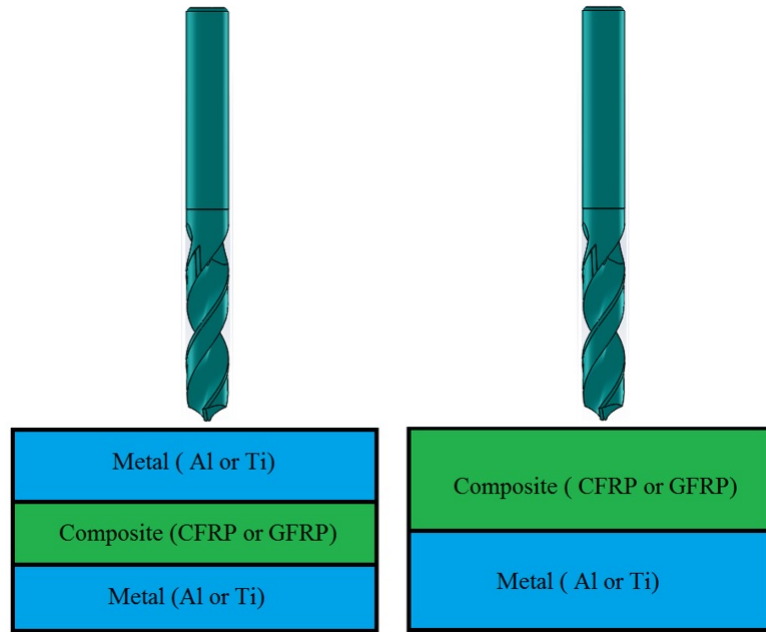
Figure 2.16: Most common stacking configurations in composite-metal stacks [190]

2.8   Machinability of GLARE

It was previously reported that good hole quality with no delamination or deformation can be achieved when choosing the proper speed/feed ratios and proper drill bits [1]. Hard metal tools are recommended when drilling GLARE on CNC machines. GLARE structures are usually produced in large panels (more than 2 metres), and machining is often required to bring those panels into the desired dimensional requirements and prepare them for assembly [1]. Machining GLARE is carried out by conventional and non-conventional material removal methods. The conventional methods most frequently used are edge milling and drilling. For example, holes are drilled into GLARE panels to join them together using mechanical fasteners while edge milling is used to give the panels the desired contour shapes for mating purposes [191]. Most machining operations on GLARE such as edge milling and drilling are performed after the components are manufactured [191]. Among the nonconventional machining processes are abrasive waterjet and laser cutting [1]. The challenges in machining GLARE arise from its hybrid structure which differs in many aspects from machining metals or composites individually. Machining GLARE can be seen as machining a material that continuously undergoes two distinctly different cutting phases. The homogenous ductile aluminium metal sheets with high thermal conductivity undergo shearing and plastic deformation followed by strain hardening and the formation of a continuous chip. The abrasive yet brittle glass fibre-epoxy prepregs and poor thermal conductivity undergo brittle fibre fracture. Also, the mismatch in the thermal expansion coefficients of metal and

composites constituents of GLARE could lead to thermal stresses which could adversely affect the machined part quality.

Despite that a signficant amount of heat is taken away by metallic chips or through the direct contact between the workpiece and the cutting tool when machining GLARE, using high cutting speeds is limited by the poor ability of glass fibre prepregs to dissipate the heat away from the cutting zone. The low thermal conductivity of the prepregs limits the tolerance of glass epoxy matrix to withstand high temperatures in high-speed machining. Adding to that the relatively low service temperature of the FM94 film adhesive (104 °C) used for bonding GLARE components together. Therefore, machining at high speeds would expose GLARE to excessive heat for a prolonged period of time which could adversely impact the quality of the machined part. Another issue to consider when drilling GLARE is the cutting tool material. The cutting tool should be capable of withstanding the abrasiveness of glass fibres and have a low tendency for chip adhesions and build up edge to improve the borehole surface quality. It was previously reported that when machining GLARE three important phenomenas should be carefully monitored and studied [1] these are:

1. Tool wear due to the abrasive nature of the glass fibres layers of the laminate: previous tests on different cutting tools materials showed that polycrystalline diamond PCD and solid cemented carbide drills with coatings are most suitable for machining GLARE. Whereas coated and uncoated high-speed steel HSS tools proved to be undesirable due to the high hardness of S2 glass fibres in comparison with most common cutting tool materials used in machining operations. The hardness of S2 glass fibres is 6.5 on mineral hardness scale Moh [192] which equals 84 HRa on a Rockwell A-hardness scale. The high hardness and abrasive nature of glass fibres in GLARE can cause rapid tool wear. Other types of fibre metal laminates such as those containing carbon fibres will also exhibit similar tool wear problems to GLARE [1]. For FMLs that contain aramid fibres, the sharpness of the cutting tool will deteriorate causing an incomplete cut and lose fibres protruding from the edges of the laminate.

2. Delamination: the delamination in GLARE was found to be related to the helix angle of the cutting tool for both drilling and milling operations. Studies on machining GLARE showed that helix angle in milling operations and feed force for drilling operations should be kept as low as possible to reduce peel and shear cutting forces and minimise delamination. In drilling, the delamination in GLARE takes place when the feed force is too high as the cutting tool is exiting the laminate, the high feed force pushes the last layers away causing them to separate from the laminate. For milling operations, a large helix angle causes the top layer to peel off the laminate leading to

delamination.

3. The heat affected zones at the edges of the laminate: the tool-workpiece interaction in milling and drilling operation raise the temperatures around the edges of the machined part. The rise in workpiece temperatures was found to increase with the increase of cutting speeds and thickness of the workpiece. The rise in workpiece temperature becomes more critical when machining thick laminates using laser jet cutting operations. The use of coolants is suggested when machining GLARE to overcome the heat issues in some machining operations such as drilling and milling.

A very limited number of studies were previously reported on the machinability of fibre metal laminates. Early literature during the development of GLARE reported that the feed rate, lubrication and laminate thickness in milling operations had a major influence on the quality of the milled edge. It was found that the tool wear and fracture increased with feed rate increase, the rise in feed rate can reduce the laminate edge quality and cause delamination [1]. The previous investigation on the cooling/lubricant influence on milling GLARE showed that using coolant is preferable over semis dry cooling especially when machining thick laminates over 6 mm or when machining at high cutting speeds and feed rates. This is due to the limited ability of the semi-dry cooling to effectively remove the heat generated during the milling process. It was concluded that semi-dry cooling is recommended for thin GLARE laminates less than 3 mm [1].

The machining of thick laminates increase the cutting forces and generated heat due to larger contact area with the cutting tool which raises the temperatures. The rise of temperatures can cause the chips and fibres to adhere on the cutting tool or protrude the laminate edges causing delamination and deformations to the material. Delamination at the upper and lower parts of the laminate is likely to occur when improper cutting parameters are used. Drilling holes in GLARE can be performed manually using a hand-held drill or automatically of up to 700 holes using stable CNC machines with good quality and no delamination or deformation [1].

The first reported study on drilling GLARE can be traced back to 1994 during the development of fibre metal laminates by Coesel [193]. The thesis was a part of the IOP-project: Manufacturing of fibre metal laminates, which investigated the factors that influence the drilling performance of GLARE. The study investigated the effect of drill type, tool material, cutting speed, feed rate and drilling machine type on hole quality in terms of its accuracy, burr height, roundness and delamination. The final quality of the machined GLARE panels was evaluated using crack initiation tests on open hole specimens and fatigue behaviour of riveted countersunk lap joints. Results from drilling GLARE indicated that solid carbide

drills had better wear resistance than HSS drills using stable drilling machines, good hole quality was achievable up to 3000 holes using the solid carbide drills. Whereas poor hole quality and delamination were observed prior drilling 150 holes.

The drilling tests were conducted under dry conditions as it was reported that cutting fluids are not required in drilling GLARE if stable drilling machines are used along with carbide and solid carbide drills. However, this could be due to the use of thin laminates (¡ 2 mm) in the study. Moreover, cutting speeds and feed rates did not show to have an influence on the hole accuracy. From the four different types used, solid carbide and HSS-TiN coated drills produced most accurate holes. The HSS-TiN drill produced holes with high roundness error. It was also found that increasing the thickness of the laminate increased thrust force and torque. The inspection for delamination from visual inspecting and C-scan techniques showed that it occurred faster when using the HSS drills, whereas for the carbide coated and solid carbide drills no delamination was observed even after drilling 3000 holes. It was also concluded that the maximum thrust force was a critical factor on delamination. Besides, the thrust peak corresponding to the bottom layer, the heat generated during the drilling process, the drill geometry and the distribution of the critical thrust force along the cutting edge all had an influence on delamination.

It was also reported that burr heights were noticeable when using HSS drills due to the rapid wear of the cutting tool and depending on the feed rate used in carbide coated drills. Additionally, solid carbide drills did not produce burrs in all holes, while thrust force and torque increased with a number of holes drilled when using HSS drills due to the increase in tool wear. It was concluded that cutting forces increased with feed rate increase and that the drill size and chisel edge had an influence on the cutting forces while drilling different layups of GLARE showed that cutting forces increased with the increase of the laminates thickness and that the increase in lay-up thickness had no influence on the hole quality. In his thesis, Coesel did not study the delamination factor due to difficulties in measuring it visually or using the C-scan method. The surface roughness of the holes was not measured due to the small thickness of the tested laminates while burr height was measured using a micrometre and it was concluded that the actual shapes of the burrs might have changed during the measurement process. Therefore, it was assumed that all burrs were crushed which means that the accuracy of the actual burr height was affected by the measurement technique used. Also, the selection of cutting speeds and feed rates were restricted because of the limitation within the CNC machine and the pre-requisites of the experiment.

A more recent study on drilling GLARE like fibre metal laminates was conducted by Tyczynski et al. [194]. Their drilling trials were carried out on fibre metal laminates samples made of Al2024 sheets with a thickness of 0.3 and 0.5 mm and the glass fibres were R-

type and prepregs which had a nominal thickness of 0.25 mm. The type of glass fibres used in the study is not the one which is used in standard GLARE grades (S2 glass fibre). Additionally, the stacking sequence of the prepreg laminates was a quasi-isotropic system made of (0/45/45/90/90/45/45/0). Also, the thickness of the prepreg layer was 0.5 mm and consisted of more than 4 prepreg layers. Their findings indicated that the cutting forces increased with the increase of feed rate and laminate thickness. Additionally, it was found that the cutting forces required for drilling GLARE were higher than those required for drilling GFRP and less than those required for drilling Al2024 alloy. The observed that poor hole quality at in the form of deteriorated edges at the exit of the hole and fibre pull out through the thickness of the workpiece when drilling at the highest feed rate. The damage in the glass fibre layers was more severe in the thicker laminates, while the hole size accuracy was not affected by feed rate. However, it was observed that the hole size in glass fibre layers was closer to the nominal size of the cutting tool than that in aluminium sheets. In addition, the internal surface quality of the drilled holes was poor and deteriorated, and burrs were formed around the hole edges and tended to increase with feed rate increase. However, no delamination was identified on the internal surfaces of drilled holes.

A very recent study on drilling GLARE was conducted by Pawar et al. [64] to understand the cutting mechanism of GLARE by analysing the cutting forces and the acoustic emission energy (AE). The study investigated the influence of cutting parameters and tool geometry on delamination, hole size and burr formation. The study compared four different types of solid carbide cutting tools including two flutes, three flute, four facet and eight facet drills as shown in Table 2.14. Their findings showed that the feed rate had the major influence on burr formation. Results also showed that the two facet drill outperformed the other cutting tools in terms of eliminating delamination and producing acceptable burr formation. The four and eight facet drills produced poor hole quality and uncut fibres around the edges of drilled holes, while delamination increased with feed rate. They also found that undersized holes were produced with exception to those drilled using the three flute drill. Burr heights were comparable and did not exceed 250 microns when drilling using the two flute, three flute and four facet drills, the eight facet drill produced large burrs which exceeded 1000 microns. The entrance burr height increased with feed rate increase while the exit burr height decreased with spindle speed increase. Similar results were found for the burr width.

Table 2.14: Summary of the previous studies on drilling of GLARE laminates.[64, 193, 194]

Material information	Cutting tools used/coolants	Cutting parameters	Areas studied	Concluding remarks	Ref.
GLARE 3-3/2-0.3 GLARE 3-2/1-0.3 GLARE3-4/3-0.3	- HSS TiN coated with 118° point angle and 5 mm diameter - HSS with 8% Co with 135° point angle and 5 mm diameter - Carbide tipped HSS with 118° point angle and 5 mm diameter - Solid carbide with 118° point angle, 5 and 5.5 mm diameter - Diamond tipped HSS with 118° point angle and 4.8 mm diameter (No coolants/dry)	Feed rates: 0.05,0.08,0.13, (mm/rev) Cutting speeds: 40,55,70,140 (m/min)	- Cutting forces - Hole accuracy - Roundness error - Visual inspection - Burr height - Crack initiation tests on riveted countersunk lap joints	- HSS drills are not suitable for use with GLARE due to excessive tool wear and poor performance - Hole quality was not influenced by laminate thickness - Solid carbide drills produce better hole quality - Hole quality influences the fatigue life of lap joints - Cutting parameters had no influence on the hole accuracy - HSS drills had a better shock load resistance in manual drilling	[193]
GLARE- like made of Al2024 sheets (0.3-0.5 mm thickness) and 0.25 mm thickness layers of polymer, fibreglass type R with a quasi-isotropic system (0/-45/-45/ 90/90/-45/-45/0)	Uncoated VHM carbide drills with 6 mm diameter and 90° point angle (%6 oil emulsion coolant was used)	Feed rates: 0.05,0.075,0.1,0.125,0.15 (mm/rev) Cutting speeds: 75.36 (m/min) (4000 rpm)	- Cutting forces - Hole size - Stress distribution - Visual inspection of drilled holes	- Axial cutting force increased with feed rate - Hole quality decreases with feed rate increase - Variation between hole size in Al2024 sheets and GFRP layers for the same hole - Delamination is affected by feed rate - The damage in GFRP layers was more severe in thicker samples	[194]
GLARE 5 3/2-0.3 GLARE 6 3/2-0.3	2,3,4 & 8 facets solid carbide drills with 120° point angle, 30° helix angle and 6.35 mm diameter (No coolants/dry)	Feed rates: 0.15,0.225,0.3 (mm/rev) Spindle speeds: 4500,6000,7500 (rpm)	- Cutting forces - Hole size - AE absolute energy variation with time - Chip formation - Delamination - Burr formation - Hole size	- Hole quality varied with cutting tool type - The 2 flute 4 facet drills produced better hole quality - Undersized holes were produced when using all cutting tools - Feed rate had the major influence on cutting forces, delamination and burr formation	[64]

2.9 Temperature measurement of the cutting tool and workpiece during the machining process

During the machining process, the heat generation occurs due to the continuous friction between the workpiece and the cutting tool. Approximately 98 % of the energy in machining is converted into heat [32]. The rise in the temperatures can adversely affect the properties of the workpiece and cutting tool materials, induce thermal damage to the workpiece causing dimensional changes, accelerate tool wear or result in chemical changes in the tool-workpiece materials reducing the quality of the machined parts [195]. Even though coolants have proven to be a powerful method for reducing machining temperatures, yet problems associated with high temperatures remains a major challenge, especially in dry and high-speed machining applications. One of the most important factors which govern the temperature build up during the machining process is the thermal conductivity of the workpiece material [130], material that has a low thermal conductivity is subject to higher increase in temperature when machined due to its inability to dissipate heat quickly. In addition, the alloy content in the material can also affect the machining temperatures, Ozek et al. [196] reported that when drilling different aluminium alloys (A5083, A6061, A7075-T651, A1050) the temperature of the workpiece can be as high as 242 °C in A5083 and 164 °C in A1050 at same cutting conditions. The heat generated when machining composites is distributed differently than when machining metals [29].

In metals, approximately 75 % of the heat is generated at the shear zone, 20 % at the chip sliding on the tool face and about 5 % is produced due to plastic deformation in the metallic workpiece [130] and between (80-85 %) of the thermal energy generated is carried away by the moving chip [197]. Indeed, the relatively high ductility of most metals compared to composites materials means that extensive plastic deformation of the chip rakes place during cutting, which increases heat generation and temperature [131]. Whereas drilling composites are limited by the softening temperature of the matrix system despite fibres having high melting temperatures, nevertheless, the temperatures generated in the machining process should not exceed the softening temperature of the matrix [126]. In addition, the lack of ductility required for plastic deformation produces very small fragments of chip coupled with a low thermal conductivity of composites, means that a large amount of the heat is dissipated by the workpiece and cutting tool.

Generally, the cutting temperature in drilling is strongly dependent on cutting speed and feed rate [29]. Fliescher et al. [198] performed an review of heat partition ratios various machining process as shown in Table 2.15, which shows that the workpiece takes a large share of the heat distribution during the drilling process, which means that the low thermal

conductivity of composites promotes for localized heat build-up in the drilling zone [126].

Table 2.15: Percentile share of heat distribution in various machining processes [47, 198].

Component	Drilling (%)	Turning (%)	Milling (%)
Tool	5-15	2.1-18	5.3-10
Workpiece	10-35	1.1-20	1.3-25
Chip	55-75	74.6-96.3	65-74.6

Measuring the machining temperatures remains a big challenge and it has been the main objective of many studies in milling and turning operations, however, there has been a limited number of research work on measuring the cutting temperatures in drilling operations due to its complexity especially in composites and FMLs. Many experimental techniques have been implemented to get an accurate reading of machining temperatures. The rise of cutting temperatures in composites can lead to matrix burnout, acceleration of fibre pull-out and can cause a reduction in the shear strength of the laminate [199]. Figure 2.17 shows a summary of some of the most common techniques used for measuring the cutting temperatures during the machining process.

2.9.1 Temperature measurements using radiation methods

Radiation methods are non-contact techniques that use thermal imaging to capture the temperatures of surfaces since all bodies and objects that possess temperatures more than the absolute zero can emit infrared radiations. Infrared cameras (IR cameras) can capture emitted forms of energy and convert them into temperatures depending on the intensity of the IR radiations. The results are then shown on the infrared capturing device in the form of different colours with each colour representing a specific value of temperature or a temperature range. The IR method has been extensively used by many researchers to study the temperatures during the machining process. However, IR methods can only capture the surface temperatures of the bodies and therefore they are suitable for milling and turning operations where the tool-workpiece interaction zone is visible at all times in contrast to drilling experiments. Nevertheless, IR methods were also used in drilling experiments using additional arrangements in the workpiece and machine setup by various researchers [200–202].
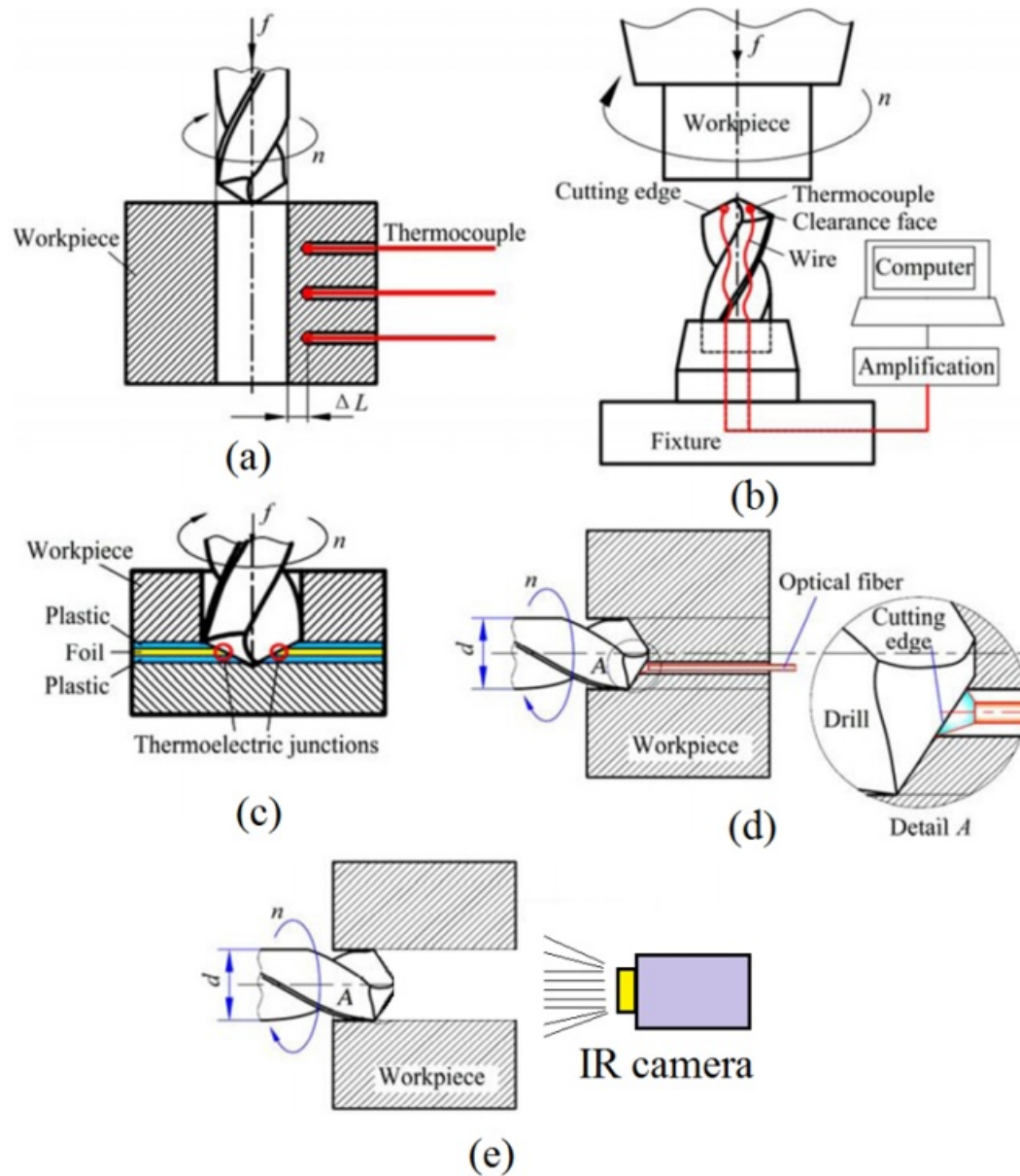
Figure 2.17: Temperature measurement methods during drilling process: (a) Thermocouple embedded in workpiece; (b) Thermocouple embedded in tool; (c) Drill-foil thermocouple system; (d) Infrared pyrometer (e) Infrared camera method [203]

2.10 Machining Coolants

As discussed earlier in the chapter, there has been little work available on the machinability of GLARE and fibre metal laminates in general. Moreover, little work has been published on the application of cutting fluids in composite machining and no reported studies on the application of cutting fluids when machining FMLs. Machining industry continuously aims to improve the machining process by reducing the production costs and by creating a safer and healthier working environment. Tackling machining costs besides health and safety regulations can be achieved by reducing the costs incurred from cutting fluids and their disposal process. According to a survey conducted by the European Automobile Industry, the cost incurred on lubricants comprises nearly 20 % of the total manufacturing cost [204, 205]. While the cost of the cutting tool is only 7.5 % of the total cost [206, 207]. The recent advancements in coolant technologies and machining operations are driven by the high costs of coolants and machining, in general, have led to alternative routes for sustainable machining. For example, using efficient cooling techniques which require small amounts of cutting fluids which do not require further treatment or dispensing at the end of their life cycle such as minimum quantity lubrication (MQL) and cryogenic cooling using liquid nitrogen (LN2) and carbon dioxide (CO2). The current chapter provides a detailed review of the cooling methods used in machining industry with a focus on minimum quantity lubrication and cryogenic cooling of metals and composites and the recent advancements in these technologies.

2.10.1 Cutting Fluids

70 % of the functional percentage of the cutting fluids is used for chip removal while 20 % and 10 % are used in cooling and lubricating respectively [208]. Cutting fluids in machining can be classified based on their composition to Oil-based cutting fluids commonly used as a lubricant between the chip, tool and the workpiece. Or water-based fluids which are usually used for cooling and heat extraction or cryogenic gases in their liquidus phase, which is mainly used for heat extraction and reduction of dimensional changes of the machined workpiece [209]. Since most of the work done in the machining process are converted to heat, reducing the heat generated due to the friction between the tool and workpiece can increase the tool life, produce better-machined surface finish and clear away the formed chips. Moreover, allowing for higher cutting speeds to be used. Flood coolant is the most commonly used cooling method in the industry [210].

The types of coolants used in machining processes were previously summarised by Yildiz et

al. [211] as shown in Figure 2.18. Generally, the characteristics of the cutting fluids mainly depend on the type of the machining process and the machined material. There are two common methods for delivering the cutting fluid in a machining process: The first method delivers the coolant externally through a nozzle targeted at the workpiece/cutting tool at the cutting zone. The second method delivers the coolant internally and is commonly used in milling and drilling operations. The method is designed to deliver the coolant more efficiently by creating holes in the cutting tool such as in drilling operations where the coolant is delivered close to the centerline of the drill bit head.
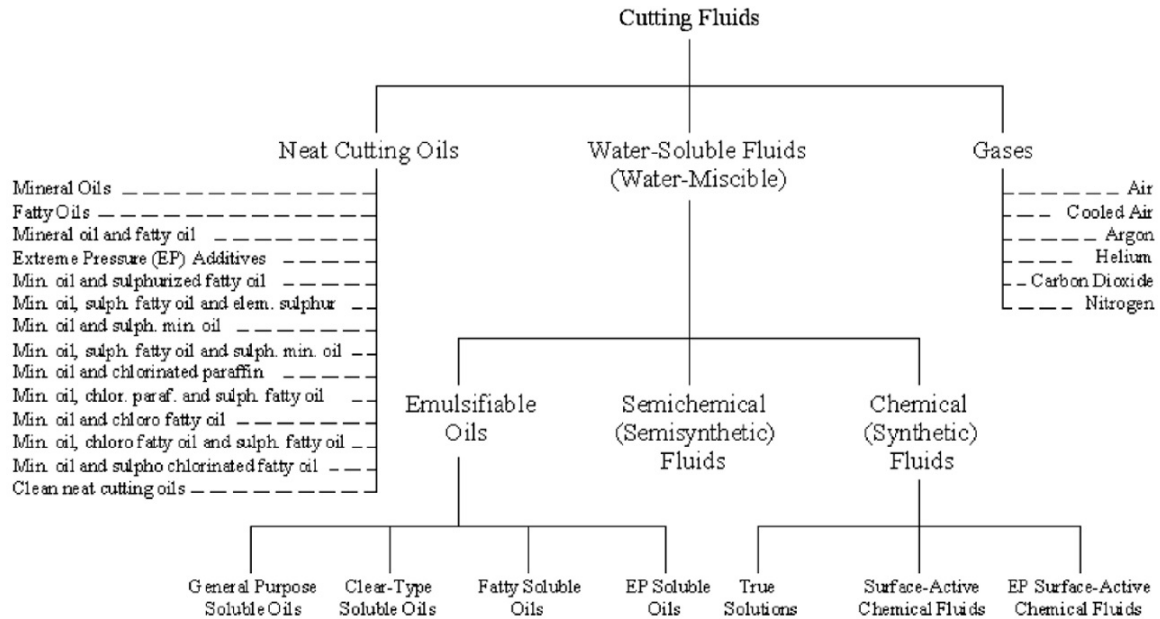
Figure 2.18: Classification of cutting fluids by Yildiz et al. [211]

The second method delivers the coolant through small holes made in the cutting tool. Cakir et al. [212] previously summarised the factors for selecting suitable cutting fluids such as the nature of the machining process and the type of workpiece cutting tool materials. Water or water soluble (mixed with oil when machining metals) coolants are rarely used when machining composites [67, 185, 213]. Unless the water can easily evaporate after the machining process causing no damages to the fibres, there is always a risk of moisture absorption, a decrease in strength properties and degradation the fibre-matrix interfacial bonding, which could compromise the long-term durability of the composite structure. Therefore, many researchers carried out their composite machining experiments without the use of any coolants [68, 80, 214–220]. the lubricants types can be classified based on the amount of lubricant used in the machining process as shown in Table 2.16.

Table 2.16: Classification of lubricant types [208].

Lubrication type	Content	Used volume
Wet machining (using coolant)	Flooding supply, full jet lubrication	10 to 100 l/min
Reduced lubrication	Minimum quantity lubrication (MQL)	50 ml/h up to 1–2 l/h
	Minimum quantity cooling lubrication (German abbrev: MMKS)	< 50 ml/h
Without lubrication	Dry machining	without

2.10.2 Dry Machining

Dry machining, from its name, implies that no coolant, cutting fluid or lubricant is used with the machining process. Thus, considerably saving large costs and keeping the process clean and environmentally friendly. Advantages of dry machining are both environmental and economical: it has no contamination risk or pollution hazards whatsoever on the environment or the operator [125, 221]. In addition, large cost savings from those usually incurred when using cutting fluids and time-money required to dispose of them. Moreover, in some cases the wastes and pieces produced from the machining process can be recycled and used again for other operations in contrast to when coolants are used as the waste material needs to undergo a special cleaning process to eliminate the coolants materials from chemical additives to small particles in order for them to be used again.

Disadvantages of dry machining are the high temperatures associated with the cutting process in the tool-workpiece cutting zone, excessive tool wear and the difficulty of chip removal especially in drilling operations, and the requirement of special cutting tools which can resist high temperature [125, 221]. Additionally, built up edge (BUE) and adhesion can form on the cutting tool and workpiece especially at high cutting speeds. Dry machining is used when the use of coolants is not suitable or recommended. Dry machining process can be enhanced by improving the cutting tool material, its coating and the method for chip removal. Sreejith et al. [155] recommended using coated cutting tools and specifically diamond coated tools when dry machining of nonferrous metals such as aluminium as they have no affinity for aluminium and their high thermal coefficient and heat diffusion. Additionally, improving the dry machining performance can be achieved by using high-pressure compressed air to help evacuate the clogged chips instead of using coolants.

2.10.3   Minimum Quantity Lubrication

Minimum quantity lubrication, near dry machining or simply MQL is one of the latest technologies for delivering precise quantities of cutting fluid to the targeted cutting region where cooling is needed. The idea is to use the least amount of cutting fluid or lubricant mixed with air, typically a flow rate of 50 to 500 mL/hour is used [222–224]. The amount of lubricant used can make a substantial difference in the cutting process by improving surface finish and tool life considerably. Advantages of MQL is that it produces drier workpiece and can provide lubrication when high-pressure of flood coolant cannot be used. It can also reduce the costs associated with the usage and waste disposal of similar cutting fluids used in high-pressure and flood coolants [208]. Moreover, it can reduce the thermal shock of the tool and the workpiece. Additionally, MQL can reduce the mist and spray generated and hence it can be used in non-enclosed machines. Disadvantages of MQL is that it cannot flush away chips and swarf from the cutting zone and limited ability to cool the machined surface [225]. The additives used in MQL can sometimes cause corrosion and slip accidents for operators if left on machined parts without removing them [225]. MQL can only reduce the heat generated from the cut chips but not the heat generated by the tool and workpiece, therefore, it is not ideal for use in a high production environment or applications which require high cutting speeds. MQL have been widely used in all machining applications; it can be supplied externally through one or several nozzles as shown in Figure 2.19.
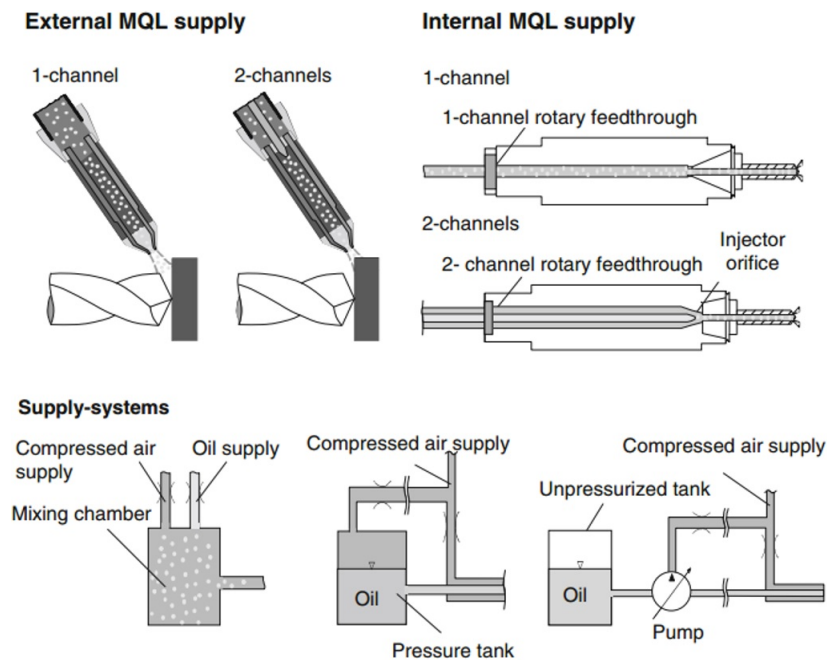
Figure 2.19: MQL supply systems designed by Klocke et al. [226]

The number of nozzles and their positions and orientation, as well as the spray pattern all, play a significant role in the machining performance [226]. The internal MQL cooling is supplied through holes created with the cutting tool such as drilling or milling processes. Indeed, the efficiency of external MQL is limited by its penetration to reach the cutting zone. The external supply of the MQL coolant is only practical up to length/diameter ratios of $l/D < 3$, for larger ratios the cooling influence becomes less effective and might require re-wetting several times which prolongs the time of the machining process [226]. MQL is compressed with air and usually sprayed from a close range from the cutting zone area. Many parameters influence the MQL efficiency such as the mist pressure and lubricant flow rate, the droplet size and nozzle distance from the cutting zone, method of supplying the MQL (internally or externally). The common fluids used are water, oil or a mixture of water and oil mixed with compressed air. The application of MQL has been used with ferrous and non-ferrous alloys such as steel, titanium and aluminium. The following section summarises some work done on the machining of ferrous alloys using MQL while the later section focuses on the near-dry machining of aluminium alloys with a focus on drilling process.

The MQL drilling of metals has been the focus study of many researchers. Most of the drilling researches were carried out using external MQL systems while few used internal ones. Milling was also investigated. The flow rate usually ranged between 5 and 250 ml/hr and air pressure between 3 and 23 bars. Generally, most of the work carried out on MQL focused on turning and grinding operations of various types of steel [223, 224, 227–233] which could be due to the better coolant penetration in those machining operations than in milling and drilling where the coolant impact could be limited when the cutting tool is engaged with the workpiece material [234, 235]. In most studies, the application of MQL in metal machining helped improve surface finish, reduce tool wear, cutting temperatures and cutting forces compared to dry and conventional cooling [223, 224, 227, 231, 233–238]. The previous studies also showed MQL improved the dimensional accuracy of the cutting process besides reductions in BUE and delay the formation of welding of chips especially at higher cutting speeds. Moreover friction and thermal distortions in the workpiece were reduced which lead to improved productivity and by allowing for higher cutting velocities and feed rates.

As discussed previously, the MQL can be supplied externally by means of nozzles attached near the cutting zone or internally by means of the tool spindle and internal cooling ducts inside the cutting tool [226], the external system is used in all machining applications while the internal MQL system was mainly developed for milling and drilling processes for better coolant impact and penetration. A drawback of external systems is that variation of the cutting tool and workpiece dimensions which require a continuous change of nozzle position

and orientation for better performance [226]. However, other studies reported that the application of MQL can be disadvantageous over flood cooling at high cutting speeds and feed rates as hole size was outside tolerance range due to the limited capacity of the MQL to remove heat from the cutting zone and the inability of MQL to minimise the adhesion of aluminium on the cutting tools [239–244]. Other studies reported that the combination of proper coating and MQL can give tool life performance which is comparable to wet machining at reduced costs [245–247].

2.11   Cryogenic Machining

Cryogenic machining is the science that studies the behaviour of machining materials at very low temperatures and the use of cryogenics in the machining process. Cryogenics are increasingly being used in machining process as a cooling agent because they can considerably reduce the high temperatures generated due to the continuous friction between the tool and the workpiece and tool-chip interface. Advantages of cryogenic machining over the conventional methods were summarized by Pusavec et al. [248] such as being cleaner, safer, environment friendly (no environmental hazards), cost saving, increase of material removal rate (higher cutting speeds), better surface finish, increase tool life, reduces friction and power consumption, increase of productivity. Liquid nitrogen is the most commonly used cryogenic coolant in the machining applications [211]. LN2 is non-flammable, environmentally friendly gas, non-toxic and does not leave any effects after being used. Moreover its low temperature of -196 °C degrees greatly reduces the cutting temperatures associated with the machining process. In most of the application, liquid nitrogen is used in its gaseous state but it is usually stored in its liquid phase in large tanks as it provides an easier and cheaper method of delivery and supply. A comparison between CO_2 and LN2 cryogenic coolants in turning Ti-6AL-4V showed that CO_2 was more effective in reducing the surface roughness, flank wear and cutting forces while LN2 proved to be more effective in reducing high temperatures associated with the machining process than CO_2 [249].

Cryogenics have been widely used as a method of the material treatment or cooling aid in different machining applications and on with many types of materials including metals and composites. Cryogenic treatment is one of the first methods used in, especially in the manufacturing, automotive and aerospace industries, where high material properties such as hardness and strength in some parts are desired in order to improve their performance and longer service life, or when more coherent structure is desired to improve its thermal and electrical conductivity. For example, having stronger engine parts such as gears and crankshafts to enhance their strength and durability, better knife blades toughness and

abrasion resistance for cutting operations, cryogenic treatment is usually performed in three stages: the slow cooling stage, soaking stage and a tempering warming stage [250]. These stages can be varied depending on the desired material properties after the treatment, time and cost, the process involves submerging the part to be treated in a bath of liquid nitrogen for a period of time. The material properties change when subjected to low temperatures leading to changes in its microstructure. For example, when ferrous metals are cryogenically treated, better thermal properties and lower surface friction are achieved which gives better surface finish after machining them. However, high costs are associated with the process which can be avoided by cooling the sample as fast as possible to the treatment temperature to reduce costs associated with time. However, the risk of thermal shocks due to the low temperatures is apparent and might damage the treated material, hence, this method is preferred when a temperature control is possible to avoid damaging the treated sample, a detailed review of the steps of cryogenic treatment process of cutting tools and its benefit on various cutting tools types were previously summarized by Gill et al. [251].

2.11.1 Cryogenic machining strategies

Cryogenic cooling methods applied in machining operations can be classified into four different groups according to Yildiz and Nalbant [211, 250] as shown in Figure 2.20:
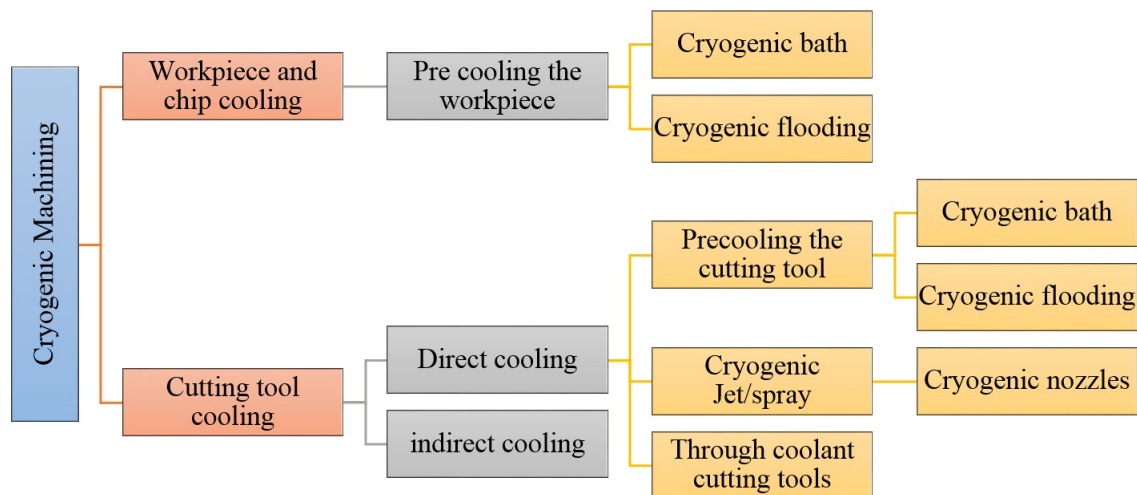
Figure 2.20: Cryogenic machining strategies

Cryogenic pre-cooling of the workpiece

The cryogenic pre-cooling is performed by either submerging the workpiece in a liquid nitrogen bath or by continuously subjecting it to a flow of liquid nitrogen to transform the material from ductile phase to brittle phase. The first implementation of this method goes back to the work of Wiggins et al [252] who used cryogenic liquid nitrogen in the drilling process of bone. Limited work was found on composites, Bhattacharyya et al. [253, 254] applied liquid nitrogen during the machining process of Kevlar composites and found that it helped to improve the surface finish. This method has been mostly applied to different grades and types of steel [255–261] since it proved to be useful in controlling chip breakability in turning operations by bringing the chip to embrittlement temperatures as well as increasing the upper limit of used cutting parameter [262–264]. The method was recently applied to aluminium alloy 6061 by precooling it to temperatures of -50 °C prior turning operations in the work of Murugappan et al. [265]. Their results showed improvements in surface roughness surface roughness over dry machining trials and better performance of the cooled workpiece at higher cutting parameters. However, this method has many disadvantages and cannot be useful in industrial applications as a large amounts of liquid nitrogen are required. Some of the problems reported in machining application when using this method changed in the dimensional accuracy of the workpiece increased cutting forces and high costs associated with liquid nitrogen purchase and storage [211, 265].

Indirect cryogenic cooling

Indirect cryogenic cooling also known as conductive remote cooling or cryogenic tool back cooling, is a method used to overcome the problems associated with pre-cooling the workpiece [211]. In this method, the aim is to remove the generated heat and high temperatures in the tool and the workpiece by heat conduction from an LN2 or CO2 chamber located at the tool face or the tool holder [250] as shown in Figure 2.21. The cryogenic coolant is supplied on the back of the cutting tool or over the rake face or by circulating the cryogenic coolants internally in the cutting tool body in order to extract heat from the cutting tool during the machining process. This method was mainly used in turning operations of steel and titanium alloys. The indirect cryogenic cooling method depends mainly on the thermal conductivity of the cutting tool material and the surface area of the cutting tool which the cryogenic coolant will be in contact with.

The indirect cryogenic cooling method is useful in reducing tool wear and preventing it from plastic deformation, thus maintaining its sharpness [267–272]. The method was also
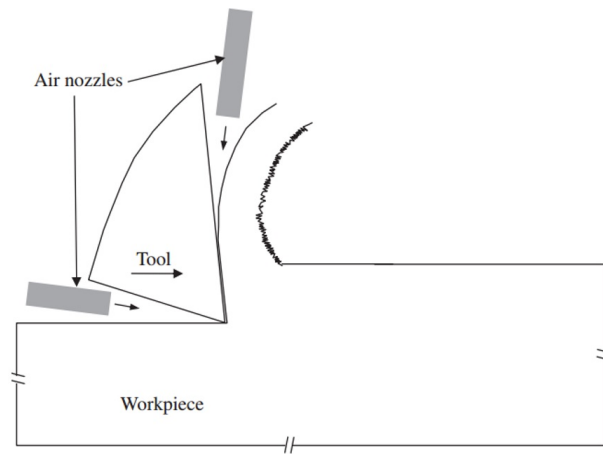
Figure 2.21: Concept layout design of indirect cryogenic cooling in machining [266]

reported to reduce cutting temperatures [266–273]. This method also helped maintain the workpiece ductility and avoid the increase in its hardness and brittleness [273]. Other studies reported that using indirect cooling improved the friction effect between the chip and the cutting tool which altered the shape of formed chip from irregular to regular shapes [266]. This method is highly dependent on the thermal conductivities of the workpiece and cutting tool, it could be further improved by increasing the cutting tool contact area with cryogenic coolant [211].

Cryogenic spraying and jet cooling

This is the most commonly used cryogenic cooling method which mainly aims to reduce the temperatures in the cutting zone and chip-tool interface [211]. The method involves directly cooling the cutting zone area by either flooding the cryogen in a similar way to conventional emulsion cooling or spraying the cryogen through nozzles to the desired regions as shown in Figure 2.22. The cryogen flooding method consumes large amounts of coolant which add high costs and can lead to cooling undesired areas or pre-cooling the workpiece [211, 274]. In such application, the direct coolant contact with the workpiece cools unwanted areas which could lead to an increase in the cutting forces. The method was mainly applied in turning, milling and to a less extent drilling operations due to the limited impact of the coolant once the cutting tools enter the workpiece. Most work was on machining steel, titanium alloys, aluminium alloys and magnesium alloys and more recently composites [275]. First, attempts for using this method was carried out by Paul et al. [276–279] in grinding steel operation by using a jet of LN2 directed by a nozzle at the grinding zone from a fixed distance. The reported that the cutting forces and residual stresses were reduced due to

better chip formation modes over dry and flood coolant conditions. Even though this method showed considerable tool life improvement, the continuous cooling of the major and minor flanks could result in premature failure due to overcooling the workpiece [264].The use of jet or spray nozzles at the cutting interaction zone have been used in conventional cooling methods and have been also extended to be used in cryogenic machining [249, 270, 280–282]. .Benefit of this method lays in its ability to remove the formulated chips and to have better penetration into the tool-chip interface zone which improves the heat removal and eliminates the BUE effect on the cutting tool and increases tool life. It is also more economical as it consumes very small amounts of coolants due to the use of nozzles in comparison to flood cooling method which considerably saves costs.
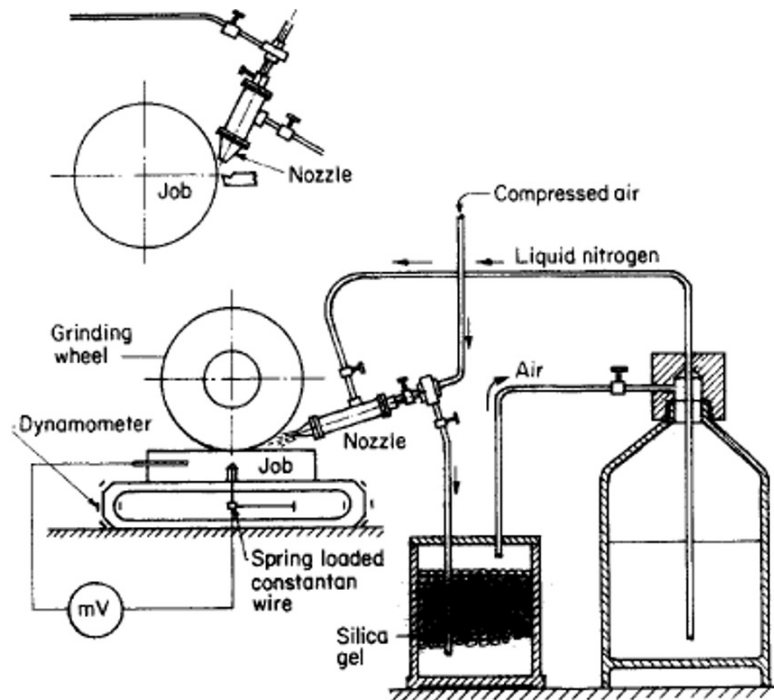
Figure 2.22: Schematic view of liquid nitrogen machining setup by Chattopadhyay et al. [283]

Cryogenic treatment

Cryogenic treatment is a heat treatment method which implies cooling down the material to cryogenic temperatures for a long period of time followed by heating to improve the wear resistance and dimensional stability [211] as shown in Figure 2.23. The method is mainly used for cryogenically treating the cutting tools prior the machining process and to increase its hardness. The method have been widely used in drilling, turningand milling operation. The cryogenic treatment of HSS cutting tools resulted in longer tool life when

drilling different types of steel [256, 284]. Kim and Ramulu [285] reported that cryogenically treated carbide drills with low cobalt percentage drill bits gave better hole quality than untreated ones when drilling thermoplastic composites.
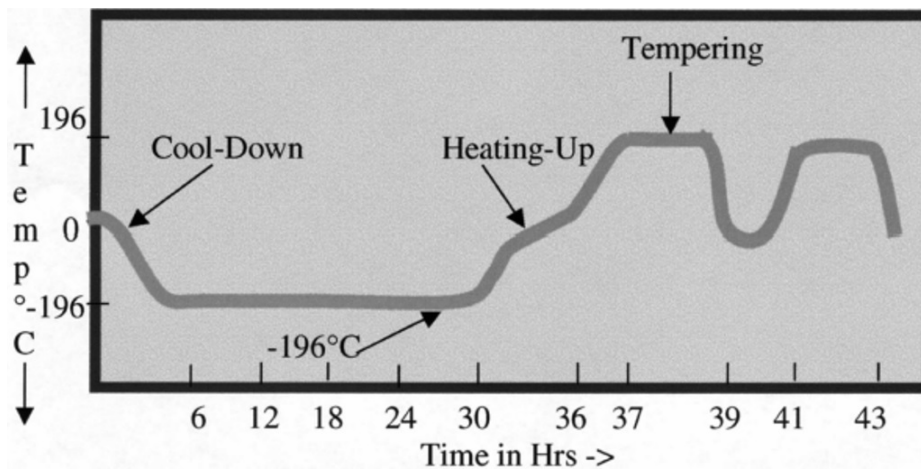
Figure 2.23: Typical cryogenic treatment for tool steels

However, the cryogenically treated bits wore faster and showed signs of pitting (indentations on the surface) and, therefore, the treatment was deemed unbeneficial. In another study by Stewart [286] on machining medium density fibre board showed that cryogenically treating carbide tools with cobalt binds reduced tool wear due to the increased corrosion and oxidation resistance. Barnes et al. [287] found that drilling CFRP with precooled drill bits increased the cutting forces compared to dry drilling and did not show any significant reduction in tool wear but using them helped reduce delamination. In another study by He et al. [259] on turning titanium alloys showed that using cryogenically treated carbide inserts reduce cutting forces, cutting temperatures, better surface finish and wear resistance compared to untreated ones especially at higher cutting speeds. Kivak et al. [288] also reported that the cryogenic treatment of reduces the size of the carbide particles increased their concertation and uniformly distributed them on the cutting tool which improved its wear resistance when machining titanium alloys. Moreover, the treatment increased the hardness of the drill bit due to the transformation of the retained austenite to martensite [256]. Some studies reported that drilling different styles of steel using cryogenically treated cutting tools reduced surface roughness, cutting forces and tool wear compared to non-treated drill bits due to microstructural alterations which increased bonding strength and deformation resistance [260, 289]. The drawback in this method lays in its instability for all machining applications and cutting conditions [211].

2.11.2   Cryogenic Machining of Composite Materials

Even though many researchers have previously investigated the effect of cryogenics in machining, most of the work done were on turning operations of metals such as steel and titanium. Little work was done on cryogenic machining of composites and more specifically cryogenic drilling of composites. This area needs to be thoroughly investigated to provide a better understanding and accurate information for the industry about its effectiveness and best approach. The following are summaries of some of the research studies and findings on cryogenic machining of composites Natural material or biological tissues such as bones and wood are considered as natural composite materials similar to the artificial composites made by humans, drilling bone have been major research in medical sciences for a long time, the importance of understanding the mechanism to drill the bone during a surgery is important to avoid the risk of fracture and temperature rise which can cause burn marks and damage to the bone [290].

Wigging et al. [252] found that lowering the temperature of bone during machining can lead to reduction in cutting energy when using liquid nitrogen. Bhattacharyya et al. [254] used ambient and cryogenic liquid nitrogen coolants in their study of drilling Kevlar composites (KA-060/ADR 240) found that in comparison with drilling at ambient temperatures, using cryogenic coolants produced better surface roughness and less hole dimensional error regardless of the drill geometry and type. Moreover, tool life increased while thrust force increased when using cryogenic cooling leading to higher delamination, especially when drilling without a backup plate. Other studies reported that using croygenically cutting tools can improve tool life during drilling of medium density fibreboard [286, 287, 291] Some studies reported an increase in cutting forces using cryogenic coolants especially when usign liquid nitrogen due to the increase in hardness of the machiend material [287]. However other studies reported a reduction in cutting forces as the cryogenic coolant acted as a lubricant at the cutting zone [286, 292].

2.11.3   Comparison studies of MQL and Cryogenic machining

Despite having numerous studies reported on the effect of using MQL and cryogenic cooling methods in machining applications. Nevertheless, there were smaller numbers of studies which compared these two cooling methods against dry and other conventional cooling applications in the same study. Previous comparison studies on dry drilling metals and composites showed that tool wear can be reduced by up 50 %, while chip contact length and thickness decreased by 20 % using MQL and cryogenic cooling over dry conditions,

especially at high cutting speeds due to proper cooling and (lubrication in MQL) [293]. The studies also agree that using MQL and cryogenic coolants can reduce the machining temperatures [294, 295]. The use of cryogenic coolants had contradicting reported results, some studies reported an increase in surface roughness considerably due to the increased workpiece hardness, cutting forces and the limited lubrication effect by the cryogenic coolant [293, 295]. However, other studies reported that the cryogenic cooling outperformed MQL in reducing tool wear and surface roughness considerably when supplied in short periods of no more than 4 minutes, as it prevented fractures, adhesions and chipping in the cutting tool which was present under MQL and dry conditions [294, 296, 297]. This could be due to the different reaction of metals to cryogenic cooling or the duration and delivery method of cryogen to the cutting zone.

2.12 Summary

- In this chapter, a brief review of the history of FMLs and GLARE have been presented. The overview briefly describes the manufacturing process of GLARE. The chapter also summarises types and characteristics of GLARE and aluminium alloys and the possible application for GLARE in the aerospace industry. The state of the art of cutting mechanisms, chip formations, and factors affecting the machinability of metals and composites and full literature of the drilling of GLARE fibre metal laminates has been presented.

- As evident from the literature, when fibre metal laminates such as GLARE are subjected to drilling operations, the defects that are likely to appear resembles those which occur in composite metallic stack structures, making the evaluation of hole quality even more complicated.

- Machining operations in GLARE can be carried out in conventional twist drilling process normally used for making holes into metallic or composite parts. However, it is necessary to take into account the need to modify the process parameters and cutting tool geometry/coatings based on its constituents.

- Although the development of FMLs has been mainly associated with aerospace applications. However, their use is still limited by the assembly difficulties and high associated costs during machining and joining operations.

- Machining operations of GLARE, such as drilling and milling can cause damage to its metal and composite constituents in the form of poor burr formations, poor surface finish, drilling-induced damage forms in composite layers, inadequate hole size, cracks

and thermal damage in the heat affected zones. In addition, the abrasive nature of glass fibres in GLARE rapidly increases tool wear which also influence the final hole quality.

- Contrary to composites, or composite metal stacks, some of the defects in GLARE laminates cannot be detected visually since metallic sheets and composite layers are permanently bonded together, and therefore, care is taken when machining those parts as they will be installed in critical locations which govern the safety and integrity of the aircraft. This has caused a barrier to the widespread of fibre metal laminates usage in other applications of aerospace structures.

- Producing high quality of holes in aerospace structures with minimum damage is a challenging aspect in the machining industry. However, despite having a decent amount of research on the machinability of metals, composites and composite metal stacks, the amount of machinability research reported in the open literature on fibre metal laminates is very limited.

- Despite dominating the coolant sector for machining applications, the use of conventional cooling methods is being slowly replaced by a more productive, economically and environmentally friendly coolants such as MQL and cryogenic cooling (LN2 and CO2).

- There has been extensive work on the performance of coolants on the machinability of various metals such as steel, aluminium and titanium alloys and to a very less extent on their effect on the machinability of CFRPs. However, the research on minimum quantity lubrication and cryogenic machining of fibre metal laminates is not reported at all.

- As evident from the literature, MQL and cryogenic machining showed a significant contribution to improving the quality of machined parts in metals and composite structures, especially in reducing the tool wear compared to dry or providing similar results to those obtained from conventional cooling, due to their ability in reducing the machining temperatures and friction between the cutting tool and the workpiece.

- The reported literature on the machinability of GLARE fibre metal laminates is very limited to several studies conducted in the past few years, and during the development of FMLs back in the 1990s. The focus of previous studies was only on the machinability of thin GLARE laminate of thicknesses up to 2 mm due to high material costs, limited availability and limited industrial applications.

- The cutting parameters used were in the range of 4000 rpm and 7500 rpm due to restrictions in the cutting range of the used CNC machines. The impact of coolants

such as MQL and cryogenic cooling on the drilling of GLARE fibre metal laminates was not previously reported in open literature due to the small thickness of tested laminates and limited cutting parameters investigated by previous researchers.

- Although previous studies carried out substantial effort in analysing the machined hole quality in GLARE laminates through the evaluation of hole size, burr formation and cutting forces, the analysis of the borehole surface roughness was not previously addressed due to the hybrid nature of the laminate. Moreover, the inspection of borehole surface for drilling induced damage through the applications of advanced scanning techniques was not previously carried out. Also, in all of the reported literature on GLARE machining, the implementation of design of experiments statistical techniques in drilling trials was not reported.

- The current research aims to fill the gaps in GLARE machinability by conducting conventional dry drilling tests on two grades of GLARE laminates and thicknesses up to 7.15 mm to evaluate the impact of fibre orientation and workpeice thickness on cutting forces and a number of hole quality parameters using design of experiment strategies, some of which have not been previously addressed in open literature. The current research will also fill the gap on the impact of using cryogenic and MQL coolants on the machinability of GLARE laminates as green machining is becoming widely used in various aerospace and automotive applications.

Chapter 3

EXPERIMENTAL SETUP AND PROCEDURES

This chapter provides a detailed description of the experimental work carried out, the setup of the machining process and the equipment used for measuring the characteristics of hole quality, to evaluate the drilling performance under different machining conditions. The chapter also describes the undertaken measurement techniques, data collection and analysis to evaluate the performance of machining coolants.

3.1 Introduction

The current research involved two experimental phases. The first experimental phase investigates the drilling of Al2024-T3 aluminium alloy, GLARE 2B and GLARE 3 laminates under dry conditions. The aim is to evaluate the impact of cutting parameters such as spindle speed, feed rate, fibre orientation and workpiece thickness (for GLARE only) on cutting forces and hole quality. The second experimental phase investigated the drilling of GLARE 2B 11/10-0.4 under two different cooling technologies: a) Cryogenic cooling using direct liquid nitrogen and b) Minimum quantity lubrication. The aim is to evaluate the influence of using those coolants on cutting forces and hole quality and to compare them with results from dry drilling condition from the previous phase. In each phase the following data was collected and analysed:

- Cutting forces (thrust force and torque).

- Average surface roughness (Ra).

- Burr formations (Burr height and burr root thickness at entry and exit sides).

- Hole size (at top and bottom locations).

- Circularity error (at top and bottom locations).

- Surface Integrity for part of the hole periphery.

- Delamination (surface delamination and damage in glass fibre layers)

- The heat affected zone around the hole edge at the exit side of drilled holes.

The following sections detail a comprehensive description of the methods and procedures which were taken to measure and analyse the collected data for each phase:

- Selection of cutting parameters.

- Machine tool details and setup.

- Cutting tool details.

- Machining coolants details and setup.

- Cutting forces measurements setup and data collection.

- Delamination inspection setup and analysis technique.

- Measurement of surface roughness.

- Measurement of burr formations.

- Setup and measurement of hole size and circularity error.

- Borehole surface inspection using scanning electron microscopy (SEM).

- Three-dimensional surface inspection using Contour GT.

- Temperature measurements of the cutting tool and hole edge at the exit side.

- The design of experiments (DOE).

3.2 Selection of Cutting Parameters

The selection of cutting parameters such as spindle speed, feed rate, and coolant flow rate and air pressure -in the case of MQL- is a significant factor for improving the cutting performance and surface integrity of machined holes. The choice of cutting parameters in this research was based on previously used cutting parameters when drilling GLARE,

aluminium and GFRP composites. As shown previously in the literature, there were limited studies available on drilling GLARE. Generally, the range of the feed rates used was between 0.05 to 0.3 mm/rev, while cutting speed used ranged between 70-140 m/min. Accordingly, the used spindle speeds -depending on the size of the cutting tool- ranged between 4000 to 7500 rpm [1, 64, 68, 193, 194]. The equations from 3.1 to 3.4 relates the cutting speed, feed rate and spindle speed to each other in a drilling process.

$$Cutting\ speed\ (V_c) = \frac{\pi.D.n}{1000}(m/min) \tag{3.1}$$

$$Spindle\ speed\ (n) = \frac{1000.V_c}{\pi.D}(rev/min) \tag{3.2}$$

$$Feed\ speed\ (V_f) = f.n\ \ (mm/min) \tag{3.3}$$

$$Feed\ per\ revolution = \frac{V_f}{n}(mm/rev) \tag{3.4}$$

Where:

- V_c = Cutting speed (m/min).
- n = Spindle speed (rev/min).
- V_f = Feed speed (mm/min).
- D = Drill diameter (mm).
- f = Feed per rev (mm/rev).

The cutting parameters were set as four levels of spindle speed (1000, 3000, 6000 and 9000 rpm), and four levels of feed rate (100, 300, 600, and 900 mm/min). Additionally, for MQL trials, three levels of flow rate (20, 40 and 60 mL/hr) and three levels of air pressure (1, 2 and 3 bars) were used. The levels values were based on previous studies on drilling aluminium alloys which used flow rates ranging from 10 mL/hr to 100 mL/hr and in some cases up to 250 mL/hr coupled with air pressures of up to 10 bars [143, 239, 241, 243, 246, 298–301], and according to the limitations in the CNC and MQL machines used in the studies. Moreover, the parameters satisfy full factorial and fractional factorial design requirements which were necessary to perform statistical analysis on the collected data, as explained later.

3.3   Experimental Design Arrays

Initially, a screening design was adopted to narrow down the number of variables which will be considered for analysis. Due to the limitation of GLARE laminates and high machining

costs, the current research verified two factors, the spindle speed and the feed rate, which were considered important for the drilling study. In addition, coolant flow rate and air pressure were considered for MQL trials. It is usually recommended to use full factorial or fractional factorial designs when screening in a study especially when the number of factors involved ranges between 2 to 4 as shown in Table 3.1. Additional details on design of experiments and analsysis is provided in Appendix A.

The full factorial design was chosen to study the response of the cutting parameters in dry and cryogenic drilling trials while the fractional factorial design was chosen for MQL trials to further reduce a large number of runs required in this method. Factorial designs are helpful in determining the effects of two or more variables and their linear interactions on a response, therefore simplifying the process. However, they do not have the ability to determine the contribution of higher order interactions or quadratic terms of each factor.

Table 3.1: Design Selection Guideline [302]

Number of Factors	Comparative Objective	Screening Objective	Response Surface Objective
1	1-factor completely randomised design	-	-
2-4	Randomized block design	Full or fractional factorial	Central composite or Box-Behnken
5 or more	Randomized block design	Fractional factorial or Plackett-Burman	Screen first to reduce the number of factors

The next step was to implement the response surface design to model the response of the output in terms of its inputs. Usually, when applying DOE to machining trials, blocking is desirable since it does not require the randomization of the trial order or sequence (randomization is useful to eliminate uncontrollable variables). In order to make the DOE results more robust, each of the experiments was repeated twice to determine the accuracy of the collected data, in the dry drilling of GLARE 2B 11/10, up to 5 repetitions were considered to check whether using two different CNC machines for this experiment had any effect on the outputs. The central composite design (CCD) also known as Box-Wilson central composite design was used in two forms shown in Figure 3.1. The CCD contains an embedded factorial design with centre points which allow for the estimation of curvature in a model. The circumscribed central composite CCC was used for dry drilling of GLARE 2B 11/10 while face centred composite design FCC was used for MQL drilling trials. The later design is recommended when it is not possible to extend the axial out to the maximum and minimum values of the chosen analysed factors. Therefore, it was used for MQL trials due to limitations in the controllable levels of air pressure and coolant flow rate from the portable MQL and the CNC milling machines. The cryogenic drilling trials were not further analysed

using RSM due to limited funding and material for this research.
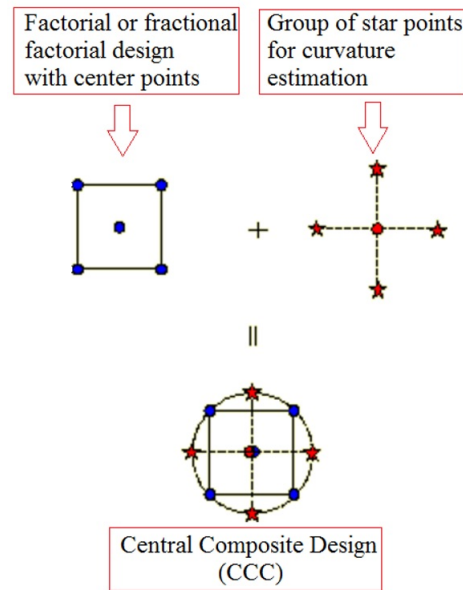
Figure 3.1: Generation of a Central Composite Design for Two Factors [302]

The analysed outputs can be correlated to the cutting parameters using non-linear regression analysis available in RSM. When using multiple regression analysis, the R2 (the regression coefficient) is obtained and is valid if $R^2 > 0.85$ for the models, a value above 0.85 indicates that the fit of the experimental data is satisfactory and that the equations obtained can be used to obtain values of the variables within the tested range of cutting speeds and feed rates (factors). Finally, confirmation tests are carried out by comparing the results of the new parameters obtained experimentally and those obtained from the mathematical equation from the regression analysis. ANOVA statistical tool is used to evaluate the significance and contribution of studied parameters on the outputs of both stages. The analysis of variance (ANOVA) will be used to determine the relative significance of the machining controllable parameters (spindle speed and feed rate), on hole quality parameters, thrust force and torque. The percentage of contribution P calculated in the ANOVA gives an indication of how much each controllable parameter influences the output parameters. The following sections describe the experimental procedure and tests used in the dry, cryogenic and MQL drilling trials. Minitab software version 17 was used to perform statistical analysis and produce ANOVA data.

3.4 Dry Drilling Trials

The dry drilling experiments combined four spindle speeds and four feed rates which represent a general full factorial design ($4^2 = 16$). In order to confirm the repeatability of the experiment, the tests were repeated two additional times and reported results are the average readings. Each set of 16 holes was drilled with a new tool to avoid any effects that might arise from the tool wear. Some of the drilling trials of GLARE 2B 11/10-0.4 were carried out on a MORI SEKI SV-500 instead of MORI SEKI NV-5000 CNC milling machines, two additional sets of the hole were drilled to eliminate the effect of using a different machine on the output results, and the variation among measurements was found to be negligible. Therefore, the average of the results was taken from a total of five sets from both machines. Table 3.2 summarises the cutting parameters used in the experiment. Several holes were drilled at very high feed rates and very low spindle speeds (1000 rpm with 600 and 900 mm/min), their results were reported in here for comparison only, these holes were drilled for the purpose of evaluating delamination and for high productivity reasons.

Table 3.2: Spindle speeds and feed rates used in the full factorial dry drilling trials.

	Level 1	Level 2	Level 3	Level 4
Spindle speed (rpm)	1000	3000	6000	9000
Feed rate (mm/min)	100	300	600	900

The next step implements the application of response surface methodology (RSM) and central composite design (CCD) to analyse the influences of dominant cutting parameters on investigated hole quality parameters when drilling GLARE. The RSM analysis was carried out on GLARE 2B 11/10 laminates only due to the limited available material and high costs associated with machining operations. The drilling trials are carried out using same plates and cutting tools from GLARE 2B 11/10 drilling trials. The design of experiment aims to further analyse the influence of the spindle speed and feed rate based on a two-factor three-level full central composite design (CCD) as shown in Table 3.3. The multiple regression analysis using response surface methodology is employed to develop mathematical models which relate input parameters (i.e. spindle speed and feed rate) to the response parameters (i.e. thrust force, torque, surface roughness ...etc.). The mathematical models are tested for their accuracy of predicting the responses and are compared with the experimental data from two additional drilling tests. The main effects and their interactions, in addition to quadratic terms of the input variables, are tested to evaluate their contribution to the predicted responses using analysis of variance (ANOVA).

Table 3.3: Central composite design levels of spindle speeds and feed rate for GLARE 2B 11/10 drilling trials

Limits				
Process variables	Notation	-1	0	+1
Spindle speed (rpm)	n	3000	6000	9000
Feed rate (mm/min)	f	300	600	900

The RSM model is designed using a blocked matrix consisting of 2 blocks, 6 centre points, 3 axial points and 3 cube points and default value of alpha of 1.414 making the total 14 runs each with coded and actual independent process variables as shown in Table 3.4. The adequacy of the developed models were tested at 95 % confidence level using ANOVA. The number of replicates was set to 3 and the measured responses were analysed using MINITAB 16 statistical software.

Table 3.4: Central composite design array for GLARE 2B 11/10 drilling trials

Exp. No	Run order	Pt type	blocks	Spindle speed (rpm)	Feed rate (mm/min)
1	1	1	1	3000	300
2	2	1	1	9000	300
3	3	1	1	3000	900
4	4	1	1	9000	900
5	5	0	1	6000	600
6	6	0	1	6000	600
7	7	0	1	6000	600
8	8	-1	2	1757	600
9	9	-1	2	10242	600
10	10	-1	2	6000	175
11	11	-1	2	6000	1024
12	12	0	2	6000	600
13	13	0	2	6000	600
14	14	0	2	6000	600

The adequacy of the developed models were tested at 95 % confidence interval using ANOVA. The final quadratic regression models of the responses -in coded input factors forms- are determined using MINITAB 16 software. The developed models were validated by carrying out additional confirmation experiments. The confirmation experiments were carried out at n= 9000 rpm and f= 450 mm/min, and 4500 rpm and 600 mm/min. Each of the confirmation experiments was repeated twice and the average value of the three tests was

used for comparison with values obtained from predicted models.

3.5 MQL Drilling Trials

Three spindle speeds and three feed rates were used MQL drilling experiments. The tests were repeated two additional times to confirm the repeatability of the results observed and all measurements were reported as mean values of the average readings obtained from the three tests. Two levels of air pressures and two flow rates were used for the analysis in addition to two spindle speeds and two feed rates with one centre point as shown in Table 3.5.

Table 3.5: Fractional factorial MQL machining parameters and their levels

Machining parameters	Low	Centre point	High
Feed rate (f) (mm/min)	300	600	900
Spindle speed (n) (rpm)	3000	6000	9000
Flow rate (ml/hr)	20	40	60
Air pressure (Bar)	1	2	3

Although preliminary trials using MQL coolant showed that the level of air pressure and the coolant flow rate had a minor influence on cutting forces, their levels affected the surface roughness; therefore, these coolant parameters were investigated further and were included in the RSM statistical model. Face centred central composite design was used to further analyse the MQL trials. The total number of runs was 31 with seven total centre points as shown in Table 3.6. The fractional factorial MQL model is capable of detecting the significance of each factor (i.e. spindle speed, feed rate, coolant flow rate and air pressure), and their interaction effects on desired outputs (i.e. thrust force, torque and surface roughness). Similar to dry drilling trials, the RSM model is used to further analyse the impact of the four controllable factors on the response outputs to detect the impact of higher order interactions such as quadratic terms.

The RSM model is designed using a blocked matrix consisting of one block, 7 centre points, and no axial or cube points. The face centred composite design alpha value = ±1 was chosen since it requires three levels of each factor making the total number of runs equal to 31, each with coded and actual independent process variables as shown in Table 3.6. The adequacy of the developed models were tested at 95 % confidence level using ANOVA. The number of replicates was set to 3 and the measured responses were analysed using MINITAB 16 statistical software. Some of the runs in the model were taken from the previous factorial design to reduce the required number of trials.

Table 3.6: Central composite design for MQL trials

Run	Spindle speed (rpm)	Feed rate (mm/min)	Flow rate (ml/hr)	Air pressure (bar)
1	3000	300	20	1
2	9000	300	20	1
3	3000	900	20	1
4	9000	900	20	1
5	3000	300	60	1
6	9000	300	60	1
7	3000	900	60	1
8	9000	900	60	1
9	3000	300	20	3
10	9000	300	20	3
11	3000	900	20	3
12	9000	900	20	3
13	3000	300	60	3
14	9000	300	60	3
15	3000	900	60	3
16	9000	900	60	3
17	3000	600	40	2
18	9000	600	40	2
19	6000	300	40	2
20	6000	900	40	2
21	6000	600	20	2
22	6000	600	60	2
23	6000	600	40	1
24	6000	600	40	3
25	6000	600	40	2
26	6000	600	40	2
27	6000	600	40	2
28	6000	600	40	2
29	6000	600	40	2
30	6000	600	40	2
31	6000	600	40	2

The final quadratic regression models of the responses in coded input factors forms are determined using MINITAB 16 software. The results were statistically validated using regression models, ANOVA and were also validated by conducting confirmation experiments. The confirmation experiments are carried out at (9000 rpm, 300 mm/min, 60 mL/hr and 1 bar) and (6000 rpm, 300 mm/min, 20 mL/hr and 1 bar). Each of the confirmation experiments was repeated twice and the average value of the three tests was used for comparison with values obtained from predicted models.

3.6 Cryogenic Drilling Trials

The cryogenic drilling trials were carried out using a three-level full factorial design with a total of nine runs and two additional centre points as shown in Table 3.7. The full factorial model is capable of predicting the significance of each input factor (i.e. spindle speed and feed rate) and their linear interactions.

Table 3.7: Spindle speeds and feed rates used in the experimental work of cryogenic trials

	Level 1	**Level 2**	**Level 3**
Spindle speed (rpm)	3000	6000	9000
Feed rate (mm/min)	300	600	900

3.7 Machine Tool

The drilling trials were carried out on a MORI SEIKI SV-500 and a MORI SEIKI NV-5000 milling machines available at the Advance Manufacturing Research Centre (A.M.R.C) as shown in Figure 3.2. MORI SEIKI NV-5000 machine was only used for a small part of the dry drilling trials.
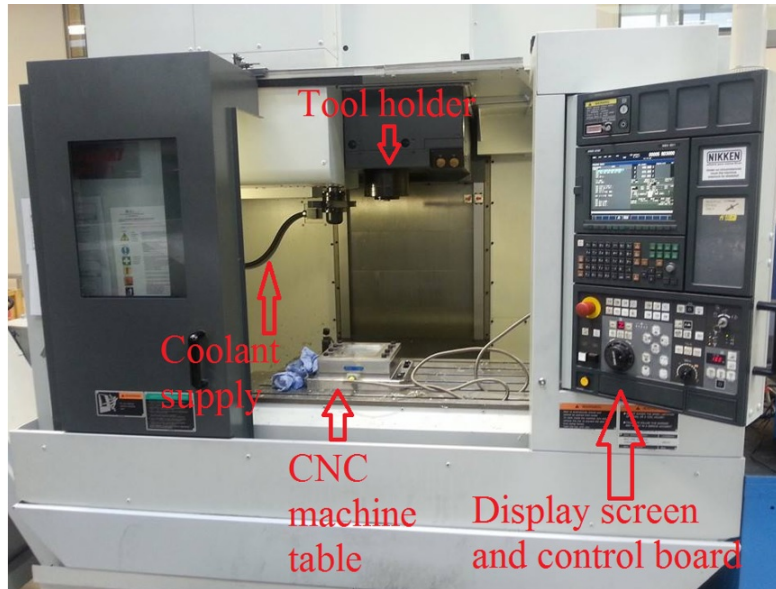
Figure 3.2: View of the MORI SEIKI SV-500 three axis milling machine

The specifications of the CNC machines are shown in Table 3.8. In order to eliminate the

effect of using a different machine on the results of cutting forces and hole quality parameters, additional hole sets were drilled for GLARE grade 2B 11/10-0.4 on each machine, and the variation among measurements of cutting forces and hole quality parameters were found to be negligible.

Table 3.8: CNC machine specifications used for performing the drilling tests

Machine brand	DMG MORI SEIKI SV-500	DMG MORI SEIKI NV-5000
Dimensions (m)	2.87x2.667x2.844	2.45x2.71x2.64
Weight (Kg)	7257	7166
Table size (m)	1.32x0.6	1.1x0.6
Max spindle speed	10000	12000
Cutting feed rate (mm/min)	2.54-16002	2.54-16002
Max table load (Kg)	1197	1000-1200
Max tool weight (Kg)	9	8
Main motor	30 HP, 220/440v, 3ph	30 HP, 220/440v, 3ph

3.8   Machining Coolants Setup

Two cooling technologies were studied in the research: minimum quantity lubrication (MQL) and cryogenic cooling using liquid nitrogen LN2. The following sections provide a detailed description of the two systems and their setup.

3.8.1   MQL trials setup

The MQL coolant tests were conducted using a portable coolants supply machine. COOL-UBE 2210 metal machining oil coolant was supplied under controlled flow rate and air pressure. The full details of the MQL system are shown in Figure 3.3. The system is capable of supplying coolant mixed with small amounts of compressed air to produce various flow rates up to 1200 mL/hr, and pressures ranging from 1-4 bars.

A holder was designed to accommodate the MQL nozzle and cryogenic coolant hose near the tool holder. The MQL nozzle was used to create an atomised spray mist to target the cutting area. The nozzle is made of brass and 316 stainless steel, a full jet standard spray nozzle with inlet connection of 3.175 mm and a nominal orifice diameter of 1.6 mm, the nozzle has a supply capacity ranging from 1.628 litres per minute at 1 bar up to 7.192 litres per minutes at 20.7 bars. The spray angle of the nozzle varies between 23-30 degrees depending on the supplied air pressure. The nozzle was chosen since it can atomise the coolant flow rate and create a cone-shaped spray mist that can cover the cutting tool tip and the surface
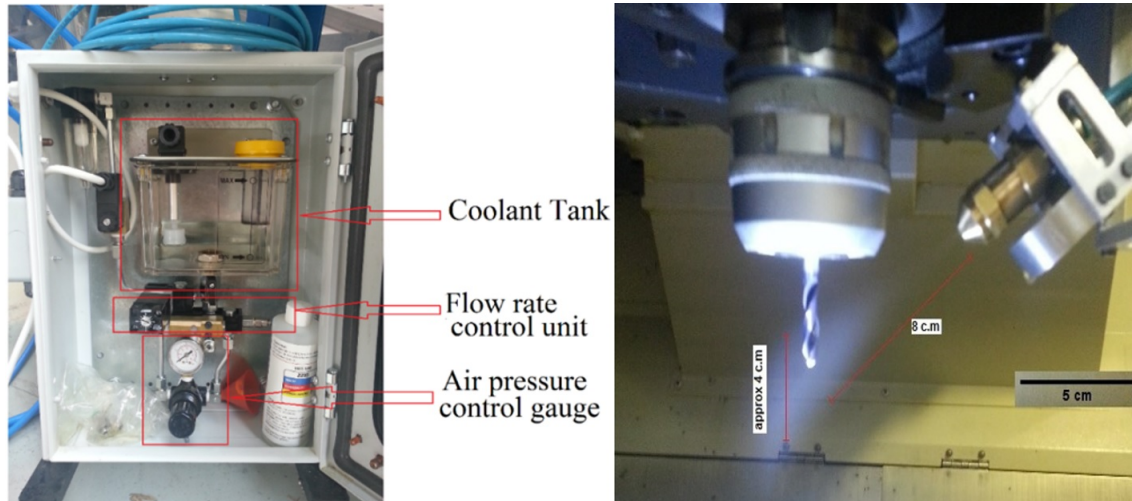
Figure 3.3: Characteristics of the used MQL unit and nozzle setup inside the CNC machine [303, 304]

of the workpiece at the drill-workpiece contact zone. Three flow rates were used, 20, 40 and 60 ml/h since previous studies on drilling aluminium alloys used flow rates ranging from 10 mL/hr to 100 mL/hr, and in some cases up to 250 mL/hr [143, 239, 241, 243, 246, 298–301]. Also, Bhowmick et al. [241] previously reported that there was no significant difference in average torque responses when changing the flow rate levels below 30 mL/hr (i.e. between 5 to 30 mL/hr) and therefore, higher flow rates were used in the experiments. In addition, three levels of air pressure were used, 1, 2 and 3 bars due to limited pressure supply from the portable MQL machine. The MQL coolant was supplied continuously since it was previously reported that it was beneficial in terms of tool life for small diameter twist drills over interrupted MQL supply. The continuous MQL supply during the drilling process would allow small amounts of cutting fluid to reach the cutting zone at greater depths [305].

3.8.2 Cryogenic trials setup

Liquid nitrogen was delivered from a portable Statebourne self-pressurized cryogenic Dewar, with a maximum capacity of 90 litres and operating pressure of 3 bars. The internal set-up is shown in Figure 3.4. The liquid nitrogen was transferred from the tank to the cutting zone through a 4 metres vacuum insulated stainless steel hose at a pressure of 2 bars. However, a realistic comparison between the two coolant technologies would require similar machining conditions, including equal pressures and flow rates. It was not possible to change the cryogenic tank pressure continuously due to safety issues and therefore, the pressure was kept constant at 2 bars. Temperature measurements of the liquid nitrogen coolant at the tip

of the hose prior machining trials showed that a period of ten seconds was required to reach the liquid nitrogen boiling temperature of -196 °C. Therefore, a minimum of ten seconds was allowed before the start of the drilling of each hole.
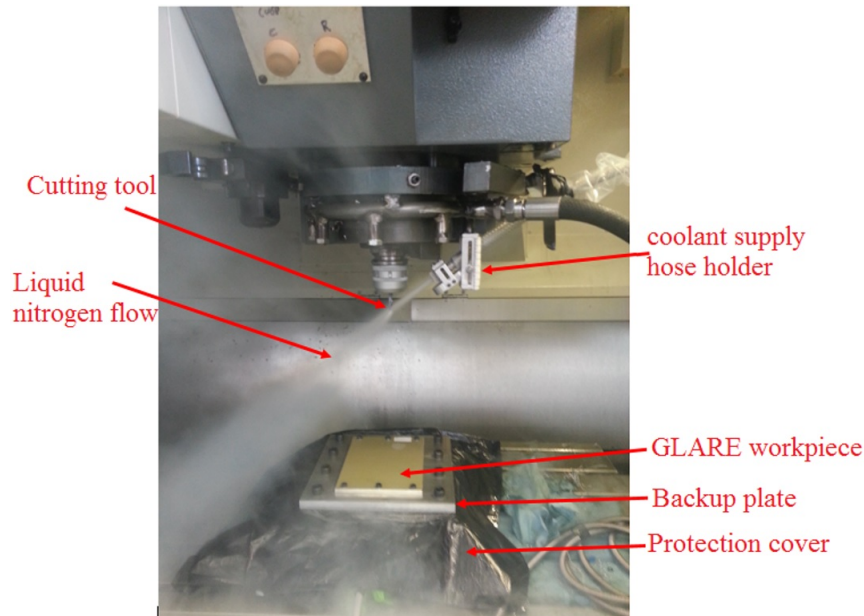
Figure 3.4: Experimental setup for cryogenic drilling trials

3.9   Nozzle holder

The CNC machines did not have a built in MQL or cryogenic coolant supply capability externally or internally. Therefore, a nozzle holder was designed and manually fitted near the tool holder. The nozzle holder allowed for external MQL and cryogenic coolants delivery during the machining process. The holder shown in Figure 3.5 can be manually adjusted in all directions and is capable of accommodating both cooling methods to provide better cooling strategy on the cutting tool-workpiece zone.

3.10   Cutting Tool Specifications

Twist drills are the most common tools used for making holes and rivets in aerospace structures [84]. The choice of drill bit geometry is of a great importance since it can affect the quality of drilled holes. In the current research, High-performance general purpose drill OSG HYP-HP-3D ϕ6 mm TiAlN (Titanium aluminium nitride) micro grain coated tungsten carbide twist drills with point angle of 140° and a flute helix angle of 30° shown

Figure 3.5: Schematic representation of the nozzle holder fitted inside the CNC machine

in Figure 3.6 were used for all drilling trials. The drill has an h7 shank diameter tolerance and an m7 drill diameter tolerance. The total length of the drill is 66 mm and the flute length is 28 mm. The type of drill was chosen according to similar previous studies on machining GLARE and composite-metallic stacks in the drilling of GLARE [193, 194]. The large point angle of 140∘ was chosen since it was previously reported that it can reduce burr formations when drilling aluminium alloys [135, 306]. Also, the large and positive helix (rake) angle was chosen because it has a direct effect on the surface topography and machining quality and to a lesser extent a minor influence on chip formation in composites. For example, increasing the rake angle of the cutting tool reduces the matrix smearing and increases the overall quality of the machined edge [29]. In addition, the recommended point angle for drilling Al2024 alloy is 130°-140° [128]. The size of the drill was chosen since it is one of the most commonly used for making holes in aerospace parts. Additionally, holes drilled in Airbus A380 structures range between 4.8 and 6.4 mm [190]. Coated cutting tools are desirable when drilling glass fibres due to their abrasive nature [1], especially when no coolants are used. Besides, coated cutting tools can significantly improve the shape of the formed burrs [307]. HSS tools were excluded since it was previously reported that they are not suitable for machining GLARE due to excessive wear [307]. Diamond coated cutting tools are an excellent choice for drilling GLARE in terms of wear resistance but they were excluded due to their high costs.

The TiAlN coating was chosen since it was previously reported that it is more stable at higher

temperatures [30] which were likely to develop in dry drilling trials at high spindle speeds and low feed rates. Kalidas et al. [308] previously reported that using TiAlN coated cutting tools produced holes closer to the nominal size when drilling aluminium alloys. Additionally, it was previously reported that the coating of the drill did not have a substantial effect on the surface roughness, hole size and radial deviation when drilling Al2024 alloy [76]. However, compared to other coatings such as TiN, the application of TiAlN coating yielded better performance and reduced the cutting forces, improved the surface roughness and gave better tool wear resistance when machining Al2024 and Al6061 alloys in dry machining applications [309]. Moreover, Heinemann et al. [305] previously reported that the high hot hardness, oxidation stability and lower thermal conductivity of TiAlN coating over TiN coating and uncoated tools provide protection to the tool substrate which gives satisfactory tool life and wear resistance under dry and MQL drilling conditions. In addition, TiN based cutting tool coatings have friction reducing property which shortens the contact length between the tool rake face and chip giving lower torque values during the initial contact of the drilling process [305].

Drill bit description		
Type	Micro grain Carbide Twist drill	
Diameter (mm)	6	
Coating	TiAlN	
Overall Length(mm)	66	
Point angle	140°	
Manufacturer	OSG JAPAN	
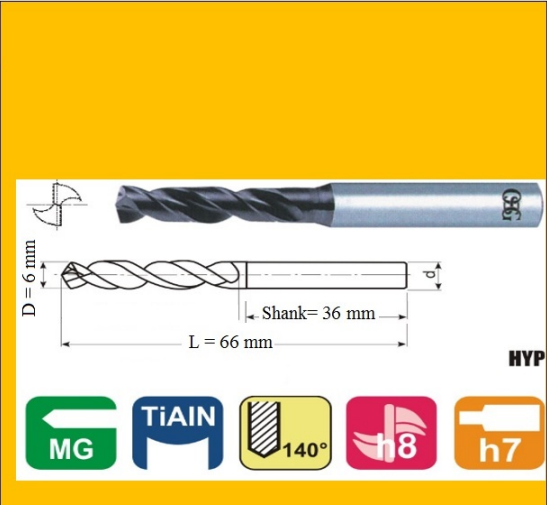
Figure 3.6: HYP-HP-3D cutting tool from OSG (courtesy of OSG)

3.11   Workpiece Material and Sample Preparation

Two types of materials were used in the current research. Aluminium alloy Al2024-T3 and GLARE fibre metal laminates. The GLARE panels were supplied by the fibre metal laminate centre (FMLC) in Holland and Delft University of Technology TU Delft. The aluminium panel was purchased from a university supplier. Each panel has dimensions of

210 mm x 150 mm. Both GLARE grades are unidirectional and their constituents have similar thicknesses. The only difference is in the fibre orientation in each prepreg. For GLARE 2B, the prepreg orientation in each fibre layer is 90/90 whereas for GLARE 3 is 0/90. For GLARE 2B, three thicknesses were used: 7.31, 5.15 and 2.41 mm. For GLARE 3 only one thickness was used 7.31 mm. 6 mm clamping holes were drilled on the upper and lower parts of each panel to mount it on the backup plate as shown in Figure 3.7.
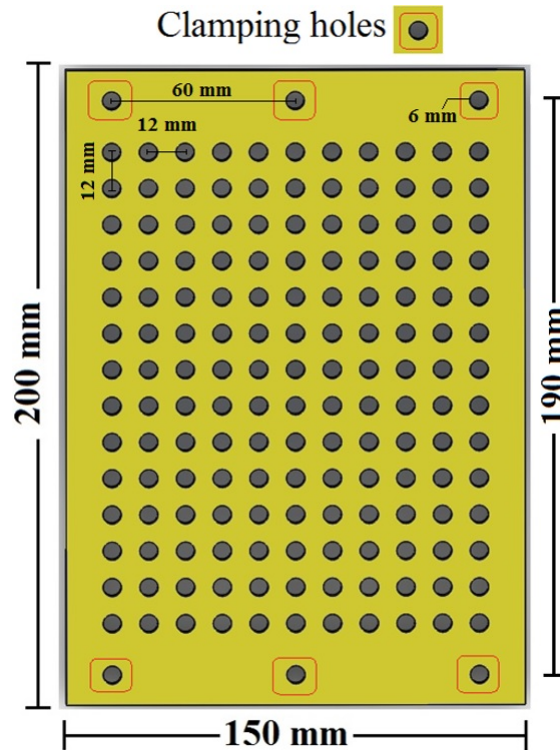
Figure 3.7: Panel details and dimensions used in the drilling tests [303, 304]

The total number of holes which can be drilled in each sample is 144. Eleven holes are drilled in each row and in total 14 rows are drilled in the panels. The distance between the centre of each two adjacent hole was kept constant at 12 mm. The dimensional properties of both materials are summarised in Table 3.9.

Table 3.9: GLARE grades considered in the drilling experiments

Material	Al2024-T3	Glare 3 8/7-0.4	Glare 2B 4/3-0.4	Glare 2B 8/7-0.4	Glare 2B 11/10-0.4
Thickness Of Aluminium Layer (mm)	7.13	0.4064	0.4064	0.4064	0.4064
Thickness Of S2 Glass Fiber Layer (mm)	-	0.266	0.266	0.266	0.266
Total Thickness (mm)	7.13	5.113	2.42	5.113	7.13
Metal Volume Fraction % (M.V.F)	100%	63.58	67%	63.58	62.69
Workpiece Size (mm)	210X150	210X150	210X150	210X150	210X150
Prepreg Orientation In Each Fibre Layer	-	$[0^\circ/90^\circ]$	$[0^\circ/90^\circ]$	$[90^\circ/90^\circ]$	$[90^\circ/90^\circ]$

3.12   Support Plate

The workpiece was mounted on a support plate and clamped to it using 6 mm bolts. The design and dimensions of the support plate are shown in Figure 3.8. The support plate was mounted on the top of the dynamometer during the drilling process to protect it from damage and to reduce bending of the workpiece.
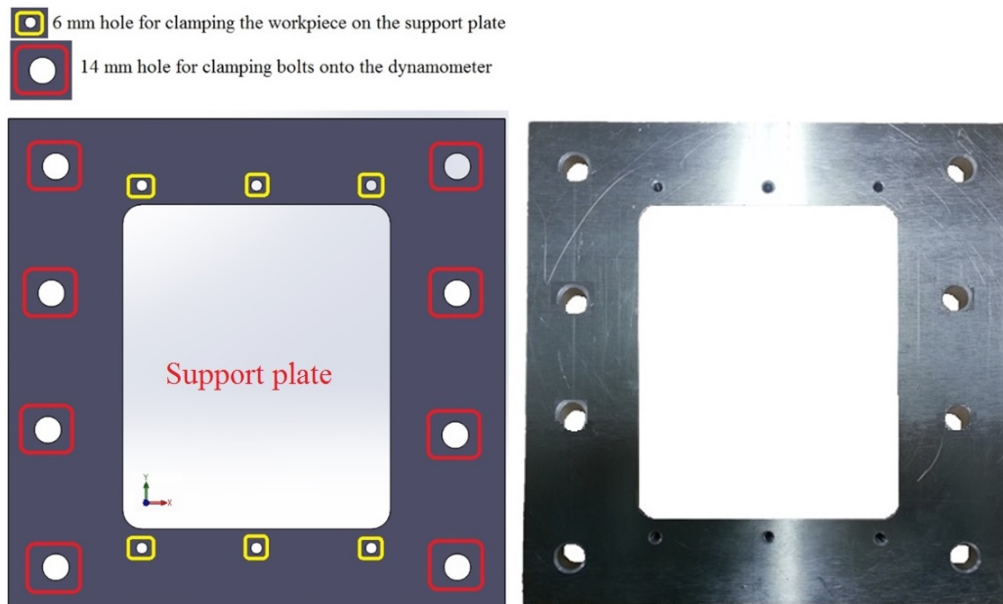
Figure 3.8: CAD model of the support plate and actual fixture [310]

3.13 Hole Quality Analysis

The evaluation of machined hole quality in GLARE is a more complex issue than that used for composites or metals because of its inhomogeneous structure. The damage caused in GLARE by the machining process can exist in metallic sheets and composite layers, it can also transform from metals to composites and vice versa. To the knowledge of the author, there are no standards which define a form of acceptable standards of the quality of machined holes in GLARE. However, strict requirements imposed by the aerospace industry demand the production of highly quality machined parts. For example, the presence of waste material pressed in the edges of milled GLARE panels is considered a primary machining defect which leads to immediate rejection of the panel, while some delamination or cracks can be tolerated if they are repairable [1]. The following sections describe in details some of the most common defects and criteria used to inspect and evaluate the machined hole quality.

3.13.1 Delamination analysis

In the current research, drilled hole in GLARE was inspected for damage and delamination using computerised tomography (CT) scan available at X-Tek Systems Ltd (Nikon Metrology UK Ltd) and AMRC. The measurements of X-ray computed tomography were carried out using Nikon Metrology XTH 225/320 ST and Nikon Metrology XTH 225/320 LC CT scan machines. The samples are stacked onto a turntable using floral foam material as shown in Figure 3.9, on which they will rotate in between an X-ray source and X-ray detectors. Care was taken to make sure that the samples are within the range of the X-ray beam. The florist foam is commonly used in CT scans due to its low density and reasonable rigidity which make it relatively transparent to X-rays. The X-ray voltage and current were set at 135 kV and 105 mA respectively. The sample exposure time was 1000 ms per projection with a total number of 3300 projections, and two frames per projection and a scanning resolution of 15 microns. Nikon Metrology Inspect-X and XT CT Pro/CT agent were used for setting up the scanner and reconstruction of CT volume. Volume graphics gmbh (VGL) software was used for the analysis of the reconstructed 3D volume from the 2D image stack, and to capture the images for delamination analysis of the glass fibre layers.
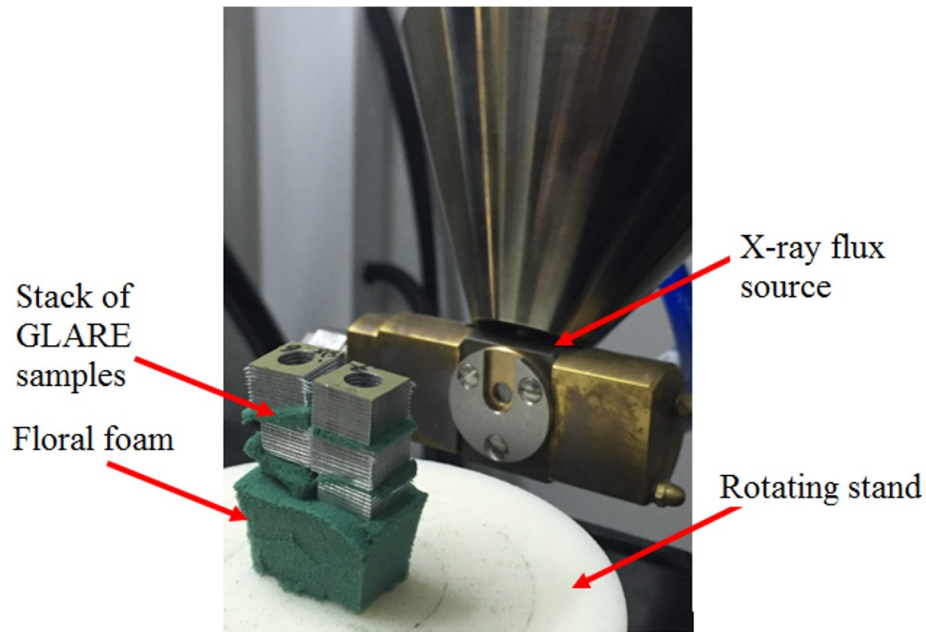
Figure 3.9: CT scan inspection of GLARE samples [311]

Figure 3.10 illustrates the steps undertaken to process the images in order to obtain the final delamination area around the hole. The concept of image processing for delamination inspection of holes drilled in composite using 2D images obtained from CT scanning or optical microscopy techniques was similar to that used previously by other researchers [80, 107, 312, 313]. The method is based on measuring the extent of damage around the hole edge depending on the contrast in the 2D image slice which was processed by an image processing software (ImageJ) [80, 107, 312–314]. First, the image brightness and contrast are adjusted to get a clearer visibility of the delaminated area around the hole in comparison to its surroundings. The image brightness is manipulated to better visualise the damage around the hole edge. The delaminated regions are then selected using the wand tool by tracing objects of uniform colour or threshold objects; the delaminated areas have a different colour intensity and can be visually observed using the software. The multiple selections of the different locations of the delaminated regions around the drilled hole are added together using the ROI (Region of Interest) Manager and the total area of delamination is calculated. To enhance the final image quality and clear the unnecessary surroundings, the fill command is used to fill the whole drilled region with the black colour foreground. Sometimes the clear outside command is also used to erase the area outside the delaminated region selection if the fill command fails to do so. Finally, the image is converted to a black and white 8-bit image.
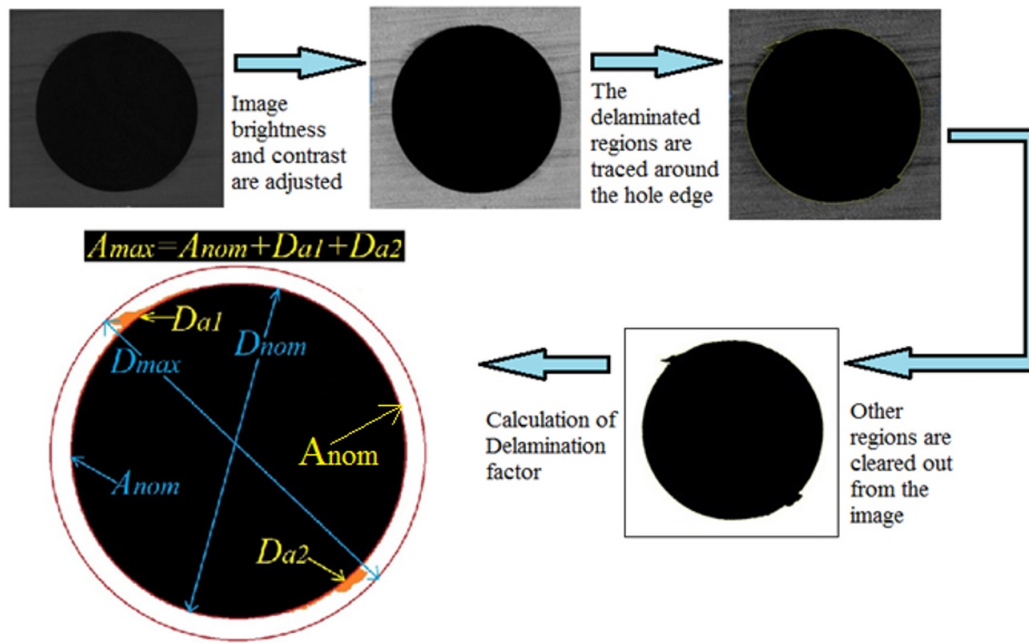
Figure 3.10: Digital image processing diagram of delamination damage around a drilled hole [311]

Since it was not possible to define an entrance or exit delamination for each layer, the delamination analysis was carried out at a plane taken in the middle of each glass fibre layer to allow for better visualisation of the damage. Due to the expensive and time-consuming nature of CT scans, only a limited number of samples were scanned for each grade of GLARE and cooling method used. Five samples were scanned from each GLARE grade used in dry and cryogenic drilling trials as shown in Table 3.10 while nine samples were scanned from the MQL drilling trials. The number of samples would be sufficient to assess the influence of the cutting parameters on delamination damage and also to conduct statistical analysis.

Table 3.10: Cutting parameters of the samples examined under CT scan for dry, cryogenic and MQL drilling trials

Dry and cryogenic drilling trials								
Spindle speed (rpm)	3000		3000		600		9000	9000
Feed rate (mm/min)	300		900		600		300	900
MQL drilling trials								
Spindle speed (rpm)	3000	9000	3000	9000	3000	9000	3000	9000	6000
Feed rate (mm/min)	300	300	900	900	300	300	900	900	600
Flow rate (ml/hr)	20	20	20	20	60	60	60	60	40
Air pressure (bars)	1	3	3	1	3	1	1	3	2

3.13.2 Surface roughness measurement

A Mitutoyo Surftest SV-600 profilometer equipped with Surfpak SV software was used to measure surface roughness of machined holes. Calibration was carried out prior to roughness measurements using a Mitutoyo Precision reference specimen with a known R_a value of 2.97 µm and error was found to be less than 5 %. The hole surface roughness was measured in the direction of the feed as shown in Figure Figure 3.11.
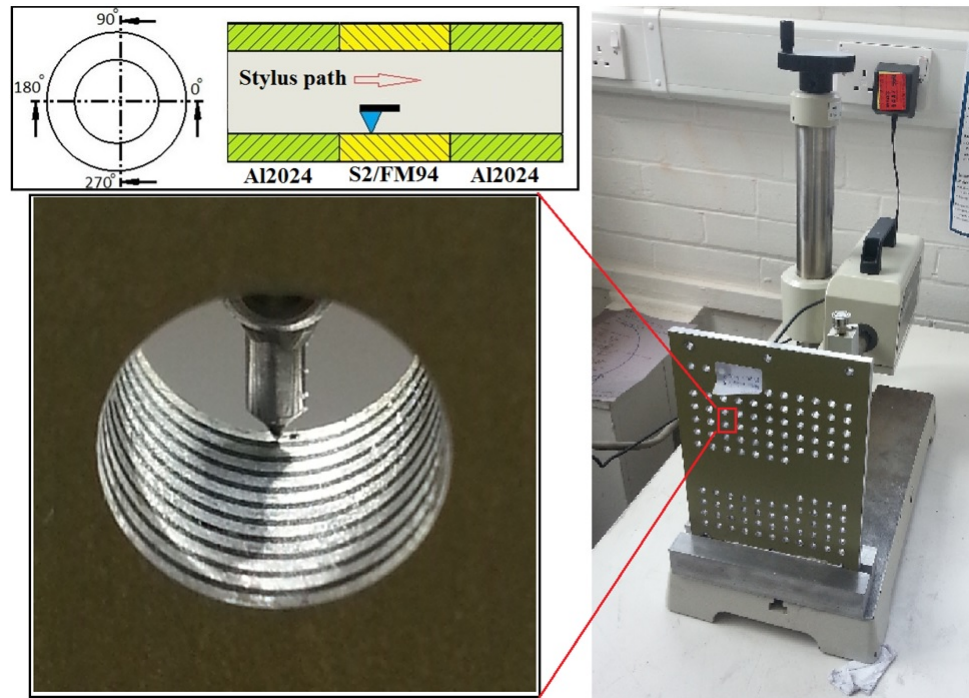
Figure 3.11: Surface roughness measurement [190]

The stylus head is made up of a 90° diamond cone shape with a 5 µm tip radius. Surfpak-SV software was used to transfer and process the collected data from the stylus to the PC. The software was set up to measure a predefined length depending on the thickness of the workpiece from near hole entry where the drill first contacts with the workpiece to the exit side. The total sample length for surface roughness measurement was set to 6.5 mm for GLARE samples 2B 11/10-0.4 and Al2024 alloy workpiece. For GLARE 2B and 3 8/7-0.4, the total sample length for surface roughness measurement was set to 4.5 mm. For GLARE 2B 4/3-0.4 the length was set to 2.2 mm which accounts for approximately 90 % of the hole depth. This was the maximum possible depth to carry out surface roughness measurements through the overall depth. The vertical measuring range can be set to 8, 80 and 600 µm with a resolution of $.0005, 0.005, 0.05$ µm, respectively [315]. The measuring range was set to 80 µm and the scan speed was set to 0.2 mm/sec.

The samples were placed such that the holes are facing the stylus from the entrance side and the stylus was inserted into the hole at the maximum possible depth, The stylus was then carefully lowered until in contact with the sample. The stylus was then traversed along the internal surface of the drilled hole across the thickness of the test sample surface and its motion profile was recorded as a profile of the surface. R_a (arithmetic mean deviation or centre line average) is recorded in the software and some of the software settings were pre-adjusted to obtain the desired measurement of surface roughness profiles. For example, the compensation in the software was set to compensate for inclination at all times to remove any effects caused by the workpiece not being completely parallel to the motion of the stylus. The measurement process was repeated four times for each hole by rotating the sample $90°$ along its side and the mean value from the four readings of surface roughness was calculated for each hole.

3.13.3 Burr formations measurement

Burr height and root thickness were measured by a surface roughness profilometer as shown in Figure 3.12. The samples were placed such that the holes were parallel and in contact with the stylus head. The stylus was then placed few millimetres away from the hole edge and was allowed to traverse along the surface of the drilled hole until it reached the drilled hole empty space. Its motion profile was recorded and the distance between the highest point on the burr root thickness surface and the surface of the workpiece was measured and burr height was recorded. This procedure was repeated four times for each hole at its entrance and its exit sides by rotating the sample $90°$ along its side and the average value from the four readings of burr height was calculated for each hole.

In this study, the burr formation around the edges of the first and last aluminium sheets was analysed by measuring the size of the burrs (height and burr root thickness). The formation of the burr is shown in Figure 3.13.a) as indicated in steps 1 to 3. These two burr parameters were defined by Schafer [316] as shown in Figure Figure 3.13.b and are widely used to characterise burr formation (burr profile shape) in machined holes (see Fig.4.b). Both burr parameters were measured using a surface roughness profilometer. The burr parameters were measured at $0°$, $90°$, $180°$ and $270°$ on the hole upper and lower aluminium sheets (see Figure 3.13.c).
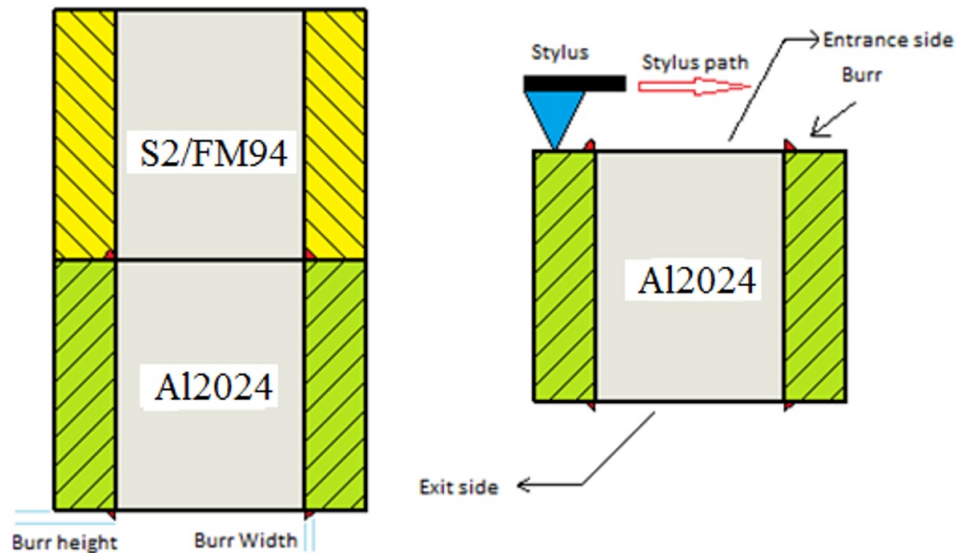
Figure 3.12: Measurement process of burr height and burr root thickness
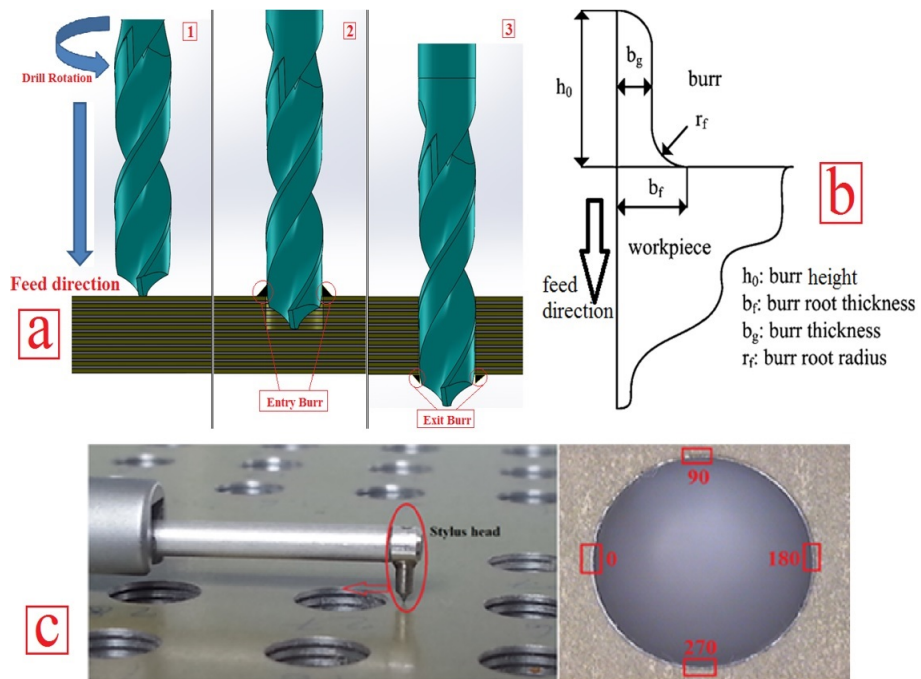
Figure 3.13: Burr profile showing a) the formation of burrs during drilling process b) detailed description of burr parameters [317] c) the measurement process and locations of burr height and burr root thickness s [303]

3.13.4 Hole size and circularity error (roundness error) measurements

The hole size and circularity were measured using SHEFFIELD CORDAX D8 CMM machine shown in Figure 3.14 and Figure 3.15. The workpiece is placed on the machine table and an optical probe continuously circulates on a particular section of the internal wall of the hole. For GLARE 2B 11/10 and Al2024 samples, the measurements were taken at 1 mm (top) and 6 mm (bottom) below the hole entry side (see A and D in Figure 3.14). For GLARE 2B and 3 8/7 the measurements were taken at 1 mm (top) and 4 mm (bottom) (see A and C in Figure 3.14), while for GLARE 2B 4/3 the measurements were taken at 1 mm (top) and 1.75 mm (bottom) (see A and B in Figure 3.14). The scanning speed for the measuring probe was 1 mm per second, allowing the probe to capture 400 points while scanning the hole. The Maximum Inscribed Circle (MIC) method was used to measure the

			Layer thickness	Total thickness	GLARE samples		
1		1	0.4064	0.4064			
1	A	1	0.266	0.6724			
2		2	0.4064	1.0788			
2		2	0.266	1.3448			
3	B	3	0.4064	1.7512			
3		3	0.266	2.0172			
4		4	0.4064	2.4236	GLARE 2B 11/10 and Al2024-T3	GLARE 2B 8/7 and GLARE 3 8/7	GLARE 2B 4/3
4		4	0.266	2.6896			
5		5	0.4064	3.096			
5		5	0.266	3.362			
6		6	0.4064	3.7684			
6	C	6	0.266	4.0344			
7		7	0.4064	4.4408			
7		7	0.266	4.7068			
8		8	0.4064	5.1132			
8		8	0.266	5.3792			
9		9	0.4064	5.7856			
9	D	9	0.266	6.0516			
10		10	0.4064	6.458			
10		10	0.266	6.724			
11		11	0.4064	7.1304			

Figure 3.14: Measurement process of burr height and burr root thickness

circularity error. An illustration of the MIC method is shown in Figure 3.16. The difference in radii between the largest inscribed circle that can be fitted in the circular profile (MIC) and the smallest external circle that can be fitted around the same circular profile gives the circularity error (roundness error). The circularity can be measured by tracing the perimeter of the cylinder with a stylus, or probe at a particular location. The stylus measures the circular profile by mapping a large number of points around the measured circle within the cylinder [318]. The MIC method is used by Sandvik metrology experts for measuring hole size. Although the least square method (LSQ) is more common in CMM machines, nevertheless, it usually overestimates the error which influence the decision on accepting or rejecting a part. Using LSQ could sometimes lead to part rejection even though they are
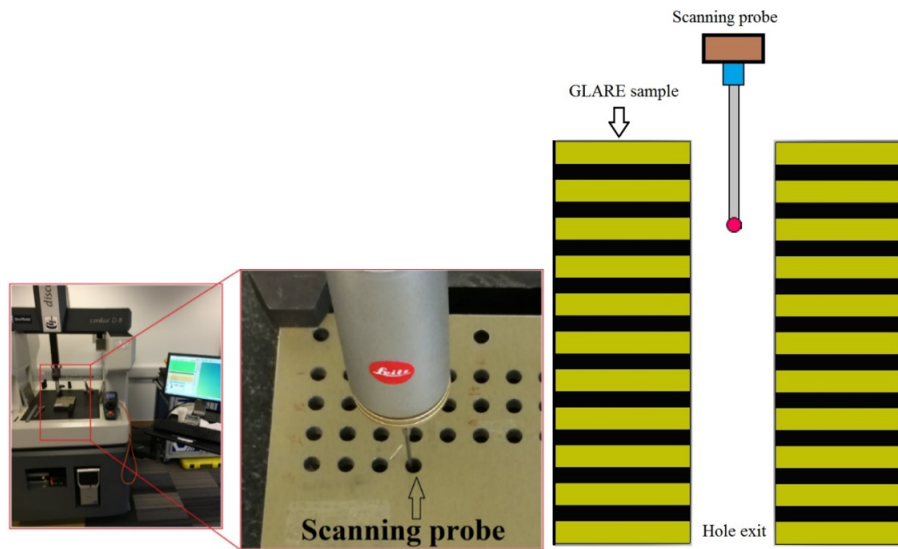
Figure 3.15: Locations of hole size and circularity error measurement for all studied samples using CMM machine

within the desired specifications [319].
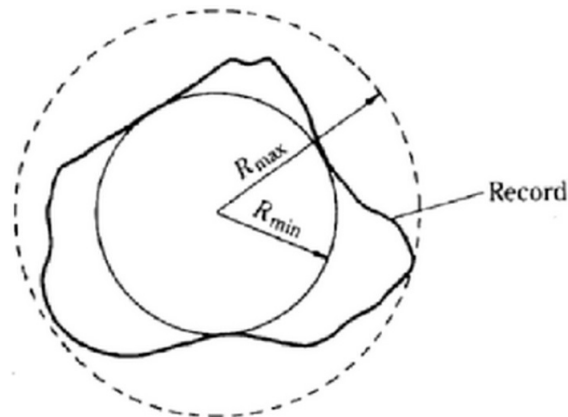
Figure 3.16: Description of Maximum Inscribed Circle method [303, 320]

3.13.5   Cutting force measurement

The cutting forces were measured using piezoelectric 3-component dynamometers. KISTLER 9255B and 9255C dynamometers were used to measure the three orthogonal components of a force during the machining process. The dynamometers are identical in dimensions but differ in their measuring range. The 9255B dynamometer measuring range is between -20 to 20 KN in the X and Y directions and -10 to 40 kN in the Z direction. The 9255C measuring range is between -30 to 30 kN in the X and Y directions and -10 to 60 kN in the

Z direction. The dynamometer has four 3-component force sensors which are sensitive to pressure in the X, Y and Z directions and are capable of measuring the cutting forces and torques in three dimensions. The dynamometer sensors are ground-insulated, rust proof and protected against penetration of coolants. A 6-component force and moment measurement was used. The dynamometer is mounted with four M18 bolts from its sides on the table of the CNC machine. The measurement signals from the sensors which represent the cutting forces acting on the dynamometers are converted into an electrical voltage in the individual channels. Therefore, the measured data from the dynamometer require signal conditioning using multichannel charge amplifier to build a complete measuring system which is controlled via DynoWare software. The dynamometer is connected to a 5070A 8-Channel Charge Amplifier using 5 metres connecting cable type 1679A5 as shown in Figure 3.17.
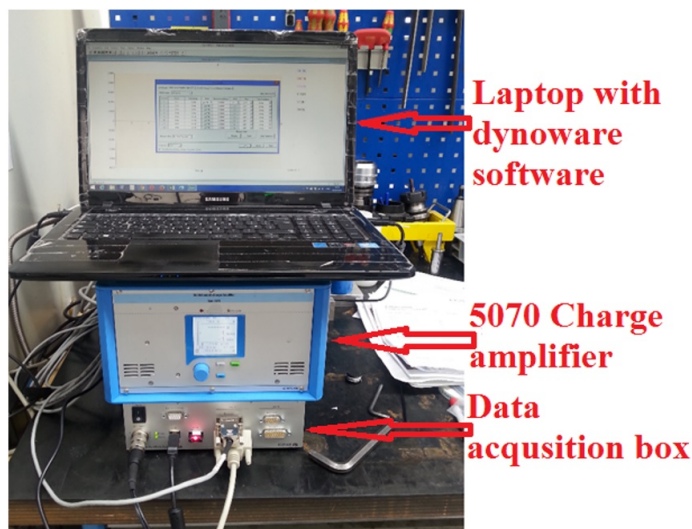
Figure 3.17: Cutting forces measurement setup [190]

The charge amplifier is controlled by a data acquisition box (DAQ) which holds the dongle (HASP) key licence. The DAQ box and the charge amplifier are connected via an RS-232 interface. The DAQ box is connected to a PC using USB 2.0 interface. The PC is running on Windows 8 and a DynoWare software is installed. The DynoWare software is used for measuring forces with dynamometers and for data post-processing. The complete setup of cutting force measurement is shown in Figure 3.18 a. Type 1a 8 channel multicomponent mode was chosen to calculate the cutting forces. The cutting forces F_x, F_y and F_z are directly calculated during the drilling process. The torque M_z is calculated by adding the location of the centre of the drilled hole with respect to the four sensors of the dynamometer in the software as shown in Figure 3.18 b. The four values of a_1, a_2, b_1, b_2 were calculated for each hole. The sampling frequency was set to 8000 Hz and measuring time was set to 20 seconds for each hole drilling.
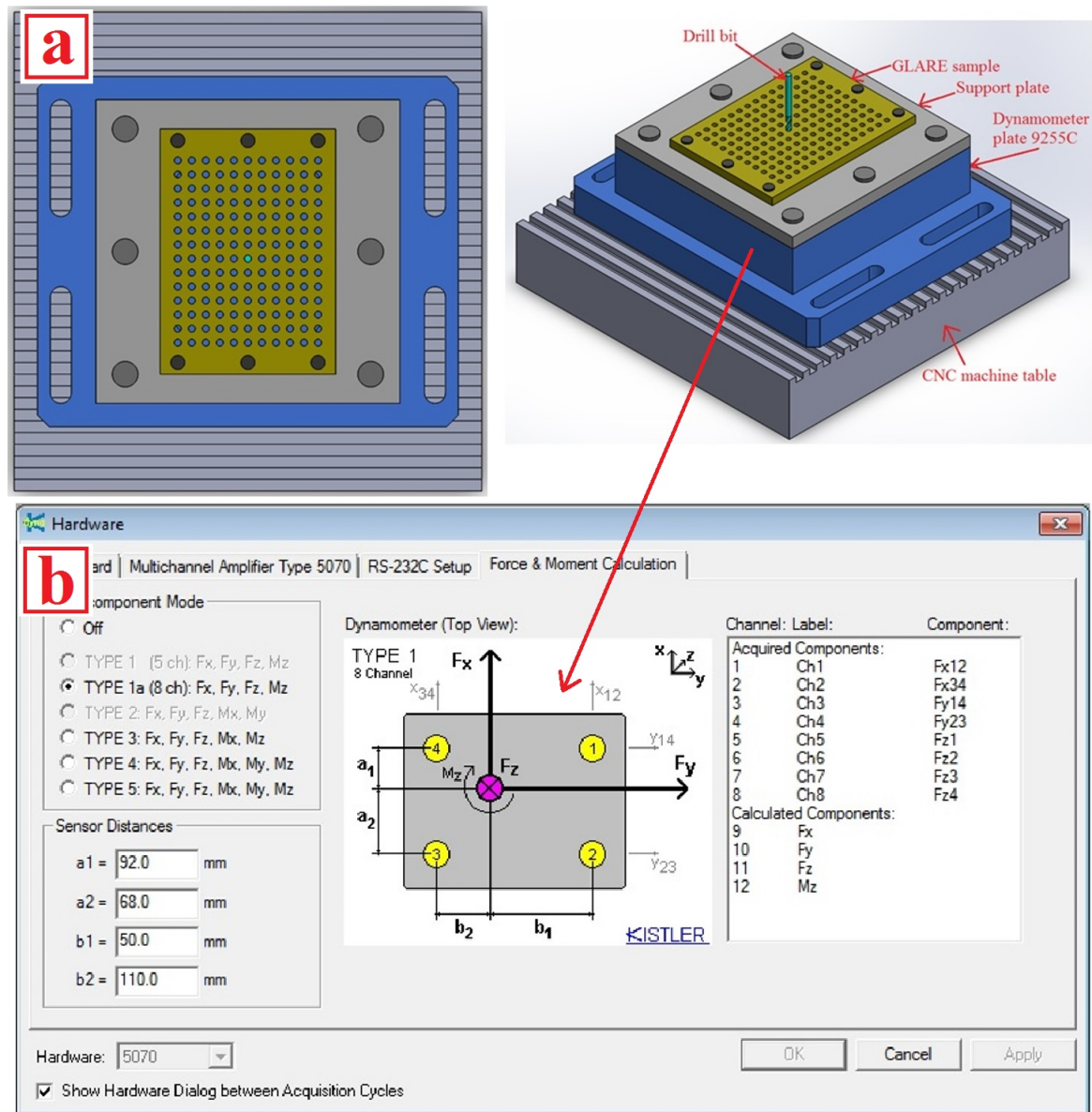
Figure 3.18: (a) 3D views of the setup of the dynamometer, the support plate and the workpiece inside the CNC machine (b) DynoWare software torque calculations setup and data input

The cutting forces components are calculated as shown in the following equations, were F_{x12}, F_{x34}, F_{y14}, F_{y23}, F_{z1}, F_{z2}, F_{z3}. F_{z4} have acquired components from the four piezoelectric sensors.

$$F_x = F_{x12} + F_{x34} \tag{3.5}$$

$$F_y = F_{y14} + F_{y23} \tag{3.6}$$

$$F_z = F_{z1} + F_{z2} + F_{z3} + F_{z4} \tag{3.7}$$

$$M_z = b_2.F_{x34} - b_1.F_x12 + a_1.F_{y13} - a_2.F_{y23} \tag{3.8}$$

Therefore, in order determine the appropriate values of a_1, a_2, b_1, b_2, the holes had to be distributed properly on the workpiece. The distance between the centres of two adjacent holes was fixed at 12 mm in each row and column. A total number of 11 holes were drilled in each row, and a total number of 14 rows can be drilled in each workpiece with a total number of 144 holes.

3.13.6 Scanning Electron Microscopy (SEM)

Scanning electron microscopy was mainly used because of the limitation of optical microscopes due to the limited poor depth of field and the large wavelength of visible light in optical microscopes. SEM technology uses focused beams of high-energy electrons which have much smaller wavelength than visible light over a solid surface to create a two-dimensional image of the surface topography with high resolution. In the current research, a HITACHI TM3030 plus tabletop scanning electron microscope was used to inspect the drilling-induced damage of the borehole surface. Each hole was cross-sectioned from its centre and was cleaned using acetone in an ultrasonic bath for ten minutes to remove glass fibre dust and any debris on the surface of the borehole as shown in Figure 3.19.a. The samples were then placed on the top of a carbon sticker and inserted inside the SEM chamber for surface inspection as shown in Figure 3.19.b. The device can operate on a variable accelerating voltage of 5 or 15 kV, the different accelerating voltages provide different types of imaging possibilities, for example using the 15 kV provides better resolution than the 5 kV and is usually used to inspect the subsurface while the 5kV cannot penetrate so far into the surface of the sample so it is used to inspect the surface and have a lower backscattered electron signal. The SEM device has a magnification range between 15X to 300000X. 3.19 shows the scanning of a GLARE hole sample using the SEM device. A 40-100X magnification was applied to view the alternating layers of aluminium and glass fibre. Due to the hybrid structure of GLARE, the scanning signal was set to the Energy Dispersive X-ray Spectrometer (EDX) which allows for multiple elemental analyses. Additionally, the mixed observation condition was selected since it is more efficient for analysing images with dual signals, which allows for better visualisation of GLARE constituents and adhered particles on their surfaces.

First, the vacuum inside the chamber is checked when the flashing blue light becomes solid, then the evacuate button is pressed to evacuate the chamber from pressure and the yellow light turns on while the blue light goes off which indicates that it is safe to open the chamber.
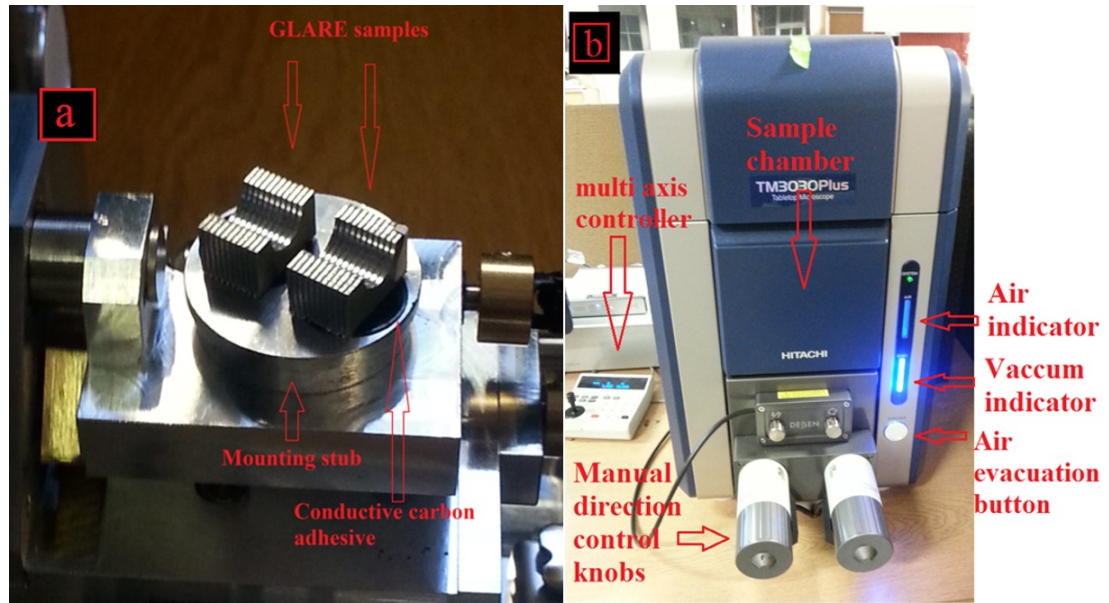
Figure 3.19: (a) SEM sample preparation (b) Hitachi TM3030 table top SEM microscope

The sample is mounted on the specimen mount using an adhesive conducting carbon tab. The samples are inserted in the main unit which is connected to an oil-free diaphragm pump and a PC running on windows 7. The specimen holder is used to make sure the sample is below the top of the holder. The chamber door is closed and evacuate button is pressed while firmly pressing the door for 2 minutes until the blue light goes on again to make sure there is no leakage or air inside the chamber. Once the blue light is on the start button on the software can be clicked and the software can be used to take SEM images of the sample.

3.13.7   3D surface roughness measurements using Contour GT

The limitation of two-dimensional surface roughness profilometry is that the measured surface roughness data are governed by the size of the stylus used, which makes it extremely difficult to detect narrow areas smaller than the stylus tip radius [190]. In addition, limitations imposed by contact methods such as the two-dimensional surface roughness devices are due to their limited flexibility in handling different geometrical surfaces and to the fact that they are measuring the surface roughness only along a straight line each time. For example, it was difficult to measure or analyse the surface roughness of individual aluminium sheets or composite layers of holes machined in GLARE due to their small thickness. Non-contact optical methods can be used to overcome the limitations of the stylus method. Three-dimensional optical microscopes provide the capability to measure an aerial surface roughness on the surface of the part rather than along a straight line. In GLARE, the use

of optical surface measurement microscopes allow for a more realistic view of the internal hole walls surface and to distinguish between the individual layers of aluminium and glass fibre. A 3D optical microscope Contour-GT as shown in Figure 3.20 was used to view and analyse the surface characteristics of the internal walls of drilled holes.
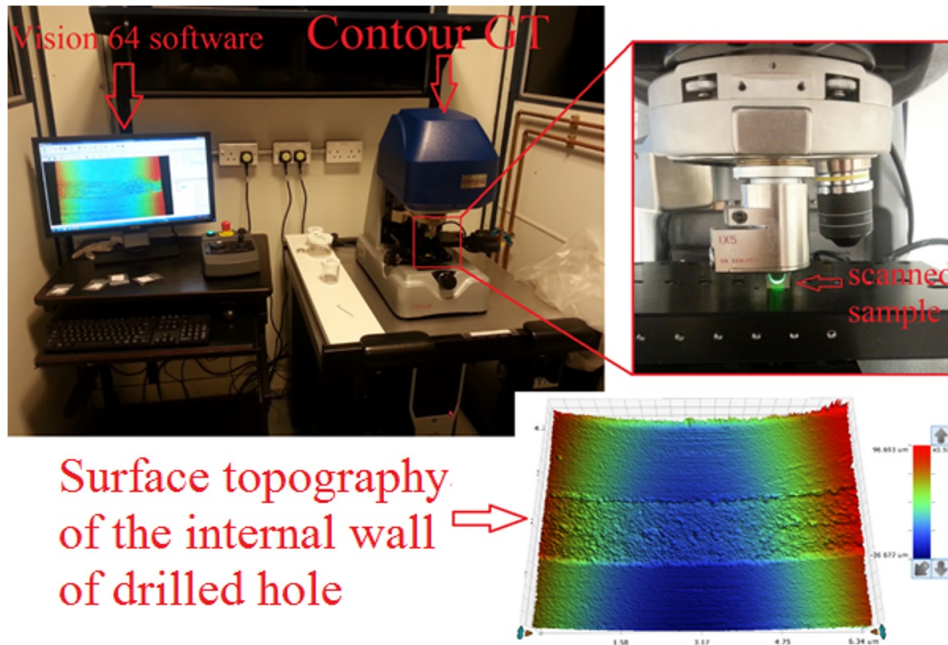
Figure 3.20: Surface topography using 3D optical microscopy scans [304]

Each hole was cross-sectioned from its centre and the internal hole walls were scanned. The Vertical Scanning Interferometry (VSI) mode was chosen since it is more suitable for measuring non-continuous surfaces. An advantage of this method is that it also allows the measurement of rough surfaces such as glass fibre prepregs that usually reflect a portion of the light back to the system. It is also suitable for materials with larger height discontinuities such as those found in GLARE due to its stacked structure. A 5X objective with 1X multiplier was used to view the sample. This allowed scanning two aluminium sheets and one glass fibre prepreg each time. The maximum measurement area was 1.259 mm in the X-direction and 0.944 mm in the Y-direction. The scanning speed was set to 1X. The back scan length was set to 100 μm and the scan length was set to 50 μm. The threshold was kept constant at 5 % at all times. The aluminium sheets are very shiny and reflective to bright light while the S2 prepregs are dark and scatter most of the light emitted from them, which reduces the amount of light reflected back to the lens. Therefore, a narrow green band light was used to view the glass fibre prepregs efficiently. A 50 % of light intensity was also applied to enable better surface viewing and results.

3.13.8   Measurement of Workpiece Temperature

The purpose of the temperature measurement using the infrared camera was to determine the impact of cutting parameters and coolants on the temperature of the machined surface at the exit side of the hole. The emissivity of the surface material is a critical input parameter when using infrared methods to measure the surface temperature which greatly influence the accuracy of the measurement results. The emissivity of GLARE laminates surfaces was measured prior to conducting the temperature measurement tests as shown in Table 3.11 using three different IR cameras. The method was carried out using calibrated infrared cameras and the thermocouples attached on the surface of the workpiece. The emissivity of GLARE was obtained by conducting three emissivity tests. Each test was carried out using different IR cameras and different types of coating/tapes all of which have known emissivity.

Table 3.11: Emissivity of GLARE fibre metal laminates using three IR cameras and thermocouple techniques [321]

Description	Test 1	Test 2	Test 3
Camera type	Electrophysic PV320 20° lens	AGEMA 550 20° lens	FLIR SC640: 0.4m away, 24° lens. FLIR B400: 0.1m away, 45° lens.
No. of cameras used	1	2	2
Type of coating/tape applied	Black spray paint	Extremely high-temperature paint & 3M Vinyl Scotch tape Super 88	3M Vinyl Scotch tape Super 88
Emissivity of coating used	0.94	0.94 & 0.95	0.95
Heat source used	Hotplate	Hotplate	Oven
Temperature level used	60-70 °C	60-90 °C	90°C
T ambient	24 °C	24 °C	24 °C
T reflect	-	21°C	21 °C
Thermocouples used	Yes	Yes	No
E1(Top and Bottom)	0.8	0.82	0.832-0.843
E2(S2-FM94 plies)	0.6	0.6	0.594-0.683
E3(Al2024 sheets)	0.4	-	0.276-0.395
Distance between camera and sample surface	-	0.45 m	0.4 m and 0.1 m

Measuring the temperature at the exit side of drilled holes

This part of experiment aim to measure the temperature in the heat affected zone at the exit side in the workpiece during the drilling process. The objective is to evaluate the extent to which using MQL and LN2 cooling technologies will contribute to reducing the cutting temperatures during the machining process. However, due to limited time, funding

and material supply, only preliminary tests were carried out on selected cutting parameters under dry and MQL conditions to evaluate the following:

- The effect of increasing the spindle speed at constant feed rate.

- The effect of increasing the feed rate at constant spindle speed.

- The effect of drilling at fixed spindle speed/feed rate ratios at 3 to evaluate the impact of reducing the drilling time on the developed temperatures.

- The effect of laminate thickness and stacking sequence of prepreg layers on the cutting temperatures.

The emissivity of GLARE surface (see Table 3.11) showed that they are not close to perfect black bodies, it was also found that the surface treatment of the upper and lower aluminium sheets in GLARE are highly reflective to light, and since thermal imaging cameras capture the intensity of radiation in the infrared part which is made up of a combination of emitted, transmitted and reflected light, the measured temperature will result from a combination of emitted, transmitted and reflected radiation which would turn to be inaccurate. Therefore, in order to eliminate the reflectivity of the surfaces, a black spray coating with known emissivity which was previously used to determine the emissivity of GLARE is applied on the lower surface of the samples as shown in Figure 3.21. Spraying the sample with black paint gives it an advantage since the coating has a high emissivity value equal to 0.94 which is close to black body definition. This means that the surface will absorb most of the heat and light and will reflect a minimum amount away from its surface.

The temperature measurement trials were carried out on the same CNC machine used for drilling GLARE. Figure 3.22 shows how the workpiece and camera are set inside the CNC machine. The infrared camera utilised in this study was a calibrated FLIR AGEMA thermovision 550 camera with a built-in 20°-140° lens and 320×240 pixels optical resolution. The camera has an operating measuring range of -20° to 140 °C, from 250 to 140 °C and up to 1500 °C with standard filter. The camera has a spectral range of 3.6 to 5 μm and a 60 Hz frame rate. The camera is operated using a FLIR tools software and is also used to process the acquired data. The camera was placed vertically with the lenses facing towards the back side surface of the GLARE sample. The sides of the fixture were then covered with dark paper to reduce the amount of light entering the chamber which could affect the measurement process.
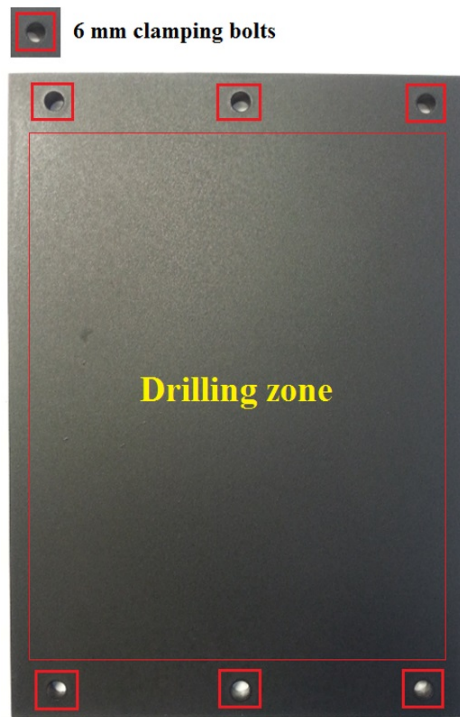
Figure 3.21: GLARE sample coated with black spray paint [321]
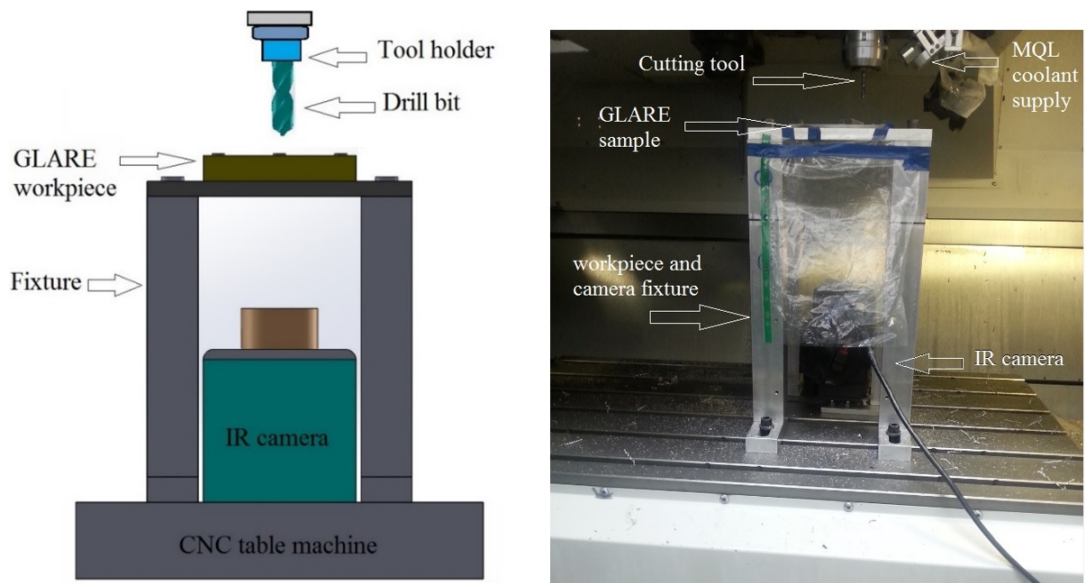
Figure 3.22: Details of the temperature measurement setup using the IR camera [321]

Due to the limited quantity of the material available and the high costs associated with machining trials, a limited number of drilling temperature measurements was carried out in GLARE 2B and GLARE 3 under dry and MQL conditions only as shown in Table 3.12. For each cutting condition, a set of 10 holes was drilled in a row on the workpiece and temperature was measured continuously at the exit and the highest temperature recorded from the ten holes was taken as the maximum temperature.

Table 3.12: Cutting parameters used in drilling temperature measurements in dry and MQL trials

	Spindle speed (rpm)		
Feed rate (mm/min)	3000	6000	9000
300	A B C D	C D	C D
600	A B C D	C D	C D
900	A B C D	C D	C D

A: G2B 11/10 B: G2B 8/7 C: G3 8/7 D: G2B 11/10 MQL

3.13.9 Measuring the post-machining micro-hardness

The hardness is the measure of a material resistance to deformation. The microhardness of the upper and lower surfaces of aluminium and GLARE samples were measured prior the drilling trials. The micro-hardness of aluminium workpiece was found to be in the range of 140 ∓3 and around 137 ∓1 HV in aluminuim sheets in GLARE samples [322]. The slightly higher hardness of the aluminium workpiece could be due to previous cutting operation applied on it to bring it to its current shape. However, the current research will use a microhardness of 137 ∓1 HV as a reference for comparison. The hardness measurements were taken near the hole edge at a distance of no more than 500 microns from the hole edge. A MITUTOYO HM-101 Micro-Vickers Hardness testing machine was used to measure the post machining microhardness around the hole edge as shown in Figure 3.23.

The device is capable of providing 10-1000 gf of tests force and 5-30 seconds of teste duration time. The device is equipped with a standard Vickers indenter (19BAA114) that have an approaching speed of approximately 60 μm per second. The device is also equipped with a color CCD camera which allows capturing live images of the indentation and sample surface. The sample surface can be observed through a 10X objective lens and the measurement is carried out using a software and an objective lens of 50X. The applied load was set to 1 kgf to all holes, the duration of applying the load was set 15 seconds of dwelling time. The hardness calculation method is carried out by applying a permanent pyramid deformation shape on the tests surface as shown in Figure 3.23 using the following equation.

$$HV = 1.854 \times F \times (d1 + d2)^2 \qquad (3.9)$$

where:

- F = Load in kgf

- d = Arithmetic mean of the two diagonals, d1 and d2 in mm.
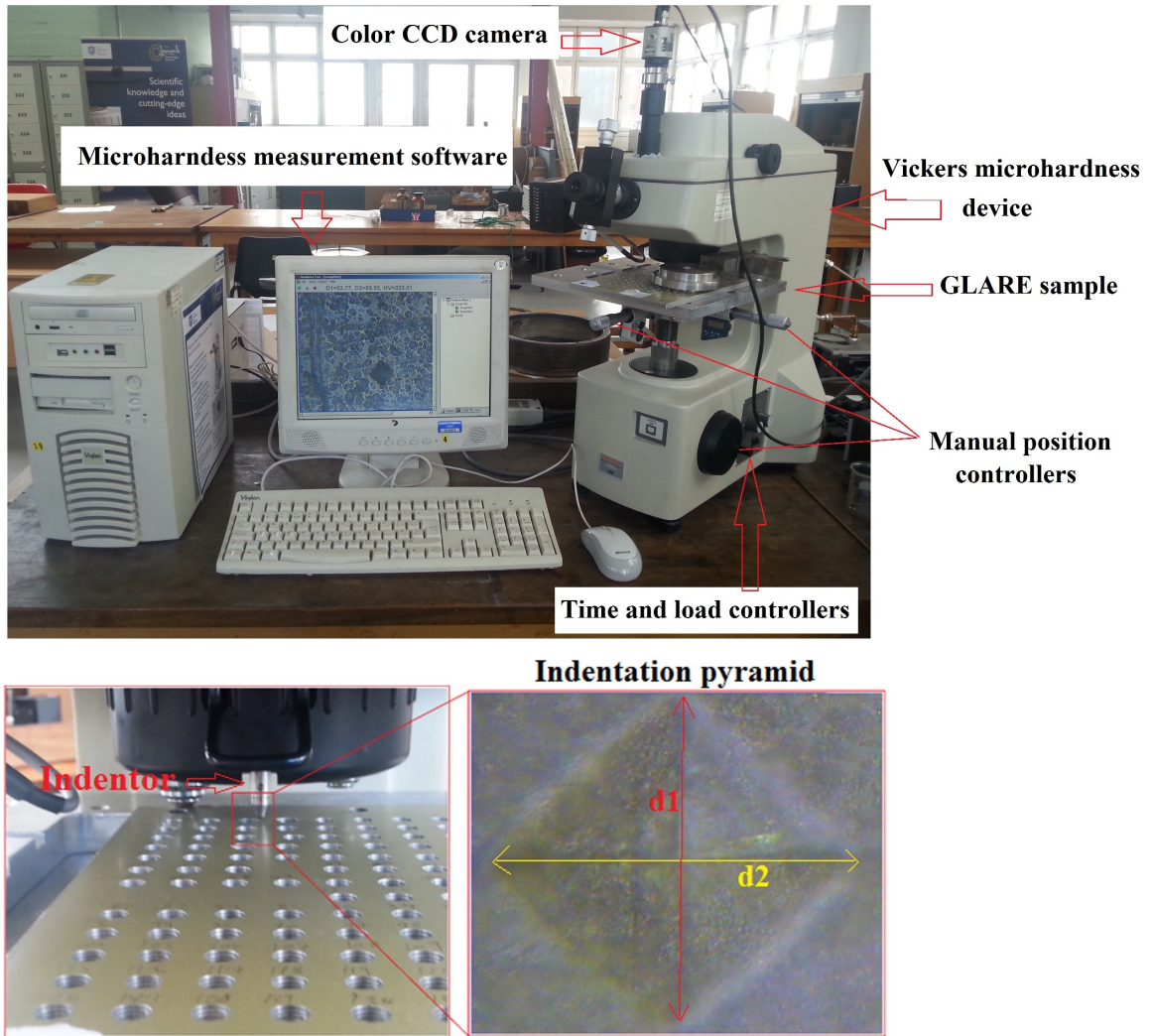
Figure 3.23: Details of the MITUTOYO HM-101 Vickers micro-hardness testing machine

3.14 Summary

In this chapter, the approaches with associated methodologies that were adopted to achieve the objectives of this research have been presented. The chapter summarises the details of the GLARE and aluminium panels used in the research, along with a description of machining process setup, cutting parameters, coolants used, cutting tool, the equipment and procedures (experimentally and statistically) employed for evaluating hole quality parameters and the methods undertaken to measure them. The following conclusions can be drawn from this chapter:

1. The Aluminium and GLARE panels for the drilling tests have been successfully prepared by determining the number of drilled holes in each panel, the distance between holes and the chosen cutting parameters.

2. Set-up and data acquisition methods for various subsequent machinability tests such as surface roughness, burr formations, hole size and circularity and workpiece thermal measurement have been developed and described I details.

3. In terms of damage, there is a significant interest regarding the mechanical damage mechanisms associated with composite machining. Therefore, scanning electron microscopy and CT scans were implemented to verify the consistent quality of the machined holes.

Chapter 4

PERFORMANCE EVALUATION OF CONVENTIONAL DRY DRILLING OF AL2024-T3 ALLOY

4.1 Introduction

This chapter presents an evaluation of the drilling performance of Al2024-T3 aluminium alloy under dry drilling conditions. The methodology of the drilling trials was previously described in chapter 3. The effects of machining parameters (spindle speed and feed rate) on cutting forces and hole quality were investigated. The results are statistically analysed using analysis of variance (ANOVA) to determine the contribution of cutting parameters on investigated hole quality parameters. The evaluation of drilling performance is based on results for, average thrust force, average torque, average surface roughness, average entry and exit burr height and burr thickness, average hole size, average circularity error and drilling damage around the borehole surface using optical and scanning electron microscopy techniques.

4.2 Results and Discussion

4.2.1 Cutting forces analysis

Figure 4.1 shows a schematic of thrust force and torque profiles respectively when drilling a hole using a spindle speed of n = 3000 rpm and a feed rate of f = 900 mm/min. The drilling process can be divided into three stages according to the chisel edge position with respect to the workpiece. Initially the cutting tool is not in contact with the workpiece and no forces are recorded. Next the cutting tool advances into the workpiece and cutting forces increases rapildy due to the continous cutting tool-workpiece contact (entry stage). At this stage the chisel edge of the cutting tool is not entirely inside the workpiece. The increase in cutting force continues until the chisel edge of the cutting tool becomes fully engaged with the workpiece. The thrust force and torque profiles remains almost constant during this stage and maximum cutting forces are observed. This steady state cutting forces period of cutting action contributes to the major proportion of total thrust force and torque of the drilling process [29, 46, 125]. The fluctuations were found to increase with spindle speed. Once the cutting tool reaches the bottom of the workpiece, the thrust force and torque falls sharply indicating the end of steady state and entering what is known as the(exit stage) similar to the entry stage which is the completion of hole drilling process.
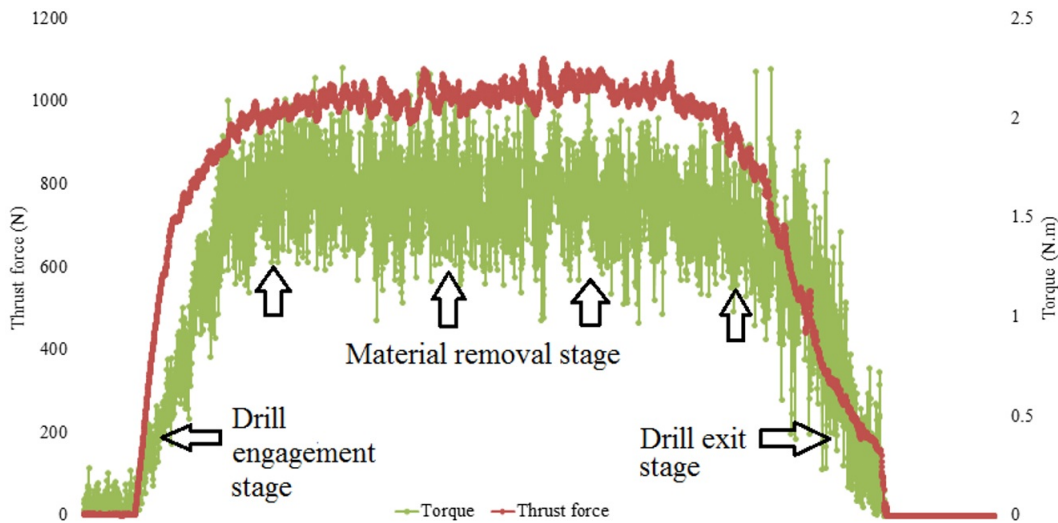
Figure 4.1: Thrust force and torque profiles in drilling Al2024-T3 (n = 3000 rpm and f= 900 mm/min) [310]

Figure 4.2 shows the influence of feed rate and spindle speed on thrust force and torque when drilling Al2024-T3 workpiece.
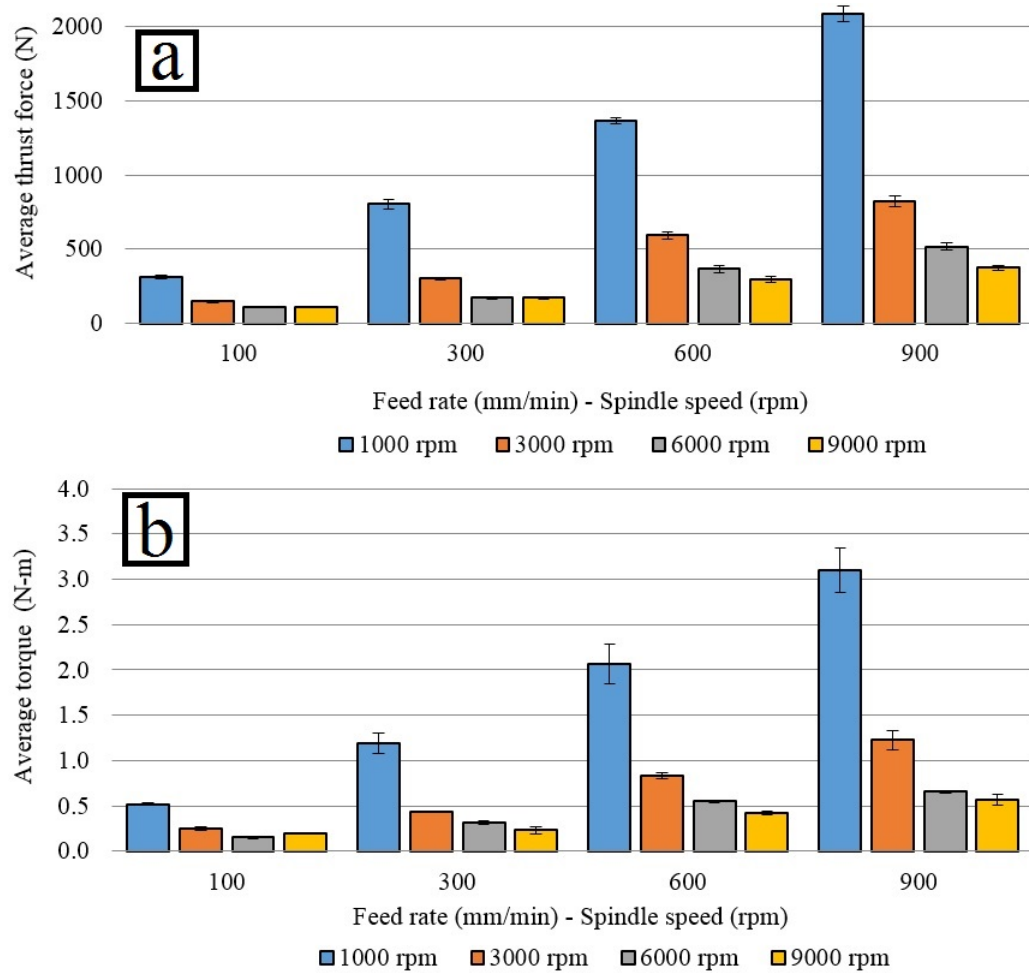
Figure 4.2: Average (a) thrust force (b) torque under different cutting conditions in Al2024-T3 [310]

Results show that the thrust force and torque increased with the increase of the feed rate and decreased with the increase of the spindle speed. The impact of the spindle speed on cutting forces was more dominant than the feed rate. The minimum thrust force was recorded when drilling at a feed rate of f= 100 mm/min and spindle speed of n= 9000 rpm. The maximum thrust forces was recorded at f= 900 mm/min and n= 1000 rpm, while the lowest torque occurred when drilling at a feed rate of f= 100 mm/min and spindle speed of n= 6000 rpm, which indicates that excessive spindle speed might increase the torque due to increased friction and vibrations of the drill. The maximum torque was obtained at f= 900 mm/min and n= 1000 rpm. It was also observed that drilling at feed rate and spindle speed combinations of 0.1 mm/rev (100/1000, 300/3000, 600/6000 and 900/9000), thrust force reduced by 4.7 % when drilling at (f= 300 mm/rev, n= 3000 rpm) compared to drilling

at (f= 100 mm/rev, n= 1000 rpm). However, drilling at (f= 600 mm/rev, n= 6000 rpm) increased cutting forces by 22-26 % compared to drilling at (f= 300 mm/rev, n= 3000 rpm). While drilling at highest feed rate and spindle speed of (f= 900 mm/rev, n= 9000 rpm) increased cutting forces by 2-3 % compared to the previous level. This clearly indicates that increasing the productivity of the drilling process would results in higher cutting forces.

Previous literature reported that the feed rate was the major contributor on increasing the cutting forces than the spindle speed [68, 188, 323]. However in the current work, it has been found the spindle speed is the dominant parameter that influences the thrust force and torque during drilling of Al2024-T3 alloy as it can be seen from the ANOVA table as shown in Table 4.1. This could be due to the lower range of cutting parameters used in those previous studies and shorter drilling periods. Table 4.1 summarises the percentage contribution of spindle speed, feed rate and their interaction on the cutting forces and hole quality parameters. Statistical analysis using ANOVA showed that for thrust force results, the spindle speed had the highest contribution of 48.368 % followed by feed rate with 32.038 %, the interaction of cutting parameters had a small effect of about 19.407 %. Similarly, for the torque, the spindle speed was more dominant with 50.847 % while the contribution of the feed rate was 29.302 % and 17.868 % for their interaction.

Table 4.1: Percentage contribution of cutting parameters on analysed factors using ANOVA in Al2024-T3 [310]

	Percentage contribution (%)			
	Spindle speed	**Feed rate**	**Spindle speed x Feed rate**	**Error**
Thrust force	48.368	32.038	19.407	0.186
Torque	50.847	29.302	17.868	1.984
Surface roughness	19.972	30.198	47.679	2.151
Bur height at entrance	25.831	31.841	21.656	20.672
Burr height at exit	26.896	33.153	29.836	10.115
Burr root thickness at entrance	22.433	21.707	17.176	38.684
Burr root thickness at exit	41.412	33.641	20.841	4.106
Hole size at top	Insignificant	Insignificant	Insignificant	63.285
Hole size at bottom	Insignificant	Insignificant	Insignificant	72.493
Hole circularity at top	Insignificant	Insignificant	Insignificant	49.858
Hole circularity at bottom	Insignificant	Insignificant	Insignificant	68.087

4.2.2   Surface roughness analysis

Figure 4.3 shows the average hole surface roughness R_a under different spindle speeds and feed rates. The surface roughness ranged from 1.159 to 7.96 μmm and was minimal when

drilling at at n= 3000 rpm and f= 600 mm/min, and maximal at n= 1000 rpm and n= 900 mm/min.
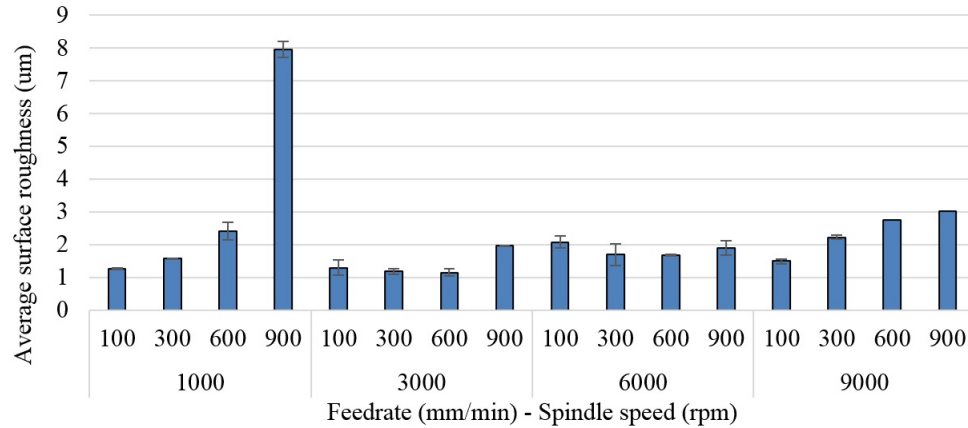
Figure 4.3: Average surface roughness in Al2024-T3 drilling trials in Al2024-T3 [310]

Generally, hole surface roughness increased with the increase of both cuting parmaters. The continuous rubbing of the drill against the borehole walls rises the temperatures in the cutting zone which increases the ductility and deformations of the workpiece material and further increase to surface roughness. The impact of the feed rate varied at different cutting conditions. For example, the surface roughness increased with the increase of the feed rate when drilling at n= 1000 and 9000 rpm. The surface roughness decreased with the increase of the feed rate at n= 3000 and n= 6000 rpm with exception of drilling at f= 900 mm/min. The influence of spindle speed on surface roughness was more signficant than the feed rate as shown previously in the ANOVA analysis in Table 4.1. The percentage contribution of the spindle speed was approximatley 19.97 % while the contribution of the feed rate was around 30.2 %. The interaction of cutting parmaters also had a significant contribution of about 47.68 %. It was also observed that drilling at feed rate/spindle speed combinations of 0.1 mm/rev tended to increase the surface roughness despite reducing the machining time, which indicates that increasing hole drilling productivity would compromise the surface quality of the hole. The surface roughness results acquired in this study are comparable to reported range of surface roughness results in the previous literature on drilling operation of Al2024-T3 alloy (1 to 3.5 µm) using similar cutting parameters and cutting tool size [75, 144, 159].

4.2.3 Burr formation analysis

Figure 4.4 shows the average burr height and burr root thickness at the hole entry and exit sides under different cutting parameters. Results indicate that both burr parameters

increased with the increase of the feed rate, and decreased with the increase of the spindle speed when drilling at n= 1000, 3000 and 6000 rpm, while they both increased with the increase of the feed rate when drilling at n= 9000 rpm. This is because burr height greatly depends on the workpiece material properties such that the higher the material ductility the greater the burr height [324]. In addition, increasing the spindle speed increases the temperatures at the cutting zone between the tool and the workpiece which increases the plastic deformation of the alloy and therefore, leading to an increase in burr height [54].
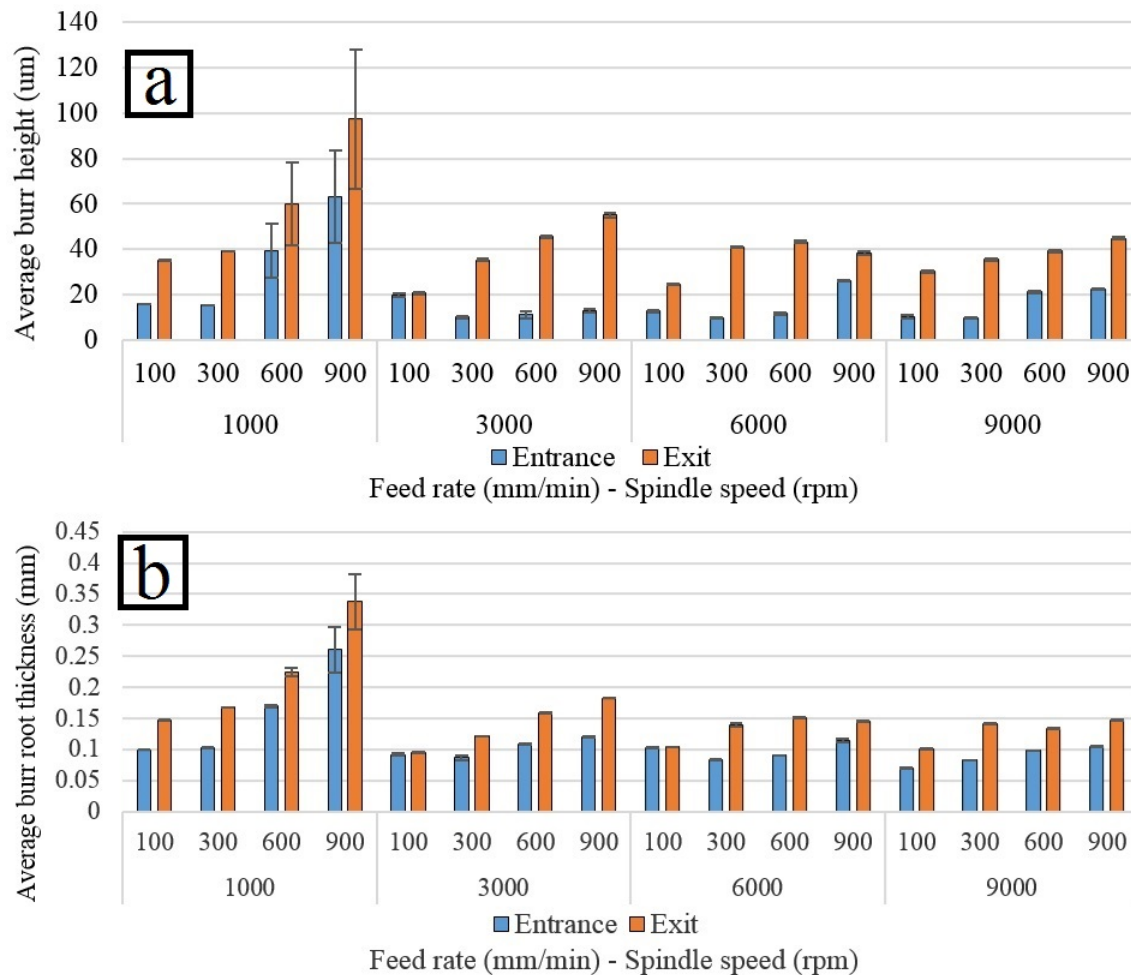
Figure 4.4: Average burr (a) height (b) burr thickness at entrance and exit in Al2024-T3 drilling trials in Al2024-T3 [310]

The results of burr height were comparable to previously reported literature on drilling Al2024-T3 alloy individually and in composite-metal stacks using CVD diamond drills [63, 189]. Moreover, the observed burr height was smaller than previously reported results on drilling Al2024-T3 alloy under comparable cutting parameters but using 8, 10 and 12 mm uncoated HSS drill [158]. This could be due to the influence of TiAlN coating of the cutting tools used in the current research and the smaller drill bit size. Coated cutting tools have

lower coefficient of friction than uncoated ones which limits the rise in cutting temperatures that trigger diffusion and prevents the migration of tool atoms to the chips [325].

The impact of the feed rate was more dominant than the spindle speed on the average burr height at both sides as shown previously in Table 4.1. The contribution of the spindle speed on burr height ranged between 25.831 % and 26.896 %, and between 22.433 % and 44.412 % for burr root thickness. The contribution of the feed rate on burr height ranged between 31.841 % and 31.153 %, between 21.707 % and 33.641 % for burr root thickness. The interaction of both cutting parameters had a significant contribution which ranged from 17176 % to 20.841 % for both burr parameters. Burr height at exit side was 2-3 times greater than at entrance side as it can be seen from Figure 4.5. This is because the contribution of the spindle speed, the feed rate and their interaction becomes more significant at the exit side of the hole due to the increased ductility and deformations with depth which increases burr formations considerably. Results also showed that drilling at a high spindle speed and a low
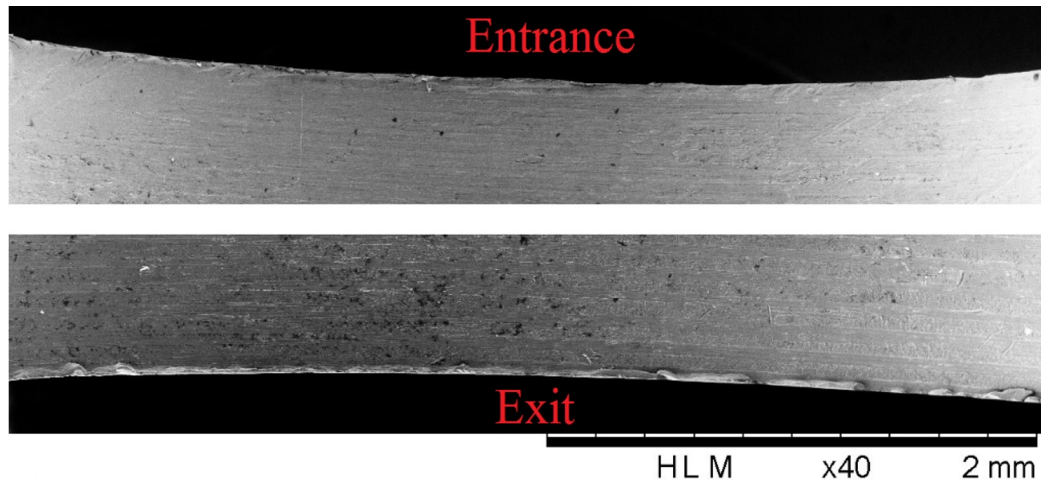
Figure 4.5: SEM image showing hole edges at entrance and exit of drilled hole at n=1000 rpm and f= 100 mm/min in Al2024-T3 [310]

feed rates produced smaller burrs on both sides, which could indicate that burr formation can be minimised when drilling under those conditions. Al2024-T3 alloy has a relatively high percentage of elongation, this directly affects the burr formation since the amount of plastic deformation is governed by the ductility of the material and its elongation [158]. Therefore, higher spindle speeds and feed rates can cause higher burr formation. The smallest burr height at hole entrance was achieved when drilling at n= 6000 rpm and f= 3000 mm/min, whereas the smallest burr height at exit was achieved when drilling at n= 3000 rpm and f= 1000 mm/min.

4.2.4   Hole size and circularity error analysis

Figure 4.6 shows the average hole size and circularity error under different cutting parameters. Oversized holes were produced at both investigated locations through the hole depth with similar results reported by Abdelhafeez et al. [63]. The hole oversize at the top was greater than at the bottom at f= 300, 600 mm/min and n= 3000, 6000, 9000 rpm which could suggest the possibility of drill wander on contact with the workpiece [63]. The top hole size decreased with the increase of the feed rate at f= 100, 300 and 600 mm/min at spindle speeds of n= 1000 and 3000 rpm, and increased with the increase of the feed rate from f= 100 to 900 mm/min at n= 6000 and 9000 rpm. The hole oversize at bottom location generally decreased with the increase of the feed rate when drilling at f= 100, 300, 600 mm/min and increased thereafter. This indicates that excessive rotation or feeding of the cutting tool might cause the hole to deviate from its nominal diameter. This might be difficulty of machining aluminium alloys under dry conditions due to their high thermal expansion coefficient compared to other metals. The continuous rubbing of the drill on the borehole walls could lead to the accumulation of hot chips and the expansion of the cutting tool/workpiece materials creating thermal distortions that influence the accuracy of the machined hole [30]. The hole oversize ranged between 0.712 to 40.32 µm. The minimum deviation in hole size was acquired when drilling at n= 3000 rpm and f= 600 mm/min. The analysis of ANOVA showed that the cutting parameters and their interactions had no impact on hole size and circularity error at the entrance, which was also reported by previous research studies on drilling Al2024-T3 alloy [63, 65, 189].

The error from the ANOVA analysis was large for hole size and circularity error, which indicates that the model is not capable of detecting the contribution of the cutting parameters and higher order models should be employed to further analyse the results which will be carried out in future work. The circularity error at top increased with the increase of the feed rate when drilling at n=3000, while it decreased with the increase of the feed rate at n=1000 and 9000 rpm. At the bottom, hole circularity error increased with the increase of the feed rate at n= 3000, 6000 rpm while it decreased with it at n= 1000 rpm. This could be due to the vibratory displacement in the cutting tool which causes dynamic instability which occurs more commonly at hole entry leading to larger hole circularity error at the top than at the bottom [76]. For feed rates and spindle speeds combinations which gives a feed rate of 0.1 mm/rev (100/1000, 300/3000, 600/6000, 900/9000), it was observed that circularity error at both sides improved or remained unaffected with the reduction of drilling time. Generally, the hole circularity error ranged between 6.92 to 27.26 µm at the top and between 4.1 to 33.84 µm at the bottom.
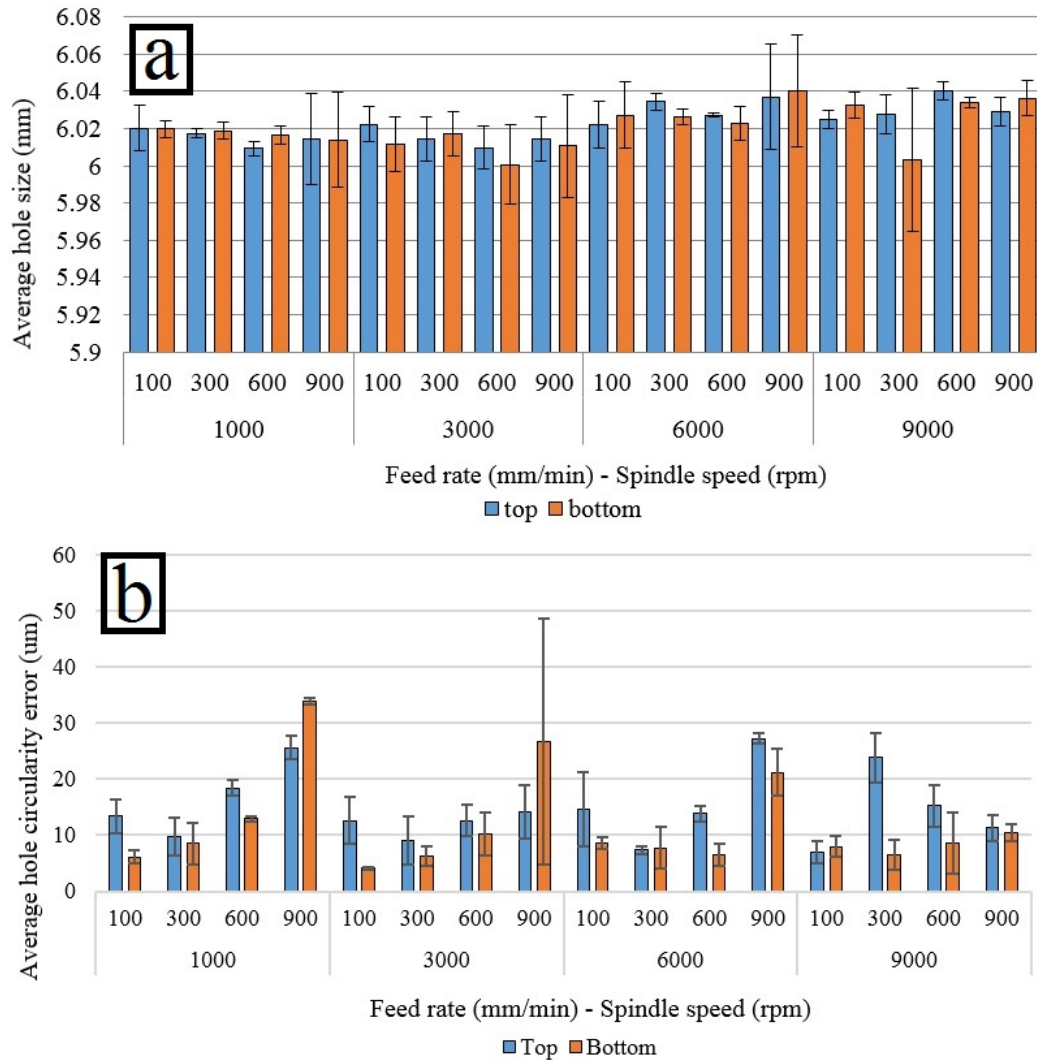
Figure 4.6: Average (a) hole size and (b) circularity error at top and bottom in Al2024-T3 [310]

4.2.5   Chip formation and post machining hardness analysis

Figure 4.7 shows samples of chips collected after drilling each hole under tested spindle speeds and feed rates. The chip formation analysis here is based on the description of the types of chip formation reported by Singal et al. [326]. It was observed that a wide range of chip thickness and lengths were formed depending on the level of cutting parameters. The chip thickness increased with the increase of the feed rate and decreased with the increase of spindle speed. The chip length decreased with the increase of the feed rate and increased with the increase of spindle speed. Short conical helical chips were formed when drilling at n= 1000 rpm and f= 100 mm/min, also at n= 3000 rpm and f= 900 mm/min. Long conical helical chips were formed when drilling at at n= 6000 rpm and f= 100 mm/min.

Loose arc chips were formed when drilling at n= 1000 rpm and f= 300 mm/min, at n= 3000 rpm and f= 600 mm/min, at n= 6000 rpm and f= 600,900 mm/min, and at n= 9000 rpm and f= 900 mm/min. Elemental chips were formed at n= 1000 rpm and f= 900 mm/min which is a sign of excessive feeding into the workpiece. Connected arc chips were formed when drilling at n= 6000 rpm and f= 300 mm/min, and at n= 3000 rpm and f= 100,300 mm/min. Lamellar chips were at n= 9000 rpm and f= 300, 600 mm/min and at n= 1000 rpm and f= 600 mm/min . Lamellar chips are a type of continuous chips which occur due to repeated inhomogeneous material flow at the cutting tool-workpice interface [327]. Long ribbon chips were formed at n= 9000 rpm and f= 100 mm/min.
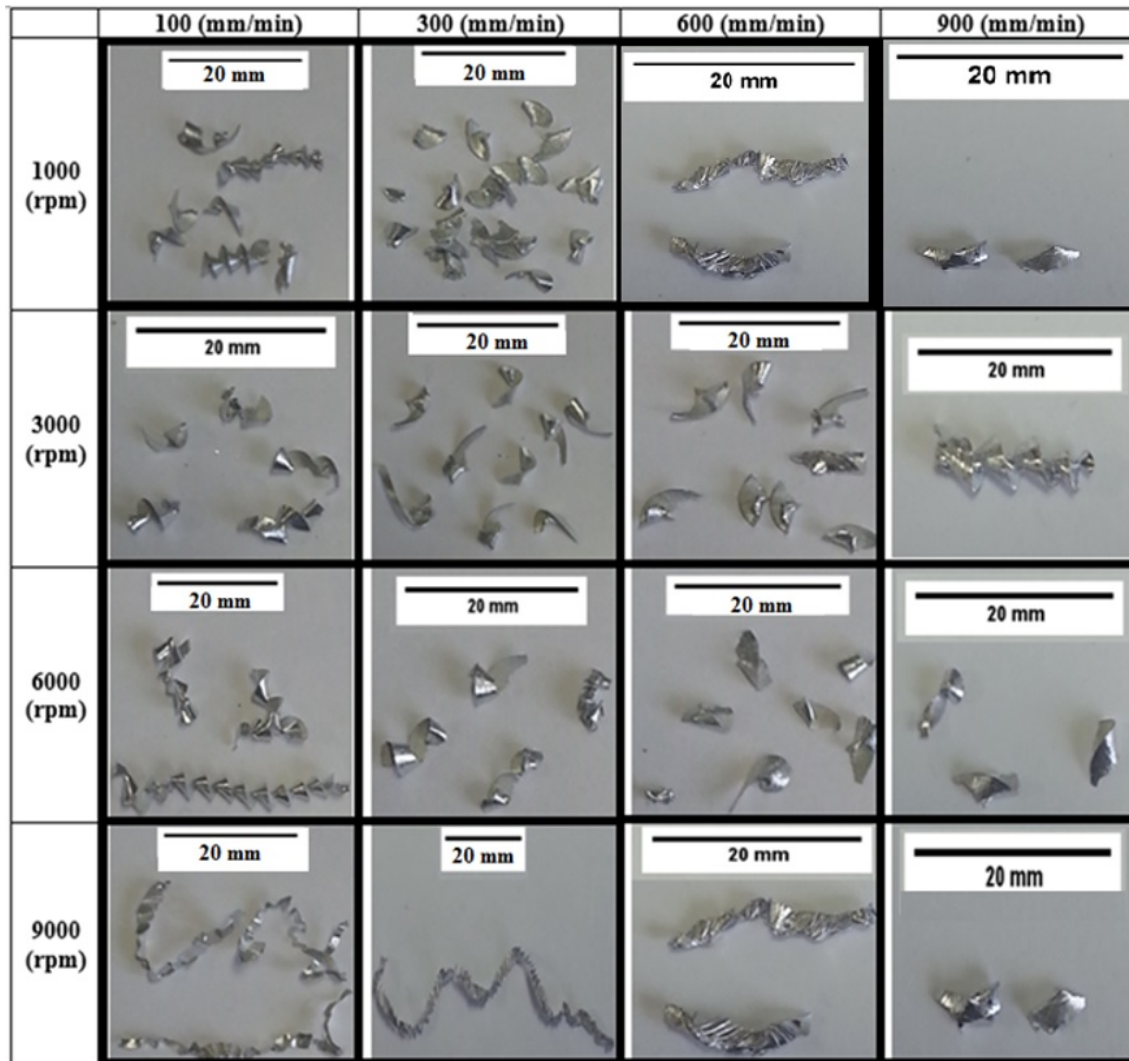
Figure 4.7: Chip formation under different cutting conditions in Al2024-T3 [310]

Regardless of their type, the chips formed at n= 6000, 9000 rpm and f= 100 mm/min, and n=9000 rpm and f= 300 mm/min were long, continuous and tended to curl around the drill shank which required manual removal. Those chips seemed to promote built up

edge on the cutting tools since it was found that Al2024-T3 particles adhered to the cutting tool facets and cutting edges. The formation of built-up edges is generally undesirable as it ends to reduce the machined surface quality and tool life [37]. The change of chip length could be due to the increase in workpiece ductility as machining temperatures rise with the increase of spindle speed. Figure 4.8 shows the post-machining microhardness at the top and bottom surfaces for each drilled hole. The increase in workpiece hardness can lead to excessive tool wear and brittleness of the workpiece material which makes it more vulnerable to damage in applications where impact and fatigue are present. The hardness increased at both sides after drilling the holes, the hardness ranged between 155 and 172 HV, which is 13 %-25.5 % increase from its typical hardness value of 137 HV. It was also found that hardness increased with the increase of spindle speed and feed rate which agrees with previous reported studies [328]. Also, the variation in microhardness of the upper and lower surfaces of the workpiece was minor with the exception of few drilled holes which indicates that the change in microhardness of the workpiece remained constant with depth.
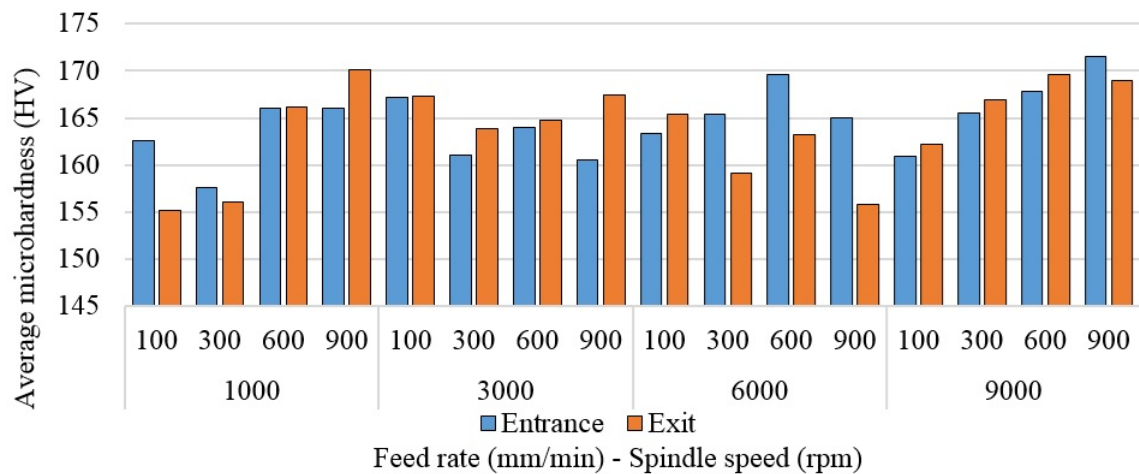
Figure 4.8: Average post-machining microhardness at entrance and exit sides in Al2024-T3 [310]

4.2.6   Hole surface inspection under optical microscopy

Figure 4.9 and Figure 4.10 show the condition of machined holes of the first drilling trial under different cutting parameters at entry and exit sides, respectively. The visual and optical inspection of the holes showed that the condition of hole surface was better at the entry than at the exit side. In addition, the hole quality at both sides seemed to decrease with the increase of the feed rate. Drilling at at n= 3000 and 6000 rpm and f= 100 mm/min gave the best hole quality among others. At those cutting parameters the edges of the hole were more uniform and with very little burr and discontinuities. Drilling at at high spindle

speeds and low feed rates tended to improve the condition of the hole at the exit side due
to the reduce feed feed force/chip load.
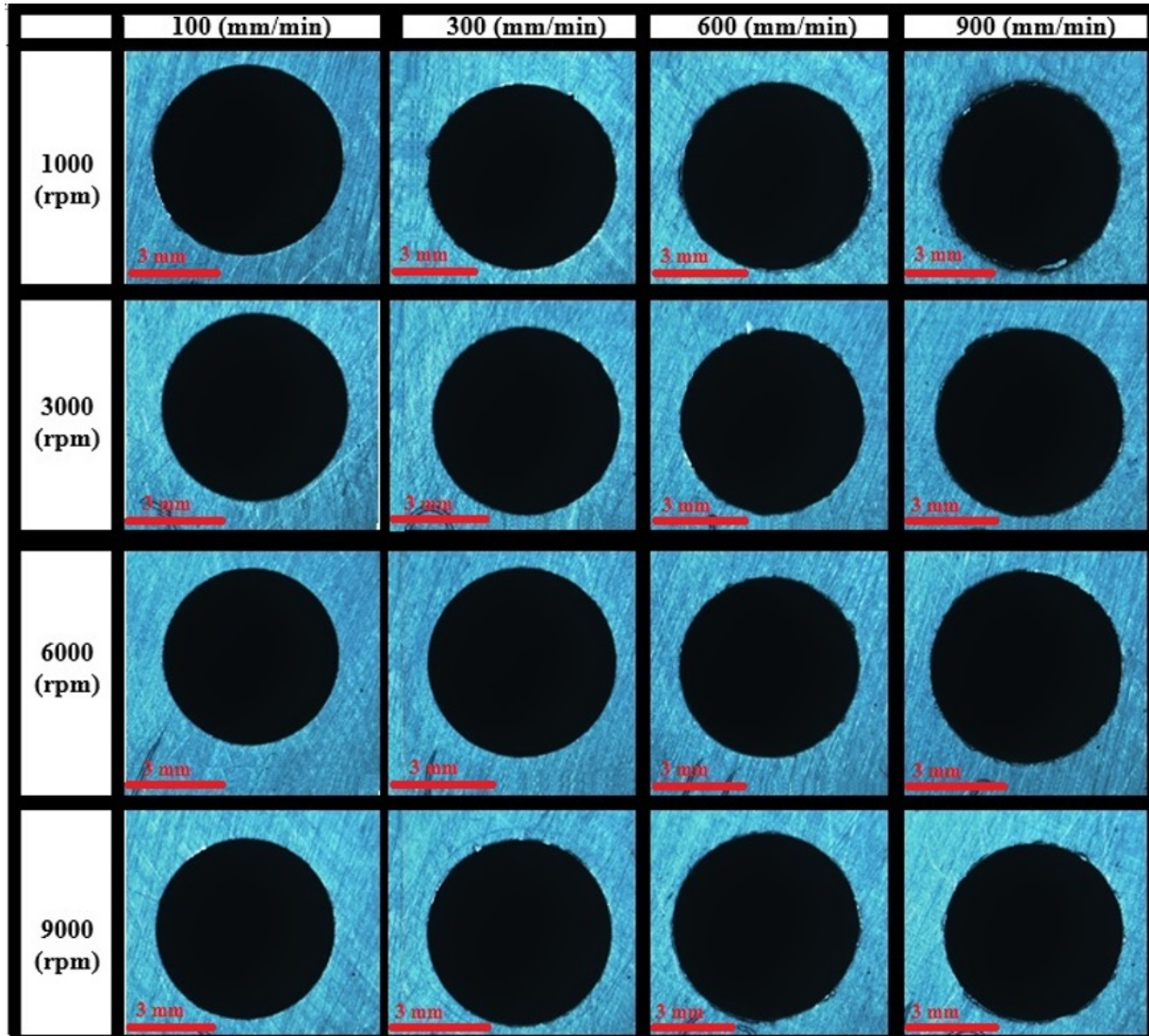
Figure 4.9: top side of drilled holes in Al2024-T3 in Al2024-T3 [310]
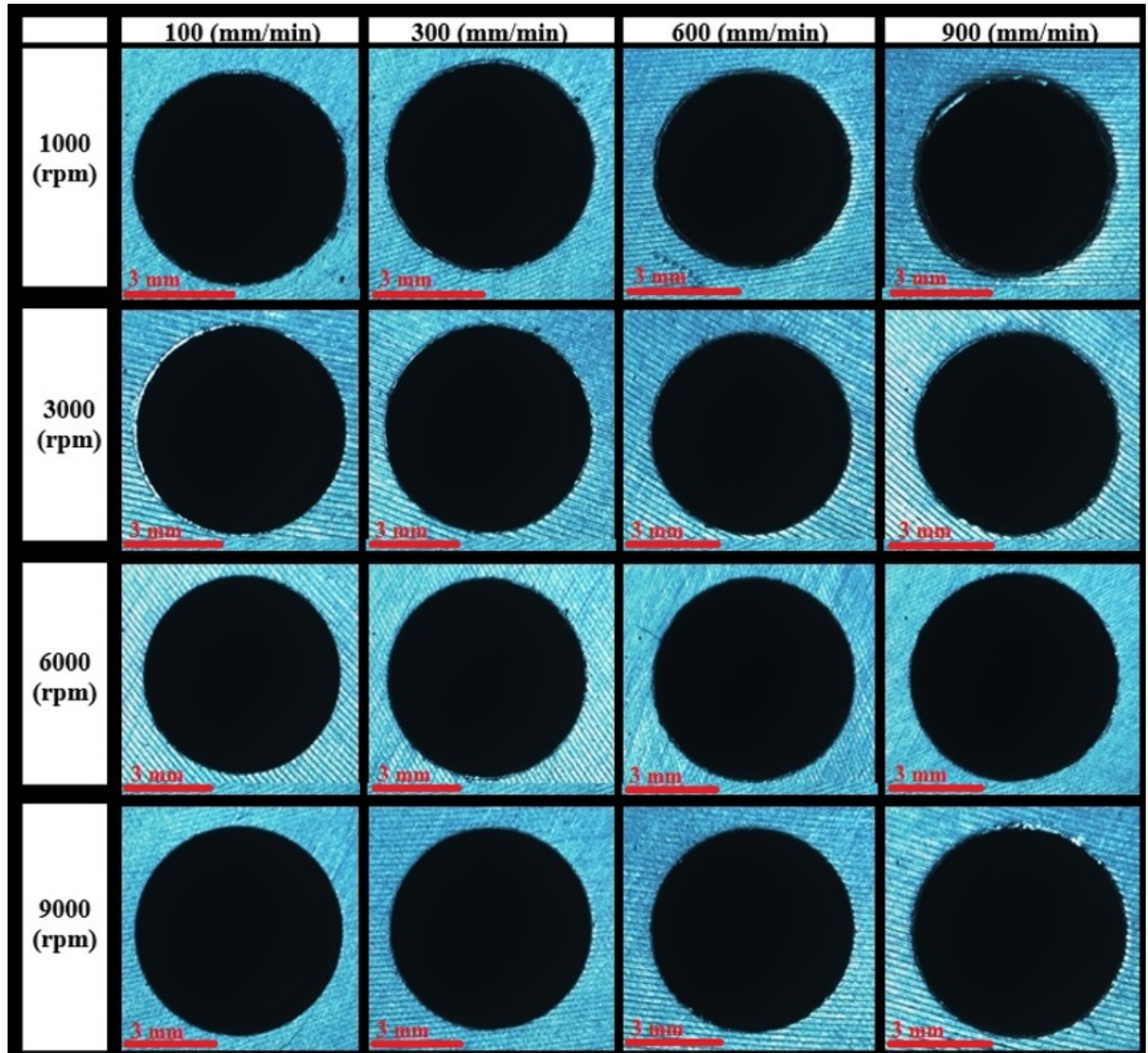
Figure 4.10: bottom side of drilled holes in Al2024-T3 in Al2024-T3 [310]

4.2.7 Post machining cutting tool inspection

Figure 4.11 presents a comparison of the condition of one of the cutting tools after drilling in Al2024-T3. Inspecting the tool used for Al2024-T3 drilling trials under the microscope showed high levels of built up edge (BUE) on the cutting edges of the drill. This indicates that interaction between the cutting tool and chip of the workpiece undergo severe friction which caused it to weld on several regions on the cutting tool (see Figure 4.11.a). It can also be noticed that the BUE continued to spread along the cutting edges away from the chisel edge, adhesion was also found on the chisel edge, the flanks and the crater of the drill, the Al2024-T3 chips melted and were deposited creating a thin layer on the cutting tool surface, which could have an impact on the surface finish and reduce hole size accuracy. The use of high spindle speeds and feed rates might be the cause of BUE and adhesions on the cutting tools, thus, it is always recommended to avoid excessive feed or speeds in machining.
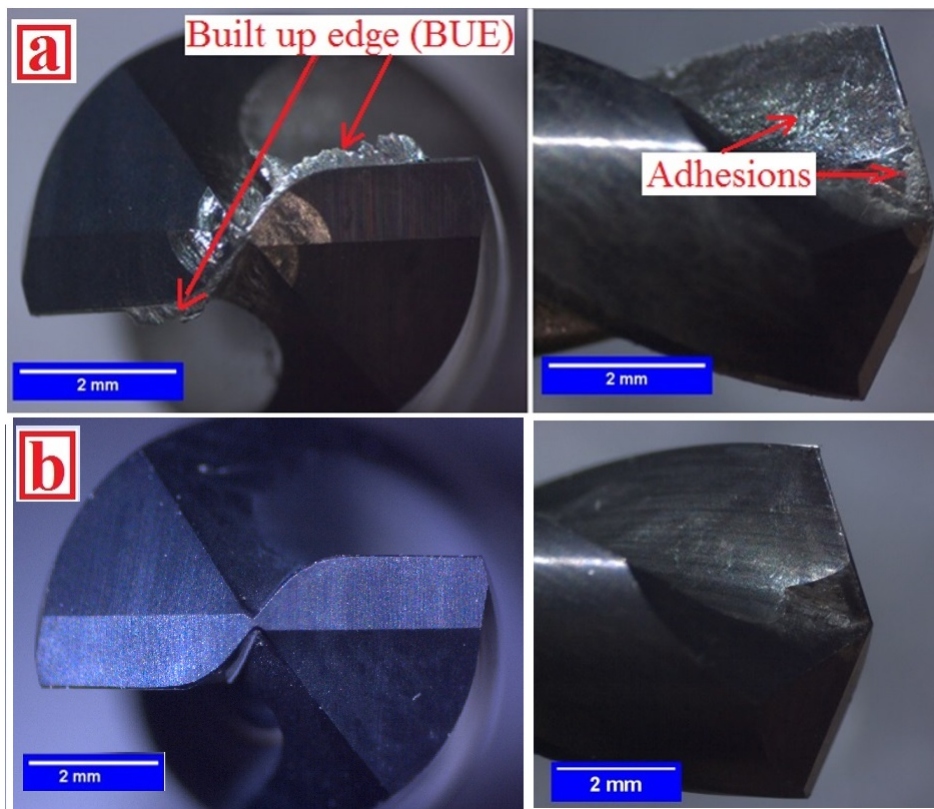
Figure 4.11: Built up edge and adhesion in cutting tools (a) Al2024-T3 (b) GLARE 2B 11/10 [310]

4.2.8   Scanning electron microscopy analysis

Figure 4.12 shows an image of machined borehole surface under SEM. The inspection of the internal hole surfaces indicated that the surface quality decreased with the increase of both cutting parameters which could be due to the increase in the cutting temperatures of the cutting tool-workpiece interface with the increase of the spindle speed, and increased chip/load deformations with the increase of the feed rate. Aluminium alloys have a strong alloying tendency and chemical reactivity with materials in the cutting tools at tool operating temperatures. The cutting tool tended to leave feed marks in the shape of spiral profile on the machined hole surface. The feed marks were observed at the upper part of some of the holes (See Figure 4.12). The size of the feed marks increased with the increase of the feed rate and showed a spiral path around the circumference of the hole. Higher feed rates produced deeper and longer feed marks which resulted in a rough finish which might have considerably influenced the accuracy and the surface finish of machined holes.
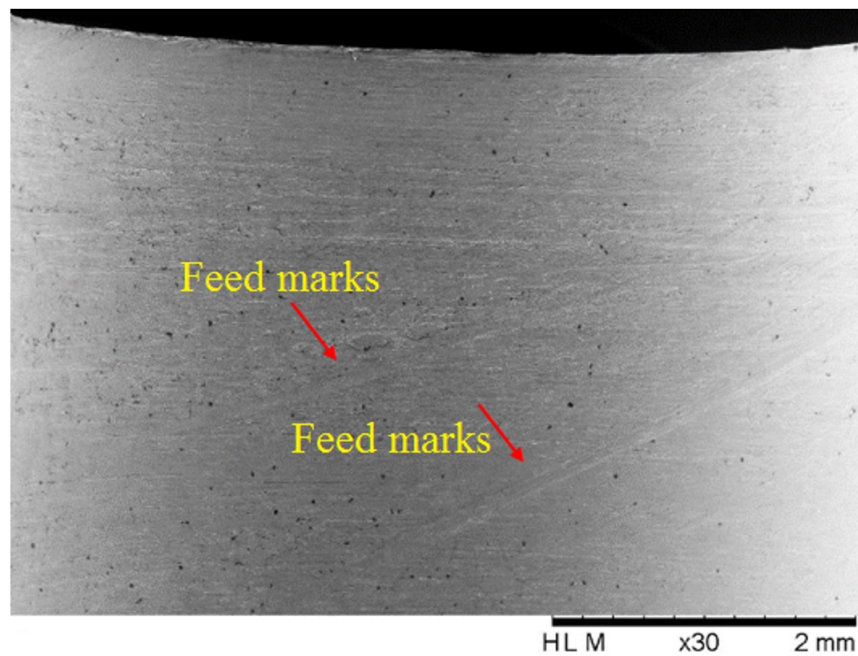
Figure 4.12: Inside hole surface condition under SEM microscopy in Al2024-T3 showing feed marks (spiral lines) [310]

Smearing was observed in all drilled holes as shown in Figure 4.13. Smearing increased with the increase of the spindle speed and the feed rate. This could be due to the increase in cutting temperatures and feed force which increases the flowing and deformations in Al2024-T3 surface during the machining process as reported earlier. No visible cracks were found on the surface under all cutting conditions. However, drilling at a spindle speed of n= 1000 rpm and feed rates of f= 600 and 900 mm/min showed severe deformations within the

hole walls and some chipping as shown in Figure 4.14, which indicates that those cutting parameters are not suitable for drilling Al2024-T3 alloy. It was also observed that the feed marks and deformations were less pronounced on the lower part of the hole (above the hole exit) rather than the upper part (below the hole entry). This could be due to the increased ductility and flow of the material with depth due to the increase in cutting temperatures which improves the cutting process and give better surface finish. Some black spots were observed on the machined surfaces as shown in Figure 4.15. The spots had various sizes and are known as hot spot/pitting spots which developed due to heat accumulation during machining under high cutting speeds.
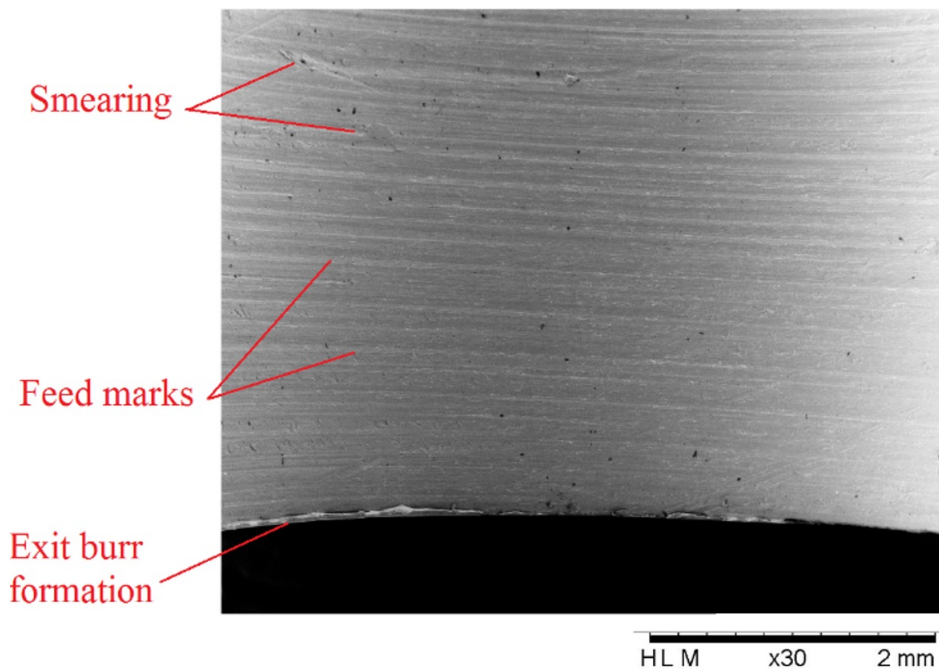
Figure 4.13: Hole surface condition under SEM microscopy (n= 1000 rpm, f= 100 mm/min) in Al2024-T3 [310]
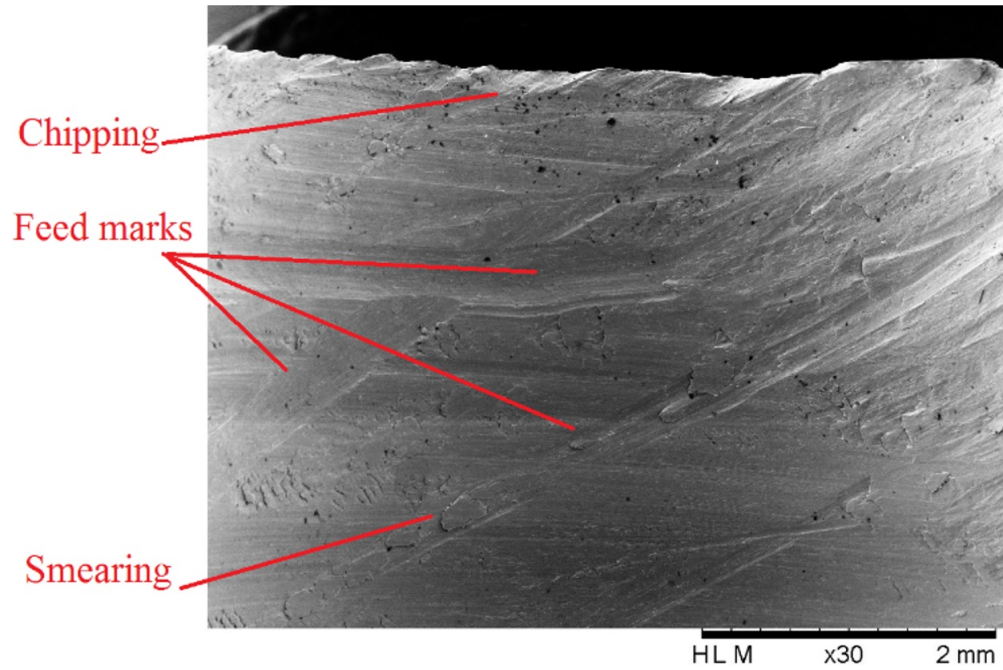
Figure 4.14: Poor hole surface condition under SEM microscopy (n= 1000 rpm, f= 600 mm/min) in Al2024-T3 drilling trials [310]
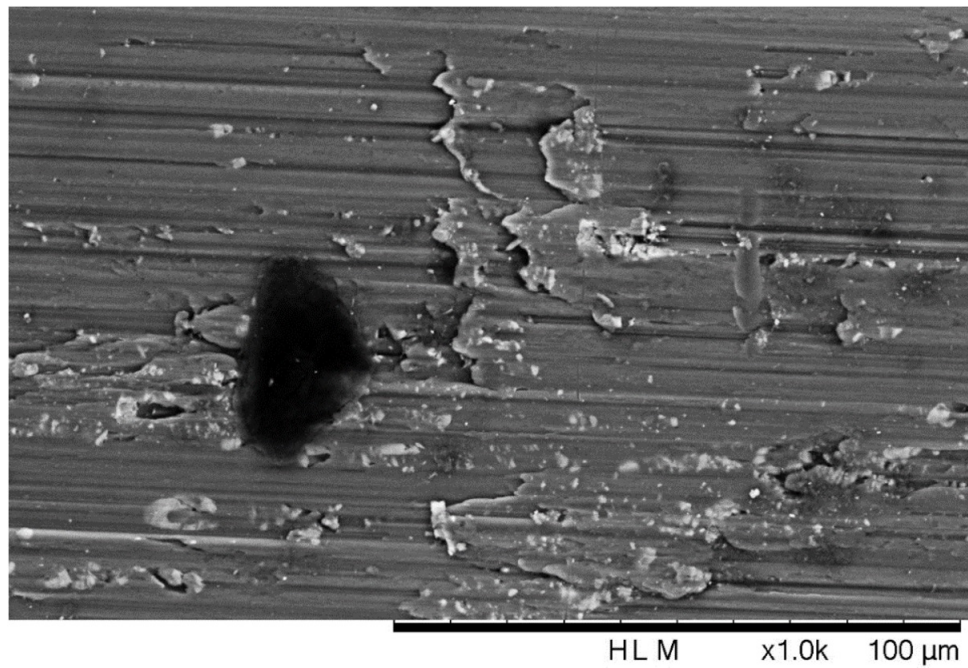
Figure 4.15: Pitting spot in drilled hole in Al2024-T3 (n= 1000 rpm, f= 100 mm/min) [310]

4.3 Concluding Remarks

The research on drilling of Al2024-T3 was mainly motivated by the major study in the current research on drilling GLARE fibre metal laminates. The aim is to draw some of the similarities and differences in their machinability since the alloy makes up the metallic part of the laminate. The study was also motivated by the fact that in most of the earlier scientific research, the cutting speeds used were below n= 5000 rpm and using fewer combinations of cutting parameters. Moreover, only a handful of studies used coated 6 mm drill diameter in their experiments which only investigated a limited number of hole quality parameters rather than a complete study. In this chapter, an experimental investigation of drilling aluminium Al2024-T3 alloy have been carried out to evaluate the effect of the spindle speed and feed rate on the cutting forces and hole quality. The experiments have been carried out under a wide spectrum of cutting parameters beyond those used in previous studies on drilling Al202-T3 aluminium alloy. The application of full factorial design and ANOVA have been employed to determine the impact of machining parameters on cutting forces and the inspected hole quality parameters. The evaluation includes inspecting the surface roughness, hole size, circularity error, entry and exit burrs, chip formations and damage in the borehole walls at the micro level (chipping, adhesions, cracks) using scanning electron microscopy. The following conclusions are drawn from the dry drilling trials of Al2024-T3 aluminium alloy:

- Both cutting parameters had a significant influence on the thrust force and torque. Increasing the feed rate increased the cutting forces while increasing the spindle speed reduced them. The spindle speed was the dominant factor on the reduction of cutting forces (48.36 % and 50.84 %) for thrust force and torque, respectively, while their interaction had a significant contribution of 17.8-19.5 %.

- The average surface roughness ranged from 1.1 to 3 μm (with the exception of holes drilled at n= 1000 rpm and f= 600 and 900 mm/min). Surface roughness increased with the increase of spindle speed and the feed rate, the influence of feed rate on surface roughness was greater than the spindle speed evidenced by the higher percentage of contribution.

- Burr height and burr root thickness increased with the increase of the feed rate, while the spindle speed had a different influence depending on its level. The spindle speed was more dominant than the feed rate on burr thickness while feed rate was more dominant on burr height. The burr height ranged from 9.5 to 26 μm at entry and from 35 to 55 55 μm at the exit. The burr thickness ranged from 70 to 170 μm at

entry and from 95 to 167 µm at the exit.

- All holes drilled in Al2024-T3 workpiece were oversized. The hole oversize increased with depth and ranged from 0.7 to 40 µm. Drilling at high spindle speeds and low feed rates can considerably influence the hole size.

- Feed rate and spindle speed had a different influence on circularity error depending on the combination of cutting parameters used. The circularity error at top and bottom increased with the increase of feed rate when drilling at n= 3000, 6000 rpm, while it decreased with feed rate at n= 1000 and 9000 rpm.

- An increase in workpiece microhardness was observed in all holes which ranged from 13 % to 25.5 % from its normal hardness value of 137 HV.

- Microhardness increased with spindle speed and feed rate and the variation of hardness between entrance and exit sides was negligible with the exception of few drilled holes.

- Various chips lengths and thickness were formed at different cutting parameters. The formation of long chips was observed at high spindle speeds and low feed rates, such chips are undesirable as they curl around the cutting tool and could deteriorate the machined hole quality.

Chapter 5

PERFORMANCE EVALUATION OF CONVENTIONAL DRY DRILLING OF GLARE

This chapter presents an evaluation of the drilling performance of two different grades of GLARE (2B and 3) under dry drilling conditions. The methodology of the drilling trials was previously described in chapter 3. Drilling trials for Glare 2B will be carried out for three different thicknesses while one thickness of GLARE 3 will be used. In Sections 5.2.1 through 5.2.11, the effects of machining parameters (spindle speed and feed rate) on cutting forces and hole quality will be investigated. Comparisons will be carried out in order to develop a basic understanding of the effect of fibre orientation and workpiece thickness on the surface integrity of machined GLARE laminates. In addition, the results are statistically analysed using analysis of variance (ANOVA) to determine the contribution of cutting parameters on investigated hole quality parameters. Finally, the effect of cutting parameters, fibre orientation and workpiece thickness on drilling performance of GLARE are discussed based on the achieved results. The evaluation of drilling performance is based on results for, average thrust force, average torque, average surface roughness, average entry and exit burr height and burr thickness, average hole size, average circularity error and damage described at the macro level (delamination area) and at the micro level (fibre matrix debonding, chipping, adhesions, cracks).

5.1 Results and discussion

5.1.1 Cutting forces analysis

Figure 5.1 shows the cutting forces profiles for a hole drilled in GLARE 2B 11/10-0.4 laminate. The variation in the magnitude of cutting forces is observed when the drill cuts through aluminium sheets and glass fibre layers. The thrust force and torque profiles when the drill cuts through the aluminium sheets [1-11] can be clearly distinguished from the cutting forces profiles generated when the drill cuts through the glass fibre layers [1-10]. The magnitude of cutting forces required to drill through aluminium sheets were greater than those required for drilling through glass fibre layers. This agrees with previously reported studies on drilling GLARE and composite-metal stacks [68, 145, 189, 193, 194]. The dissimilar generated cutting forces magnitudes and profiles for drilling through the aluminium sheets and glass fibre layers is due to the difference in their mechanical properties. The young modulus of aluminium is 31 % higher than that of glass fibre (in loading direction) and nine times higher than that of glass fibres in other directions. Also, the shear modulus of aluminium Al2024-T3 alloy is higher than the shear modulus of glass fibre layers which means that amount of cutting force required to cut through aluminium sheets is greater than those required to cut through glass fibre layers.

Initially, the thrust force and torque increase steadily with depth once the cutting tool enters into the workpiece and continues to increase until the chisel edge of the drill is in full contact with the workpiece (see 5.1). Next, the cutting forces remain constant through the thickness of each aluminium sheet and glass fibre layer (point 2 to 10). When the drill reaches the last aluminium sheet and glass fibre layer, the cutting forces decrease due to reduced workpiece resistance to the drill feed force (see point 11). Finally, when the drill cuts through the last aluminium sheet while exiting the workpiece, the cutting forces drop down rapidly until they reach zero (after point 11) indicating the end of the drilling process. Cyclic cutting forces are observed when cutting through the unidirectional glass fibre laminates as shown Figure 5.2 which is an illustration of the torque profile for one of the drilled holes in GLARE 3 showing variation when the drill cuts through different layers of aluminium and glass fibre. It was also observed that the thrust force in the first and last aluminium and glass fibre layers were lower than the remaining ones. When the chisel edge starts to engage with the first aluminium sheet the cutting tool is not in full contact with the workpiece and lower cutting forces are recorded. Similar results are observed when the cutting tool exits the workpiece from below.
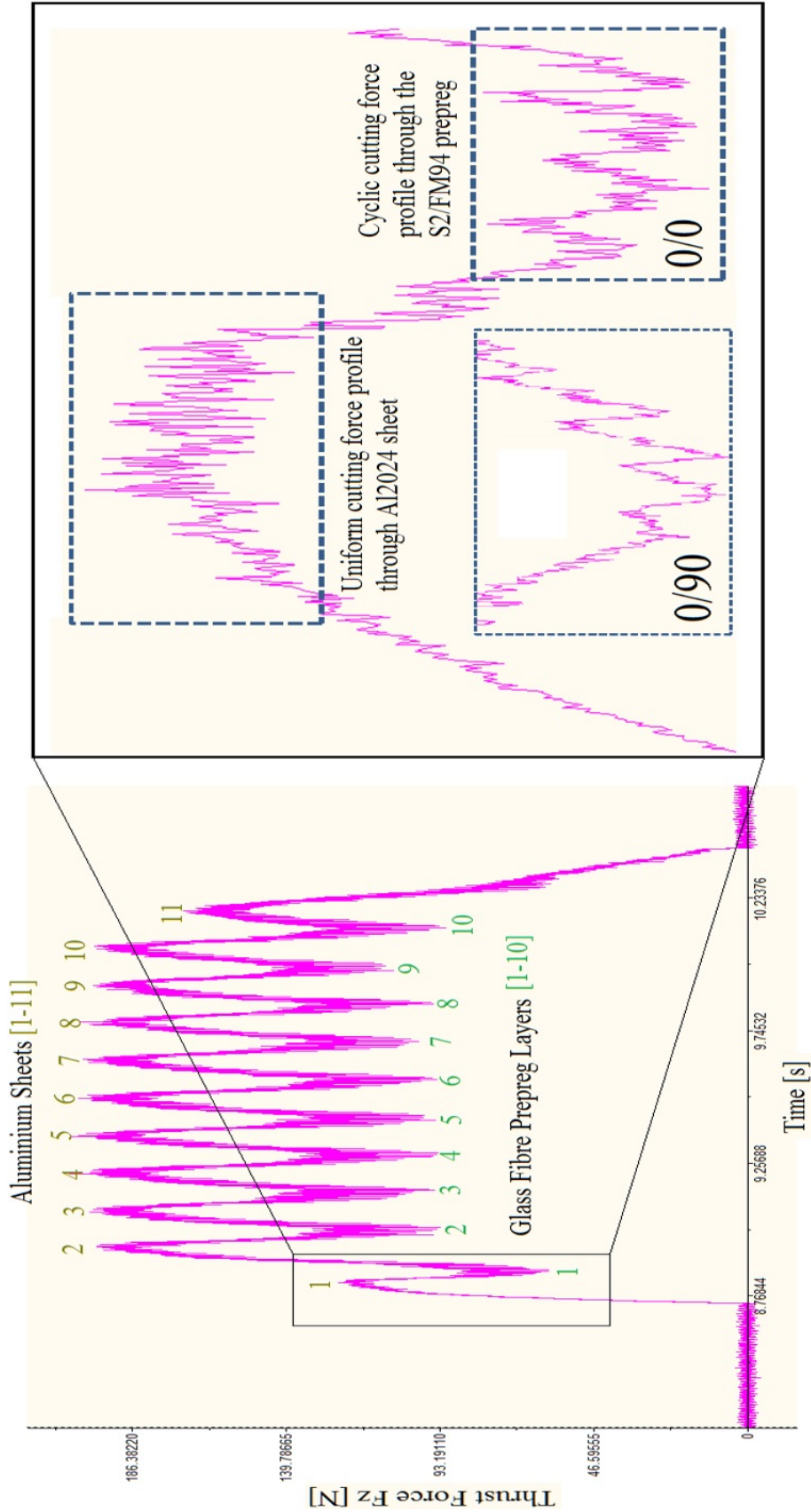
Figure 5.1: Thrust force profile when drilling GLARE 2B 11/10-0.4 at Spindle speed of 3000 rpm and feed rate of 300 mm/min [190]
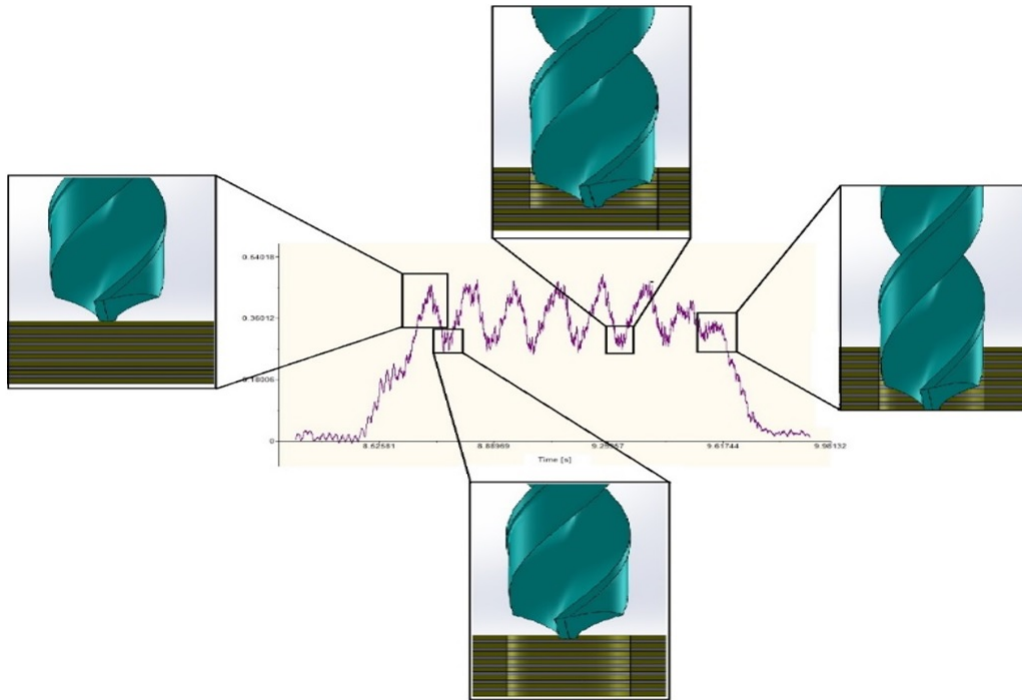
Figure 5.2: Torque profile at 3000 rpm and 300 mm/min showing the position of cutting tool at different depths for GLARE 3 8/7-0.4 [190]

The influence of ply orientation on cutting forces

Previous studies on machining composites showed that ply orientation can influence the dynamics of the machining process which could impact the quality of the machined part. Machining angular layers is easier than machining unidirectional ones [126]. The effect of fibre orientation was investigated in many studies and it is well known that the mechanical properties of composites are dependent on the fibre orientation. The way in which the fibres are cut can influence the cutting forces and surface roughness [114, 329]. Previous studies showed that delamination and fibre pull out are more likely to occur at specific angles between the cutting direction and fibre orientation [114, 330, 331]. The severity in fibre pull-out is more likely to be higher when fibres are oriented at 90° or 135° especially at the exit side of the drilled hole [332]. Drilling GFRP layups with fibres oriented at 0° or 90° was found to reduce thrust force [113, 333]. The fluctuation in cutting forces primarily depends on the fibre orientation which is highly related to the chip formation mode occurring when cutting in the particular fibre orientation [29].

In drilling GLARE, however, there was no clear effect on the degree of cutting forces fluctuations with ply orientation on cutting forces. The average and maximum thrust force and

torque for the two investigated grades were almost identical. The small thickness of the glass fibre layers in GLARE could be insufficient to cause a substantial impact on cutting forces. Figure 5.3 shows cutting force profiles for two drilled holes in GLARE comparing the layers oriented at $0°/90°$ and $0°/0°$ for GLARE 3 and 2B, respectively. The thrust force profiles of both grades match well with each other.
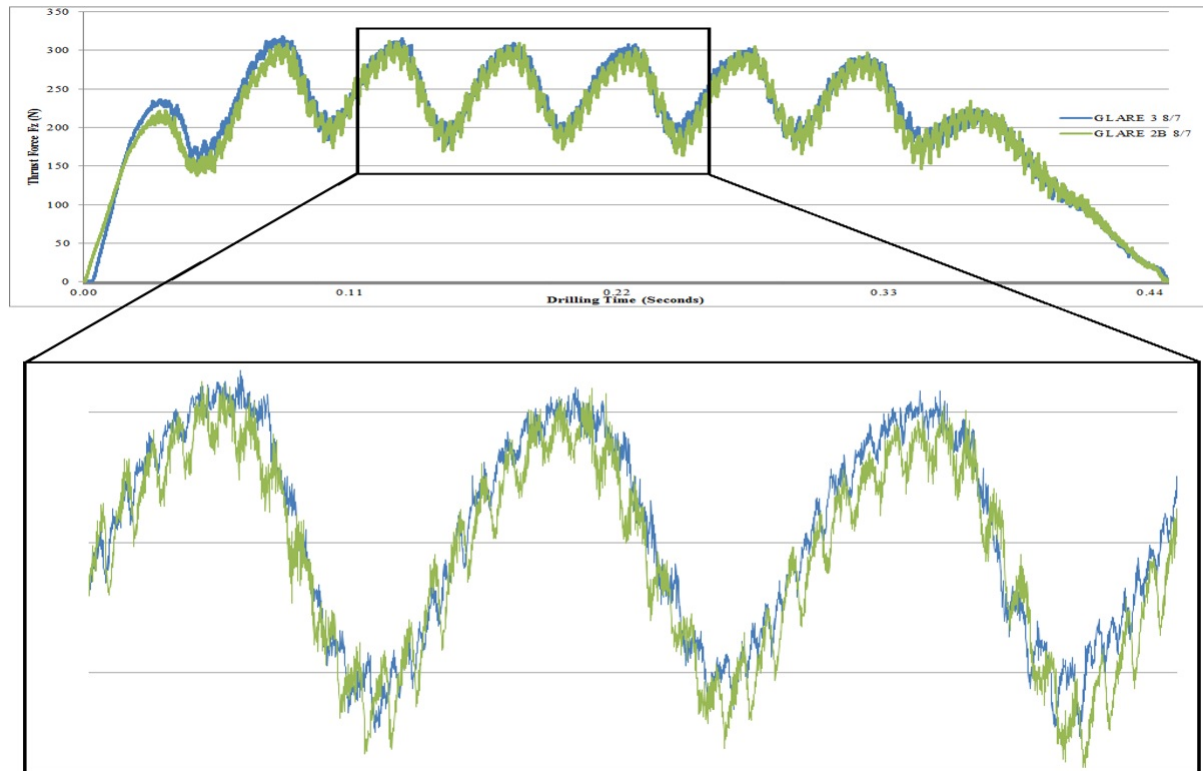
Figure 5.3: Typical representation of cutting force profiles for GLARE 3 and 2B showing the S2/FM94 layers [190]

Figure 5.4 shows a comparison of the average thrust force and torque for two grades of GLARE (2B and 3) under different spindle speeds and feed rates. The results show that the ply orientation did not have a significant effect on thrust force under all cutting parameters. However, it was observed that the magnitude of torque was generally higher in GLARE 2B than in GLARE 3 under the same cutting parameters with few exceptions. For example torque was higher in GLARE 3 than in GLARE 2B when drilling at n= 1000 rpm and f= 600 and 900 mm/min. It was previously reported that the amplitude of thrust force and torque are primarily dependent on fibre orientation. The thrust force significantly decreases when drilling cross ply and quasi-isotropic laminates [29] such as the case in GLARE 3 $(0°/90°)$ which could explain the slightly higher thrust force found in GLARE 2B $(0°/90°)$. The cyclic pattern in the cutting forces profiles is due to the change in the mode of chip formation [29] as the presence of $90°$ plies in the propagation plane appears to form an

obstacle to the propagation of delamination [334], which could explain the slight increase in torque in GLARE 2B than GLARE 3.
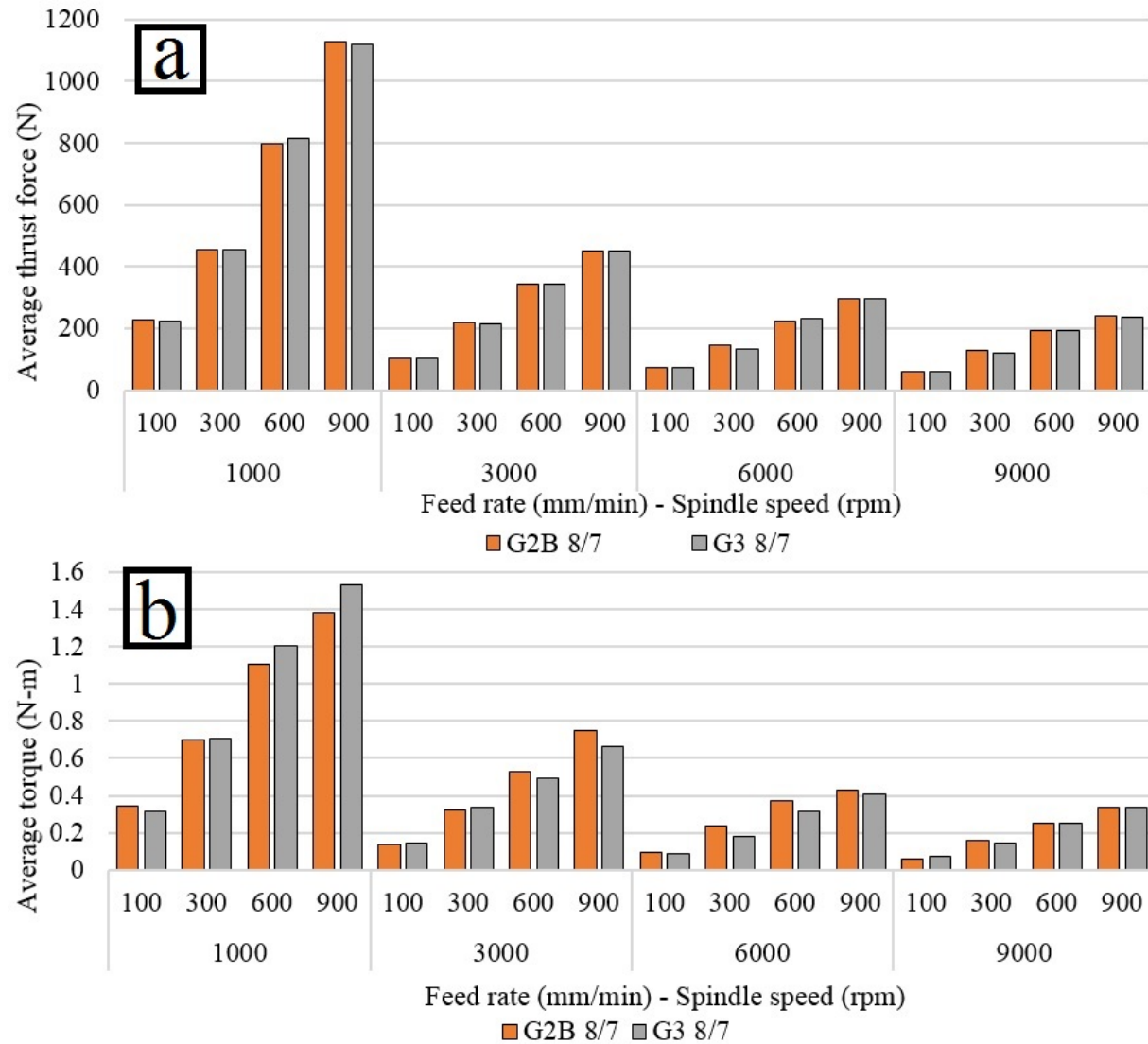
Figure 5.4: Average mean (a) thrust force (b) torque for different GLARE grades

The influence of workpiece thickness on cutting forces

Figure 5.5 shows the influence of the laminate thickness in GLARE 2B on thrust force and torque. Both cutting forces increased with the increase of workpiece thickness. The increase in drilling depth could cause improper conditions of chip evacuation and increased heat which would in return increase the cutting forces [130]. The change of hole depth is more pronounced on the torque than on the thrust force due to the elastic recovery of the cylindrical surface of the hole. The surface of the cutting tool is continuously subjected to

normal stresses while drilling through the workpiece. The greater the surface area means larger forces will be acting on the periphery of the drill leading to significant increase in torque [335]. It was also observed that the time period-although very small-required to reach maximum cutting force decreased with the increase of the workpiece thickness. The reduction in workpiece thickness was accompanied by a substantial out of plane bending during drilling as shown in Figure 5.6, which could indicate that bending deformations are more likely to occur in thin laminates especially with the lack of a support plate beneath the laminate.
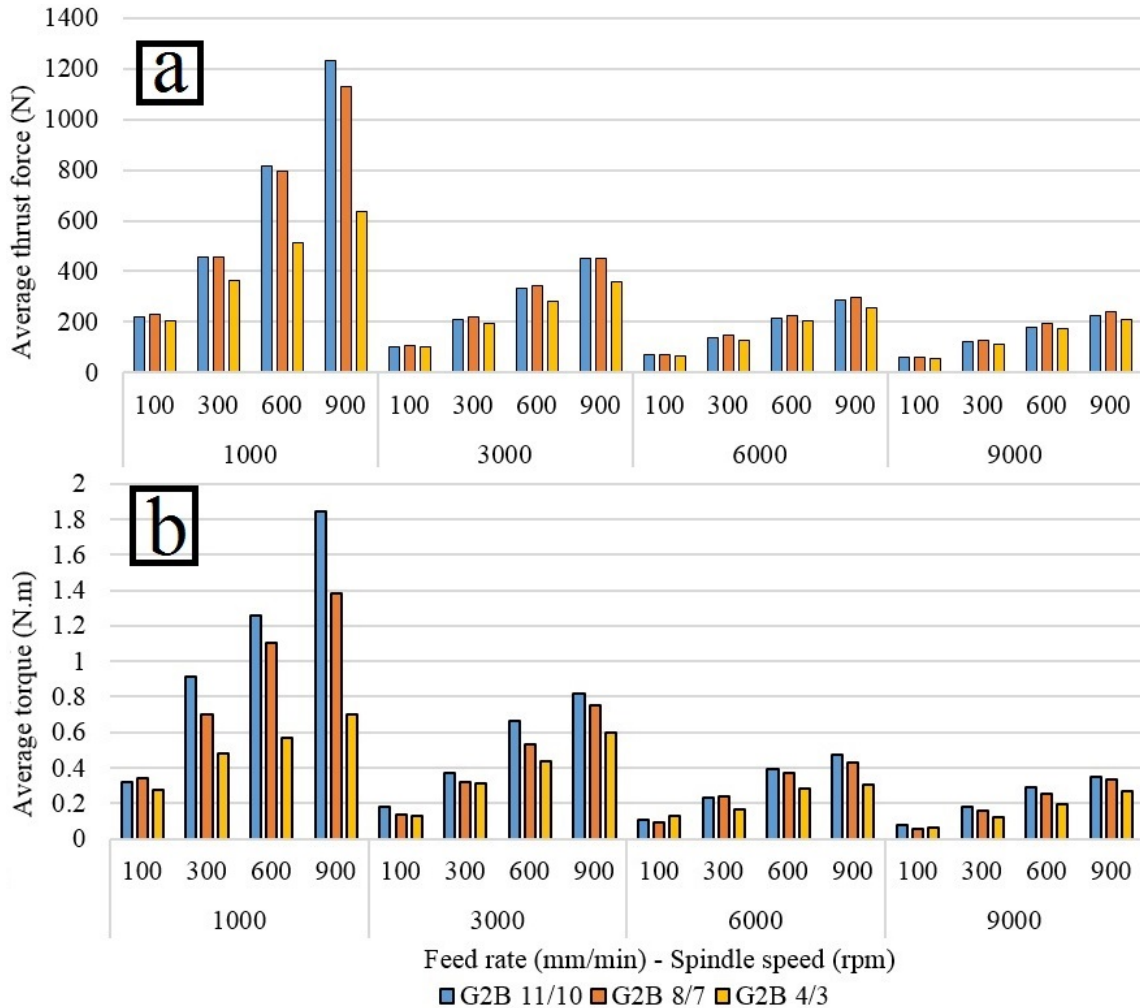
Figure 5.5: Average mean (a) thrust force (b) torque for different GLARE grades and thicknesses [190, 311]
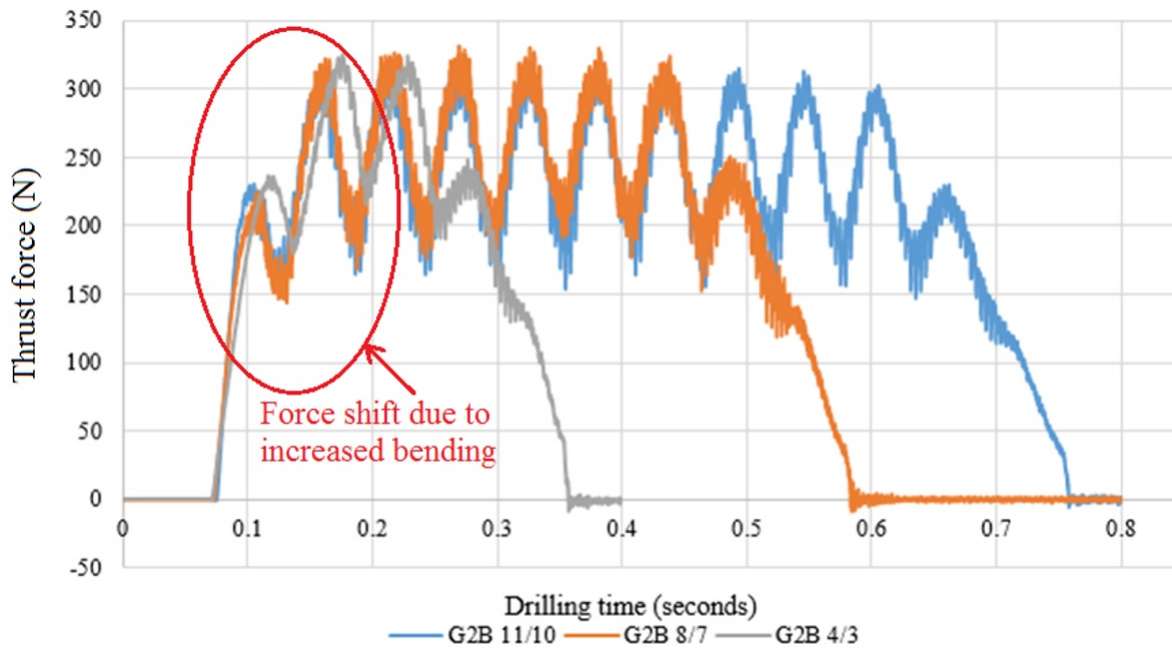
Figure 5.6: Thrust force profiles for different GLARE thickness of the same grade

The influence of cutting parameters on cutting forces

Figure 5.7 shows thrust force profiles of holes drilled in GLARE 2B 11/10 under different spindle speeds and feed rates. Drilling at n= 1000 rpm , the maximum thrust force can reach up to 700 N when drilling through aluminium sheets and up to 450 N when cutting through glass fibre layers (see Figure 5.6). The reduction in thrust force becomes negligible when drilling at n= 9000 and 6000 rpm (see Figure 5.6 b) which indicates excessive rotation of the cutting tool that could cause premature wear and chatter. The difference is roughly around 200-300 N. The difference in thrust force between aluminium and glass fibre becomes smaller when increasing the spindle speed. It is well known that increasing the spindle speed increases the temperatures at the cutting zone which, in return, would increase the ductility of the aluminium sheets and softens the epoxy matrix of glass fibre layers, therefore reducing the forces required to cut through the material. This indicates that increasing the spindle speed could have a greater influence on aluminium sheets than that on glass fibre layers during the drilling process. Reducing the spindle speed relative to the feed rate could prevent the cutting tool from having enough time to cut through the material properly and therefore, forcing the flutes to take off too much material. Forcing the cutting tool into the material rather than cutting it properly will considerably increase the cutting forces and deformation in the hole as it was seen when drilling at feed rates of f= 600 and 900 mm/min and spindle speed of n= 1000 rpm. For this combination of feed rate and spindle speed,

the drilled holes were severely damaged, the aluminium sheets were highly deformed and pulled upwards at entry and pushed downward at the exit. Loose fibres were clearly visible especially at the entrance and exit.
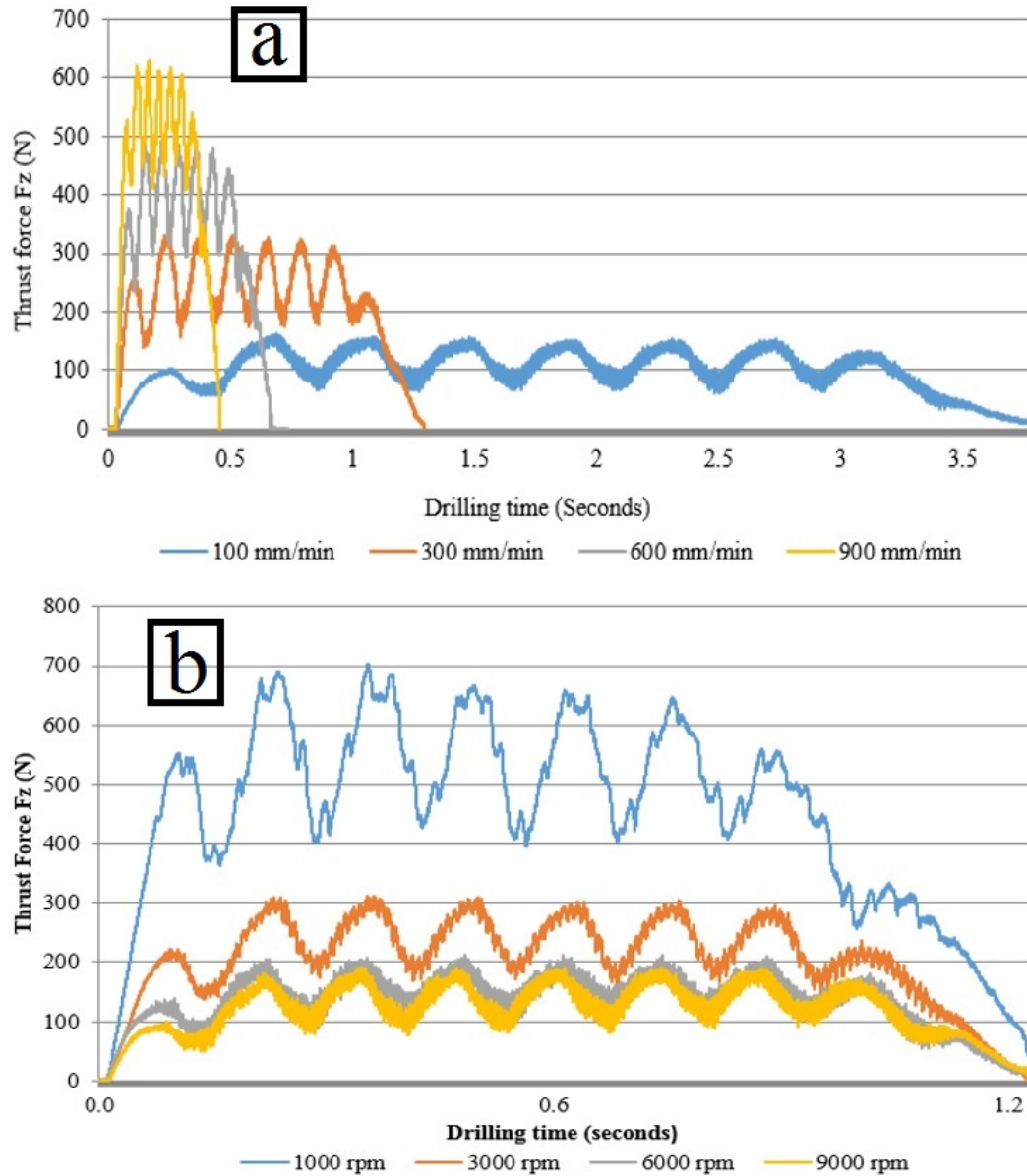
Figure 5.7: Typical representation of thrust force for GLARE 2B 11/10-0.4 (a) at 3000 rpm and various feed rates (b) at 300 mm/min and different spindle speeds

Feeding too much into the workpiece caused high chip load and the cutting tool to push through the laminate layers without allowing sufficient time to cut through properly as shown in Figure 5.8. It was also observed that the higher the feed rate the larger is the deformed area in the upper and lower aluminium as shown in Figure 5.9. The white circle around the hole is related to the light reflection from the microscope lights, which shows

the region at which the metal sheet start to pull out from the laminate, forming a conical frustum shape around the hole centre.
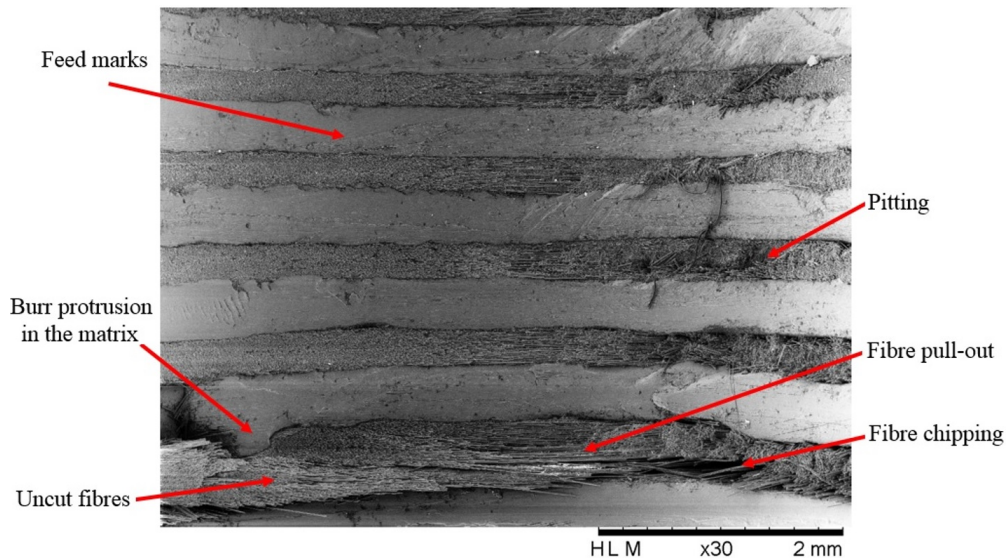
Figure 5.8: SEM image of hole quality in GLARE 2B 11/10 at f= 900 mm/min and n= 1000 rpm
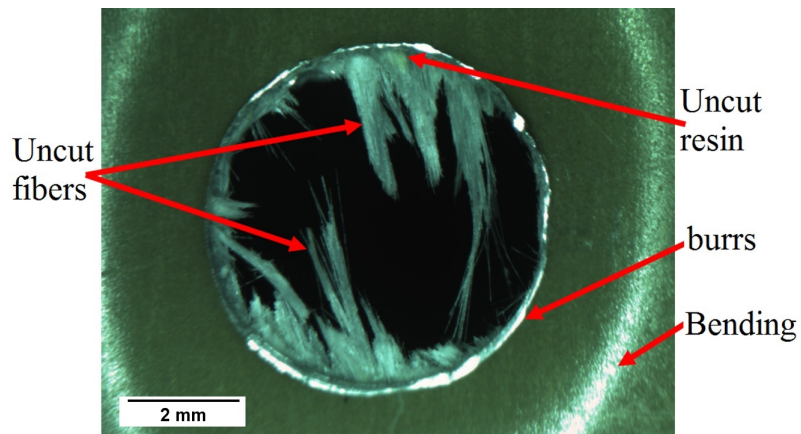
Figure 5.9: Optical image of hole quality in GLARE 2B 4/3 at f= 900 mm/min, and n= 1000 rpm

The results indicate that the spindle speed and feed rate had a significant impact on the cutting forces. Thrust force and torque increased with the increase of feed rate and decreased with the increase of spindle speed. This is because increasing the feed rate increases the unit cutting thickness of workpiece material and therefore increases the amount of forces required while increasing the spindle speed reduces the uncut thickness and increases the heat at the cutting zone, which softens the workpiece constituents and reduces their resistance to the cutting process. This could also be due to the increase of friction between the tool and

workpiece with the increase of the feed rate [336]. The lowest thrust force was recorded when drilling at a spindle speed of n= 9000 rpm and a feed rate of n= 100 mm/min. The highest thrust force and torque were recorded when drilling at 1000/600 and 1000/900 feed rate/spindle speed combinations. ANOVA results from the full factorial analysis show that the contribution of the feed rate on cutting forces was greater than that of the spindle speed. The percentage contribution of each parameter obtained from ANOVA analysis was used to illustrate the effect of cutting parameters on cutting forces for different GLARE grades and thicknesses as shown in Table 5.1. The results show that both cutting parameters had a significant contribution to the cutting force. The influence of the spindle speed on cutting forces was more significant than that of the feed rate and ranged between 51-54 % while the feed contribution ranged between 30-40 %. The interaction of both parameters seemed to have a significant influence which ranged between 6-18.6 %.

Table 5.1: Percentage contribution results for thrust force and torque of different grades of GLARE

	G 2B 11/10		G 2B 8/7		G2B 4/3		G3 8/7	
Cutting forces	Fz	Mz	Fz	Mz	Fz	Mz	Fz	Mz
Spindle speed	51.2	52.0	52.0	52.2	53.95	51.12	52.2	54.2
Feed rate	30.2	31.2	31.9	34.4	38.85	40.13	31.98	30.6
Spindle speed* Feed rate	18.6	14.44	15.9	10	6.33	6.0	15.76	13.35
Error	0.021	2.34	0.175	3.33	0.87	2.7	0.030	1.79

Figure 5.10 shows the state of the entry and exit sides of the drilled holes from the first drilling set of GLARE 2B 11/10-0.4. The visual and optical microscopy investigation showed the absence of loose fibres and damage within the glass fibre layers around the wall of the drilled holes. The only exception was when drilling at a spindle speed of n= 1000 rpm and feed rates of f= 600 and 900 mm/min. For that combination of feed rates and spindle speed, the drilled holes were severely damaged, the aluminium sheets were deformed and loose fibres were clearly visible especially at the entrance and exit. This indicates that feeding too much into the workpiece caused high chip load and the cutting tool to push through the laminate layers without allowing sufficient time to cut through properly The quality of the holes at the exit side were worse than at its entry.
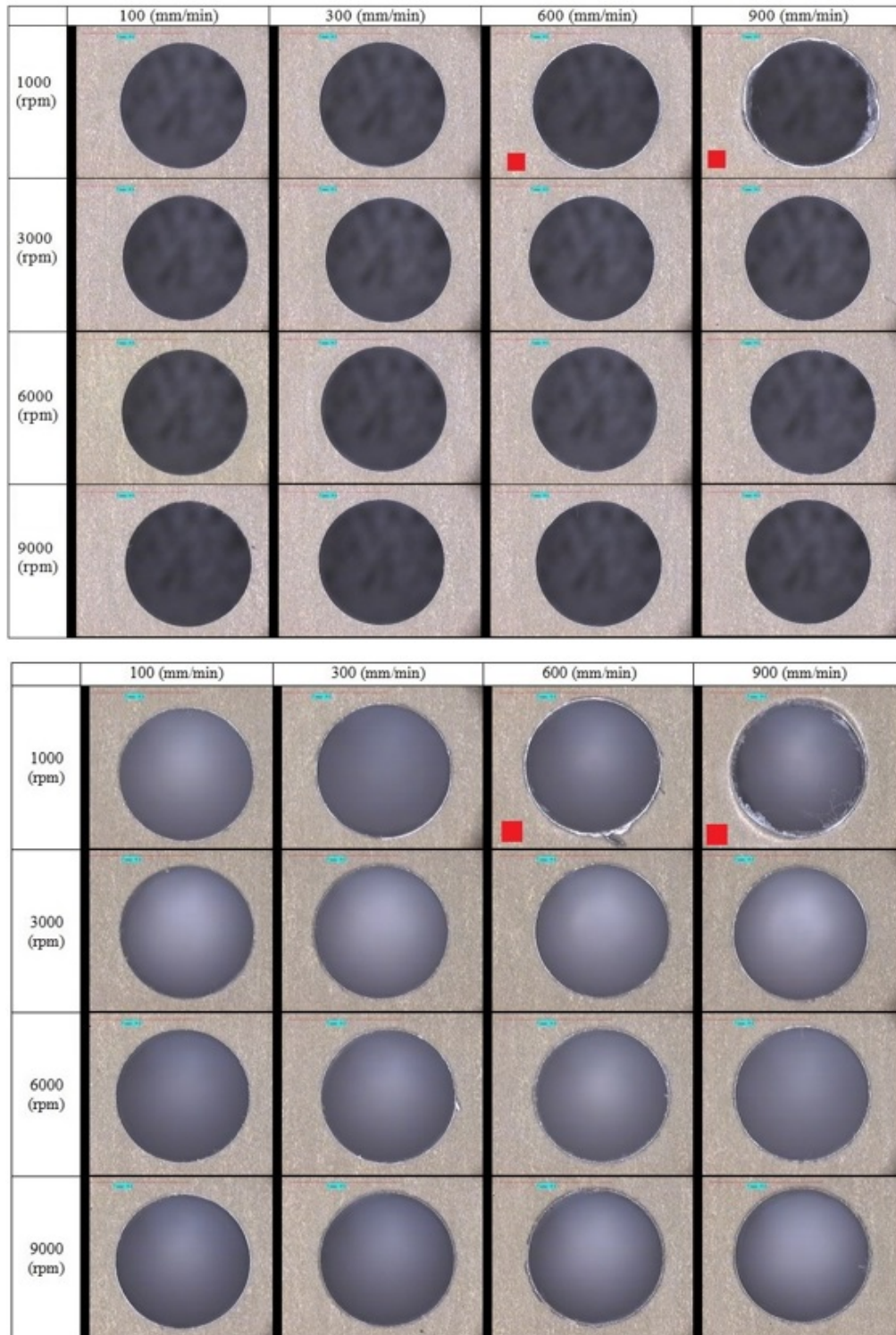
Figure 5.10: Images of holes of the first drilling trial for GLARE 2B 11/10-0.4 (a) entry side (b) exit side [190]

5.1.2   Surface roughness analysis

The surface roughness values reported in the study are a combination of the surface roughness of the aluminium sheets and the glass fibre layers; it was not possible to measure the surface roughness of the two materials individually using the 2D surface profilometer due to their small thicknesses. It was observed that the surface roughness of the aluminium sheets was always lower than that of the glass fibre layers as shown in Figure 5.11, which shows a representation of surface roughness profile for one of the drilled holes in GLARE 2B 11/10-0.4. This is due to the heterogeneous nature of composite materials and the effect of fibre orientation relative to the direction of cut [337], and to the fibrous nature of glass fibre layers which are prone to fibre pull-out and matrix degradation during the drilling process. In addition, voids (pockets) of complete fibre/matrix loss are common when drilling composite/metal stacks partially caused by the evacuated aluminium chips rubbing against the internal surfaces of the hole, as evidenced by the scratch marks on aluminium sheets surfaces and forced chips into glass fibre layers.
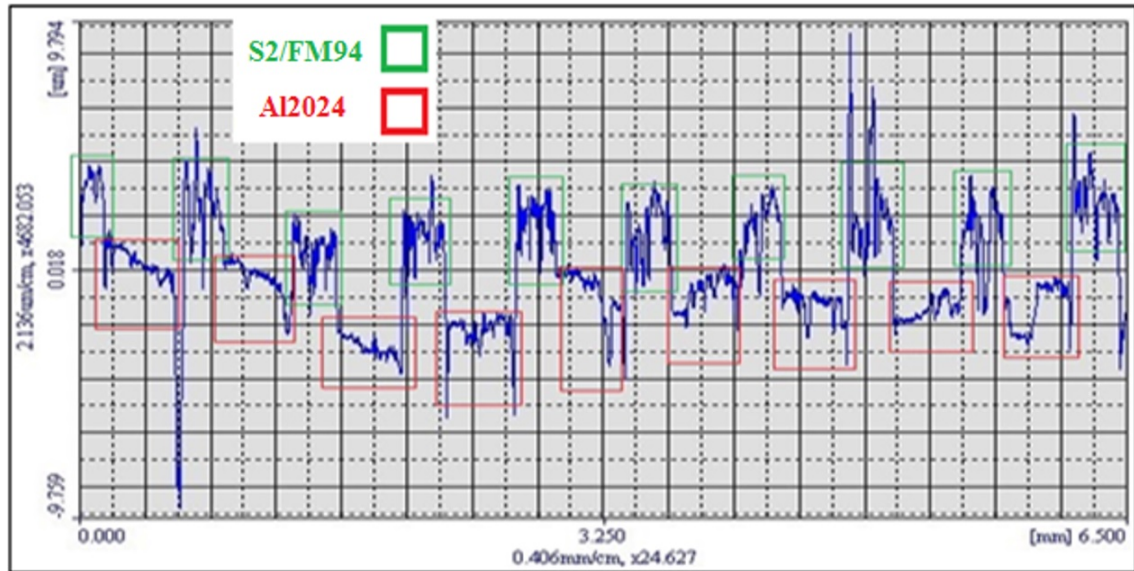
Figure 5.11: Average surface roughness profile for a drilled hole in GLARE 2B [190]

The influence of fibre orientation on surface roughness

Figure 5.12 shows a comparison of the average surface roughness for GLARE 2B 8/7 and GLARE 3 8/7 under different spindle speeds and feed rates. The surface roughness in GLARE 3 was generally higher than in GLARE 2B by 3.9 % and up to 64 % with the increase of the feed rate. Results showed that the fibre orientation in GLARE can influence the surface roughness regardless of the cutting parameters used. The direction of measurement with respect to ply orientation seems to have an influence on surface roughness. GLARE laminates with plies having different orientations (cross-ply configuration) show an increase in surface roughness compared to laminates with plies having a unique orientation (unidirectional plies). It can be concluded that the microstructure of the machined surface is a function of the fibre orientation [87]. This could due to the fact that the bent fibres -due to the cutting process- tend to retain back to their initial state after the cutting tool edge passes them, creating fuzzy surface texture and higher surface roughness [29].
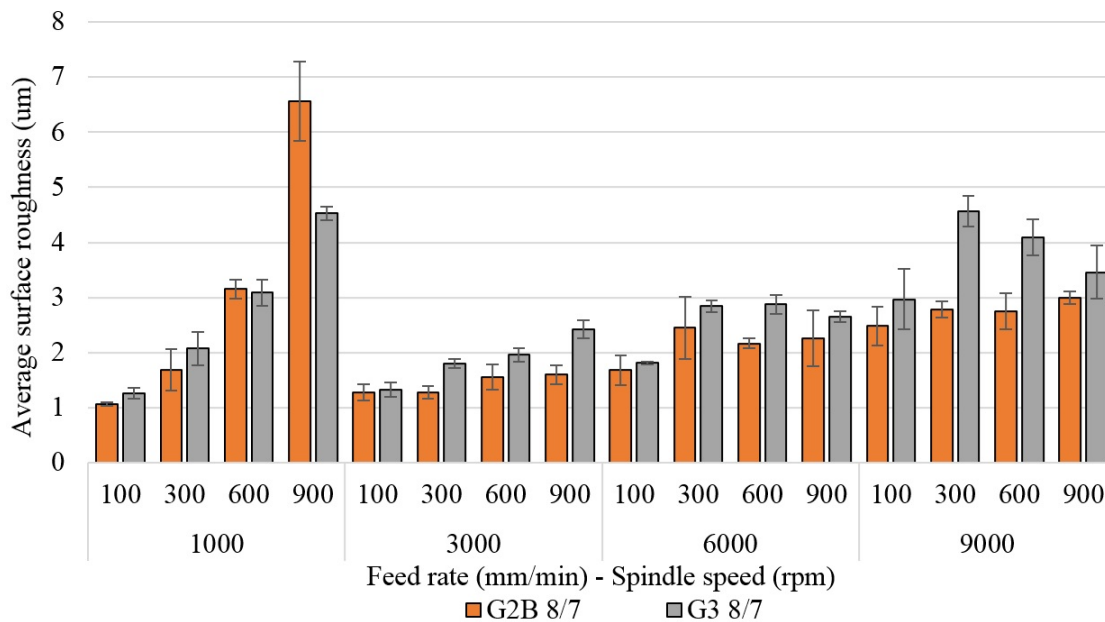
Figure 5.12: Average Surface Roughness of drilled holes in different GLARE grades and thickness

As reported earlier in chapter 2, the contact method for measuring surface roughness of machined composites might be affected by the size of the fibres and their orientation or the possibility of fibre hooking to the stylus whic can cause errors during the measurement process [337]. Therefore, using non-contact methods such as optical microscopy to measure the surface roughness in composites is highly desirable. To further clarify the influence of ply orientation on surface roughness, 3D surface images were taken from a section of the

internal wall of the drilled holes for each grade. The average area surface roughness of was generally higher when the plies are oriented in different directions such as in GLARE 3. The 3D surface analysis also showed that there were three different cases when it comes to the value of surface roughness in tested GLARE grades at inspected regions. The first case which exists in GLARE 2B is when the fibres are normal relative to the stylus motion path across the hole depth shown in Figure 5.13.a. In this case, the surface roughness showed highest readings of surface roughness. The second case which exists in GLARE 3 is when half of the fibre layers point towards the center of the hole and the adjacent fibre layers are normal relative to the stylus motion path as shown in Figure 5.13.b. For this case the surface roughness shows lower readings than in the first case but higher than in the third case.
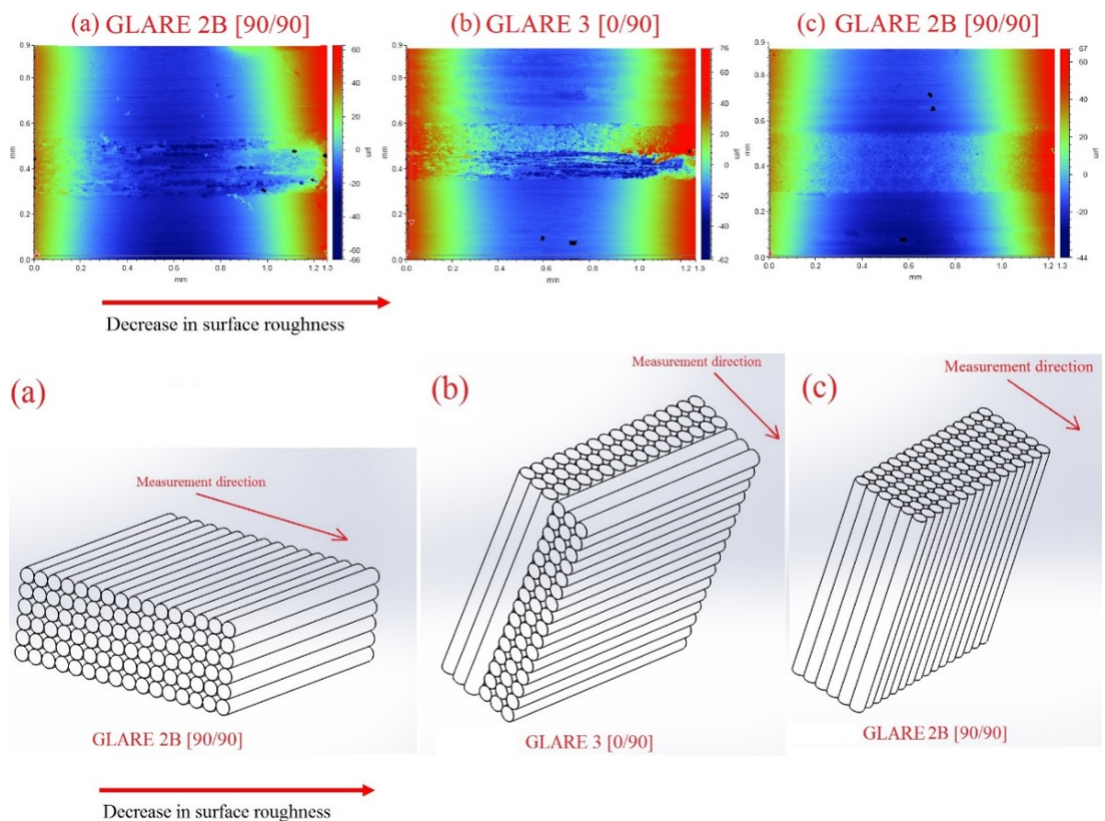
Figure 5.13: Cases of surface roughness values depending on the prepreg orientation in each fibre layer [304]

The third case which also exists in GLARE 2B is when the fibres are pointing outwards towards the centre of the drilled hole as shown in Figure 5.13.c. The measured surface roughness, in this case, was lowest compared to the first and second case. Therefore, when measuring the surface roughness in GLARE 2B at the stated locations described previously in chapter 3, there will be two high readings of surface roughness and two low readings. For

example, the average surface roughness of the last glass fibre layer in GLARE 2B 8/7 and GLARE 3 8/7 for a hole drilled at n= 1000 rpm and f= 300 mm/min were found to be 1.867 and 1.368 µm respectively. The 3D surface images of glass fibre layers surfaces revealed that when the work material is cut from the side as it is the case in Figure 5.12.a and partially in Figure 5.13.b, the cutting process yields undesirable burr which mainly consists of fibres backed up by the matrix and adjacent aluminium sheets which limits the compressive stresses around the cutting edge from shearing or breaking the fibres [338]. Therefore, it could be concluded that surface roughness is affected by the fibre orientation around the borehole surface [29]. Takeyyama [338] previously reported that the roughness of the machined surface in reference to the fibre angle showed that surface roughness increases steeply at fibre angles greater than 60° due to the generation of larger compressive strains within the work material resulting in larger surface roughness. The maximum surface roughness of the first two and last aluminium sheets and the middle glass fibre layers between them were measured using 3D surface roughness contour GT device. The analysis revealed that the surface roughness is higher when the fibres are oriented at 90°Âř and lower when the fibres are oriented at 0° as shown in Figure 5.14. The results also showed that the surface roughness of glass fibre layers is likely to increase with the decrease of workpiece thickness.
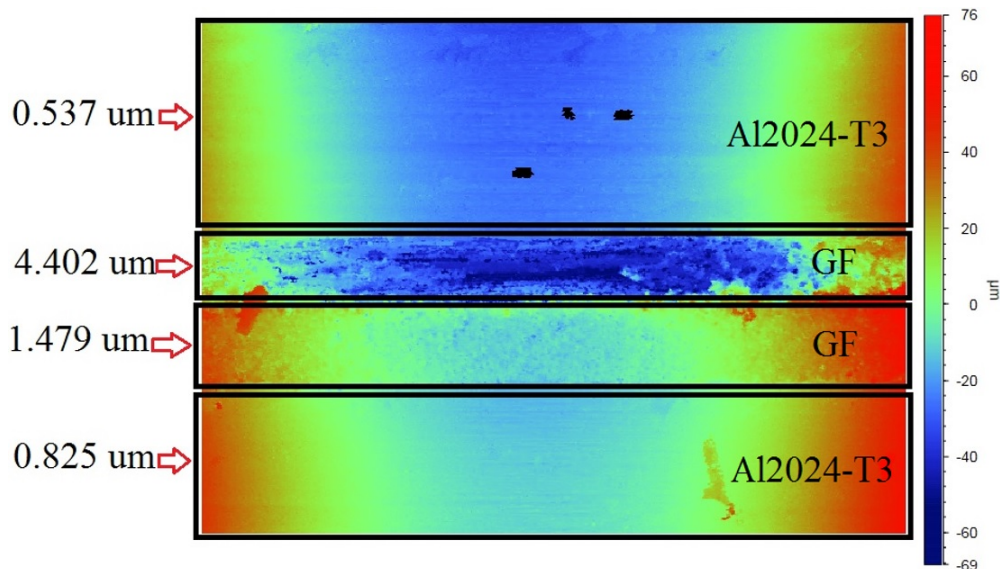
Figure 5.14: 3D surface texture condition of drilled holes in GLARE 3 at hole entry [304]

Large magnification from scanning electron microscopy images shown in Figure 5.15 indicates that the machined surfaces condition at 0° and 90° were different. The machined surface of the 0° fibre orientation shows that the matrix surrounding the fibres seems to have been pulled out during the machining process, leaving behind fibres exposed. In addition, bundles of broken fibres can be seen left on the machined surface after the cutting process,

creating somewhat a rough surface compared to fibres oriented at 90°. The fibres oriented at 90° are pointing outwards towards the centre of the hole and remained intact with each other during the machining process creating a smoother surface.

The results showed that both the spindle speed and feed rate had an impact on surface roughness. The surface roughness increased with the increase of feed rate and spindle speed. The measured roughness ranged between 1 μm up to 4.5 μm (excluding holes drilled at n =1000 rpm and f = 600 mm/min and 900 mm/min). Additionally, it was observed that when drilling at a feed rate/spindle speed ratios of 0.1 mm/rev, the surface roughness increased considerably. For example, the surface roughness in GLARE 3 8/7 when drilling at n = 9000 rpm and f = 900 mm/min was 20.2 %, 91.6 % and 176 % higher than when drilling at 600/6000, 300/3000 and 100/1000 (mm/min/rpm) respectively, which indicates that reducing the drilling time would be at the expense of reduced surface quality. The analysis of surface roughness in terms of the cutting parameters leads to the conclusion that using lower feed rates gives a better surface quality regardless of the ply orientation and spindle speed used but higher spindle speeds might have a significant impact on the developed machining temperatures.
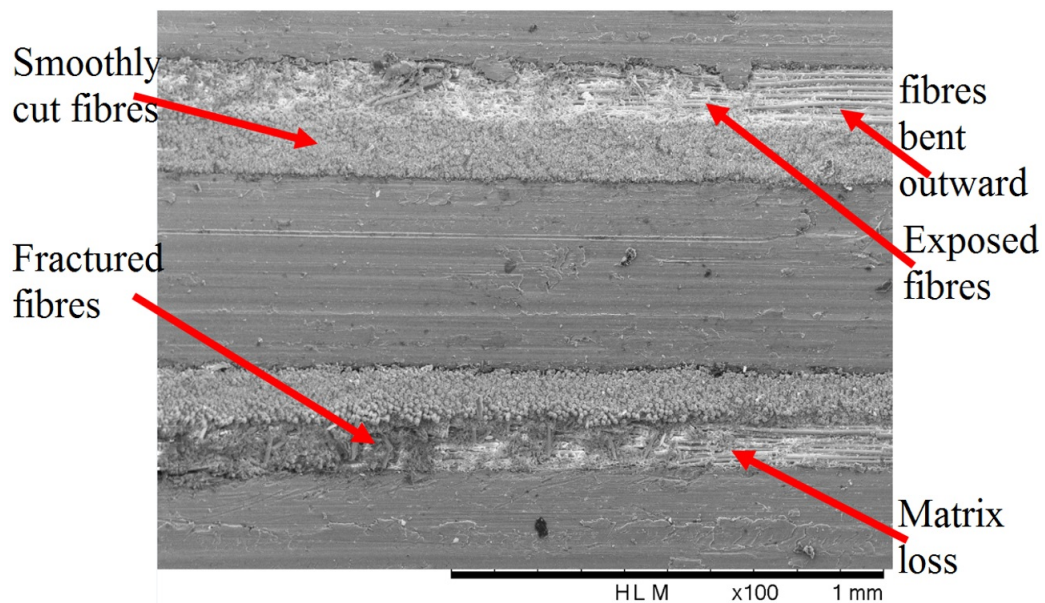
Figure 5.15: Average Surface Roughness of drilled holes in different GLARE grades and thicknesses

The influence of workpiece thickness on surface roughness

Figure 5.16 shows the average surface roughness of different thicknesses of GLARE 2B under various spindle speeds and feed rates. The data for GLARE 2B 4/3 for holes drilled at n = 1000 rpm and f = 600 and 900 mm/min are not provided since it was difficult to measure the surface roughness due to severe hole deformation and fibre pull-outs. The results did not reveal any relation between surface roughness and workpiece thickness when drilling at a spindle speed of n = 1000 rpm. However, it was observed that the surface roughness is likely to be slightly higher in thinner samples with the increase of feed rate. At spindle speed of n = 3000 rpm, the surface roughness was higher in thinner laminates, while at spindle speeds of n = 6000 and 9000 rpm, the surface roughness tended to be higher in thicker laminates. This could be due to the increase in cutting temperatures and vibrations with depth. It was also observed that within the same hole, the surface roughness of different aluminum sheets and glass fibre layers was no affected by depth. In some holes it was found that the surface roughness was slightly higher near the entry side of the hole than near the exit side, which could be due to continuous contact between the chips and the surface of the machined hole. A conclusion can be made that, with the experimental conditions used, a better hole surface quality in GLARE was obtained when drilling at spindle speeds n = 3000 and 6000 rpm and feed rates of f =100 and 300 mm/min.
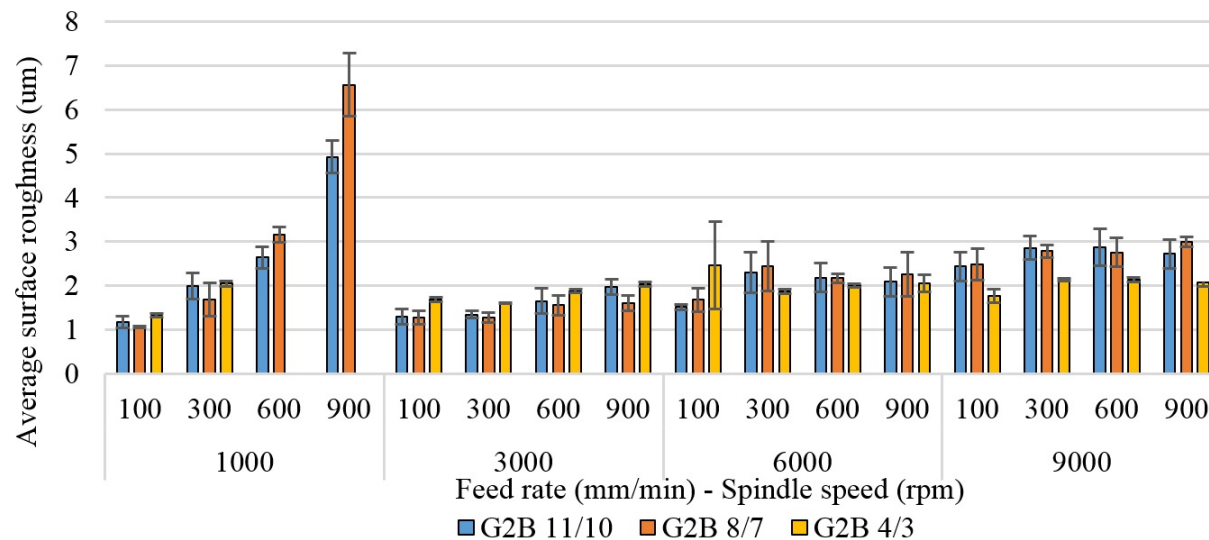
Figure 5.16: Average surface roughness for different thickness of GLARE 2B samples [190]

The ANOVA results given in Table 5.2 reveal that both cutting parameters had equal effect on surface roughness when drilling GLARE 2B, with feed rate contributing equally with spindle speed in GLARE 2B 11/10 and 8/7, while in GLARE 2B 4/3 the spindle speed had a significant contribution of 42.9 %, followed by feed rate with 26.97 %. The interaction of

cutting paramaters was insignificant, however, the error contribution was large with 20.75 %, which means that the model might have higher order interactions contributing to the surface roughness. In GLARE 3 8/7, the spindle speed had a greater influence on surface roughness than the feed rate. This indicates that the direction of measurement with respect to the fibre orientation had an influence on the surface roughness and again it can be concluded that the microstructure of the machined surface is a function of the fibre orientation [87]. GLARE laminates with different ply orientations are likely to have higher surface roughness compared to the GLARE laminates with unidirectional ply orientation.

Table 5.2: Percentage contribution results for surface roughness of different grades of GLARE

GLARE grade	G 2B 11/10	G 2B 8/7	G2B 4/3	G3 8/7
Spindle speed	27.9	24.4	39.86	42.9
Feed rate	26.76	24.15	18.92	26.97
Spindle speed* Feed rate	37.3	45.0	Insignificant	24.16
Error	8.0	6.37	20.75	5.94

To conclude on surface roughness analysis and results during dry drilling of GLARE laminates, the range of surface roughness under tested cutting parameters was between 1and3 μm in GLARE 2B and between 1and4 μm in GLARE 3. As reported from the literature, there is no available data on the acceptable surface roughness for GLARE or composite metal stack materials recommended by the aerospace industry for machining/drilling process. However, as mentioned in chapter 3, Sandvik [52] reported common hole quality requirements by aerospace industry to be less than 3.2 μm in CFRP and less than 1.6 μm in Al or Ti. Table 5.3 shows the range of surface roughness values measured at the upper and lower section of each drilled hole in all tested GLARE laminates. For GLARE 2B 11/10, GLARE 2B 8/7 the surface roughness was measured at 90°/90° section of the hole, while for GLARE 2B 4/3, the surface roughness was measured at 0°/0° section of the hole and therefore was lower than the value in the other two thicknesses of GLARE 2B. The surface roughness in aluminium sheets was around 0.5 μm on average. For glass fibre layers, the surface roughness varied from 1 μm to 5.195 μm The results clearly indicate that the surface roughness of aluminium sheets satisfy the recommended values by the aerospace industry. For glass fibre layers, despite exceeding the recommended roughness values, it was observed that the measured maximum surface roughness occurs only in a narrow region at the edges of the glass fibre layer (between aluminium sheets and glass fibre layer or between glass fibre layers with different fibre orientation). It was aslo below the recommended maximum roughness for the remaining regions of glass fibre layer surface. This could be due to the sudden change in surface texture height when going from aluminium surface to glass fibre layer surface or when the fibres alternate from 0° to 90°. The surface roughness values of glass fibre layers

are generally within the range of previously reported studies of surface roughness in drilled GFRP and CFRP/metal stacks [65, 79, 189, 339–341]

Table 5.3: Range of surface roughness for selected aluminium sheets and glass fibre layers in drilled holes in GLARE laminates

Surface roughness (µm)	GLARE 2B 11/10	GLARE 2B 8/7	GLARE 2B 4/3	GLARE 3 8/7
1st aluminium sheets	0.478-1.675	0.533-1.153	0.447-1.113	0.527-0.943
1st glass fibre layer	1.287-4.484	2.762-6.786	1.021-2.431	3.26-9.735
2nd aluminium sheet	.456-1.719	0.503-0.765	0.468-1.062	0.465-1.029
Pre last aluminium sheets	0.509-1.309	0.528-0.909	0.451-1.205	0.541-1.036
Last glass fibre layer	1.492-5.195	3.515-13.681	1.229-5.978	3.774-7.137
Last aluminium sheets	0.433-1.607	0.465-0.72	0.442-1.074	0.457-0.756

5.1.3 Burr formation analysis

Figure 5.17 shows the average exit and entry burr height and thickness in GLARE 2B 11/10 under different spindle speeds and feed rates. The exit burr height and thickness were always greater than at entry by up to 4-6 times in all GLARE samples. Entry burr size is small < 15 µm and the drilled holes can be considered burr free at the entrance. Figure 5.18 shows SEM images of burr formation at entry and exit side of a hole drilled in GLARE 2B 11/10. The edge quality at the exit was more deteriorated than at the entry side which could be due to the absence of backup plate which is known to reduce burr formations [342, 343]. Burr height and thickness increased with the increase of feed rate and spindle speed. All the burrs formed -with the exception of holes drilled at high feed rates and low spindle speed of f= 600 and 900 mm/min and n= 1000 rpm- were very small and mostly uniform. Some of the formed burrs could not be seen with the naked eye as shown in Figure 5.19. The type of burr formed in GLARE laminates does not exhibit evidence of material that can break away and is generally acceptable in machining operations which do not require deburring, unless it can affect the assembly of holes in mating parts or the contact between surfaces.
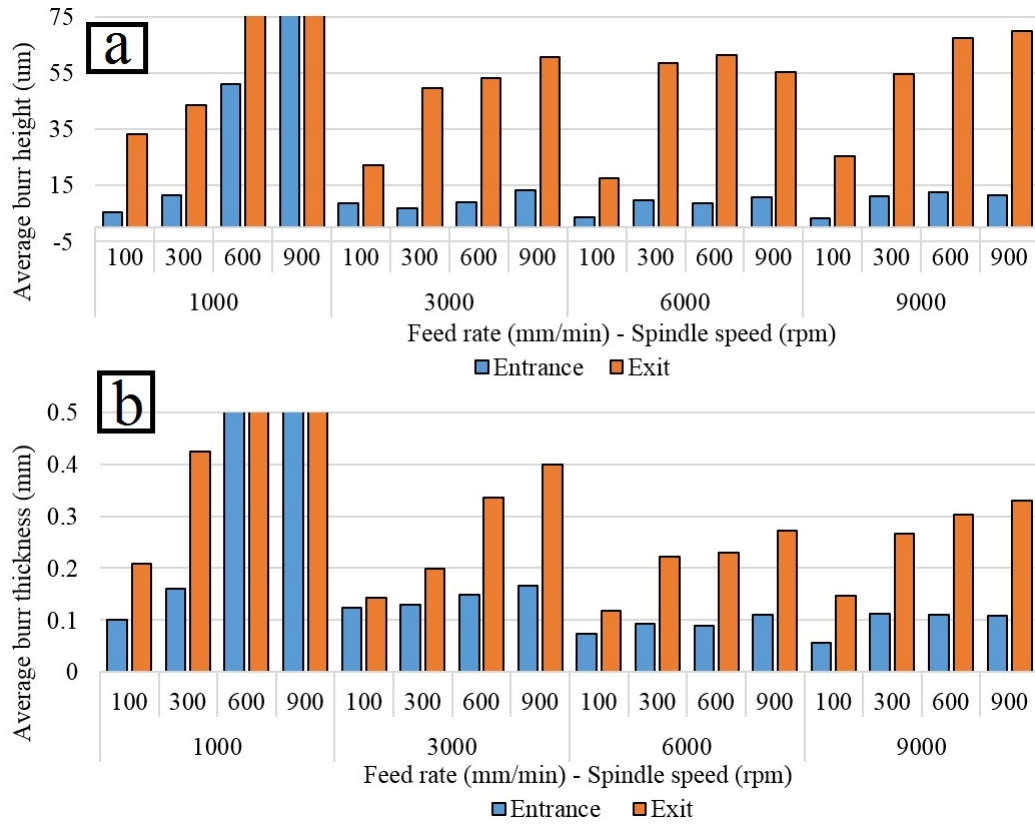
Figure 5.17: Comparison of (a) average burr height (b) burr thickness, at entrance and exit for GLARE 2B 11/10
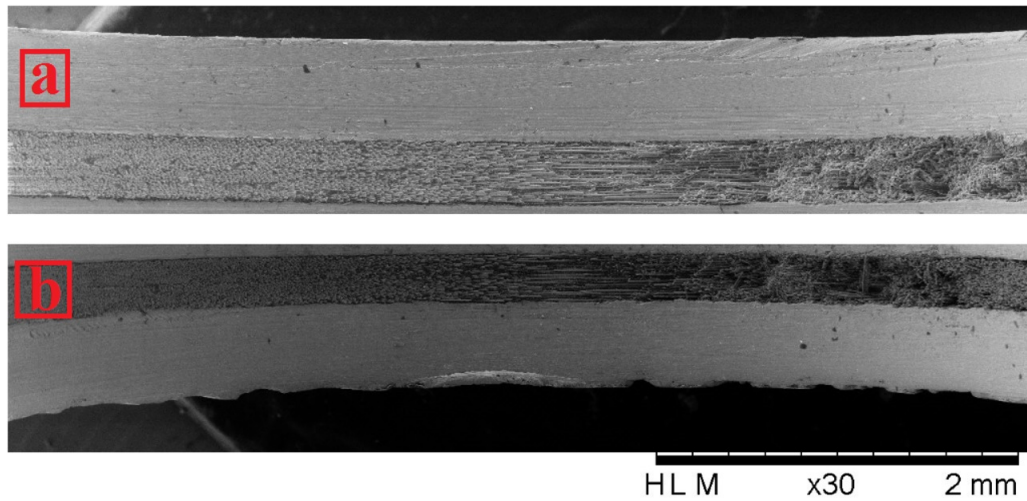
Figure 5.18: SEM images of (a) entrance burr and (b) exit burr in GLARE 2B 11/10-0.4 at n= 9000 rpm and f= 100 mm/min
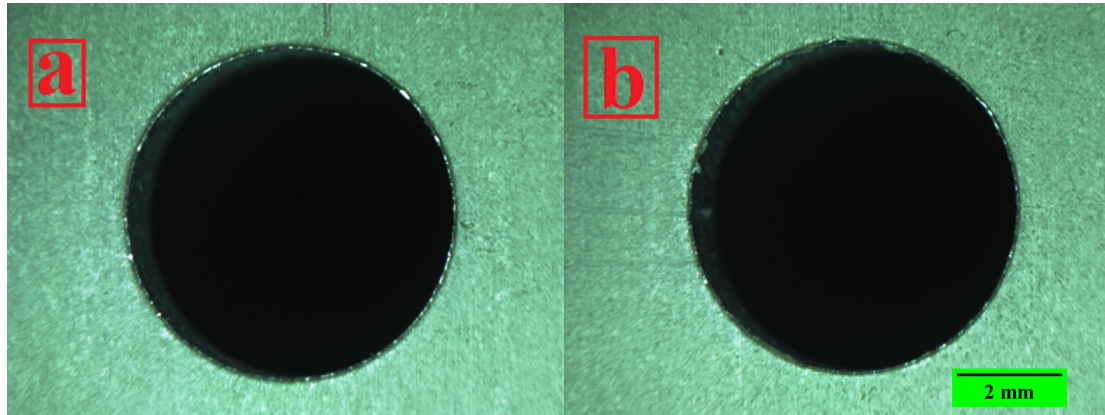
Figure 5.19: Exit burr formation for hole drilled at (a) n= 9000 rpm and f= 900 mm/min (b) n= 3000 rpm and f= 300 mm/min

The influence of ply orientation on burr formations

Figure 5.20 shows the average entry and exit burr height and thickness in GLARE 2B 8/7 and GLARE 3 8/7 under different spindle speeds and feed rates. Results showed that burr height is likely to be larger when glass fibre layers are stacked in the same direction. The increase in entry burr height in GLARE 2B was greater than that in GLARE 3 with the increase of the feed rate. This could be due to the fact that the energy transfer from one composite layer to another is easier if they both have same fibre orientation such as in GLARE 2B. As a result, the severity of the damage is greater than what it would be if the fibres in each layer had different orientations such as in GLARE 3, which allow it to fail at higher loads [110]. Conversely, the entry burr thickness did not show any significant relationship with fibre orientation. The exit burr thickness was higher in GLARE 2B than in GLARE 3. A maximum burr height of $23.09\,\mu m$ and $15.64\,\mu m$ were recorded at hole entry when drilling at n = 9000 rpm and f = 600 mm/min for GLARE 2B and n = 3000 rpm and f = 900 mm/min in GLARE 3 respectively. A maximum burr height of $78.51\,\mu m$ and $65.15\,\mu m$ were recorded at hole exit when drilling at n = 6000 rpm and f = 300 mm/min for GLARE 2B and n = 3000 rpm and f = 900 mm/min in GLARE 3 respectively.
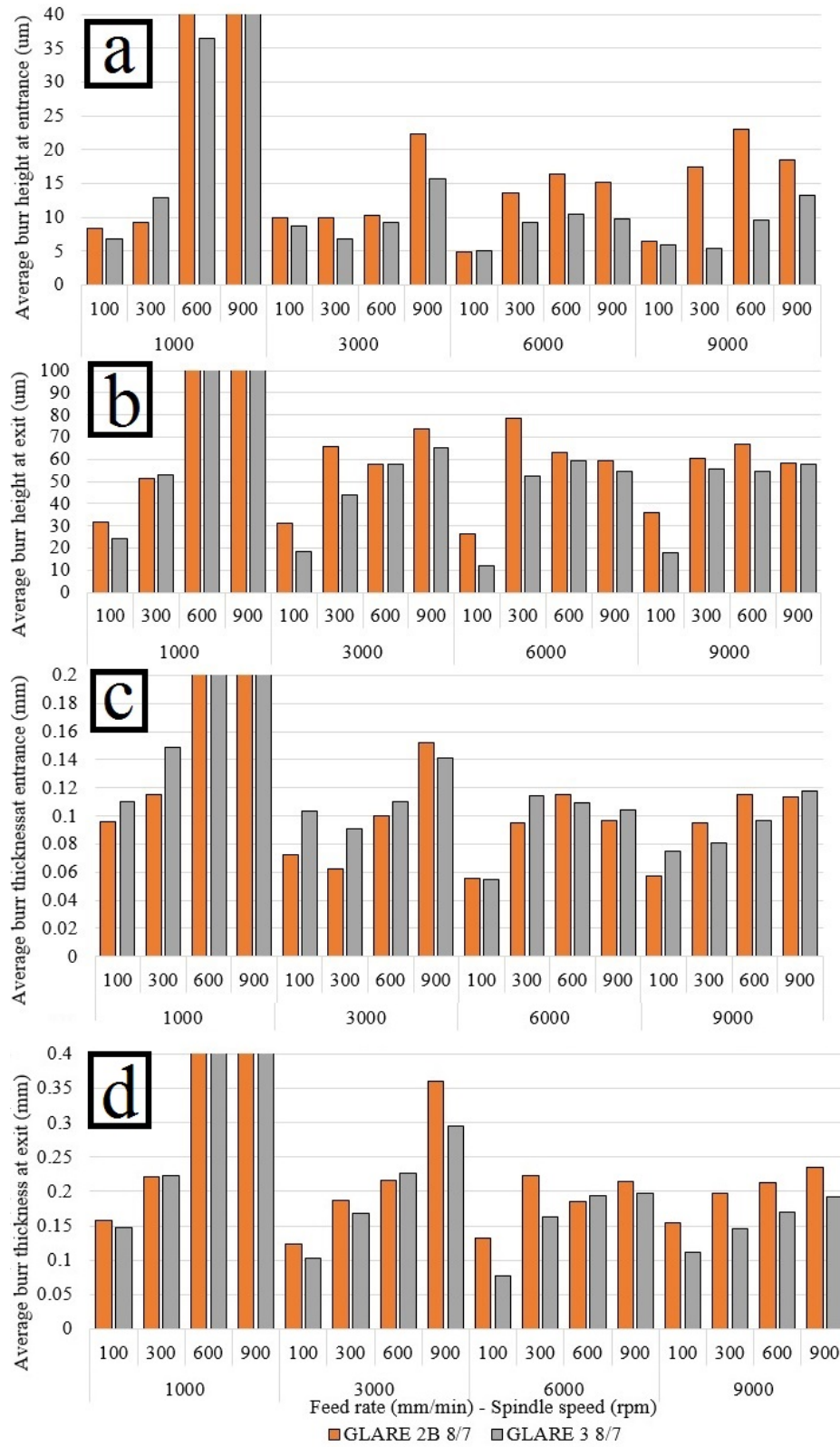
Figure 5.20: Influence of fibre orientation on average (a) entry burr height (b) exit burr height (c) entry burr thickness (d) exit burr thickness

Interlayer burr was formed in the drilled holes as shown in Figure 5.21. Interlayer burr was difficult to measure, non-uniform and randomly distributed around the edges of aluminium sheets by protruding glass fibre layers. The interlayer burr is usually formed when the elastic bending deformation of two different materials stacked together occurs at different degrees due to the mismatch in physical and mechanical properties. In addition, when the cutting tool drills through the stack, the upper part of the workpiece undergoes elastic recovery while the lower part undergoes large elastic bending deformation due to the acting of the feed force especially when no backup plate is used. The bending of the workpiece allows for the formation of small gaps which provide suitable conditions for interlayer burr formation. The formed chips can be also forced onto the glass fibre layers surfaces while the cutting tool is cutting through or retracting from the workpiece.
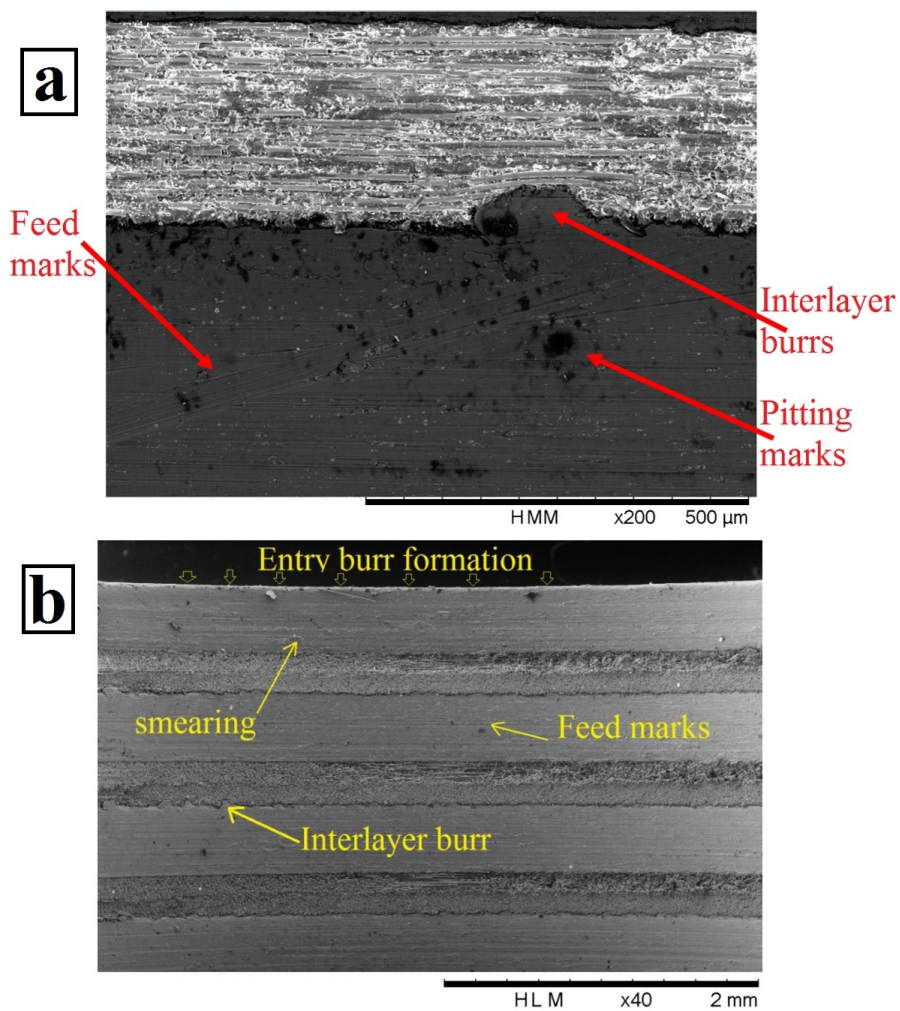
Figure 5.21: SEM image showing (a) interlayer burr formations of hole in GLARE 2B 8/7 drilled at 1000 rpm and 300 mm/min (b) entry burr formations of hole in GLARE 3 8/7 drilled at 3000 rpm and 300 mm/min

Table 5.4 shows the percentage contribution of cutting parameters on burr formations. The spindle speed was more dominant than the feed rate for all grades and thickness, while their interaction showed significant contribution. The spindle speed was found to have a larger effect on burr formation at entry, while the feed rate impact was greater at exit.

Table 5.4: Percentage contribution of cutting parameters on burr formation

Burr height (μm)							
	GLARE 2B 11/10		GLARE 2B 8/7		GLARE 2B 4/3		GLARE 3 8/7	
	Entrance	Exit	Entrance	Exit	Entrance	Exit	Entrance	Exit
Spindle speed	32.23	29.03	30.72	28.57	36.93	37.28	32.40	28.02
Feed Rate	20.54	23.87	19.53	21.30	15.73	17.5	23.61	23.47
Spindle speed * Feed rate	46.37	38.76	8.87	49.75	36.87	35.98	42.63	48.33
Error	0.849	8.325	10.86	0.362	10.46	9.22	1.34	0.147
Burr thickness (mm)							
	GLARE 2B 11/10		GLARE 2B 8/7		GLARE 2B 4/3		GLARE 3 8/7	
	Entrance	Exit	Entrance	Exit	Entrance	Exit	Entrance	Exit
Spindle speed	38.55	43.45	41.59	37.50	41.68	39.31	36.40	40.69
Feed Rate	17.55	20.99	16.31	18.01	15.88	20.20	16.89	17.79
Spindle speed * Feed rate	41.71	35.33	40.65	43.93	35.89	37.08	42.92	41.10
Error	2.17	0.214	1.43	0.548	6.53	3.39	3.774	0.407

The influence of workpiece thickness on burr formations

Figure 5.22 shows the average entry and exit burr height and thickness in GLARE 2B under different spindle speeds and feed rates for three thicknesses. The entry burr height increased with the increase of the feed rate and spindle speed. The entry burr height in GLARE 2B 8/7 was greater than that in GLARE 2B 11/10 and 4/3, especially with the increase of the feed rate and spindle speed. As previously reported by Gillespie [344], the entry burr in drilling is formed as a result of tearing, a bending action followed by clean shearing, or lateral extrusion when the chip is forming and impacting the cutting edges.

Burr thickness at both sides in GLARE 2B 11/10 was greater than in GLARE 2B 8/7 and 4/3 while the latter two did not show much difference in burr thickness compared to each other. This could indicate that burr thickness becomes more critical after a certain drilling depth has been reached. The feed rate had more influence on increasing the burr thickness with the increase of hole depth on the entry side. The burr thickness increased with hole depth and increased with the increase of feed rate and spindle speed. The increase of burrs with the increase of cutting parameters could be due to the increase of plastic deformation under dry condition and high-temperature rise may which result in larger burrs formation [342]. There was no clear relation between the size of burr and drilling depth. However, it was observed that the exit burr height tended to increase with workpiece thick-
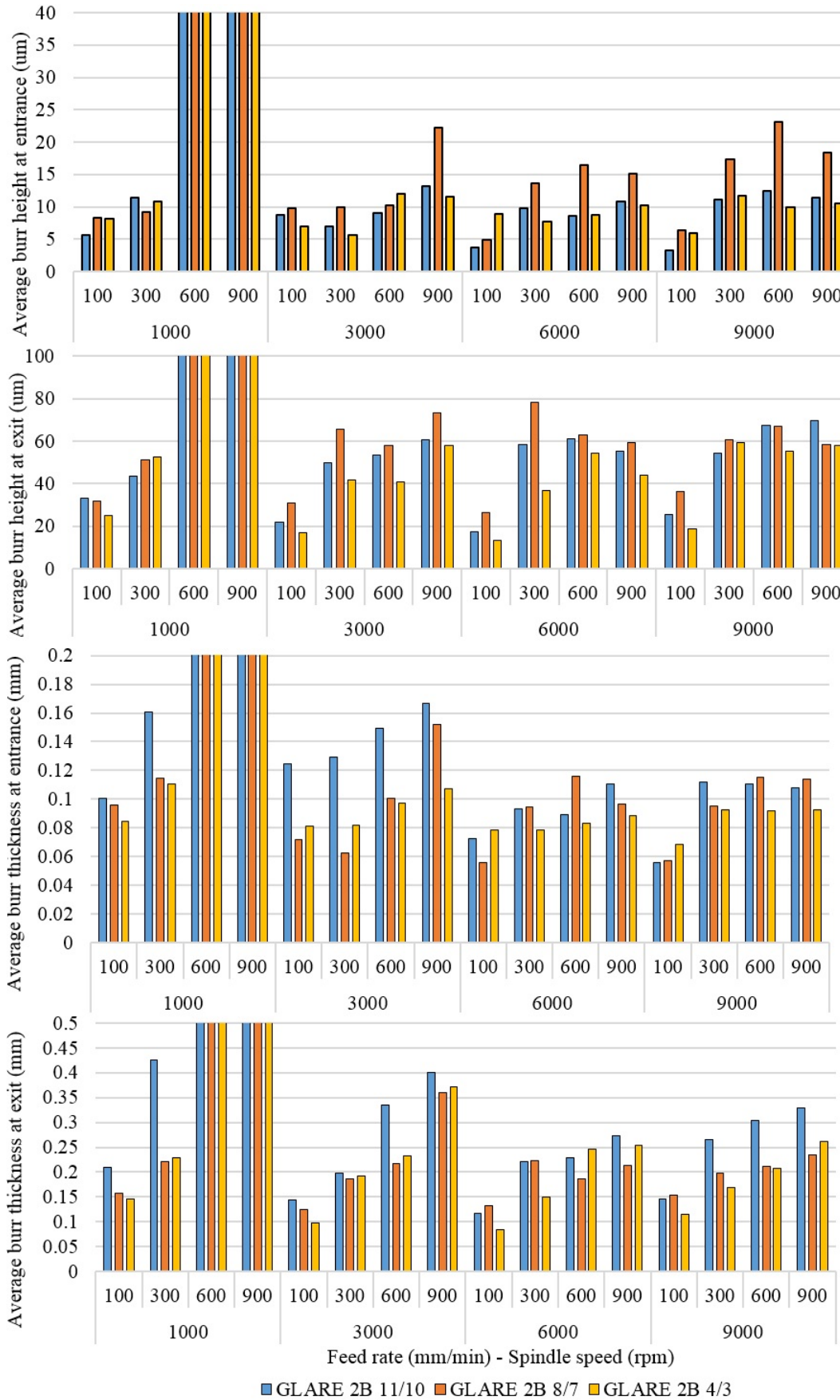
Figure 5.22: The influence of workpiece thickness on the average (a) entry burr height (b) exit burr height (c) entry burr thickness (d) exit burr thickness

ness, or when increasing the spindle speed, or when decreasing the feed rate.

To conclude on burr height and thickness analysis and results during dry drilling of GLARE laminates, as reported from the literature, there are no available data on the acceptable burr height or thickness for GLARE, composite metal stacks or monolithic aluminium for machining/drilling process. However, comparing the obtained data with previous studies on drilling aluminium alloys and GLARE fibre metal laminates shows that exit burr height could reach anything between 10 to 80 μm. Generally, the burr height obtained from all drilling trials are within or below those obtained in previous studies on drilling GLARE and aluminium alloys shown previously in chapter 2 [54, 63, 64, 189, 345].

Table 5.5: Range of average burr height and thickness in drilled GLARE laminates

Burr formation	GLARE 2B 11/10	GLARE 2B 8/7	GLARE 2B 4/3	GLARE 3 8/7
Entry burr height (µm)	3.32-13.1	4.83-22.28	5.98-11.95	4.83-23.09
Exit burr height (µm)	17.5-69.88	26.42-78.51	13.09-58.20	12.25-59.28
Entry burr thickness (µm)	55.8-166.85	55.9-152.1	68.8-107.33	54.66-140.91
Exit burr thickness (µm)	116.95-399.85	98.08-360.66	84.41-372.25	77.08-294.66

5.1.4   Hole size analysis

Figure 5.23 shows the average hole size in GLARE 3 8/7 under different spindle speeds and feed rates at both locations (top and bottom).
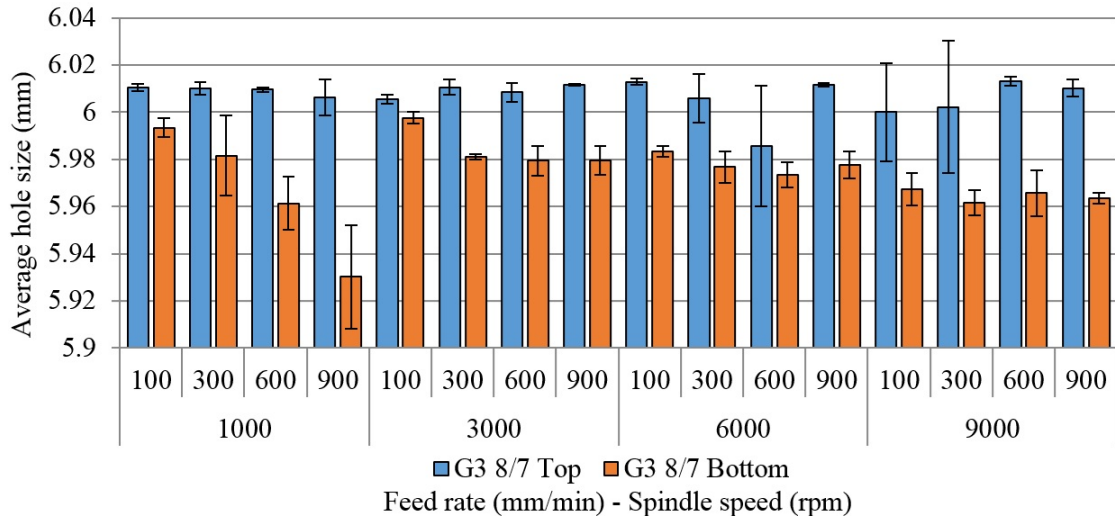
Figure 5.23: Average hole size at top and bottom for GLARE 3 8/7

The holes at the top in GLARE 3 were found to be oversized under all cutting parmaeters

and ranged from 0.11 to 13.2 μm with the exception of the holes drilled at n= 6000 rpm and f= 600 mm/min. The diameter of the drilled holes at the bottom in GLARE 3 was found to be undersized for all conditions tested ranging from $30 - 70$ μm. At the top location, the deviation from nominal hole size increased with the increase of the feed rate (with the exception of holes drilled at n= 6000 rpm). While the influence of spindle speed varied depending on the cutting parameters used. At the bottom location, the diameter of the hole decreased with the increase of the feed rate and spindle speed which could be due to the increase in frictional heating induced by the high spindle speeds. The glass fibre-epoxy matrix and metal sheets in GLARE react differently to the developed temperatures in the cutting zone. For example, in metal machining, up to 70 % of the heat generated by the cutting, the zone is carried away by chips [29], while for glass fibre-epoxy matrix, the low thermal conductivity means that the generated heat does not conduct quickly to the cutting tool. The heat transfer occurs only in a thin layer at the interface between the aluminium sheets and the prepregs throughout the laminate. The poor thermal conductivity of the glass fibre prepregs compared to Al2024 aluminium sheets causes the prepregs to expand. Additionally, the mismatch coefficient of thermal expansion of GLARE constituents could result in residual stresses and changes in the hole size [29]. Indeed, undersized holes are common when drilling laminated GFRP composites [346] due to the elastic bending and tightening of the reinforcement fibres during machining followed by relaxation of the lamina [347]. This was evidenced by the fact that the reduction in hole size at a bottom location in GLARE 2B 11/10 was greater than that in GLARE 2B 8/7, which indicates that the reduction in hole diameter increases with the increase of drilling depth.

The influence of ply orientation on hole size

Figure 5.24 shows a comparison of the influence of ply orientation on the average hole size in GLARE 3 8/7 and GLARE 2B 8/7 under different spindle speeds and feed rates at both locations (top and bottom). The diameter of the drilled holes at the top in GLARE 2B 8/7 was also found to be oversized for all conditions tested by up to 18.7 μm and 0.53 μm with the exception of the holes drilled at 1000 rpm and 600 and 900 mm/min. The diameter of the drilled holes at the bottom was found to be below the nominal hole size for all conditions tested by 10.5 μm, while some holes were oversized at both locations. At the top location, the diameter of the hole increased with the increase of spindle speed and decreased with the increase of feed rate. At the bottom location, the diameter of the hole increased with the increase of spindle speed and decreased with the increase of the feed rate.
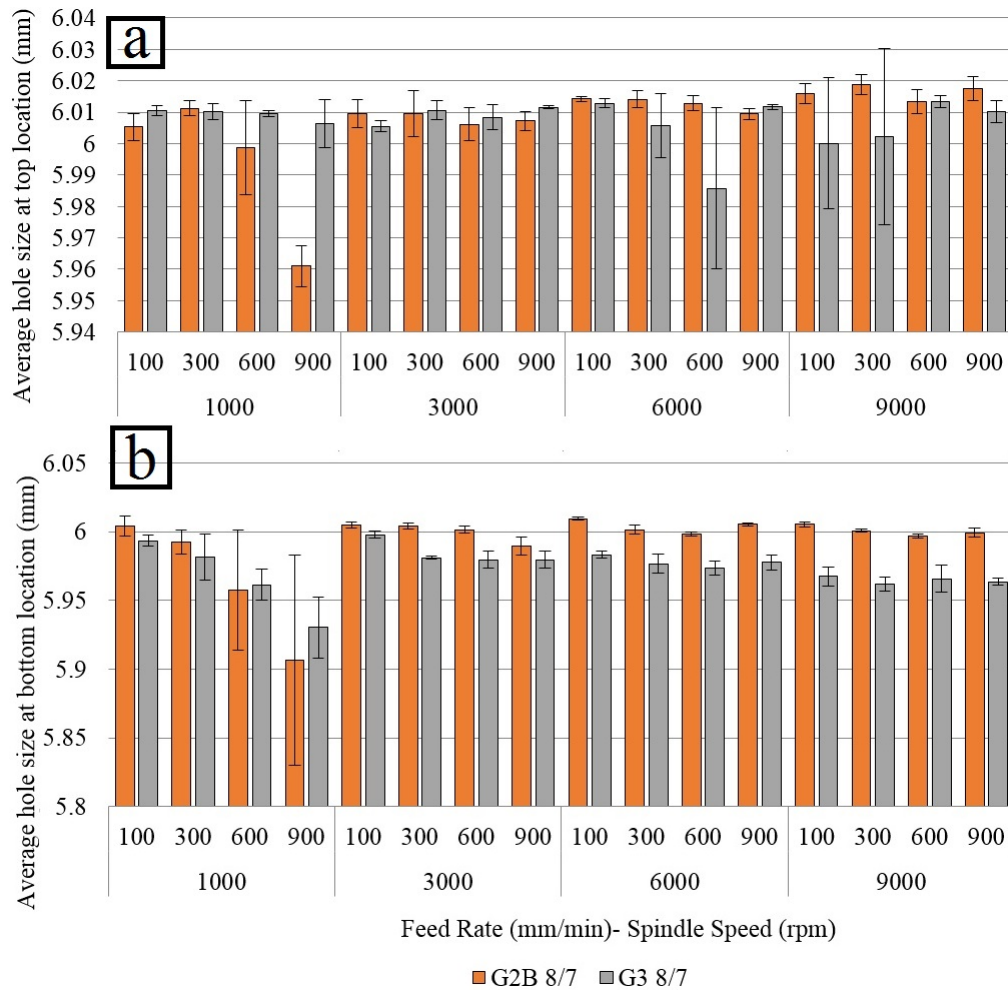
Figure 5.24: Comparison of hole size at (a) top and (b) bottom locations for GLARE 2B 8/7 and GLARE 3 8/7

The diameter of the hole measured at the bottom in GLARE 3 was smaller than in GLARE 2B (8/7 and 11/10) for all drilled holes which could indicate that the ply orientation influence the hole size. The majority of holes size in GLARE 2B 8/7 were also greater than in GLARE 3 8/7. Additionally, the difference in hole size at the bottom between the two different grades was greater at the bottom than at the top, which could indicate that the ply orientation becomes more critical on hole size with the increase of hole depth. It is well known that the thermal expansion coefficient in unidirectional plies varies with direction. For example, the thermal expansion coefficient of a cross-ply in the fibre direction $\alpha 1$ is 6.1×10^{-6} $1/^{\circ}C$ while the thermal expansion in the transverse or out of plane direction is 26.2×10^{-6} $1/^{\circ}C$ [11] which is due to the transverse isotropy of the glass fibre epoxy [14]. The heating and cooling in GLARE during the drilling process causes thermal expansion and shrinkage of the glass fibre-epoxy layers and since the thermal expansion coefficients are different relative to the fibre direction, the contraction in glass epoxy layers in cross-ply configuration tend to act in

different directions and, therefore, the retraction to its original position will be slower than that in unidirectional ply configuration. The 0° fibres expand in the longitudinal direction while the 90° fibres contract in the transverse direction, which leads to geometric mismatch and residual stresses in glass fibre layers [126]. The geometric mismatch influences the dimensional accuracy of the drilled hole at the glass fibre and causes them to have a smaller size than the nominal size of the drill. Another explanation could be that in the cross-ply system, half of the plies in the stack have fibres pointing towards the hole centre while in unidirectional ply system the fibres will be either pointing towards the centre of the hole or perpendicular to the centre of the hole. This could adversely affect the measurement of hole diameter as there will be more fibres protruding towards the centre of the hole in the cross-ply system and therefore, generating a smaller hole diameter than that in a unidirectional ply system.

The influence of workpiece thickness on hole size

Figure 5.25 shows a comparison of the influence of drilling depth on the average hole size in GLARE 2B under different spindle speeds and feed rates at both locations (top and bottom). The hole diameter measured at the top location was oversized with few exceptions in some holes drilled in GLARE 2B 11/10. The hole size increased with the increase of feed rate and spindle speed at the bottom. Oversized holes were produced in GLARE 2B 4/3 under all cutting parameters and ranged between + 4.45 μm and + 24.7 μm and between +7.63 μm and + 13 μm which could be due to its relatively small thickness. For GLARE 2B 11/10 and 8/7, oversized and undersized holes were produced depending on the cutting parameters.

The deviation of the hole from its nominal diameter in GLARE 2B 11/10 at the top ranged between +12.84 μm and -7.9 μm, and between -0.255 μm and -17.8 μm at the bottom. For GLARE 2B 8/7 the deviation of hole size at the top ranged between +17.4 μm and +5.32 μm and between +1.32 μm and -7.63 μm at the bottom. The results clearly indicate that the hole diameter is likely to shrink with depth which is common when drilling GFRP composites due to the relaxation of the lamina. The hole size tolerance described previously in chapter 2 indicates that under most cutting conditions used, the hole size can be considered acceptable with optimum spindle speeds being 3000 and 6000 rpm and optimum feed rates of 300 and 600 mm/min.
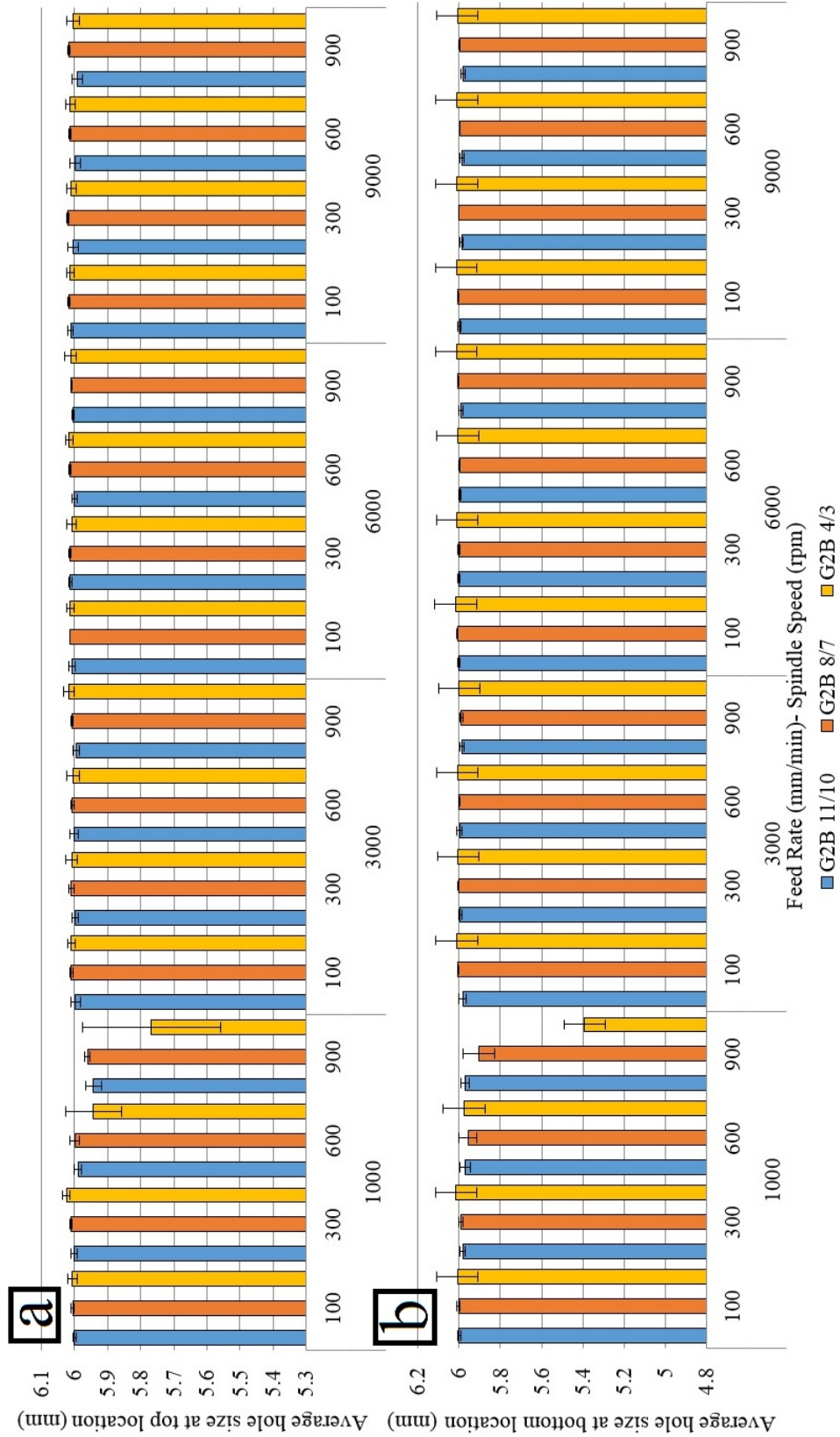
Figure 5.25: Comparison of hole size at (a) top and (b) bottom location for different thicknesses of GLARE 2B

To conclude on entry and exit hole size and circularity error analysis and results during dry drilling of GLARE laminates, as reported previously from the literature in chapter 3 section 3.3.3, SANDVIK tool manufacturer, typical hole demands when drilling composite metal stack materials commonly required to achieve an H7 hole tolerance fit based on the ISO 286 standard. This means that the hole should not vary more than ±12 microns but more relaxed tolerances such as H8 ±18 microns or H9 ±30 microns were allowed to be used when drilling composites due to the difficulty in achieving H7 tolerances, for example, SANDVIK recommends that drilled hole tolerance in a composite metal stack should be between ±20 and ±40 microns [52]. The hole circularity error ranged between 6 and 35 microns in all GLARE grades and thicknesses used under dry drilling condition. Generally, smaller circularity error is preferred and there was no specific requirement found from the literature on the matter for comparison but previous studies showed that it could be anything between 6 μm and as high as 312 μm. The results were similar to those reported by Zitoune et al. [68]. Table 5.6 shows the percentage of contribution of cutting parameters on hole size at top and bottom. The ANOVA analysis results showed somewhat large error percentage which is mainly due to the large variation in the repeated drilling trials.

Table 5.6: Percentage of contribution of cutting parameters on hole size

Hole size								
	GLARE 2B 11/10		GLARE 2B 8/7		GLARE 2B 4/3		GLARE 3 8/7	
	Top	Bottom	Top	Bottom	Top	Bottom	Top	Bottom
Spindle speed	19.68	11.96	35.96	22.07	1.03	6.71	Insignificant	21.31
Feed Rate	14.84	11.31	15.69	12.24	0.41	0.63	Insignificant	22.11
Spindle speed * Feed rate	19.78	Insignificant	33.65	Insignificant	5.58	5.88	Insignificant	30.62
Error	45.68	64.98	14.69	44.46	92.96	86.76	75.05	25.94

5.1.5   Hole circularity error analysis

Figure 5.26 shows the average deviation from circularity in GLARE 3 at top and bottom locations under different spindle speeds and feed rates. The deviation from circularity increased with the increase of both the feed rate and spindle speed on both sides. The deviation of circularity measured at the bottom was considerably greater than at the top which indicates that it is likely to increase with drilling depth. The individual contribution of spindle speed and feed rate were determined by means of the ANOVA analysis. Figure 5.27 shows a comparison of the average deviation from circularity in GLARE 3 and GLARE 2B 8/7 at top and bottom locations under different spindle speeds and feed rates. The deviation from circularity at the top in GLARE 2B was greater than that in GLARE 3 when drilling at spindle speeds of n= 1000 and 3000 and less when drilling at spindle speeds

of n= 6000 and 9000 rpm. The ply orientation and level of cutting parameters seems to have an influence on the deviation of hole circularity. At the bottom, the hole circularity was greater in GLARE 3 with few exceptions. The deviation in hole circularity increased with the increase of feed rate and spindle speed, the circularity seemed to be more severe in GLARE 3 than in GLARE 2B when drilling at high spindle speeds which could indicate that the damage in GLARE 3 is likely to be worse at those cutting parameters.
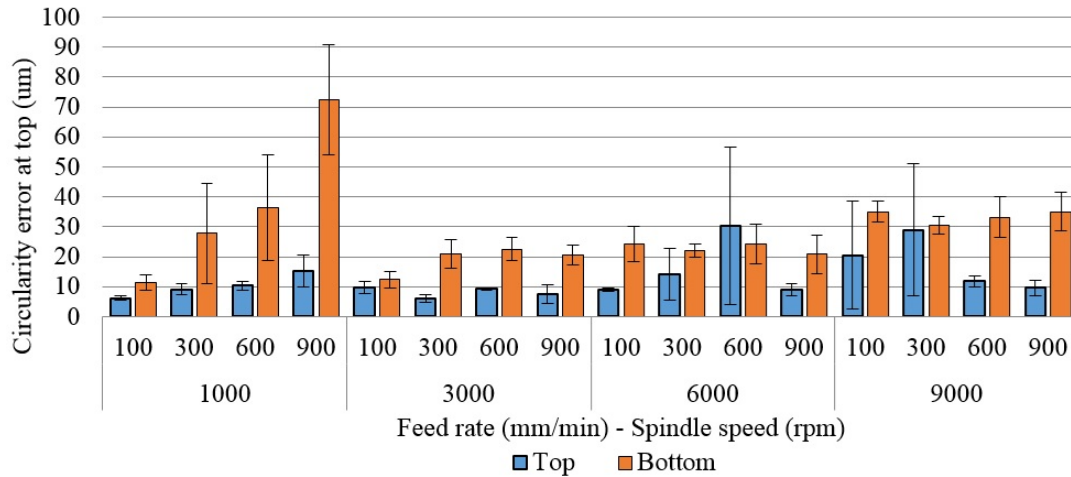
Figure 5.26: Average hole circularity at top and bottom in GLARE 3 8/7

The influence of workpiece thickness on hole circularity

Figure 5.28 shows a comparison of the average deviation from circularity in GLARE 3 and GLARE 2B 8/7 at top and bottom locations under different spindle speeds and feed rates. There was not a very clear indication of the influence of workpiece thickness on circularity. The circularity error at top decreased with the increase of drilling depth with few exceptions when drilling at a high spindle speed of n= 9000 rpm. This could be due to the increased bending of the workpiece during the drilling process for smaller depths. The circularity error at the bottom increased with the increase of the workpiece thickness. The circularity at the top in GLARE 2B 4/3 ranged between 10 µm and 19.6 µm, and between 7.84 µm and 12.51 µm in GLARE 2B 8/7 while for GLARE 2B 11/10 it ranged between 6.56 µm and 21.44 µm. The circularity at the bottom in GLARE 2B 4/3 ranged between 7.37 µm and 16.85 µm, and between 11.35 µm and 24.68 µm in GLARE 2B 8/7 while for GLARE 2B 11/10 it ranged between 10.37 µm and 28.5 µm. Comparing the circularity results in GLARE with those obtained from previous published studies on metals and composites shows that the observed hole circularities and their discrepancies were not considered high.

Percentage of contribution extracted from ANOVA analysis is given in Table .5.7. The
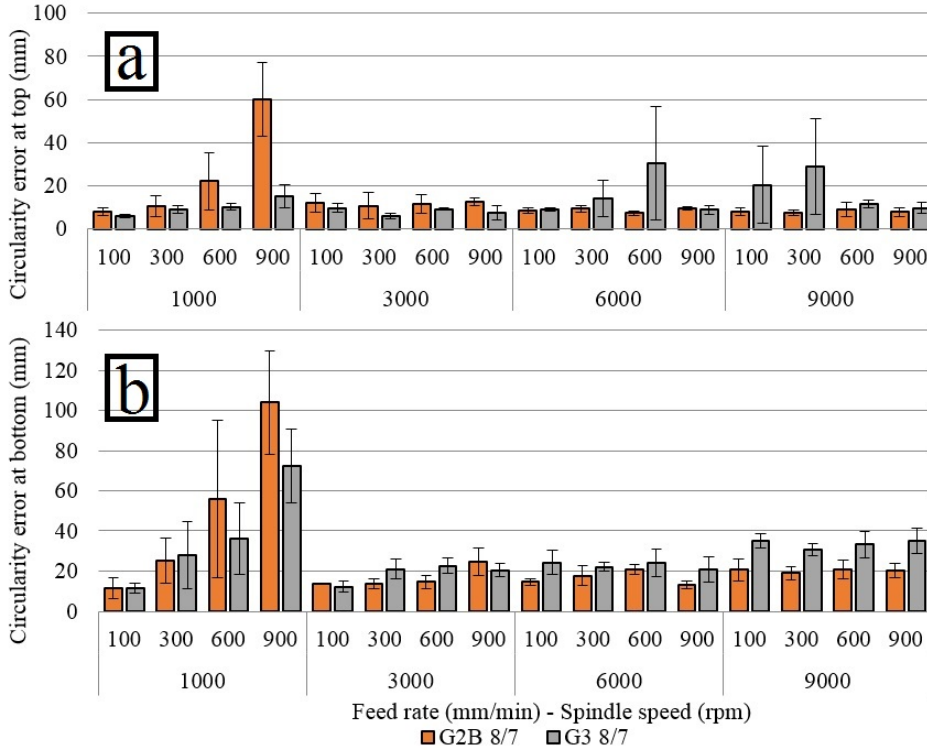
Figure 5.27: Average hole circularity at (a) top and (b) bottom
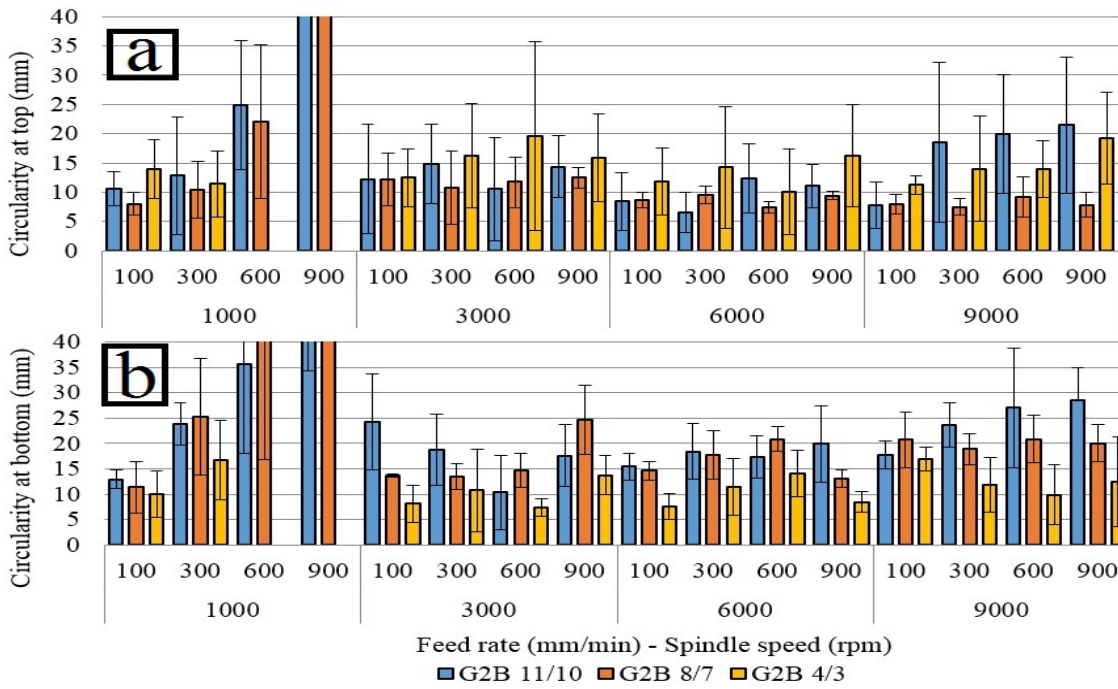
Figure 5.28: Comparison of hole circularity at (a) top and (b) bottom for different thicknesses of GLARE 2B

result indicate that the feed rate and the spindle speed had slightly higher impact on the hole circularity when drilling GLARE 2B 11/10 with 18.64 % and 13.34 % for spindle speed and feed rate respectively, while their interaction had a significant contribution of 27.02 % and similar to hole size the error in the model was large. For GLARE 2B 8/7, the influence of the spindle speed was more significant than the feed rate with 24.45 % and 27.92 % at top and bottom respectively. The feed rate contribution was around 14.5 %. The interaction between the spindle speed and the feed rate seemed to have a significant influence which ranged between 34.08 to 41.43 % which indicates that the influence of spindle speed becomes more significant with depth. For GLARE 3 8/7, the influence of the spindle speed on hole size at the bottom was approximately higher with 20.73 % for the feed rate and 13.88 % for feed rate while their interaction significantly contributed by 36.04 %. Hole circularity error at the top showed that both cutting parameters and their linear interaction were insignificant which could be due to the presence of quadratic terms in the model that affect the input parameter, this is evident by the large error present in the model 66.19 %. Therefore, the model requires further statistical analysis which will be carried out in a future study.

Table 5.7: Percentage of contribution of cutting parameters on hole circularity error

	GLARE 2B 11/10		GLARE 2B 8/7		GLARE 2B 4/3		GLARE 3 8/7	
Hole circularity error								
	Top	Bottom	Top	Bottom	Top	Bottom	Top	Bottom
Spindle speed	18.64	12.75	24.45	27.92	18.19	0.35	Insignificant	20.73
Feed Rate	13.34	13.36	14.80	14.33	10.33	0.63	Insignificant	13.88
Spindle speed * Feed rate	27.02	23.711	41.43	34.08	2.99	11.53	Insignificant	36.04
Error	40.98	50.17	19.30	23.66	68.48	87.47	66.19	29.34

To conclude on hole size and circularity error analysis, typical hole demands when drilling composite metal stack materials commonly requires to achieve an H7 hole tolerance fit based on the ISO 286 standard. This means that the hole should not vary more than ∓ 12 microns but more relaxed tolerances such as H8 (∓ 18 microns) or H9 (∓ 30 microns) were allowed to be used when drilling composites due to difficulty in achieving H7 tolerances, for example, SANDVIK recommends that drilled hole size tolerance in a composite metal stack should be between ∓ 20 and ∓ 40 microns [52]. The hole circularity error ranged between 6 and 35 microns in all GLARE grades and thicknesses under most cutting parameters. Generally, smaller circularity error is preferred and since there was no specific acceptable standard for hole circularity, comparing the results with circularity results from previous literature from chapter 2, circularity error could range anything from 6 to 312 μm. The results in the current study were similar to those reported on machining composite metal stack materials by Zitoune et al. [68].

5.1.6 Chip formation analysis in GLARE

Limited chip analysis was carried out from the collected chips after GLARE drilling trials. The chip formation analysis here is based on the description of the types of chip formation reported by Singal et al. [326]. Drilling GLARE laminates exhibits the formation of two different chip modes: those formed from the glass-epoxy matrix and those formed from aluminium sheets. In machining aluminium, the ductile material flows plastically and is pushed ahead of the cutting tool until the compression stresses are high enough to cause plastic deformation [29] and the chips undergo further deformations while chip flows upward exiting the workpiece along the face of the cutting tool. In machining composites, the cutting mechanism takes place due to fracture of the matrix and fibres. The formed chip was collected after the drilling of each hole and the analysis of the chip shows that fragmented and powdery chips were formed from cutting through the glass fibre layers due to the brittle fracture of the fibres-matrix in the laminate [29]. The generation of dusty chips indicates the absence of chip formation and that the material is separated locally, directly at the cutting edge [348]The metallic chips collected from GLARE 2B and 3 were similar at same cutting parameters. Therefore, only chips collected from GLARE 2B are shown in Figure 5.29.

The chips formed from aluminium sheets were analysed and it was observed that the chip thickness and length increased with the increase of the feed rate and decreased with the increase of the spindle speed. Different chip forms and lengths (small, middle and long chip) were observed under different cutting parameters. For example, long type helical chips were formed when drilling at a spindle speed of n= 1000 rpm and at a feed rate of f= 100 mm/min,as shown in (1). Increasing the feed rate to f= 300 mm/min produced short type helical chips as it can be seen from (2). Further increasing the feed rate to f= 600 and 900 mm/min as in (3 and 4) produced loose fragmented chips with glass fibre layers attached to them which is an indication of excessive feeding. Drilling at n= 3000 rpm and feed rates of f=100 and 300 mm/min produced long conical helical chips as shown in (5 and 6). Increasing the feed rate further to f=600 and 900 mm/min produced snarled-long helical chips and snarled conical helical chips, respectively as shown in (7 and 8). At spindle speed of n= 6000 rpm, long washer type helical chips were produced using feed rates of f= 100 mm/min as shown in (9) and washer type snarled helical chips at f= 300, 600 and 900 mm/min as shown in (10,11,12). Finally drilling at spindle speeds of n= 9000 rpm and feed rates of f=100 mm/min produced snarled ribbon chips as shown in (13), while at drilling under the feed rates of f=300,600 and 900 formed conical chips with long ribbon from one end.

Figure 5.29: Chip shapes produced when drilling GLARE 2B

Generally, the chips formed at low feed rates of f = 100 mm/min at various spindle speeds were associated with a good surface finish. In addition, chips produced at feed rates of f = 100 and 300 mm/min and spindle speeds of n = 1000 and 3000 rpm were evacuated easily from the cutting zone and did not wrap around the cutting tool. Long and continuous stringy chips with small curling were formed at high feed rates of f = 600 and 900 and high spindle speeds of n= 6000 and 9000 rpm. They chips tended to wrap around the cutting tool which would turn to be unproductive for continuous an automated machining operations where chip formation due to drilling large number of holes should not stop the production [349]. These long and continuous chips were found to damage to the borehole surface which clearly indicates a trade-off between spindle speeds and feed rates in order to achieve good hole quality and efficient machining process. Drill burr caps were formed in each hole but tended to separate after the tool exited the hole from the bottom side of the workpiece. Several burr caps were formed in each hole, some of which were torn while others were in full shape. This could be due to the coating of the cutting tool which significantly

improves the shape of the formed burr and making them easier to separate from the hole edges due to the improved contact between the drill, chips and the borehole periphery which reduces the friction and cutting temperatures in the contact zone [307].

5.1.7   Scanning electron microscopy analysis

The status of the boreholes surface was analysed by SEM to detect any defects or damage in the metal sheets and glass fibre layers. Initial observations showed that debris and chips were more likely to adhere to the borehole surface when drilling at high spindle speeds of n= 9000 rpm and feed rates of f= 100, 300 mm/min or at feed rates of f= 900 mm/min and spindle speeds n= 1000, 3000 mm/min. It was also observed that the thickness of the laminate influences the surface quality, this is because a larger thickness means that the cutting tool will need more time to drill the hole which in return produces more heat. At higher temperatures the chips and fibres adhere to the cutting tool, or could be forced to the surface of the machined hole and its edges creating what is called waste material. The waste material can lead to rejection of the part or require an additional process to remove it. Indeed, it was previously reported that the laminate thickness is important for the quality of the machined part. For example, previous studies on milling GLARE recommended that if the thickness of the laminate does not exceed 3 mm under semi-dry conditions, feed rates up to f= 1500 mm/min can be applied, whereas for thick laminates over 6 mm, recommended feed rates are f= 600 mm/min or less under dry or semi-dry milling [1]. It was observed that when drilling at high spindle speed and feed rates the subsequent removal of glass fibre layers and aluminium sheets could sometimes leave small segments and debris which adhere to the hole surface. The debris were more likely to adhere in thicker laminates which could be due to the increase of cutting temperatures with depth. The poor thermal conductivity of glass fibre layers contributes to the adherence of the debris (waste) on the inner surface of machined holes.

In GLARE 3 (0/90 ply orientation), it was observed that the delamination type chip formation (Type I) which usually occurs in the 0° fibre orientation was present on the inspected glass fibre plies. The mode I fracture occurs due to the advancement of the cutting tool into the workpiece which causes the peeled glass fibre layers to bend like a cantilever beam [29]. The uncut fibres either bend permanently or could sometimes return to their original shape and position after the cutting tool progress forward due to the absence of plastic deformation as shown in Figure 5.30 a.
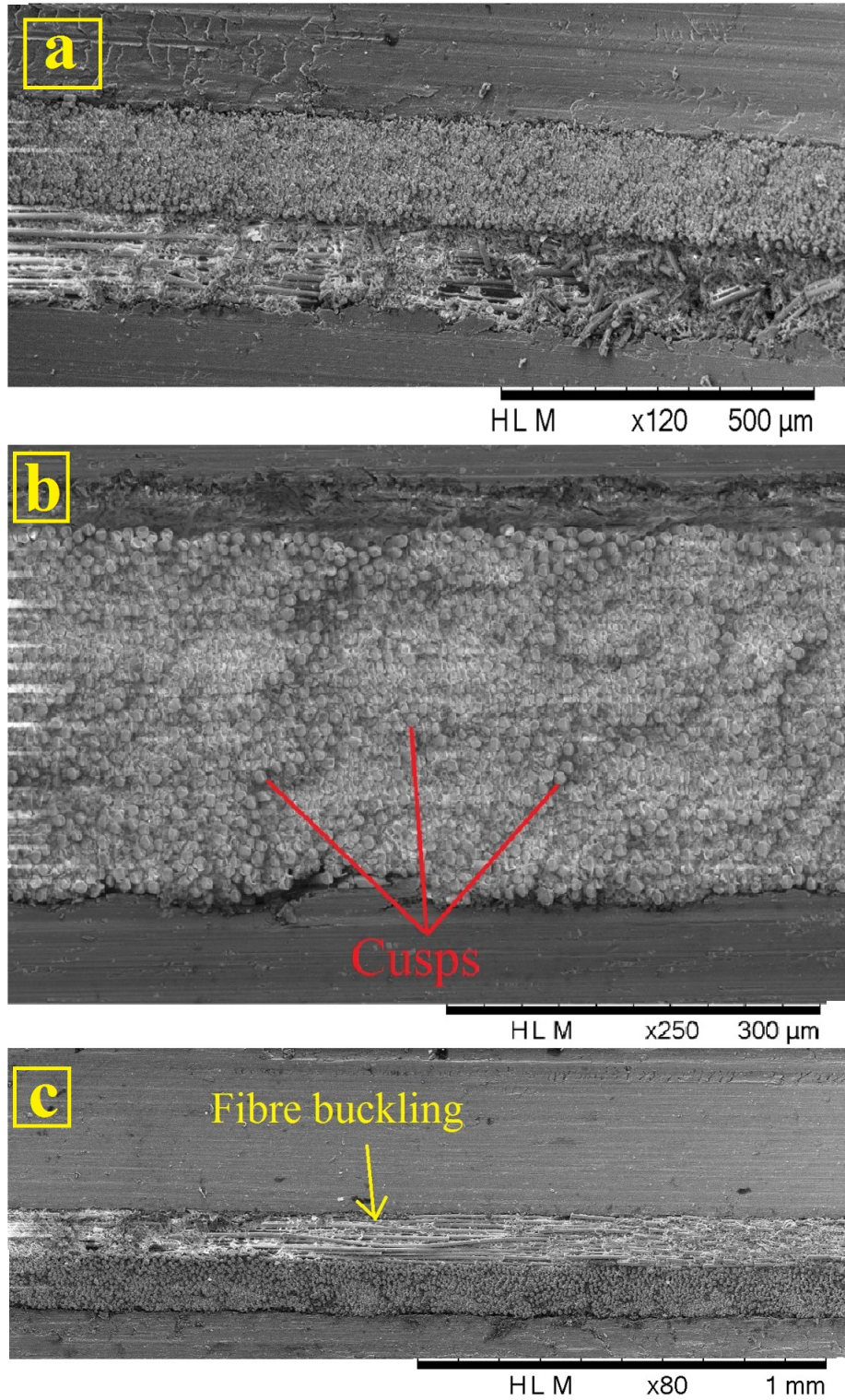
Figure 5.30: (a) Delamination type chip in GLARE (b) Smooth fibres "Cusps" formed at 0° fibre orientation in GLARE 2B 4/3 (c) an example of fibre buckling in drilling GLARE 2B

The inspection of machined hole surface microstructure shows that fibres have partly impeded in the epoxy matrix due to the elastic recovery [29]. The fracture pattern of the matrix suggests it was stretched in Mode I loading before fracture as discussed previously in chapter 2 [29]. The fibres on the machined surface are fractured perpendicular to their direction due to the compression of the cutting tool edge against the surface and micro-buckling of fibres [29]. Usually, the fibres positioned at a relative orientation of 0° to the cutting edge undergoes a minimum damage [126]. The 0° fibres were sheared from the supporting epoxy matrix which led to the formation of smooth fibre and socket surfaces commonly known as 'Cusps' [29] as shown in Figure 5.30 b. A type II fibre buckling of the chip can be also seen in Figure 5.30 c.

Fibre buckling occurs when the fibres are subjected to compressive loading along their direction [29]. Another very common phenomenon was the irregular surface created when the fibre ends stick out of the surface with varying lengths as shown in Figure 5.31. The sticking out of the fibres is because cutting by fracture occurs at different points along the fibre lengths [29]. Matrix cracking can be clearly seen in Figure 5.32 in GLARE 2B 4/3 at high feed rates equal or above f= 300 mm/min. This due to the small thickness of the laminate which is unable to resist the feed force acting during drilling.
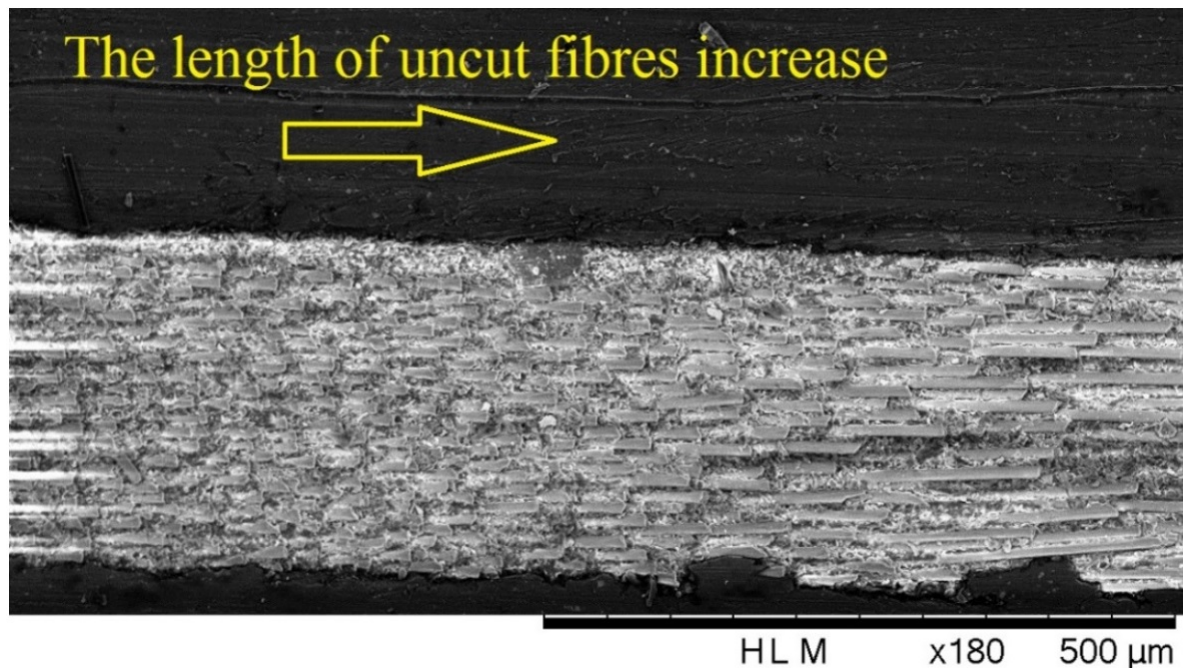
Figure 5.31: Delamination type chip in GLARE
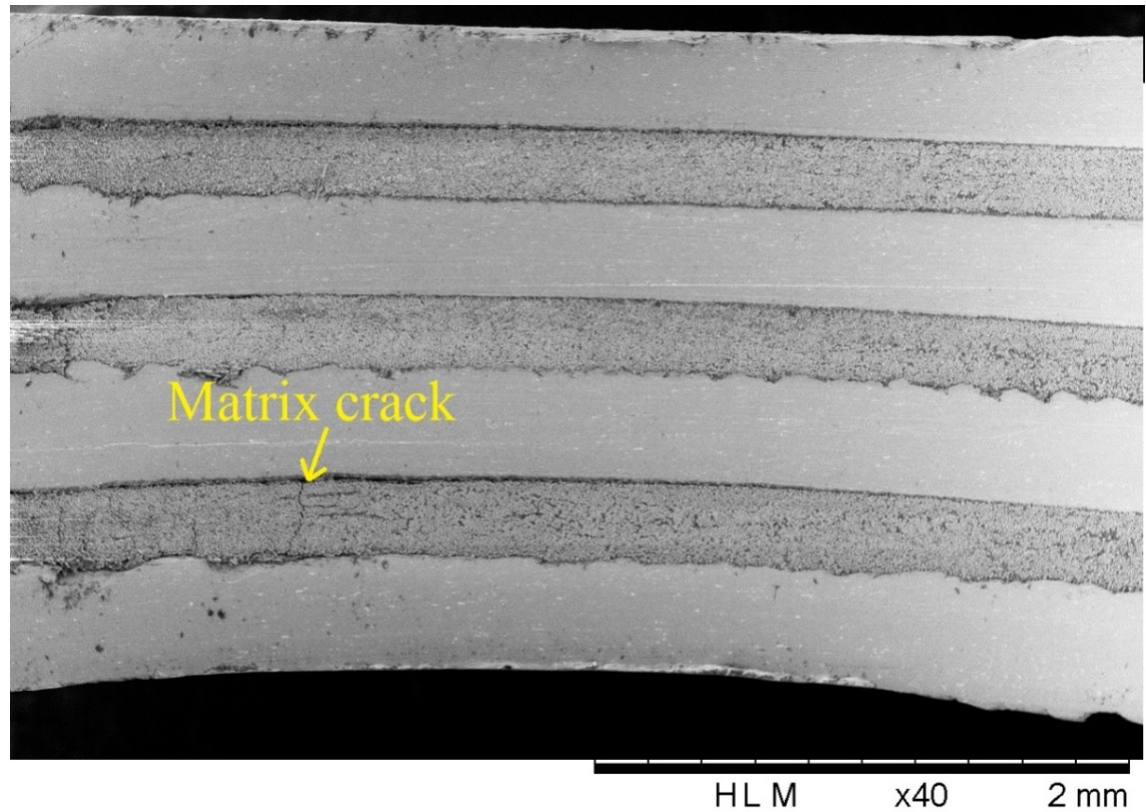
Figure 5.32: Fracture extending through the glass fibre layers in GLARE 2B 4/3 at n= 1000 rpm, f= 300 mm/min

Smearing was present when drilling at high spindle speed and feed rates, the high cutting parameters caused intense adhesion of the cutting tool coating and smearing of the softer composite matrix and aluminium on the surface of the machined hole. The smearing of the work material was more present near the exit edge of the hole which could be due to the rise of cutting temperatures with depth as shown in Figure 5.33.a . SEM images of common glass fibre chips are shown in Figure 5.33.b which were taken before cleaning the samples in an acetone bath shows that drilling glass fibre layers produce powdery bent chips.
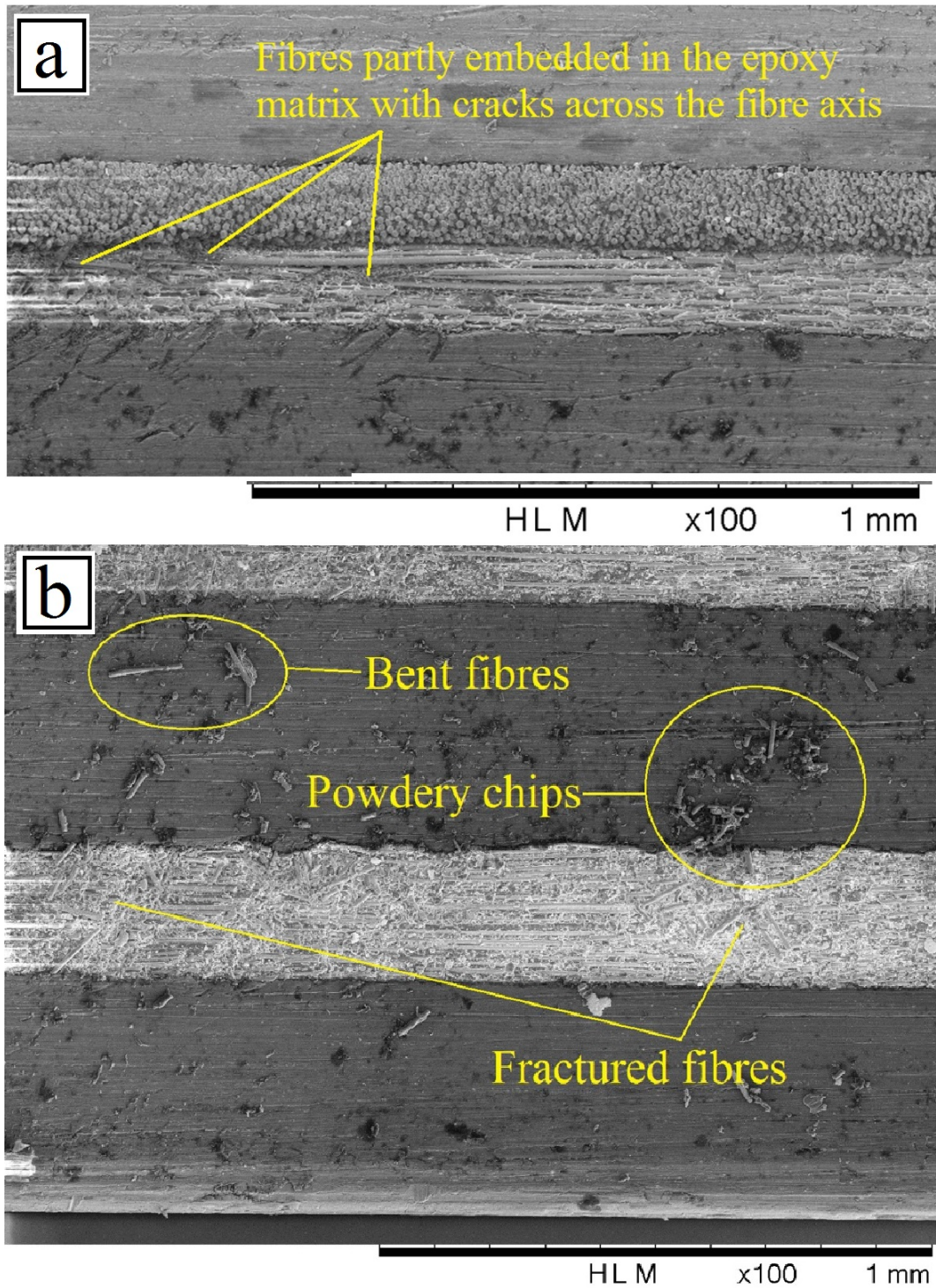
Figure 5.33: (a) SEM image of the machined surface resulting from drilling GLARE 3 8/7 showing fibres partly embedded in the epoxy matrix and cracks across the fibres at 9000 rpm and 300 mm/min (b) Fracture extending through the glass fibre layers in dry GLARE 2B 11/10 at n= 9000 rpm, f= 600 mm/min

5.1.8   Delamination analysis

SEM revealed that the region between fibre interlayers tended to separate exclusively either at the fourth or the last glass fibre layer which indicates that it is a possible location for internal delamination. The separation occurred when drilling at spindle speeds of n= 9000 rpm and feed rates of f= 900 mm/min in GLARE 3, also at a spindle speed of n= 1000 rpm and feed rates of f= 600 and f= 900 mm/min in GLARE 3 and GLARE 2B 8/7 as shown in Figure 5.34.
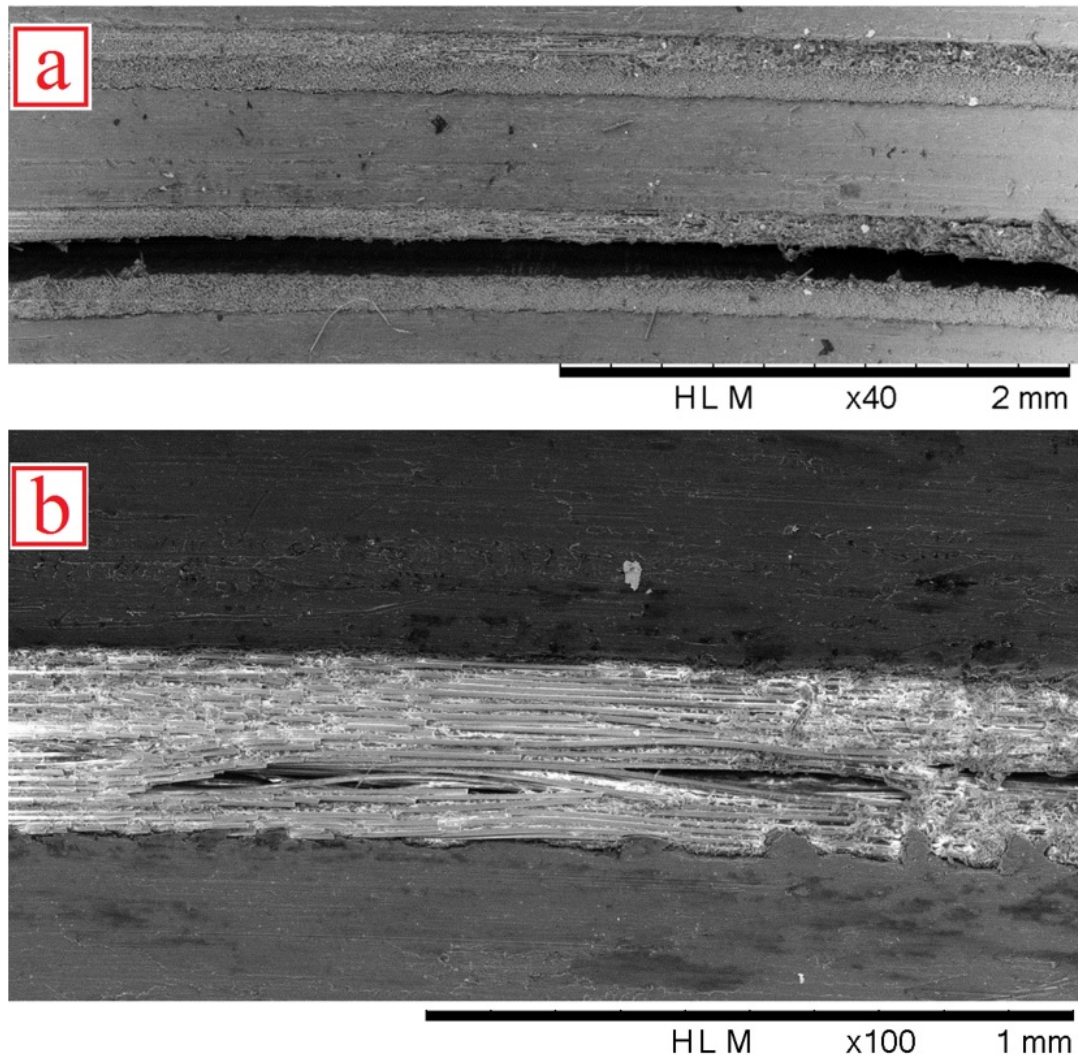
Figure 5.34: Delamination in glass fibre layer in (a) GLARE 3 8/7 at n= 9000 rpm, f= 900 mm/min (b) GLARE 2B 8/7 at =1000 rpm, f= 600 mm/min

The separation in GLARE 3 was more severe than in GLARE 2B. The delamination in the last glass fibre layer is due to push-out delamination due to the action of the feed forces which pushes away the laminate directly under the drill especially as it approaches the end

of the workpiece. The uncut thickness becomes smaller and the resistance to deformation decreases when at some point the loading exerted by the feed force exceeds the interlaminar bond strength, leading to what is known as push-out delamination [93].

The delamination in the middle of GLARE 3 laminates is due to the continuous shear and compressive action of the cutting tool while cutting through GLARE which creates three-dimensional interlaminar stresses in glass fibre layers that could lead to internal delamination between adjacent plies. The rotational and axial motion of the cutting edge of the drill towards the bottom of the workpiece tends to pull the abraded material away along the flute by introducing peeling forces acting upwards against the downward thrust force. The material spirals up before it is machined completely causing the upper laminas from the uncut portion to separate from the lower laminas being pushed by the thrust force [93]. Moreover, it is well known that the fibre layers undergo severe plastic deformations during the drilling process which directly influence the strains. The strains in the fibre direction are much larger than in the traverse direction which means that for cross ply configuration laminates such as GLARE 3, it is more likely for delamination to take place due to dissimilar fibre directions. This means that the two prepregs in GLARE 3 residing between two aluminium sheets will produce different strains in each direction depending on fibre orientation and therefore, increasing the potential for delamination. Indeed, as evident from literature, when drilling composites the quality of drilled hole depend on more on fibre than the matrix [109].

A critical factor that affects the damage tolerance in composites is the fibre direction. Generally, the energy can be easily passed from one composite layer to the other if they both have same fibre orientation and as a result, the severity of damage is greater than what would be if the fibres in each layer had different orientations, since this will have a transfer of energy between layers and allow it to fail at a higher load. Therefore, from a crack resistance point of view, a [0/90/0/90] stacking sequence is preferred over [0/0/90/90] or [0/90/90/0] [110]. However, from a separation resistance point of view, the interlaminar interface between laminates with different ply orientations (i.e. cross-ply configuration) are mechanically weak and therefore, local separation of the laminate from one another is a common form of damage in such configurations [111]. This can be explained by the fact during the drilling process, the feed force is always perpendicular to the fibre direction in the laminate. The feed force exerts bending stresses on the aluminium sheets and glass fibre layers. Some of the uncut material around the hole does not undergo plastic deformation and is only limited to plastic deformation. The bending of the GLARE laminate causes yield stresses which in return results in small amount of energy storage prior plastic deformation starts [350]. The amount of stored energy is inversely proportional to the elastic modulus of

the laminate (i.e the elastic modulus of the aluminium sheets and glass fibres). Therefore, in cross ply configuration laminates, the energy stored will be different in each fibre direction which increases the potential for spring back which results in delamination. It was also observed that in drilling process of GLARE laminates, the delamination always grew in fibre direction.

As previously discussed in chapter 3, the visual inspection of delamination in GLARE is not possible since glass fibre layers are surrounded by aluminium sheets from both sides. Visual inspection using optical microscopy turned to be cumbersome due to limited contrast and magnification to resolve the defects. Besides, the aluminium sheets are highly reflective since their surface is polished after drilling which reduces the applicability of optical microscopy. In addition, the destructive analysis of internal damage on the drilled surface by chemical erosion of metallic sheets might create more damage and would over/underestimate the true damage around the hole edge. For these reasons, the computerised tomography (CT)-scanning analysis was adopted to examine the damage in glass fibre layers of holes drilled in GLARE laminates. The methodology of delamination assessment was previously described in chapter 3. The different characteristics of metals and composites in GLARE can affect the machining performance and result in a compromise. For example, the CT scan images revealed that some of the glass fibre plies were eroded in the GLARE stack by metallic chips. This phenomenon is known as composite erosion which is caused by the evacuation of metallic chips during drilling as shown in Figure 5.35.

The maximum depth of erosion was found to be around 150 μm and tended to increase with the increase of the feed rate due to the increase in chip thickness. In addition, the erosion seemed to be more likely to occur in all glass fibre layers when drilling thinner laminates which could be due to an increase in downward bending of the workpiece making the glass fibre layers more exposed to the cutting tool and evacuated chips. Inspecting glass fibre layers in each hole for surface delamination showed that it was minor and therefore it was not reported in the current research. The layered structure of GLARE with glass fibre layers located between two metallic sheets can be compared to a composite workpiece stacked between two metallic plates. Tsao and Abrato previously reported that the use of a backup plate can significantly reduce the delamination by providing support and minimising deformations [351, 352]. Peel up and push-out delamination was minor in glass fibre layers. Only minor damage was observed which could be due to the act of interlayer burrs and evacuated chips eroding the inner surface of the hole. This was also observed in the work of Zitoune and Shyha when drilling composite metal stacks [65, 68]. The absence of surface delamination could be also attributed to the cutting tool high hardness (45 GPa) and heat resistance (up to 1200 °C) of the coating material used in the drill bits.
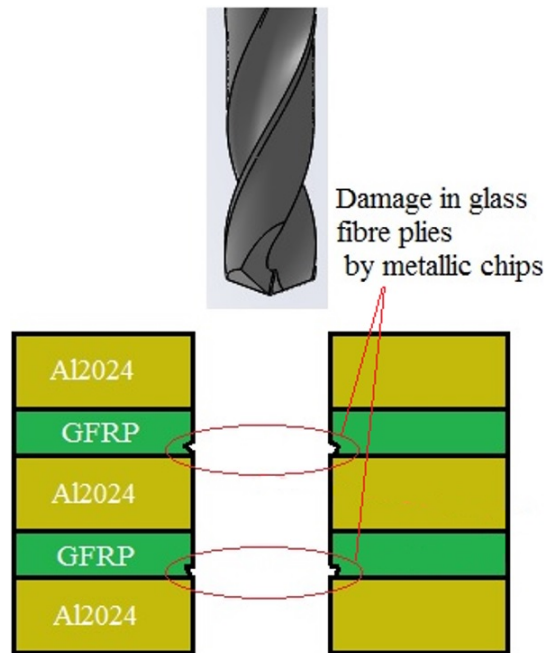
Figure 5.35: Schematic representation of erosion of glass fibre layers in GLARE by metallic chips

In GLARE, there are two different types of interfaces: the interface between aluminium sheets and the epoxy, and the interface between the fibres and the epoxy. Both interfaces contribute to load transfer in the laminate [1]. The bond between aluminium and epoxy and between the fibre-epoxy interfaces can be degraded by the rise of temperatures in the laminate. This is evidenced by the erosion observed on the hole boundaries as shown in 5.39. Surface pitting is common when drilling composites which could be attributed to the fibre breakouts when the cutting direction is 45° to the fibre direction [353]. This can be usually avoided by using cutting tools with high axial rake angles (27°) at the outer diameter, or by using feed rates of less than half a ply thickness per tool revolution [353]. The softening of the fibre-matrix during the drilling process reduces its ability to transfer the local strain disruptions to the fibres and provide them with sufficient stability against the cutting action of the twist drill [126]. As a result, fibres fracture and debonding can be seen on the edge of the hole when the feed force exceeds the ultimate strength of the fibre causing them to fail under compression, tension or shearing mode depending on the fibre orientation relative to the cutting edge of the drill [126]. The erosion can be seen to happen at ± 45° with respect to 0° fibre orientation as shown in Figure 5.36.c which could be due to the compressive and bending loads of the drill bit acting on fibres in that region eroding them by pushing them down with respect to the transverse plane.
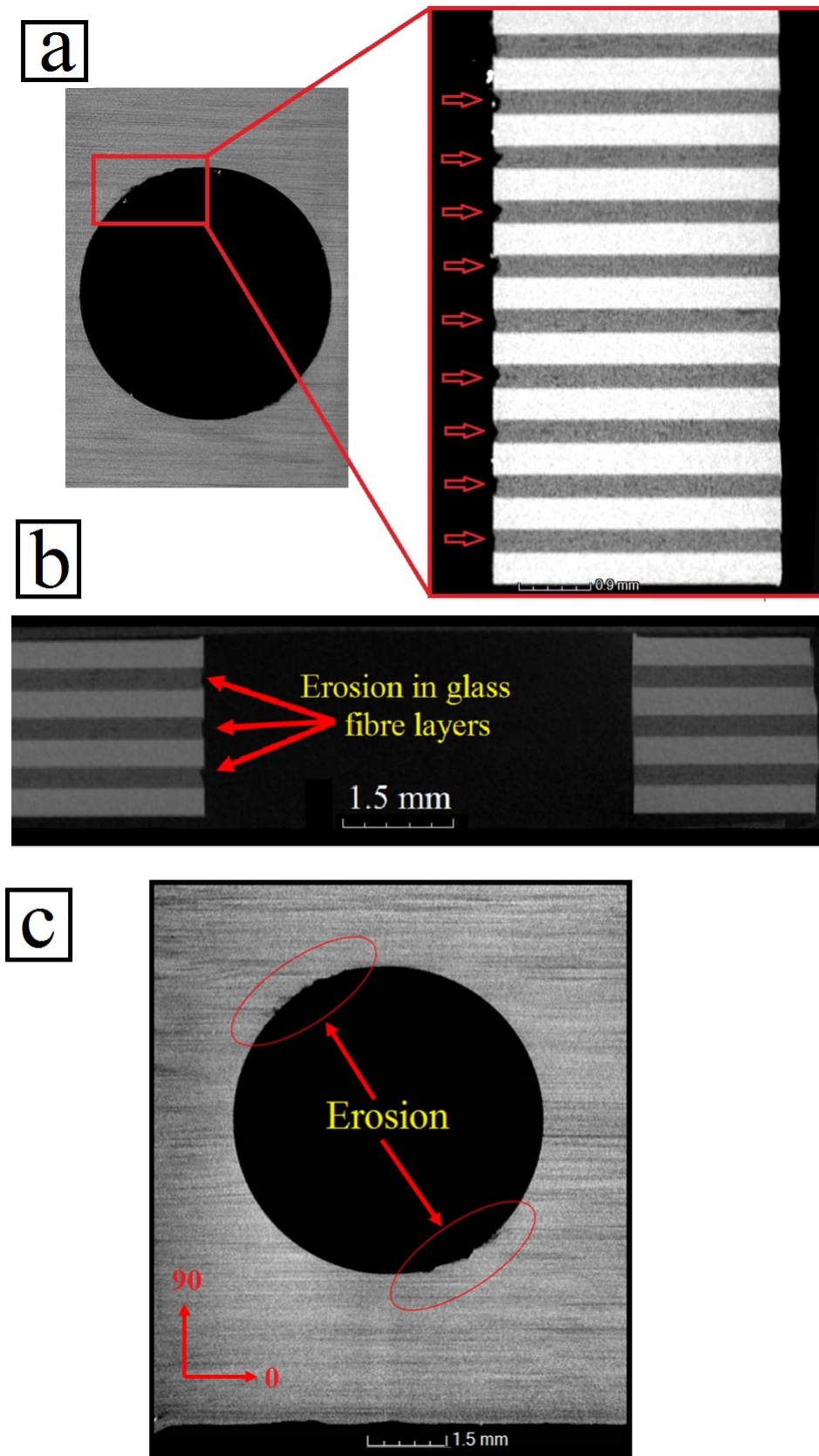
Figure 5.36: Erosion of glass fibre layers in in (a) GLARE 2B 11/10 at n=3000 rpm and f=300 mm/min (b) GLARE 2B 4/3 at n=9000 rpm and f=300 mm/min (c) GLARE 3 8/7 at n=3000 rpm and f=300 mm/min

Delamination factor F_a

As mentioned earlier in the chapter, the size of surface delamination around the hole edges and its variation with cutting parameters was negligible in all inspected holes. Glare grades and thicknesses (less than 1 %). For example, when the feed rate was increased from f= 300 mm/min to f= 900 mm/min at a constant spindle speed of 9000 rpm in GLARE 2B 4/3 - the delamination factor increased only by 0.05 %, while increasing the spindle speed from f= 3000 rpm to f= 900 rpm at a constant feed rate of f= 300 mm/min, showed that the delamination factor increased by 0.11 %. It is envisaged that this effect is caused by the presence of aluminium sheets in GLARE laminate which act as a backup structure for glass fibre layers locally preventing their out-of-plane bending and resulting in inferior normal forces.

Inspecting every glass fibre layers in each of the scanned drilled holes showed that delamination around the drilled hole was small and increased with depth. In fact, some of the inspected layers were damage-free which could be attributed to the alternating structure of GLARE. The aluminium sheets act as a backup structure and help to reduce the risk of entry and exit delamination [354]. Results showing the evaluation of surface delamination damage in the last glass fibre layer in terms of delamination factor (F_a) in GLARE 2B 4/3 are presented in Figure 5.37.
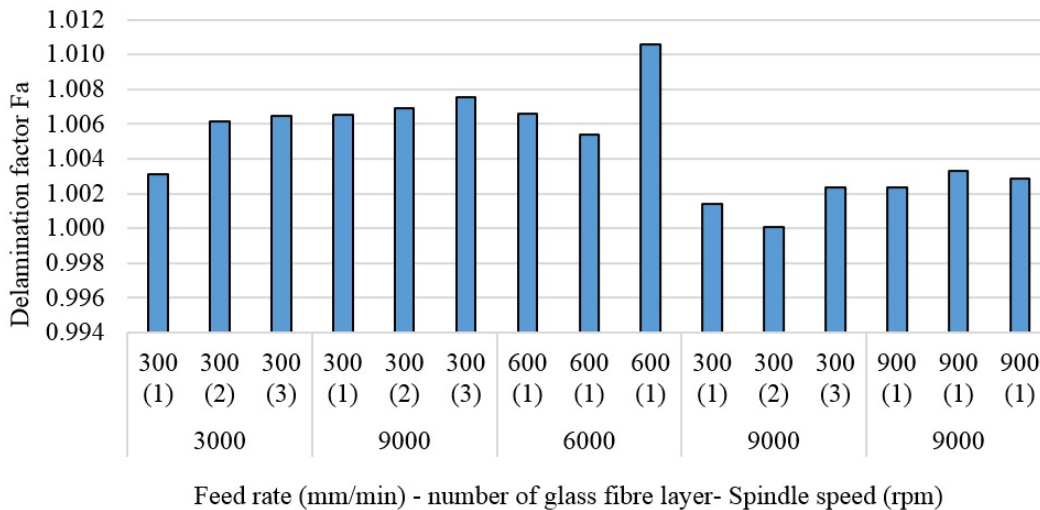
Figure 5.37: Delamination factor (Fa) in GLARE 2B 4/3-0.4 under different cutting parameters taken at the centre of each fibre layer [311]

Another reason for minimal delamination in GLARE laminates could be due to its stacking nature of having glass fibre layer stacked between two aluminium sheets. When drilling composites, the accumulated cutting heat during the drilling process softens the fibre-epoxy

and affects its interlaminar fracture strength which is directly related to delamination. In addition, the poor thermal conductivity of most composites -including glass fibre used in GLARE- and the rise in cutting temperatures can affect the strength of the workpiece allowing the push-out delamination to occur at lower levels of critical thrust force. However in GLARE, the adjacent aluminium sheets in contact with glass fibre layers from both sides contribute to partial heat removal during the drilling process due to their high thermal conductivity and dissipate heat with the cutting tool and the surrounding in a faster rate than glass fibre layers do and therefore, contribute to a reduction of delamination damage in GLARE.

It is worth to mention that despite using CT scan for analysing the internal damage -if any- within the glass fibre layers, the technique itself is limited by the maximum damage resolution it can detect. As mentioned previously in chapter 3, the internal damage which could be detected using CT scan was limited to 15 microns, which means that any damage -if it exists- smaller than 15 microns cannot be detected. Applying higher resolutions during CT scan means that a fewer number of samples could be scanned each time in a single run. In addition, the time required to complete the scanning process would increase considerably and the file size of the scanned sample/s would be so large that it would require a powerful PC with a high-end CPU and large random access memory (RAM) to open and visualises the samples in the software. Therefore, only a few samples were scanned from each test which was enough to reach a conclusion on the effect of cutting parameters on drilling-induced damage. An ideal situation would be scanning all samples and their repetitions to guarantee best results and minimise any variation in collected data. The alternative was using scanning electron microscopy by cross-sectioning the samples from their centre. However, this method cannot detect the internal damage within glass fibre layers due to the stacking nature of GLARE laminates, and it would only allow the visualisation of borehole surface for any defects and damage. The cross-sectioning and SEM inspection of the samples is more practical due to shorter process time and ease of handling which allows for inspecting a larger number of samples compared to CT scanning technique. However, the cross sectioning process of GLARE samples for SEM inspection might have caused some form of additional damage, but this could be avoided by taking proper care and handling of the samples during the cross sectioning process. Due to very limited surface delamination observed in other grades and thickness of GLARE laminates, the results of delamination factor were not calculated further.

5.1.9   Drilling temperatures analysis

The thermal conductivity of S2/FM94 adhesive epoxy system is 1.1-1.4 W/m.K (1.45 W/m.K for S2 glass fibres) while that of Al2024-T3 alloy is 121 W/m.K [6, 8] and that of solid carbide drills is around 110 W/m.K, which means that glass fibre prepregs in GLARE are poor conductors of heat. During the drilling process, the heat accumulates in glass fibre layers and is then conducted to the adjacent aluminium sheets and to the cutting tool. The rise of temperature in glass fibre prepregs can influence the physical properties of the epoxy system, such that the increase in cutting temperatures can soften the epoxy matrix and induce greater instability in the fibres due to micro-buckling [126]. Previous studies on drilling temperature showed that it could range between 90 °C and 580 °C depending on the cutting parameters used and the thermal conductivity of the composite material [116, 199, 355, 356, 356, 357]. The temperature of the twist drill used for drilling GFRPs was reported to reach up to 168 °C at the cutting edges under dry conditions [358], which indicates that the drilling temperatures could exceed the softening temperature of the epoxy such as that used in GLARE which has been reported by CYTEC to have a service temperature (glass transition temperature Tg) of 103 °C in dry conditions [1]. The rise in cutting temperatures weakens the epoxy and affects the bond interface between the glass fibre and the matrix, which plays a significant role in the transfer of stresses to glass fibre layers during the drilling process.

Figure 5.38 shows the temperature readings of two holes drilled in GLARE 2B 11/10, Figure 5.38.a shows the temperature profiles for the last aluminium sheets just before being removed from the workpiece, while Figure 5.38.b shows the maximum temperature profiles of a burr cap separating from the workpiece. The temperature contour profile of the hole in each figure shows that different regions of temperature forms uniformly around the hole periphery during the drilling process. It was found that the temperature decreases when moving away from the hole centre (see Figure 5.38.a) the centre of the hole and up to its edges showed the highest temperature readings with maximum temperature recorded to be around 192.3 °C in this case, and with an average reading of 176.1 °C up to the hole vicinity. Figure 5.38.b shows an aluminium burr cap prior separating from the bottom surface of the hole which gives an estimation of the temperature of the evacuated chips during the drilling process indicating that it can also reach high temperature levels similar to those observed on the machined hole surface.
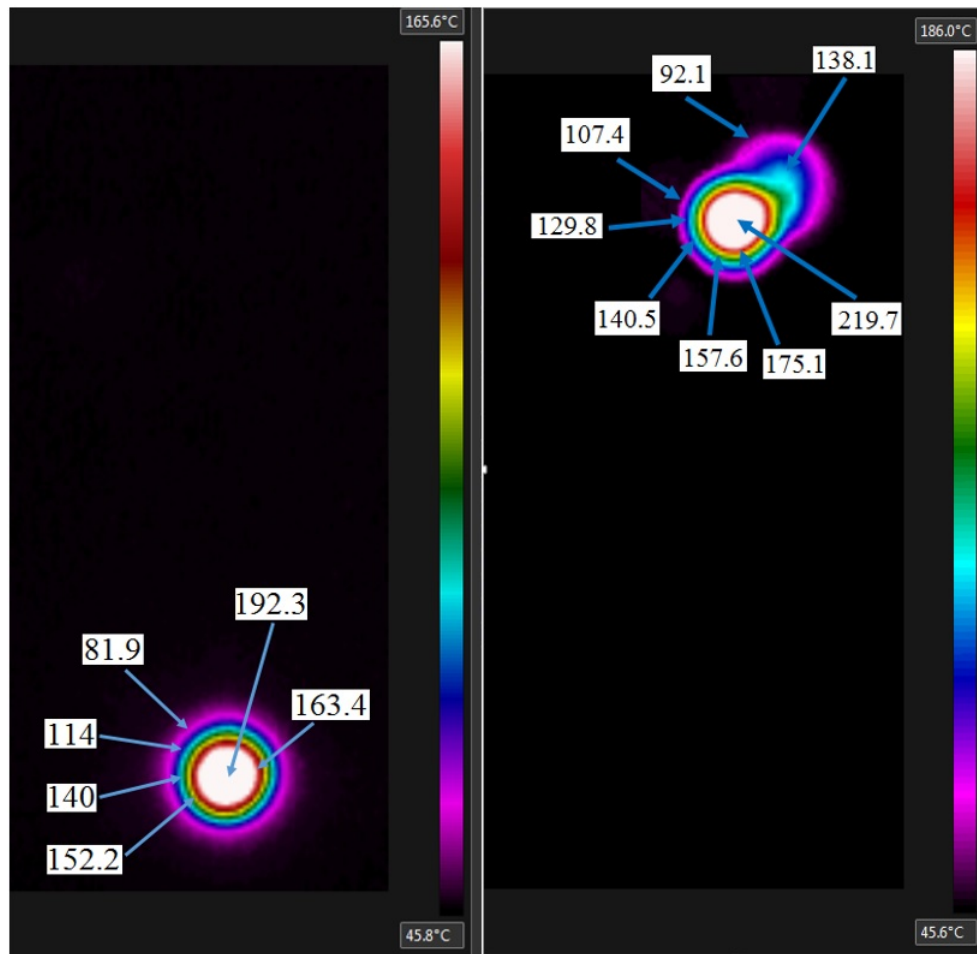
Figure 5.38: Maximum temperature readings when drilling GLARE 2B 11/10 at (a) 6000 rpm and 300 mm/min (b) 9000 rpm and 900 mm/min [321]

The heat generated during the drilling process also contributes to the rapid deterioration of the compressive strength of the fibres. The hole surfaces undergo softening of the matrix material which causes smearing over the hole boundaries due to the heat generated during drilling. Therefore, some thermal work was carried out to determine the maximum drilling temperature around the edges of the hole when the tool exits the workpiece using IR camera. AS evident from Figure 5.39 Results showed that the drilling temperature increased with the increase of the feed rate. For example, when increasing the feed rate from f= 300 mm/min to 600 mm/min at a constant spindle speed of n= 3000 rpm in GLARE 2B 8/7, the drilling temperatures increased from 163.2 °C to 185.6 °C. Increasing the feed rate to f= 900 mm/min increased the drilling temperatures slightly further reaching 188.1 °C, which could be due to the increase in chip thickness and friction with increasing feed rate. As feed increases the chip is thicker and larger thickness-to-surface area of the chip is cut per revolution which means there is less opportunity for the heat to be dissipated, hence

temperature increases. The finding disagrees with previous studies on drilling monolithic aluminium alloy, CFRP/Al7075-T651 and CFRP/Al6061-T6 stacks [164, 359, 360] which observed that the cutting tool temperature decreased with an increase in feed rate for the same spindle speed and drilling depth values. However, in another study on drilling titanium alloys, increasing the feed rate increased the drilling temperatures for the same spindle speed and drilling depth [361].
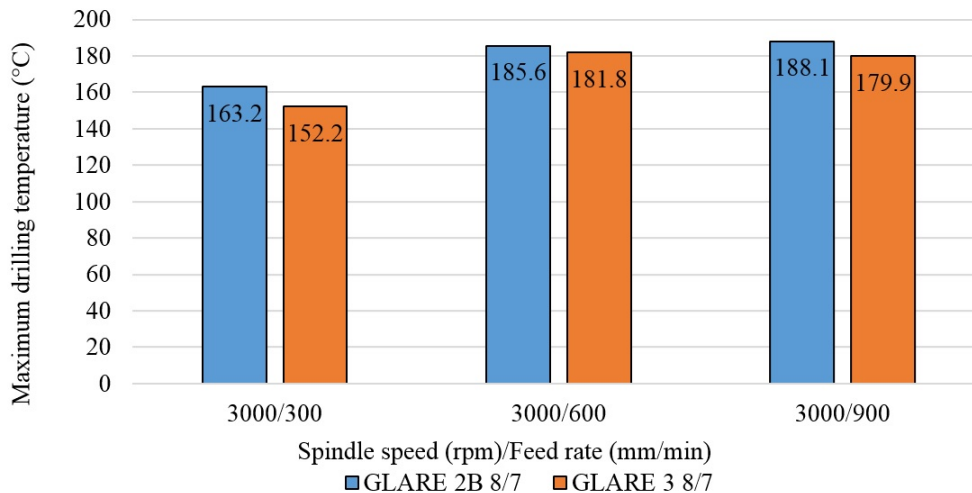
Figure 5.39: Maximum drilling temperature and the influence of fibre orientation in GLARE [321]

The rise in temperature with feed rate increase may also be accounted for in burr formation. As temperature and thrust force increase, the bottom aluminium sheet experiences increased ductility which increases the size of formed burrs. The results also showed that the maximum drilling temperatures in GLARE 3 8/7 were lower than in GLARE 2B 8/7 which indicates that the fibre orientation in GLARE can influence the machining temperatures. For example, when drilling at f= 900 mm/min feed rate and n= 3000 rpm spindle speed, the maximum drilling temperature reached 188.1 °C in GLARE 2B 8/7 and 179.9 °C in GLARE 3. The variation in thermal conductivity exhibited by the matrix due to different fibre orientation affect the temperature rise during the drilling process. The results agree with findings of Ghafarizadeh et al. [116] who previously reported that the fibre orientation has significant effects on the cutting forces and cutting temperature when milling unidirectional CFRPs such that the maximum and minimum values are obtained at fibre orientations of 90° and 0°, respectively. The difference in drilling temperatures did not exceed 10 °C for the tested cutting parameters which could be due to the small thickness of the glass fibre layers in GLARE. As shown previously in cutting forces results, there was no significant difference in thrust force between GLARE 2B and GLARE 3 arising from the difference in fibre orientation for the same thickness. However, it was observed that the

torque in GLARE 2B was higher than in GLARE 3 at same tested cutting parameters (refer to Figure 5.4) which could have been due to higher friction between the cutting tool and the workpiece causing a greater temperature rise in GLARE 2B. In addition, the relatively small thickness of glass fibre layers might not be enough to promote a significant temperature rise due to change in fibre orientation. The observed temperature values are within the range obtained from previous studies on drilling aluminium alloys such as Al2024-T3, Al6061-T6 and Al7075-T6, which showed that maximum temperatures ranged between 131 °C and 360 °C when drilling monolithic aluminium and up to 199 °C in composite metal stacks [164, 356, 359–362].

The influence of elevated machining temperatures on the deformation and delamination in GLARE laminates can be directly related to the residual stresses which take place in the laminate. The residual stresses is directly related to the thermal expansion coefficients of the constituent materials. The rise in workpiece temperature during machining softens the adhesive reducing the maximum allowed shear stresses -including those which occur in the interfaces at the hole edge through its thickness- which are directly related to the internal stresses described earlier. The reduction in maximum shear stresses causes delamination to occur earlier due to the reduction in bond strength between the glass fibre prepregs and between the aluminium sheets and fibre layers. The higher the rise in workpiece temperature during machining the more likely to cause a dramatic loss of delamination resistance in the laminate.

5.1.10   Post machining cutting tool condition

The cutting tools were inspected using optical microscopes after the end of each drilling trial. Limited tool wear was observed on the cutting tools, as shown in Figure 5.40. Some adhesions from aluminium sheets were observed on the primary and secondary facets in each of the cutting tools used, the concentration was at the centre of drill on the chisel edge, which might take place when drilling at spindle speeds of n= 1000 rpm and feed rates of f= 600 and f= 900 mm/min. Minor built up edge was found on the outer part of the cutting lips which could occur when drilling at feed rates of f= 100 mm/min and spindle speeds of n= 3000, 6000 and n= 9000 rpm. Generally, the cutting tools did not show any signs of severe wear or damage after drilling 16 holes under different spindle speeds and feed rates.
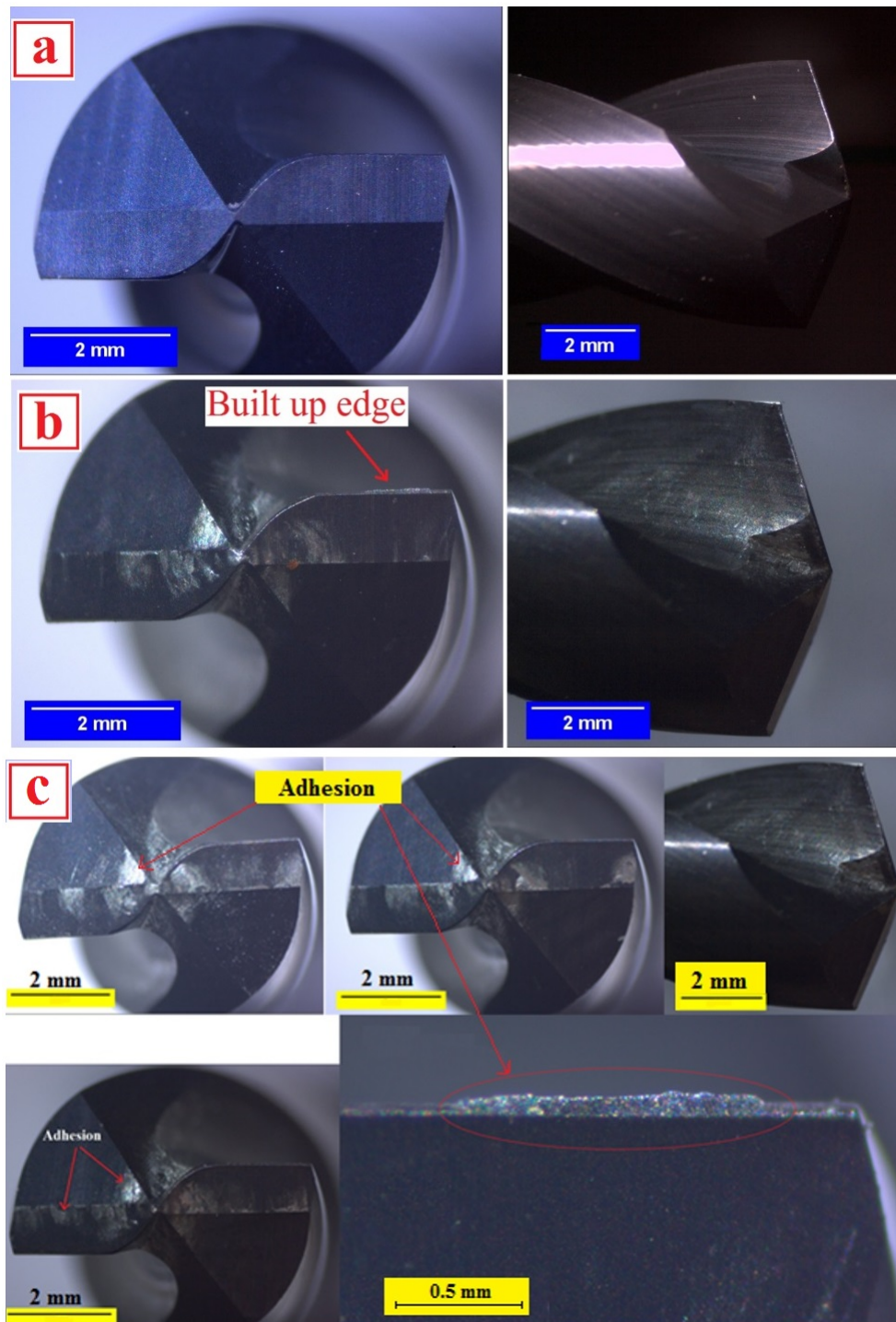
Figure 5.40: Cutting tools used in drilling trials for GLARE laminates (a) Before drilling (b) After drilling in GLARE 2B 8/7 (c)After drilling in GLARE 2B 11/10 and GLARE 3 [190]

5.1.11 The influence of input machining parameters on response outputs using response surface methodology

In this section, the application of response surface methodology and central composite design were implemented to analyse the influence of significant cutting parameters on cutting forces, surface roughness burr height, burr thickness, hole size and circularity error when drilling GLARE 2B 11/10. The percentage contribution analysis of thrust force and torque shows that the quadratic terms of controllable input factors were significant with spindle speed contribution ranging from 9 % to 12.46 %, and from 1.29 % to 4.73 % for feed rate. The coefficient of determination R^2 indicates how much of the variation is justified by the input factors and their interactions. The R^2 values for thrust force and torque were 97.68 % and 96.91 % respectively which indicates adequate models. For surface roughness, burr heights and thickness the adequacy of the model drops as R2 ranged around 69 % which means that 31 % of the variation is unaccounted for in the model due to the large error of about 30 % in each of the responses. The quadratic terms of surface roughness were insignificant with less than 0.5 % contribution. For burr height and thickness, a minor contribution can be seen from quadratic terms ranging from 2.37 % to 14.38 %. The case is similar for hole size and circularity error since R^2 is below 50 % with large errors up to 70 %. The quadratic terms contribution on hole size at both sides were minor with around 1 %, and from 1 % to 9.4 % in circularity error. Generally, a large error in the model indicates the need for a transformation or addition of extra terms that could improve the quality of the model and the predicted responses which are not investigated in this research. The larger percentage error in hole size and circularity is due to the large variation in the replicates data under same cutting parameters.

Confirmation tests shown in Table 5.8 indicate that the thrust force can be accurately predicted with an error of less than 7 %. For example, when drilling at n= 9000 rpm spindle speed and 450 mm/min feed rate, the average experimental thrust force was found to be 163 N while the predicted thrust force from the regression model gave an estimate of 153.4 N, which means that the model can accurately predict the thrust force. Similarly, the regression models were able to predict torque and surface roughness accurately with minor errors of 2.47 % and up to 13.38 %. The burr height, burr thickness and hole size regression models showed somewhat inaccuracies in predicting experimental measurements. The accuracy of predicting the circularity error using the regression models was very poor and therefore should not be used for future predictions. Ideally the error should be minimal and therefore in this case, requires further research. However, the majority of the error could be due to noise, defects in GLARE samples, human error and vibrations during the measurement process. Such drivers might not be completely eliminated and are not

discussed any further in the analysis model.

Table 5.8: Confirmation tests to validate the regression model

	@ 9000 rpm and 450 mm/min			@ 4500 rpm and 600 mm/min		
	Experimental	Predicted	Error %	Experimental	Predicted	Error %
Thrust force (N)	163	153.4	6.25	270	290	6.9
Torque (N.m)	0.288	0.254	13.38	0.512	0.525	2.47
Surface roughness (μm)	3.03	2.77	9.3	1.995	2.05	2.68
Entry burr height (μm)	3.96	5.94	33.34	3.36	3.78	11.11
Exit burr height μm	20.8	27.76	25%	18.67	20.47	8.8
Entry burr thickness (mm)	0.0974	0.1064	8.45	0.1008	0.1109	9.1
Exit burr thickness (mm)	0.2259	0.1539	46.8	0.2225	0.1178	8.9
Entry hole size (mm)	13.74	10.93	25.7	6.95	7.38	5.8
Exit hole size (mm)	-6.409	-4.87	31.6	-1.59	-3.52	54.8
Entry circularity error (μm)	9.255	56.98	515	8.39	55.43	560
Exit circularity error (μm)	28.365	97.99	256	22.15	97.94	342

Table 5.9: Percentage contribution of controllable parameters on response parameters

Response parameters Input factors	Thrust force	Torque	Surface roughness	Burr height		Burr thickness		Hole size		Circularity error	
				Entry	Exit	Entry	Exit	Top	Bottom	Top	Bottom
n	47.25	51.69	65.89	0.11	0.06	25.55	0.33	12.27	1.55	4.87	14.65
f	32.52	26.58	0	7.43	4.05	10.6	8.81	18.87	13.93	12.2	7.88
n^2	12.46	9.057	0.37	14.38	14.14	6.18	13.24	3.91	11.75	14.63	0.094
f^2	1.287	4.729	0.32	9.16	8.62	2.37	11.76	1.85	1.04	9.40	2.91
$n.f$	2.88	3.68	2.74	5.03	0.14	8.29	3.98	0	0.20	1.04	7.981
$Error$	2.325	3.095	30.62	31.59	31.05	35.66	30.94	60.93	70.17	56.45	65.35
$R^2\%$	97.68	96.91	69.38	68.41	68.94	64.34	67.98	39	29.81	43.69	34.66

Table 5.10: Estimated regression coefficients for MQL drilling trials and their percentage contribution

Factors	Thrust force	Torque	Surface roughness	Burr height		Burr thickness		Hole size		Circularity error	
				Entry	Exit	Entry	Exit	Top	Bottom	Top	Bottom
Constant	227.361	0.409278	2.25328	3.3804	18.2631	0.101764	0.101764	6.00881	5.99664	0.00865	0.024826
n	-98.826	-1.90E-01	0.4272	0.1631	0.6668	-1.45E-02	-7.52E-03	2.22E-03	-8.00E-04	7.65E-04	2.55E-03
f	81.985	1.37E-01	-0.00103	1.317	5.228	-9.36E-03	3.84E-02	-2.76E-03	-2.36E-03	1.22E-03	1.87E-03
n2	5.28E+01	8.30E-02	3.35E-02	1.91E+00	1.02E+01	7.44E-03	4.90E-02	-1.30E-03	-2.26E-03	1.37E-03	-1.90E-04
f2	-1.70E+01	-6.00E-02	-3.09E-02	1.52E+00	7.94E+00	4.61E-03	4.62E-02	-9.00E-04	6.70E-04	1.09E-03	-1.19E-03
nxf	-3.45E+01	-7.19E-02	-1.23E-01	-1.53E+00	1.41E+00	-1.17E-02	-3.65E-02	-9.00E-05	-4.00E-04	-5.11E-04	2.67E-03

Figure 5.41 and Figure 5.42 shows contour plots for measured responses of RSM study of GLARE 2B 11/10. Since only two input parameters were analysed, it was easier to determine the most suitable cutting parameters which reduce the response outputs to an optimum level. In Figure 5.42 it can be seen that increasing the spindle speed and decreasing the feed rate is recommended for reducing the cutting forces. However, to achieve lower surface roughness values, drilling at lower spindle speeds and feed rates is desired. Therefore, depending on what response needs to be controlled or minimised, the contour plot charts can give a good indication of the levels of cutting parameters to choose or to avoid. Figure 5.42 shows that
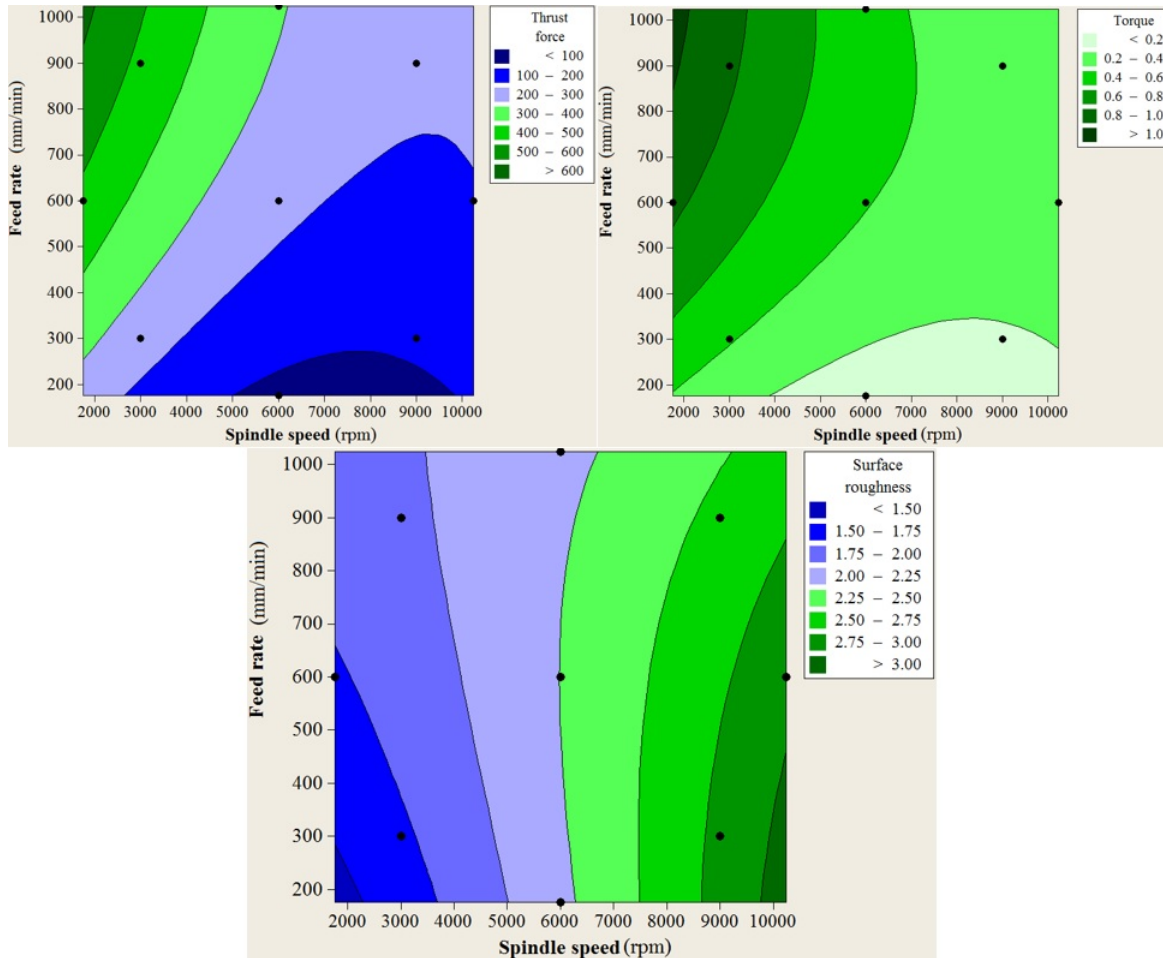
Figure 5.41: Contour plots for GLARE 2B 11/10 (a) Thrust force (b) Torque (c) Surface roughness

the models are all highly non-linear with the exception of entry burr height. They all show that a preferred cutting zone (sweet spot) for machining GLARE 2B would correspond to spindle speeds of roughly between n= 3000 rpm and no more than n= 6000 rpm, and feed rates between f= 200 mm/min and up to n= 600 mm/min.
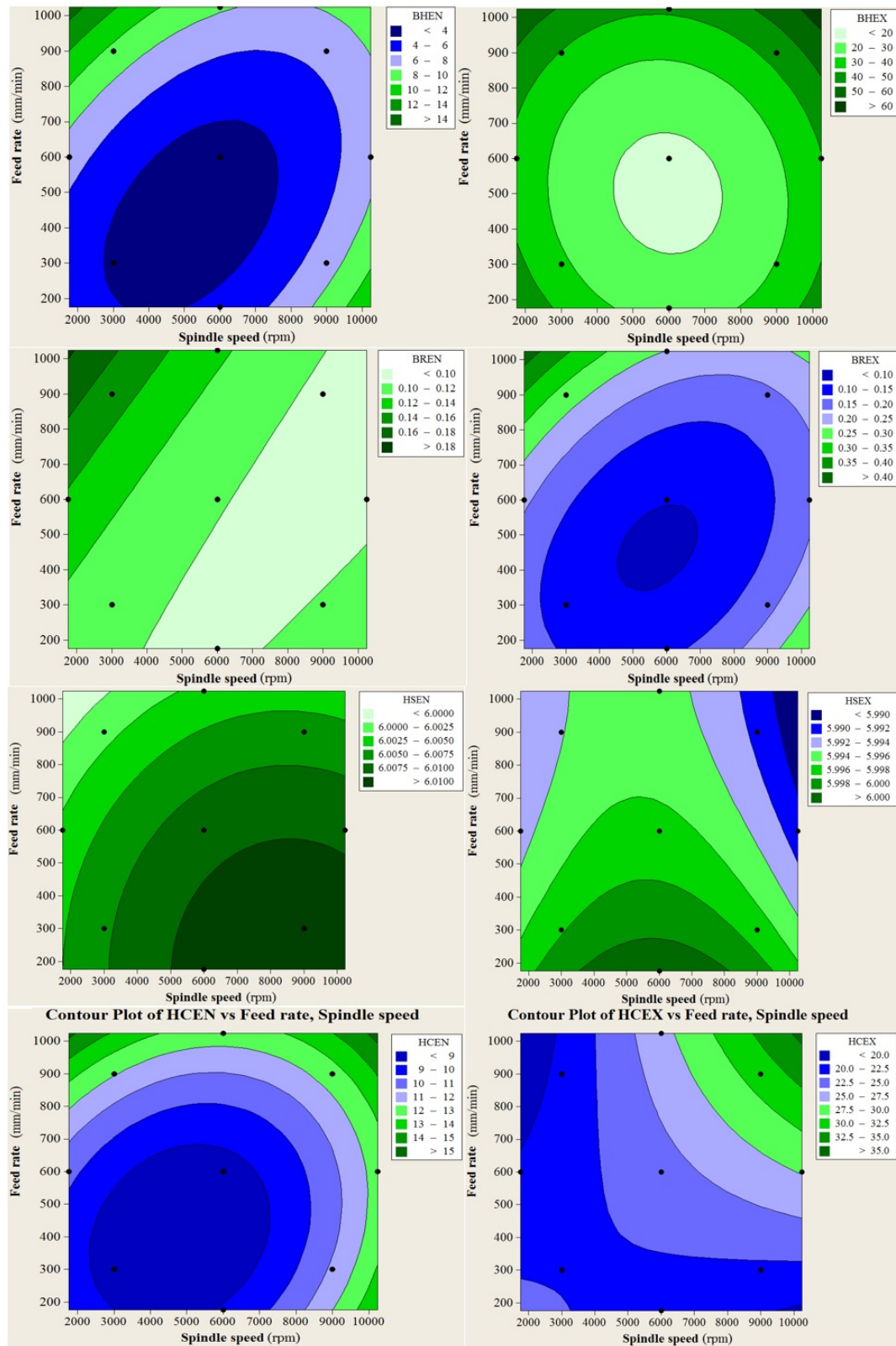
Figure 5.42: Contour plots for GLARE 2B 11/10 (a) Entry burr height in 13 μm (b) Exit burr height in μm(c) Entry burr thickness in mm (d) Exit burr thickness in mm (e) Top hole size in mm (f) Bottom hole size in mm (g) Top circularity error in μm(h) Bottom circularity error in μm

(Note) It was not possible to create contour plots for full factorial designs used in GLARE 2B 8/7, GLARE 3 8/7 and GLARE 2B 4/3. The use of normal contour plots without referring to DOE design showed similar trends for those reported previously in Figure 5.41 and Figure 5.42 for the other tested grade and thickness. However, this method does not use the models from the DOE to predict the process output so it could only give rough idea on the effect of input parameters on the responses.

5.2   Concluding Remarks

As discussed in Chapter 2, several conventional machining processes such milling and drilling were used to machine metals, composites and composite metal stacks in order to comply with the aerospace industry requirement for tolerances and dimensional accuracy. Despite the reported literature and knowledge in machining of all those materials, there has been a little work reported on machining fibre metal laminates such as GLARE due to its limited applications in the aerospace sector. Only few studies reported experimental results on limited aspects of GLARE drilling indices. The previous work on drilling GLARE has been approached only by few researchers which looked into the results of machining quality and performance of thin GLARE laminates such as GLARE 3, 5 and 6. The literature review on the machining of fibre metal laminates indicates that a full machinability investigation of drilling GLARE using design of experiment techniques has not been reported. Moreover, the machinability of thick laminates for wing parts have not been yet investigated since the thickness of GLARE samples tested in all previous studies were less than 2 mm. The current study aims to fill the gap in this part of machining GLARE by exploring the machinability of GLARE 2B fibre metal laminates using various thicknesses of up to 7.15 mm. Moreover, the drilling of GLARE 3 fibre metal laminates was also carried out to evaluate the effect of fibre orientation on hole quality and cutting forces in comparison with GLARE 2B of the same thickness. Apart from that, the quality of machined borehole surface in terms of surface roughness and drilling-induced damage in glass fibre layers and aluminium sheets were not disclosed in previous studies. This is due to complexity in inspecting those indices which require state of the art scanning techniques. Therefore, the main objective is to determine the impact of cutting parameters on some of the primary machinability indices using full factorial designs and response surface methodology statistical methods. The experiments were carefully designed by investigating two experimental factors (spindle speed and feed rate) consisting of several levels to cover a wide range of cutting parameters.

In this chapter, an experimental investigation of drilling GLARE (grades 2B and 3) has been carried out to evaluate the effect of the spindle speed and feed rate on the cutting forces

and hole quality. The application of full factorial and RSM for modelling the influence of machining parameters on cutting forces and hole quality has also been investigated. Mathematical models were developed from the response surface methodology based on central composite design statistical technique and tested through analysis of variance ANOVA to determine the contribution of cutting parameters on investigated hole quality parameters for GLARE 2B 11/10-0.4. The following conclusions are drawn from the dry drilling trials of GLARE. The evaluation includes inspecting the surface roughness, hole size, circularity error, entry and exit burrs, chip formations and damage described at the macro level (delamination area) using computerised tomography CT scan, and at the micro level (fibre matrix debonding, chipping, adhesions, cracks) using scanning electron microscopy. Conclusions from section 5.1

- Both spindle speed and feed rate had a significant impact on the cutting forces, where increasing the feed rate increased the cutting forces and increasing the spindle speed reduced the cutting forces when drilling at constant feed rates. The influence of fibre orientation on thrust force was not significant. However, it was observed that the torque was generally higher in GLARE 2B than GLARE 3 under similar cutting parameters, and it increased with the increase of the feed rate by up to 12 % when drilling at a spindle speed of n =3000 rpm and feed rate of f= 900 mm/min.

- GLARE grades with a cross-ply configuration such as GLARE 3 produced holes with relatively higher surface roughness compared to unidirectional ones such as GLARE 2B. The hole depth did not seem to have an impact on the surface roughness when drilling the same grade of GLARE. However, it was observed that the surface roughness was slightly higher in thinner samples with the increase of feed rate. Within the experimental conditions used a better hole surface quality in GLARE was obtained when drilling at spindle speeds n= 3000 and 6000 rpm and feed rates of f= 100 and 300 mm/min.

- From the ANOVA analysis, the contribution of spindle speed and feed rate on surface roughness was equal in unidirectional GLARE 2B 11/10 and 8/7, while the contribution of spindle speed in GLARE 2B and 3 was more significant than the feed rate. Increasing spindle speed and feed rate increased surface roughness. Within the experimental conditions presented in this chapter, n= 3000 rpm spindle speed and f= 100, 300 and possibly up to 600 mm/min feed rates are recommended for a better surface finish.

- The minimum cutting forces were achieved when drilling at the spindle speed of n= 9000 rpm and feed rate of f= 100 mm/min. The minimum surface roughness was

achieved when drilling at spindle speed n= 1000 rpm and feed rate of f= 100 mm/min. However, this is generally considered low for practical applications in aerospace and automotive components (in terms of productivity rate).

- The damage around the hole entrance and exit side increased with the increase of both cutting parameters; good hole quality was achieved when drilling at low feed rates between 100, 300 mm/min and spindle speeds of n =3000 and 6000 rpm. Keeping the feed rate at those levels is recommended to reduce damage at the edges of the holes.

- The variation of hole size between top and bottom locations was greater in GLARE 3 than in GLARE 2B. Undersized holes are produced when drilling GLARE fibre metal laminates and the hole size drilled in GLARE laminates is likely to shrink with depth. A reduction in hole size at exit can be seen with increasing the spindle speed and decreasing the feed rate. Moreover, circularity error in GLARE 3 was greater than in GLARE 2B at the bottom location. Circularity error increased with workpiece thickness and the increase in the feed rate.

- Different feed rates and spindle speeds produced different burr heights, thickness and chips formations. Burr formation cannot be eliminated completely, but rather minimised by proper selection of cutting parameters. Results show that smallest burrs occur when feed rate is minimum. Exit burrs were much larger than at entry burrs and within the tested range of feed rates and spindle speeds. The best surface quality was achieved at a feed rate of 100 mm/min and various spindle speeds, this cutting condition gave low burr formation, circularity and close to nominal hole size.

- Overall, it is observed that the dimensional variations in hole increased with the increase of spindle speed. The mismatch in thermal expansion coefficients in the fibres longitudinal and transverse directions, and between the fibres and epoxy matrix could cause residual stresses and variation in hole size and its circularity error.

- The damage in borehole surface is related to the workpiece thickness and fibre orientation. Interlaminar failure during drilling is more likely to occur in GLARE 3 than in GLARE 2B because laminates with cross-ply configuration are mechanically weaker than unidirectional ones which mean that the influence of the feed rate is greater in GLARE 3 than on GLARE 2B. Analysis of borehole surface shows the presence of microcracks, fibre pull out, fibre-epoxy matrix shearing and interlayer burr formation in limited regions at $\pm 45°$ with respect to the $0°$ fibre orientation.

- Various chip shapes and sizes were formed at different cutting speeds and feeds, chip thickness increased with feed rate and decreased with spindle speed.

- Composite central design statistical techniques can be employed to establish mathematical models which can predict cutting forces, surface roughness and to a lesser extent burr formations in GLARE. Predicting the hole size and circularity error using the developed models was not possible and further analysis is required to improve the quality and accuracy of the models. ANOVA clearly shows that the spindle speed and the feed rate are both dominant parameters in drilling GLARE and aluminium alloys, and both contribute to reducing the cutting forces and improving surface quality.

- The recommended drilling process parameters are feed rate in the range of 100 and 300 mm/min and spindle speed in the range of 1000 and 6000 rpm, which results in minimum cutting forces, improved surface finish and dimensional hole accuracy. Best hole quality can be achieved when drilling n = 3000 rpm and f= 300 mm/min.

- Microscopic analysis of the drill bit showed signs of built up edge in the form of adhesions of aluminium material formed on the its flank face.

Chapter 6

PERFORMANCE EVALUATION OF MQL AND CRYOGENIC COOLING IN CONVENTIONAL DRILLING OF GLARE

This chapter will present an evaluation of drilling performance of GLARE when machined with minimum quantity lubrication and cryogenic cooling technologies. In Section 6.1, the drilling performance of GLARE when machined under MQL will be discussed. The performance is evaluated based on the effect of varying the cutting parameters (spindle speed and feed rate), coolant flow rate and air pressure in order to develop the basic understanding of the effect of semi-dry cooling during conventional drilling of GLARE fibre metal laminates. The evaluated parameters are the same to those reported previously for the dry drilling process in chapter 5. The evaluation includes the assessment of cutting forces and hole quality parameters. In addition, the hardness of the upper and lower surfaces of aluminium sheets will be investigated. In Section 6.2, the drilling performance of GLARE when machined with a liquid nitrogen (LN2) cooling system will be evaluated and discussed similarly to section 6.1. The analysis in this chapter also includes examining the drilled holes using optical, CT and SEM analysis methods to inspect the morphological characteristics of drilled holes under each cooling condition.

6.1 Evaluation of Drilling Performance of GLARE under Minimum Quantity Lubrication

6.1.1 Results and discussion

This section will evaluate the drilling performance of a GLARE 2B 11/10 laminate cut from the same large panel used in dry drilling trials reported in the previous chapter. The drilling process involves the application of minimum quantity lubrication cooling technology. The evaluation of drilling performance is based on results for cutting forces (thrust force and torque), average surface roughness, entry and exit burr formations (burr height and burr thickness), upper and lower hole size and circularity error. In addition, scanning techniques are employed to study the delamination and internal damage throughout the laminate layers. The methodology of the drilling trials and evaluation of the drilling performance in this section were previously described in chapter 3.

Analysis of cutting forces

Figure 6.1 shows the average thrust force and torque under different cutting parameters at various flow rates and air pressures. For ease of observation, holes drilled using the same spindle speed and feed rate but different flow rates and air pressure share the same bar colour. Results indicate that flow rate and air pressure had a negligible effect on the cutting forces. Increasing flow rate from 20 mL/hr to 60 mL/hr and air pressure from 1 to 3 bars when drilling at 3000 rpm and 300 mm/min reduced thrust force by 2.35 %, which could be attributed to the improved lubrication and penetration with depth which allows for the formation of a thin boundary film between the tool and the workpiece interface. In some cases increasing air pressure and flow from 20 mL/hr to 60 mL/hr and air pressure from 1 to 3 bars when drilling at n= 3000 rpm and f= 900 mm/min increased thrust by approximately 1.3 %, which could be attributed to reduced penetration ability of the MQL lubricant at the tool-workpiece interface with increasing the feed rate. Mendes et al. [363] previously reported that drilling Al-1050 alloy using high flow rates of cutting fluid in MQL might increase the feed force and power consumption. This indicates that using higher coolant flow rates can sometimes be unnecessary [221].
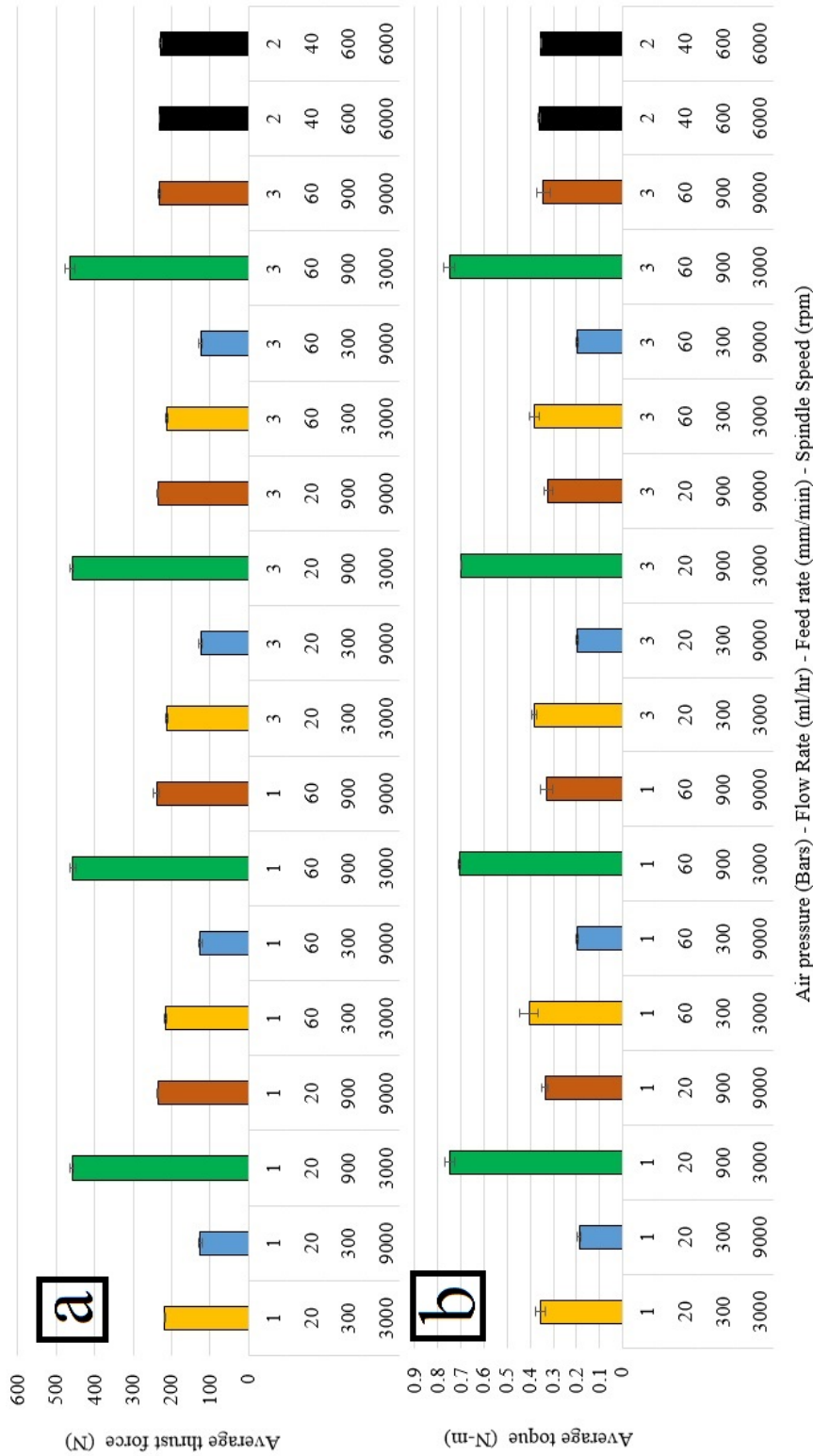
Figure 6.1: (a) The average thrust force for MQL drilling trials (b) The average torque for MQL drilling trials

In addition, excessive lubrication can sometimes wet the glass fibre dust making it stick on the borehole surface rather than allowing the tool flutes to drive it out and causing an increase in cutting forces [364]. There was no evidence for a lack of fit in the thrust force results as it can be seen from Table 6.1 which shows the percentage contribution of input parameters and their linear interactions on the output parameters. The values were calculated from the full factorial ANOVA analysis using MINITAB 16 statistical software.The regression model seems adequate to describe the thrust force data. In addition, the p-value of the curvature is extremely high, which suggests that there is no evidence of curvature.

Table 6.1: Percentage of contribution of input parameters on outputs from factorial ANOVA analysis

Source	% Contribution										
	F	T	R	ENBH	EXBH	ENBT	EXBT	HST	HSB	CET	CEB
Main effects	91.9	91.31	51.65	81.64	69.08	60.69	64.65	12.79	9.63	10.75	6.54
Spindle speed	40.07	54.08	44.68	5.10	-	3.88	-	5.8	-	-	-
Feed rate	51.83	37.17	4.64	75.11	65.30	39.32	56.09	-	-	-	-
Flow rate	-	-	0.92	0.35	0.71	15.62	-	-	-	-	-
Air pressure	-	-	1.43	1.08	2.98	1.88	8.51	-	-	-	-
2-way interaction	7.31	6.75	38.94	1.58	23.85	31.48	11.63	2.54	5.92	6.92	11.59
Spindle speed*Feed rate	7.31	6.68	33.81	0.47	-	-	0.63	-	-	-	-
Spindle speed*Flow rate	-	-	-	-	0.98	-	3.31	-	-	-	-
Spindle speed*Air pressure	-	-	-	-	1.99	-	3.68	-	-	-	-
Feed rate*Flow rate	-	-	-	-	2.21	2.55	1.07	-	-	-	-
Feed rate*Air pressure	-	-	4.69	-	18.55	26.83	2.36	-	-	-	-
Flow rate*Air pressure	-	-	-	0.75	-	0.26	0.58	-	-	-	-
3- Way interaction	0.01	0.32	2.02	3.66	3.36	2.51	11.97	3.60	10.92	3.31	15.28
Spindle speed*Feed rate*Flow rate	-	-	-	-	-	0.76	-	-	-	-	-
Spindle speed*Feed rate*Air pressure	-	-	0.5	0.71	1.18	0.43	3.48	-	-	-	-
Spindle speed*Flow rate*Air pressure	-	-	1.45	-	2.16	1.13	7.99	-	-	-	-
Feed rate*Flow rate*Air pressure	-	-	-	2.70	-	0.19	0.41	-	8.80	-	-
4-Way interaction	0.00	0.12	0.08	1.50	1.07	2.91	2.18	1.98	0.50	1.86	1.85
Spindle speed*Feed rate*Flow rate*Air pressure	-	-	-	1.50	1.07	2.91	2.18	-	-	-	-
Curvature	0.59	0.76	4.96	8.41	-	1.43	7.19	26.14	1.77	-	-
Residual Error	0.15	0.74	2.18	2.90	1.93	0.95	2.20	45.84	58.78	69.11	56.31
Lack of fit	-	0.73	-	-	-	0.94	-	-	-	68.36	-
Pure Error	0.00	0.01	0.34	0.23	0.03	0.01	0.03	0.82	7.88	0.75	1.85
R^2	99.85	99.26	97.82	97.1	98.07	99.05	97.8	54.16	41.22	30.89	43.69
R^2 predicted	98.89	97.25	88.95	82.52	95.28	95.81	85.42	0	0	0	0
R^2 adjusted	99.77	98.88	96.7	95.61	97.07	98.56	96.67	30.59	10.99	0	14.74

The results show that feed rate was the major contributor to thrust force with 52 %. Thrust force increased with the increase of feed rate due to the increase in chip load and decreased

with the increase of spindle speed. The contribution of spindle speed on thrust force was approximately 40 %. Neither coolant flow rate nor air pressure showed significant effects on cutting forces, including their linear interactions. With respect to torque, the influence of spindle speed was more pronounced at 54 %, while the contribution of the feed rate was 37 %. The linear interaction of spindle speed and feed rate had a minimal effect on cutting forces with 7.31 % and 6.68 % on thrust force and torque respectively. There was a minor evidence for a lack of fit in the torque (see Table 6.1) but generally, the regression model seems adequate to describe the torque data. In addition, the p-value of the curvature less than 0.05 indicates a significant curvature in the model, which means that the use of quadratic terms might need to be introduced in the regression model (possible non-linearity in the model).

Figure 6.2 shows the interaction plots for data means of thrust force which better show the effect of each of the input parameters on the variation of thrust force. As it can be seen changing the flow rate and air pressure does not have any impact on thrust force. Similar results were observed for torque as shown in Figure 6.1 .b. The use of amounts of flow rates proved to be ineffective as it tended to increase torque. However, it was observed that using high-pressures of 3 bars helped evacuate the chips from the cutting zone and reduced the chance of chips to curl around the cutting tool shaft. A low coolant flow rate and high air pressure are recommended for better results of cutting forces. The thrust force and torque increased with the increase of the feed rate and decreased with the increase of the spindle speed.
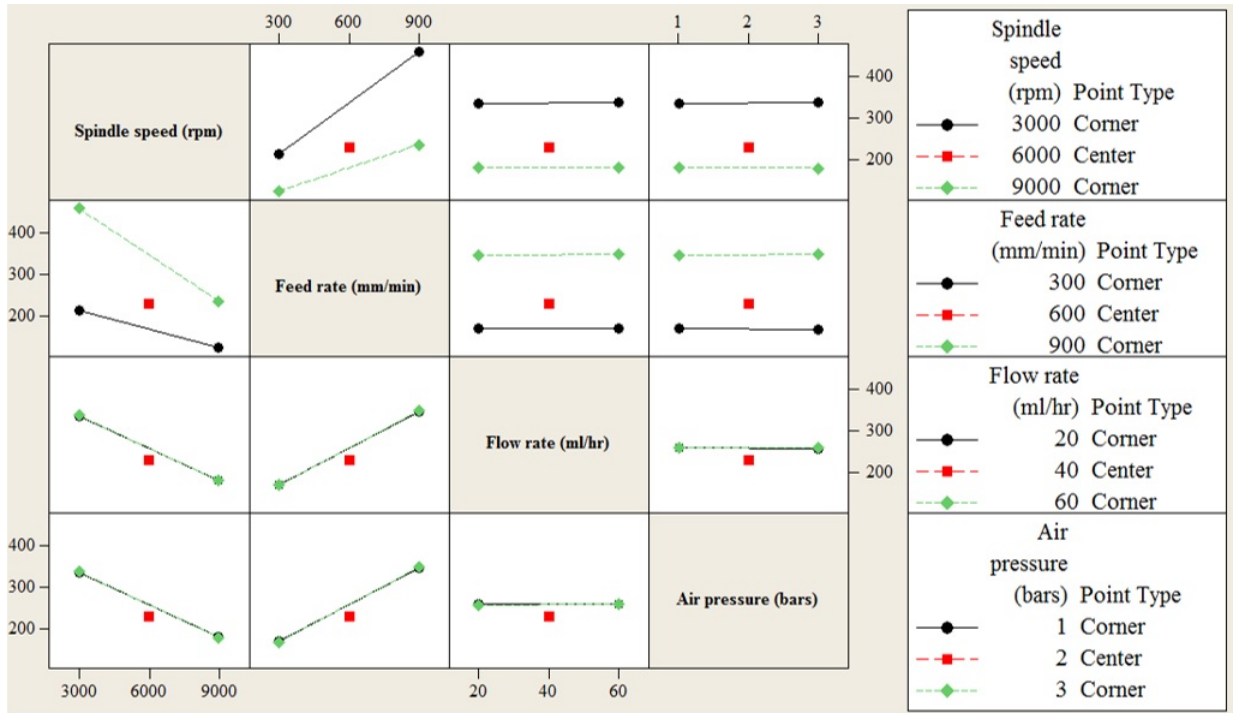
Figure 6.2: Interaction plots for data means of thrust force

Analysis of surface roughness

Figure 6.3 shows a comparison of the average surface roughness in MQL trials, according to different flow rates and air pressures for the tested cutting parameters. The average surface roughness values ranged between 1.17 to 2.56 μm. Results show that the variation in the feed rate, spindle speed, flow rate and air pressure all had an influence on surface roughness. At low feed rates of f= 300 mm/min, increasing the flow rate and air pressure from 20 mL/hr and 1 bar to 60 mL/hr and 3 bars increased the surface roughness up to 19 %. Increasing the flow rate from 20 mL/hr to 60 mL/hr leads to an increase of 10 % and 2 % in R_a at n= 3000 and 9000 rpm, respectively. Increasing air pressure from 1 bar to 3 bars increased the surface roughness by 17.7 % and 6 % at n= 30000 and 9000 rpm, respectively. It can be concluded that increasing the flow rate and air pressure should be accompanied by an increase in the spindle speed to avoid excessive cooling which could, in turn, increase surface roughness. Indeed, Nandi et al. [300] reported that increasing flow rate can sometimes increase the surface roughness when machining aluminium alloy AA1050 at high cutting speeds.

This was also observed for high feed rates of f= 900 mm/min and low spindle speeds of n= 3000 rpm. For these cutting parameters, air pressure seemed to help reduce the surface
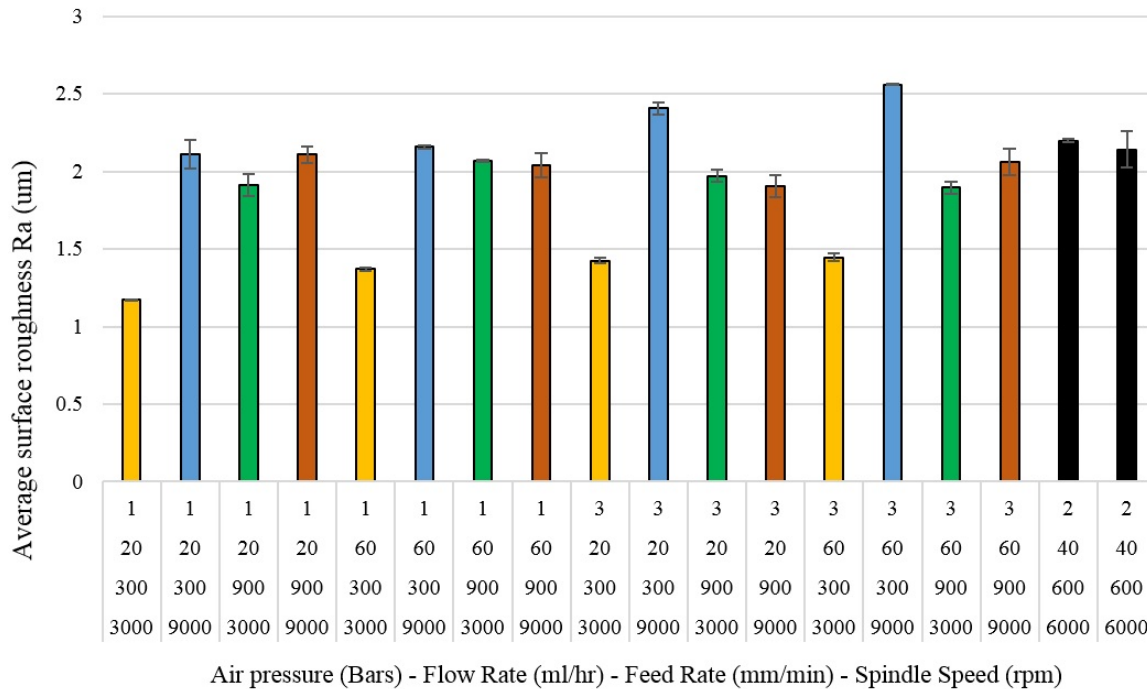
Figure 6.3: Average Surface roughness in MQL drilling trials

roughness, while increasing the coolant flow rate increased it. On the contrary, using higher flow rates and air pressures at high feed rate of f= 900 mm/min and high spindle speed of n= 9000 rpm had a negligible impact on surface roughness. The increase in surface roughness was greater when increasing the spindle speed at a low feed rate of 300 mm/min, while increasing spindle speed at high feed rates of f= 900 mm/min had little impact on surface roughness. Additionally, drilling at feed rate/spindle speed ratios of 0.1 mm/rev (300/3000, 600/6000, 900/9000) regardless of flow rate and air pressure, and increasing the feed rate three times from f= 300 to 900 mm/min, increased the surface roughness from 26 % to 43 %, which means that increasing the productivity would be at the expense of increased surface roughness.

From the percentage of contribution analysis and interaction plot for data mean values of the fractional factorial analysis (see Table 6.1), the results show that the spindle was the major contributor to the surface with 44. 68 %. The contribution of the feed rate was 4.64 % while the coolant flow rate and air pressure showed minor contributions of 0.92 % and 1.43 % respectively. The linear interaction between the spindle speed and the feed rate had a significant contribution of 33.81 %, which indicates that their effect on surface roughness varies depending on the value of the other predictor variable. The linear interaction of the feed rate with air pressure had a minor contribution of 4.69 %. The lower the feed rate

the more likely the air pressure has sufficient time to blow away the evacuated chips exiting from the drill flutes, which reduces the chances of chips clogging and therefore reduces their heat flow impact on both the workpiece and the cutting tool. The linear interaction between spindle speed, flow rate and air pressure had a minor contribution of 1.45 %. Increasing the air pressure improves the coolant penetration which can reach more depth at the drill-workpiece interface, therefore improving the lubrication and reducing surface roughness. The model data show that there is a sign of curvature in the ANOVA analysis which could be a sign of the presence of higher order interactions (i.e. square terms). In addition, there was no sign of a lack of fit in the surface roughness results (see Table 6.1).

Analysis of burr formations

Figure 6.4 shows the average entry and exit burr height under different cutting conditions using MQL. The exit burrs were always greater than the entry burrs. The maximum burr height on both sides was measured at n= 9000 rpm, f= 900 mm/min, (3 bar and 20 mL/hr at the entrance, 1 bar and 20 mL/hr at the exit) and the minimum burr height on both sides was measured at n= 3000 rpm, f= 300 mm/min, (3 bar and 60 mL/hr at the entrance and 1 bar and 20 mL/hr at the exit). The maximum burr root thickness at the entrance and the exit was measured at n= 9000 rpm, f= 900 mm/min, (1 bar and 20 mL/hr). The minimum burr root thickness at the exit was measured at n= 9000 rpm, f= 600 mm/min, 1 bar and 60 mL/hr, and at n= 3000 rpm, f= 300 mm/min, 3 bar and 20 mL/hr at the entrance. Both burr parameters increased with the increase of spindle speed and feed rate.

The influence of the feed rate was most dominant on burr height at both sides ranging between 65 % and 75 %. The spindle speed contribution was around 5 % which indicates that burr height is primarily a function of feed rate. The air pressure and coolant flow rate had a minor effect on the burr height with flow rate having 0.35 % and 0.71 %, air pressure having 1.08 % and 2.98 % on entry and exit burr heights, respectively. The interaction of the spindle speed with the feed rate and the interaction of coolant flow rate with air pressure had minor contributions of 0.47 % and 0.75 % respectively. While the interaction of spindle speed with the coolant flow rate, the interaction of spindle speed and air pressure and the interaction of feed rate with coolant flow rate had minor contributions of 0.98 %, 1.99 % and 2.21 % on exit burr height, respectively. On the other hand, the interaction of the feed rate and air pressure had a significant contribution on exit burr height (18.55 %).

Figure 6.4: The average (a) burr height (b) burr thickness at entry and exit in MQL drilling trials

It is well known that the burr formation and its size is highly affected by the ductility of the workpiece material, such that the more ductile the material the larger are the formed burrs [324]. The air pressure contributes to heat and chip removal from the cutting zone which reduces the rise of the workpiece ductility with the increase of cutting temperatures. The entry burr height analysis indicated that a curvature existed unlike for exit burr height. Interlayer burrs were formed on the upper side of aluminium sheets in some specific locations as shown in Figure 6.5.
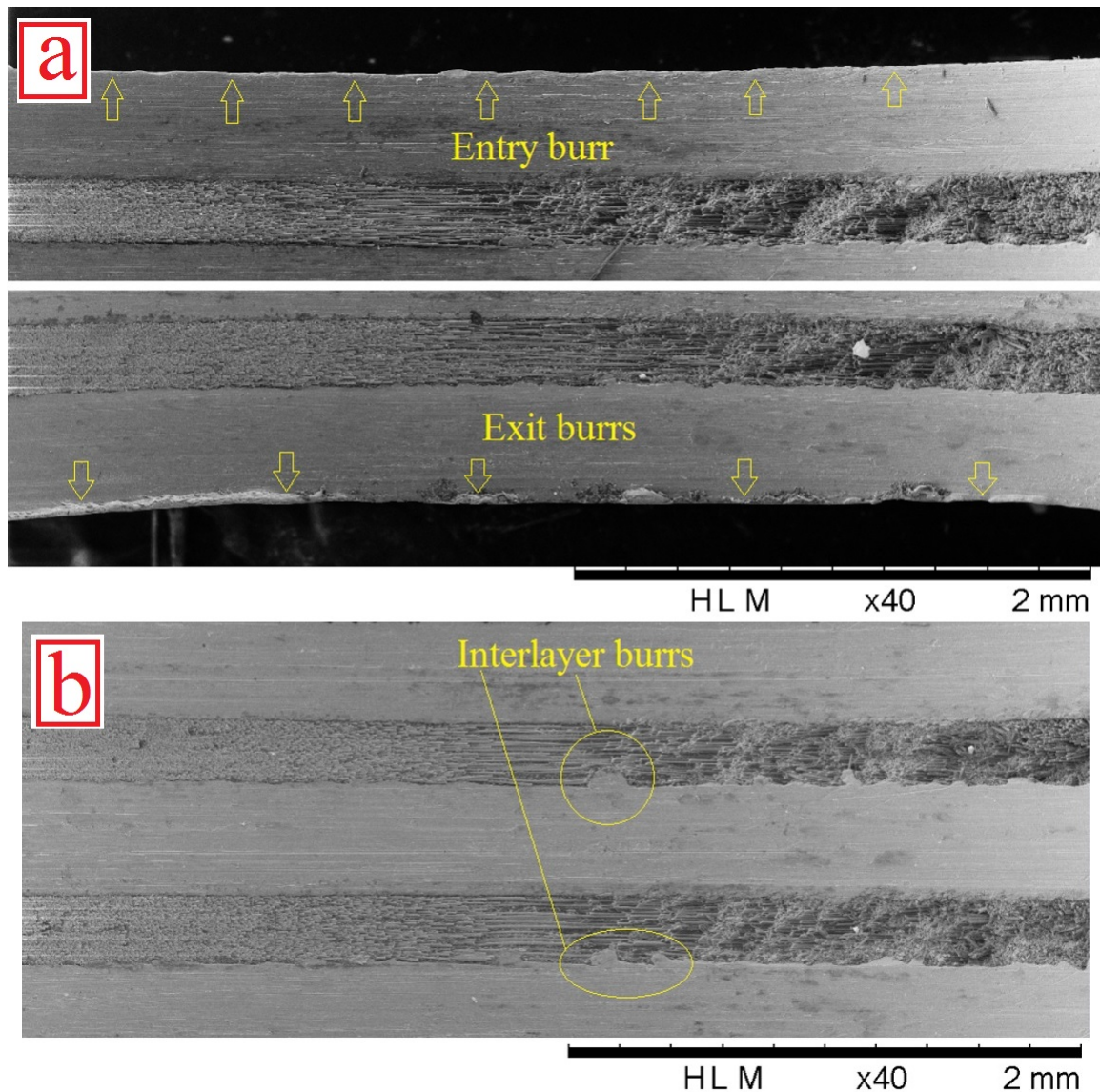
Figure 6.5: SEM image showing (a) burr formation for hole drilled at 9000 rpm, 900 mm/min, 60 mL/hr and 1 bar (b) interlayer burrs for hole drilled at 9000 rpm, 900 mm/min, 20 mL/hr and 1 bar

The formed burrs were not uniform and of a small size. They were most likely to fill in the small pockets in glass fibre layers which have been eroded during drilling. The interlayer

burrs increased with the increase of the feed rate and spindle speed due to the increase in workpiece ductility, and the increase of the feed force which increase the bending of GLARE constituents creating larger gaps for burrs to fill in. The feed rate was the primary contributing parameter on burr root thickness on both sides (39-56 %), followed by the flow rate (15.62 %) on the entrance burr root thickness. The spindle speed and air pressure had a minor contribution on entrance burr root thickness of around 3.88 % and 1.88 % respectively. The interaction of the feed rate and air pressure had a significant contribution on entrance burr root thickness 26.83 % and to a lesser extent the interaction of the spindle speed and the feed rate with the flow rate of 1.83 % and 2.55 % respectively. The air pressure had 8.51 % contribution on the exit burr root thickness while the interaction of spindle speed with air pressure and flow rate had a 7.99 % contribution. The interaction of spindle speed with feed rate and air pressure had a 3.48 % contribution and the two interactions were less significant with contributions below 3.7 %. These results indicate that burr root thickness is also a function of feed rate while the effect of spindle speed is not prominent for burr formation compared to the feed rate. The analysis indicates that a curvature exists with a minor lack of fit for burr thickness at entry and exit.

Analysis of hole size and circularity error

Figure 6.6 shows the holes size under different cutting conditions at top and bottom locations. Oversized holes were produced at the top whereas undersized holes were produced at the bottom indicating the hole size shrinks with depth. Hole size deviation ranged between +13.5 μm and - 20.456 μm. The minimum hole deviation was achieved when drilling at n= 3000 rpm, f= 300 mm/min, 60 mL/hr and 1 bar. The deviation of hole size increased with spindle speed. ANOVA results show that the spindle speed was most dominant at 5.8 % on hole size at the top while all other parameters did not show any significance of contribution since the P-value is greater than alpha= 0.05, which indicates that the model does not fit the data. Increasing the coolant flow rate reduced the deviation of hole diameter from its nominal size at the top location and increased it at the bottom. Increasing air pressure reduced the deviation of hole diameter from its nominal size at the top but had no influence on the bottom. According to ANOVA results (see Table 6.1), there is no significant contribution from the feed rate, coolant flow rate and air pressure at the top or the bottom. Only the interaction of the feed rate with the coolant flow rate and air pressure had a significant influence of 8.8 % at the bottom. The ANOVA analysis of hole size at the top and the bottom showed a large sign of curvature but no lack of fit.
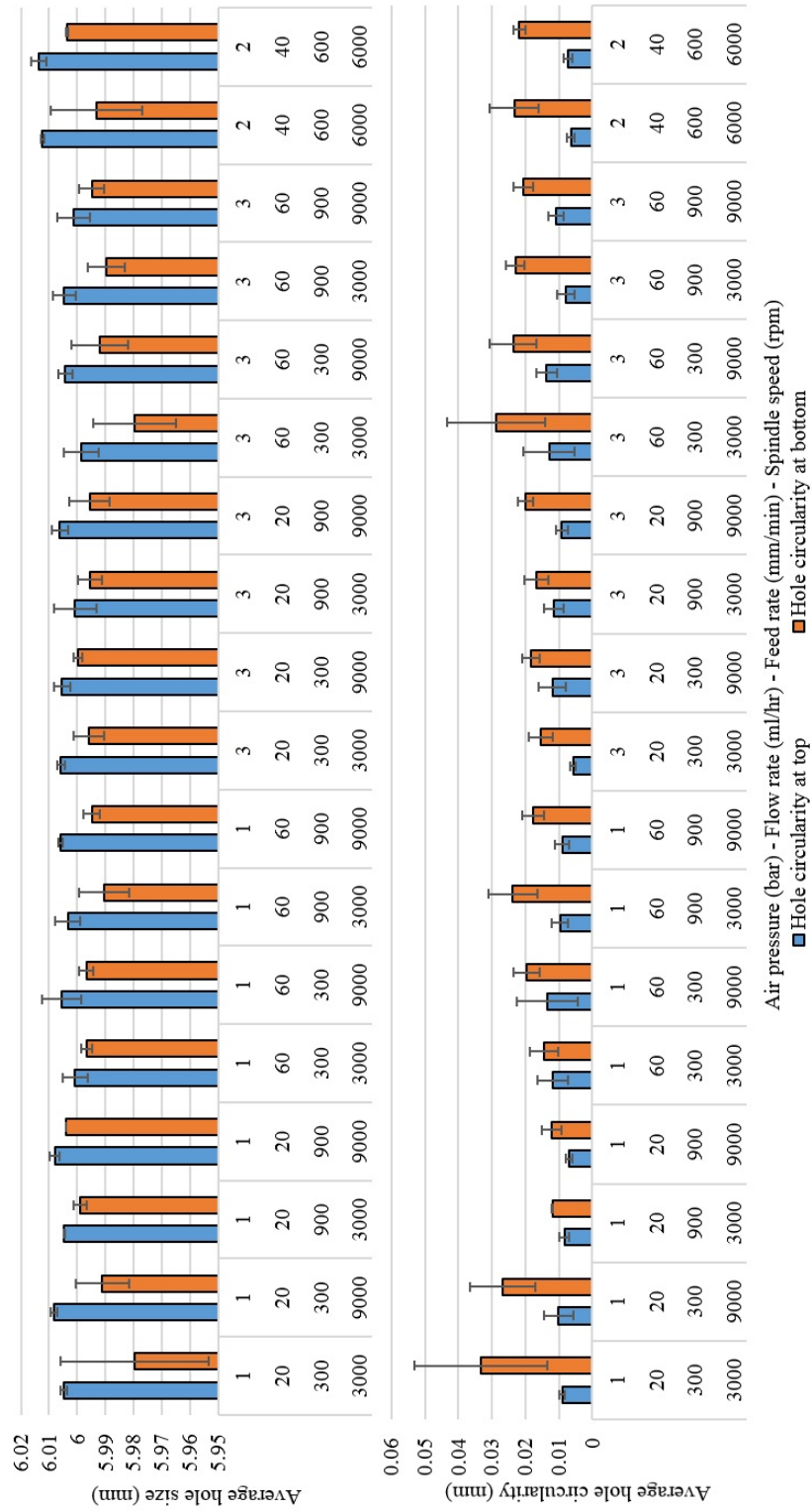
Figure 6.6: The average (a) hole size (b) hole circularity error at entry and exit in MQL drilling trials

The ANOVA analysis models for hole circularity error at the top and the bottom showed no sign of curvature but the lack of fit was evident at the top. The hole circularity error measured at the bottom was greater than the top. This indicates that the hole circularity error is likely to increase with depth. The hole circularity error did not exceed 14 μm at the top and 33 μm at the bottom. ANOVA results show that none of the four parameters nor their interactions had any contribution on hole circularity error the top and bottom. It was also observed that the residual error was large for hole size and circularity error at both locations which could indicate a problem in the regression model. Minitab analysis showed that the lack-of-fit test for the replicates of the collected data had a considerable random variation which can cause differences between the observed response values.

Post-machining microhardness near the hole edge of the upper and lower aluminium sheets

Figure 6.7 shows the average post-machining Vickers microhardness of the upper and lower aluminium sheets near the hole edge.
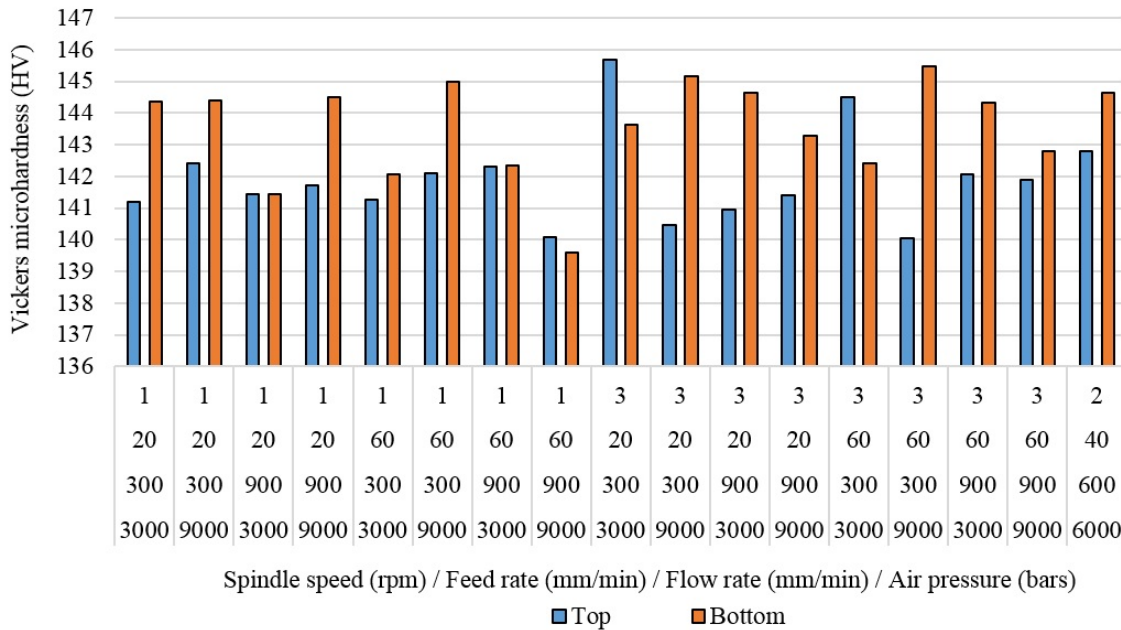
Figure 6.7: Average post-machining microhardness under different cutting conditions in MQL drilling trials

The results show that the increase in microhardness from its standard value of 137 on Vickers scale in the last aluminium sheet was higher than in the upper one, which indicates that the microhardness is likely to increase with depth. However, the change is negligible. Increasing the spindle speed increased the hardness while increasing the feed rate decreased it. There was no indication of the influence of the coolant flow rate and air pressure on the

microhardness but it was observed that the higher the flow rate and air pressure the lower the hardness at the top due to enhanced cooling from the direct contact of the coolant and air with the upper aluminium sheet. Generally, the post-machining microhardness was 2 % to 6.5 % higher than its standard value of 137 HV.

Scanning electron microscopy SEM of holes drilled using MQL

In addition to delamination damage inspection in glass fibre layers of drilled holes using CT scan, the internal damage at the borehole walls in the form of material chipping, uncut fibres, smearing and internal delamination was observed for MQL similarly to dry drilling tests. These types of surface damage are typical forms of damage common when drilling composite-metal stacks which indicate the quality of the drilling process with the variation of cutting parameters as shown in Figure 6.8.
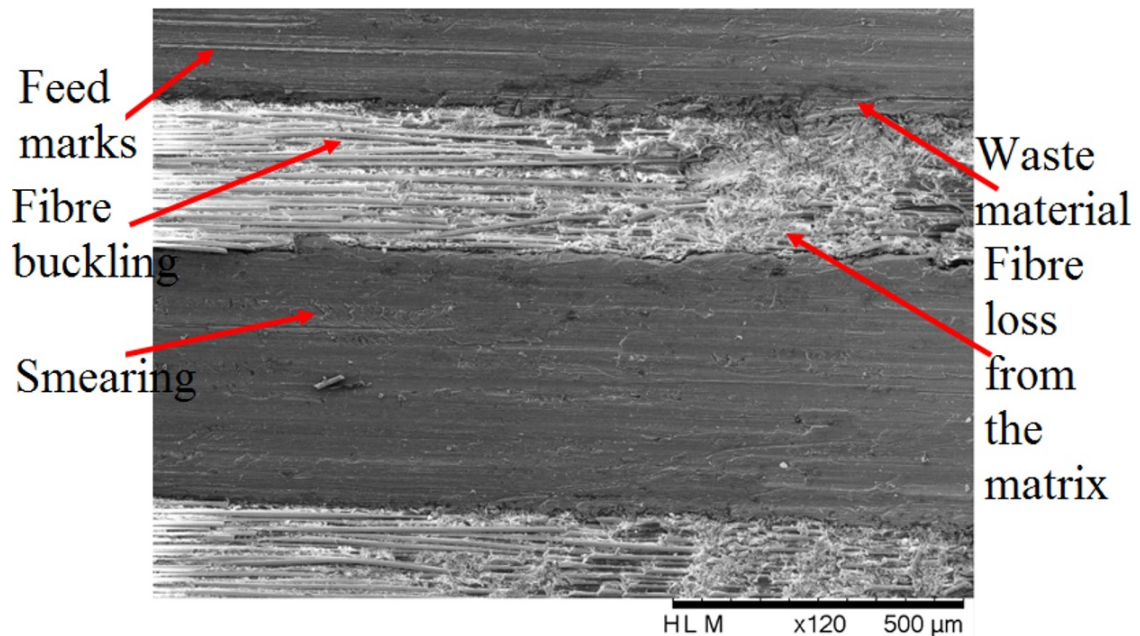
Figure 6.8: SEM images of hole surface quality drilled at 9000 rpm, 300 mm/min, 60 mL/hr and 1 bars

The status of the borehole surface was analysed using SEM to detect any defects or damage in the metal sheets and glass fibre layers. Images showed that debris and chips were more likely to adhere to the borehole surface when drilling at spindle speeds of n= 9000 rpm and feed rates f= 300 mm/min regardless of the coolant flow rate and air pressure used (see Figure 6.9.a). It was also observed that minimum waste and debris adhered to the borehole surface when drilling at n= 3000, 6000 rpm and f= 300, 600 mm/min (see Figure 6.9.b).
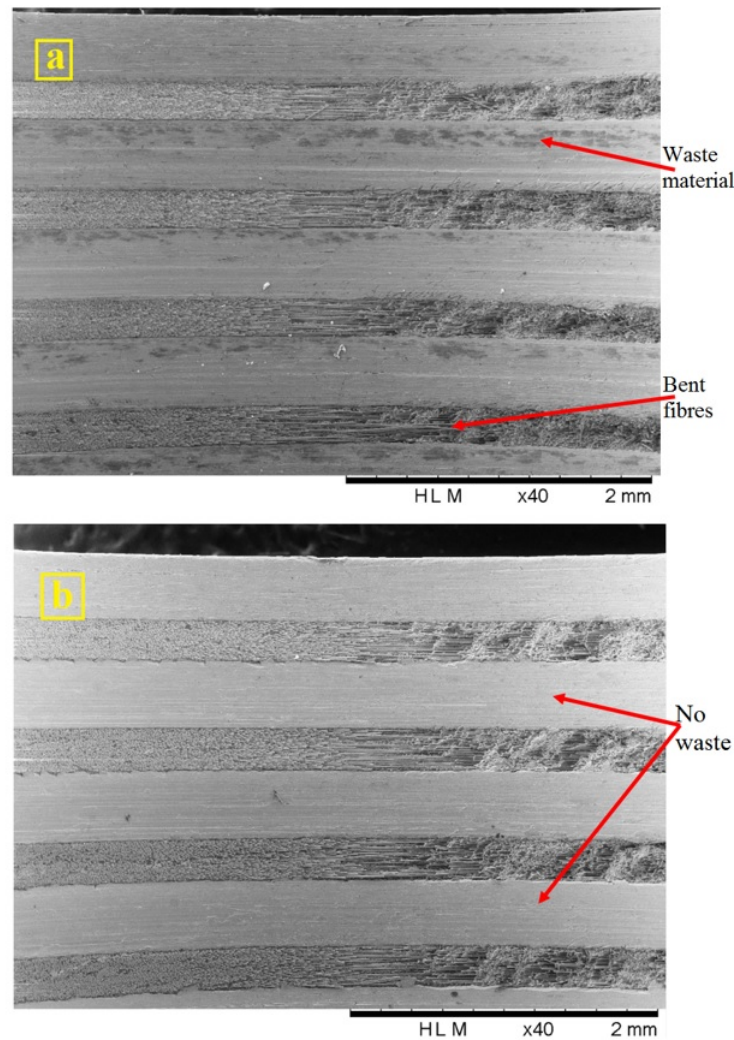
Figure 6.9: SEM images of hole surface quality drilled at (a) n= 9000 rpm, f= 300 mm/min, 60 mL/hr and 3 bars (b) n= 3000 rpm, f= 300 mm/min, 60 mL/hr and 1 bar

Using higher levels of coolant flow rate and air pressure (i.e. 60 mL/hr and 3 bars) seemed to reduce the waste and debris adhesion on the aluminium sheets surface. This could be due to the excessive lubrication of the cutting tool giving it smoother rubbing against the hole walls while increased air pressure levels helped evacuate the chips and debris therefore, reducing their tendency to adhere to the surface. The cutting mechanisms and damages in holes drilled using MQL were similar to those observed under dry drilling conditions. Interlayer burrs were formed at several locations around the upper and lower edges of the metal sheets. Metal chipping occurred randomly and seemed to be more present when drilling at feed rates of f= 900 mm/min and spindle speeds of n= 3000 rpm regardless of the applied coolant flow rate and air pressure. Similar to the observation made from dry drilling trials, the SEM images revealed that some of the glass fibre plies were eroded in the GLARE stack by the evacuated metallic chips as shown in Figure 6.10 and Figure 6.11.
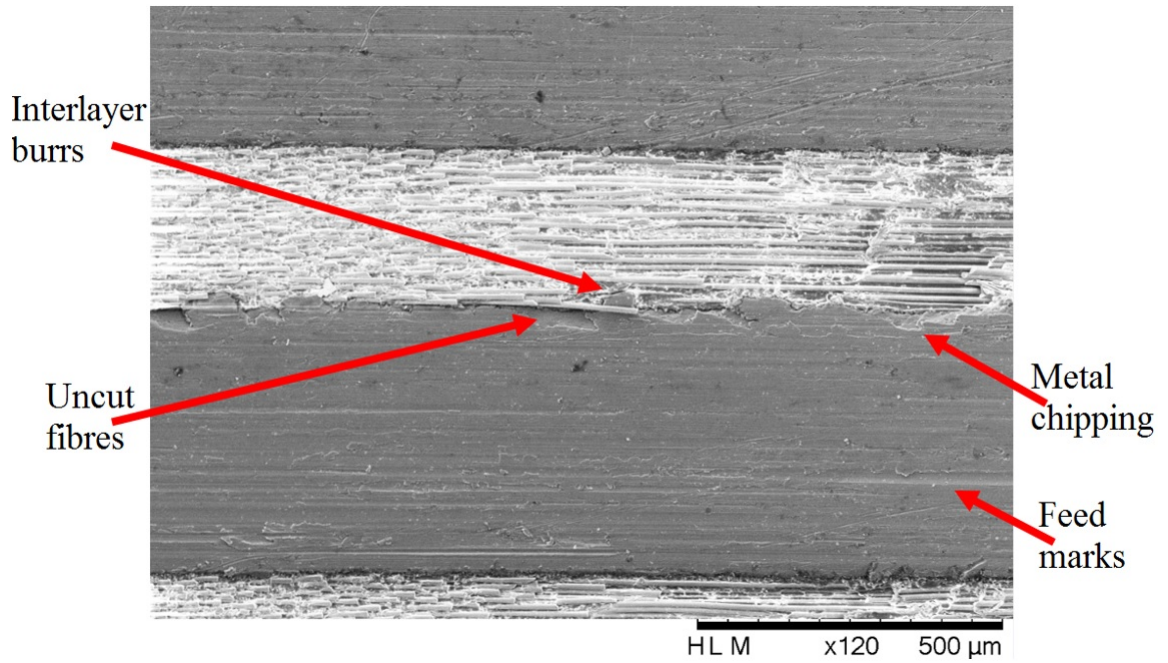
Figure 6.10: SEM image of hole surface quality drilled at 3000 rpm, 300 mm/min, 60 mL/hr and 1 bar
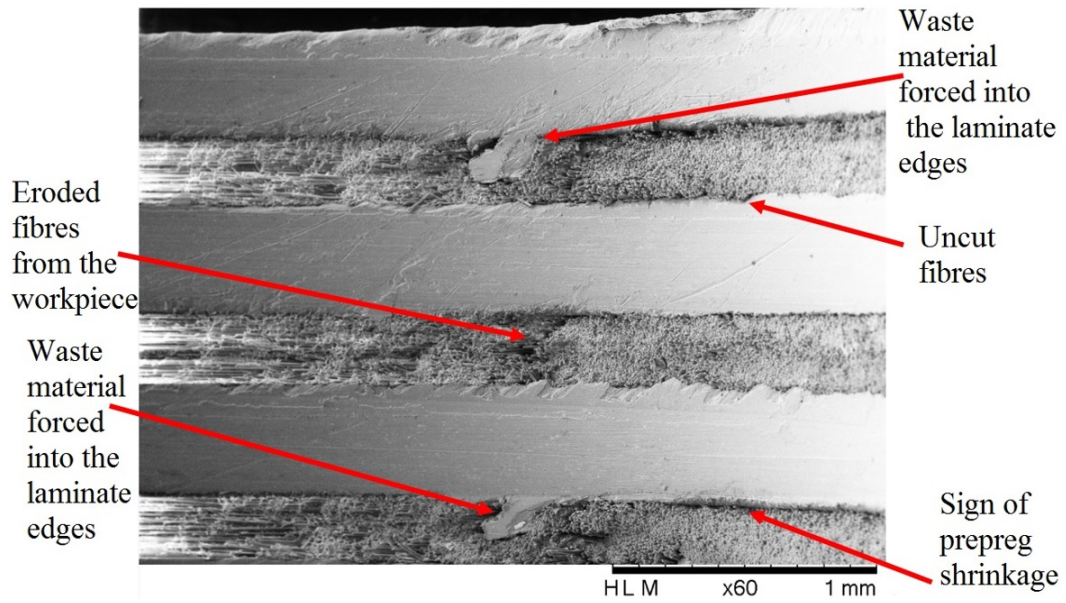
Figure 6.11: SEM image of hole surface quality drilled at 3000 rpm, 900 mm/min, 20 mL/hr and 1 bar

Delamination analysis of hole drilled using MQL

Figure 6.12 shows CT scan images of the last glass fibre layers in a hole drilled using MQL. It is observed that the surface delamination was absent and only minor chipping exists around the hole edges. The calculated delamination factor in the last glass fibre layer for each hole indicates that the delamination as a result of the drilling process is less likely to occur. As explained previously, it is suggested that the stacking nature of GLARE which puts glass fibre layers between two aluminium sheets provides a form of support and resistance from cutting forces during drilling, which reduces the potential for delamination.
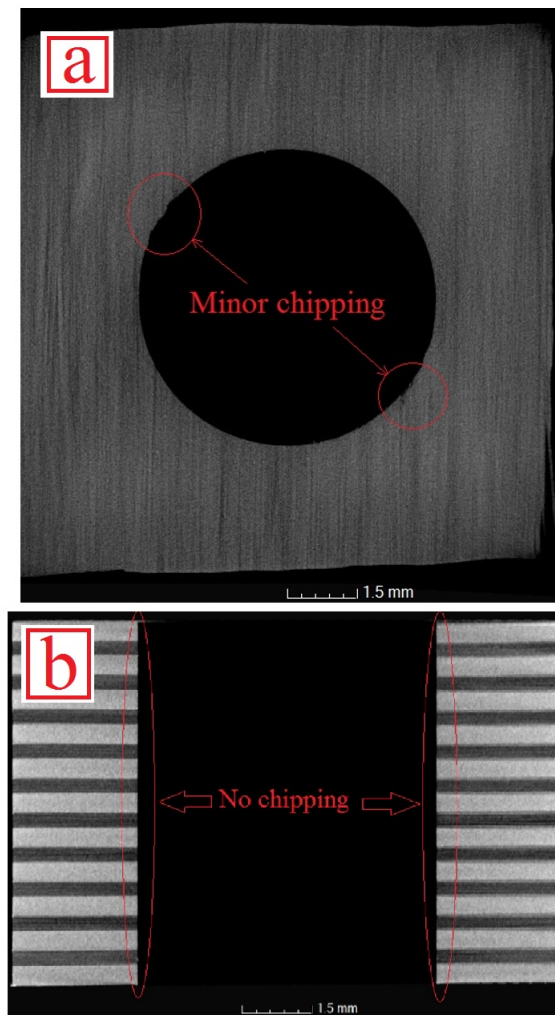
Figure 6.12: CT scan images of last glass fibre layer in hole drilled at (a) n= 9000 rpm, f= 900 mm/min, 60 mL/hr and 3 bar (b) at n= 3000 rpm, f= 300 mm/min, 20 mL/hr and 1 bar

The presence of a backup metal plate beneath or above a composites workpiece during drilling have been previously reported to reduce delamination damage due to peeling up and push-out forces [254, 352]. This would also explain the tendency of GLARE to allow larger feed rates without delamination damage. Another suggestion for the minor presence of delamination is that the air and coolants used contribute to removing part of the accumulated heat during the drilling process and therefore, lessens the impact of a rise in temperature on delamination damage. Therefore, it can be concluded that no significant delamination damage could be observed in any of the inspected glass fibre layers under all cutting conditions when using MQL. In addition, minor chipping and erosion were found on all inspected holes at approximately $\pm 45\hat{\ }\circ$ with respect to $0°$ fibre orientation similar to dry drilling results.

Hole quality inspection under optical microscopy using MQL

Figure 6.13 and Figure 6.14 show the entry and exit hole state when drilling GLARE 2B 11/10 using MQL.
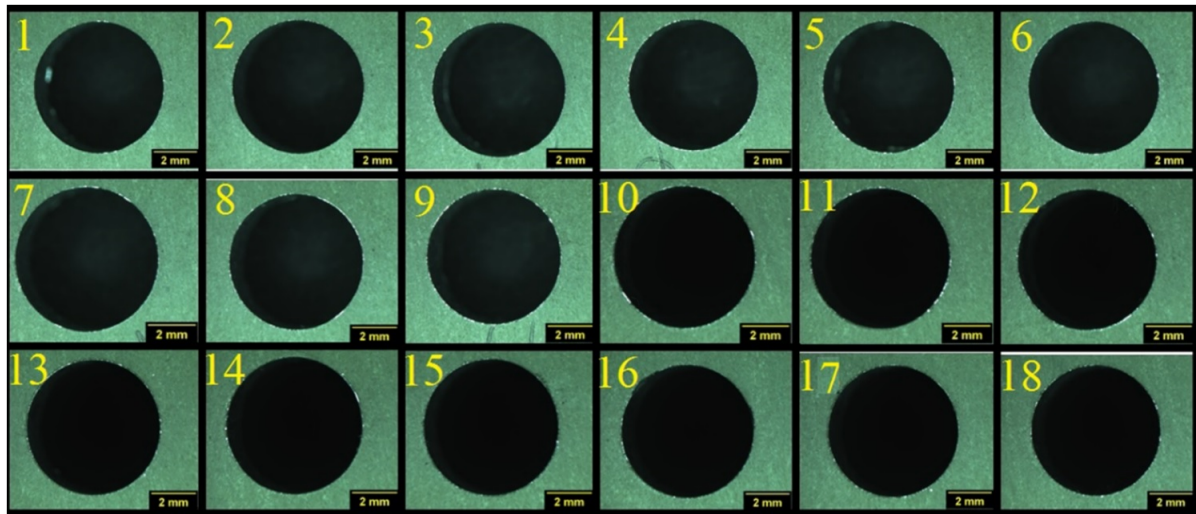
Figure 6.13: Optical microscopy images hole exit under MQL at Entrance

Under the investigated cutting parameters, no visible damage was observed on the hole edge and through its thickness. No signs of spalling, fibre fraying, fuzzing or edge chipping fracture were found in all inspected holes. The hole quality at the entry side was in better condition than at the exit side especially in terms of burr formation and edge shape. The presence of aluminium sheets which essentially function as backup/support material to glass fibre layers stacked in between was thought to minimise their susceptibility to drilling-induced damage. In addition, it was observed that the hole edges at the exit side suffered from coating loss of the bond primer which gives aluminium sheets the yellowish colour.
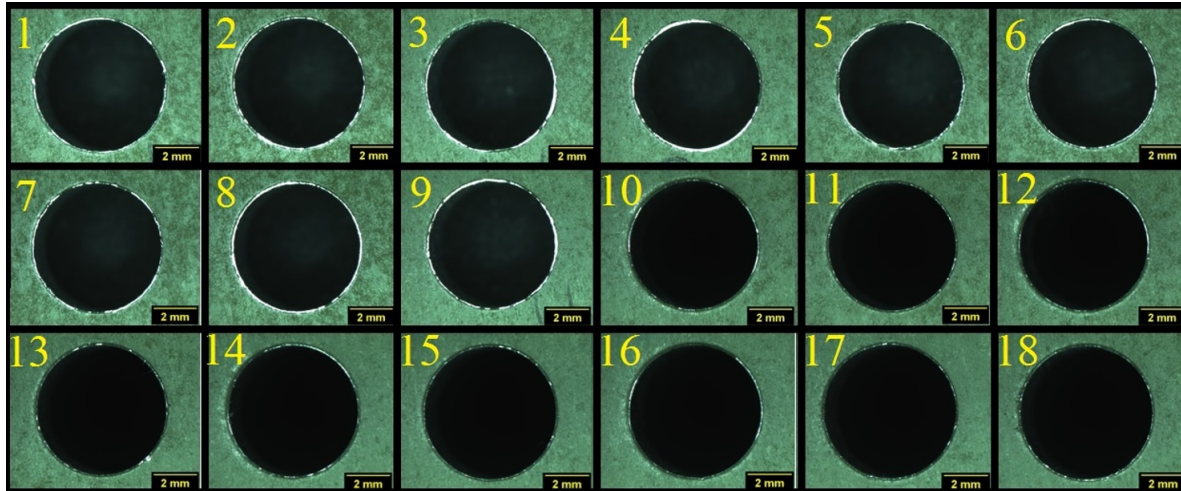
Figure 6.14: Optical microscopy images hole exit under MQL at Exit

The loss was observed when drilling at feed rates of f= 300 mm/min and was absent from hole drilled under feed rates of n= 900 mm/min.

Response surface methodology evaluation using MQL

As stated previously in chapter 3, RSM was carried out after conducting a full factorial analysis for GLARE 2B 11/10 under dry and MQL conditions. RSM approach is helpful in determining the relationship between input machining parameters with responses from the machining inputs in order to assess the impact of their higher order interactions. The following section will discuss the RSM method used for MQL drilling trials, the generated regression models, the percentage contribution of input parameters from ANOVA tables to test the models ability in predicting new cutting parameters within the tested range of parameters. Table 6.2 shows the percentage contribution of input parameters on outputs from ANOVA analysis in RSM and the regression coefficients of the nonlinear models. The percentages indicates that linear and square interactions of cutting parameters were most significant on thrust force, torque and surface roughness. Whereas linear and square interactions of the coolant flow rate and air pressure were not significant. Similarly, the linear and square interactions of the spindle speed with the feed rate are most significant on burr height. In addition, the remaining linear interactions between input parameters had some level of significance but to a lesser extent. Burr thickness was dominated by the feed rate on both sides followed by the coolant flow rate at entry side. Spindle speed had a small influence on hole size at top and bottom, feed rate impacted the circularity error at the exit while neither coolant flow rate and air pressure had any impact on hole size or circularity error.

Table 6.2: Percentage of contribution of input parameters on outputs from RSM ANOVA analysis

Source	Percentage contribution (PCR)										
Blocks	F	T	R	ENBH	EXBH	ENBT	EXBT	HST	HSB	CET	CEB
Regression	99.48	93.32	81.52	87.06	87.3	67.99	56.09	-	-	-	41.45
Linear	90.86	85.04	40.10	39.31	13.01	43.94	23.32	10.17	9.07	3.66	4.11
Spindle speed	40.40	51.57	37.7	2.86	-	2.08	-	6.67	5.25	-	-
Feed rate	50.46	33.41	1.22	35.90	12.49	30.42	21.33	-	-	-	3.06
Flow rate	-	-	-	-	-	10.30	-	-	-	-	-
Air pressure	-	-	-	-	-	-	-	-	-	-	-
Square	2.09	2.81	15.87	46.93	69.26	0.29	28.84	7.4	9	12.57	29.1
Spindle speed*Spindle speed	1.84	0.38	14.36	37.16	52.75	-	-	3.91	-	-	-
Feed rate*Feed rate	0.24	2.07	-	5.51	8.99	-	-	-	-	-	-
Flow rate*Flow rate	-	0.33	-	2.52	3.93	-	-	-	-	-	-
Air pressure*Air pressure	-	-	-	1.74	3.59	-	-	-	-	-	-
Interaction	6.53	5.47	25.55	0.82	5.03	23.77	3.94	1.59	5.8	2.78	8.22
Spindle speed*Feed rate	6.52	5.41	22.18	-	-	-	-	-	-	-	-
Spindle speed*Flow rate	-	-	-	-	-	-	-	-	-	-	-
Spindle speed*Air pressure	-	-	-	-	-	-	-	-	-	-	-
Feed rate*Flow rate	-	-	-	-	-	1.92	-	-	-	-	2.95
Feed rate*Air pressure	-	-	3.08	-	3.91	20.26	-	-	-	-	-
Flow rate*Air pressure	-	-	-	-	-	-	-	-	-	-	3.5
Residual Error	0.52	6.68	18.48	12.94	12.70	32.01	43.91	80.8	76.13	80.96	58.57
Lack of fit	-	-	7.61	7.73	5.39	7.86	-	-	-	-	-
Pure Error	0.41	5.67	10.87	5.21	7.31	24.15	36.71	72.29	63.76	73.36	45.46
R^2	99.48	93.32	81.52	87.06	67.99	87.3	56.09	19.18	23.87	19.02	41.44
R^2 predicted	99.26	91.57	74.08	81.52	57.29	83.14	42.94	0	0	0	4.99
R^2 adjusted	99.38	92.12	78.20	84.73	62.25	85.02	48.21	4.67	10.21	4.84	30.93

Table 6.3 shows the coefficients A0 to A4 of input parameters which represent the response (Y). The coefficients include a constant A0, linear terms (A1, A2, A3, A4, quadratic terms (A5, A6, A7, A8, and the coefficients of interaction terms between inputs (A9, A10, A11, A12, A13, A14). The general equation can be written according to the four input parameters used in MQL study in uncoded form as shown below:

$$
\begin{aligned}
Y_{response} \;=\; & A_0 + A_1 X_1 + A_2 X_2 + A_3 X_3 + A_4 X_4 + A_5 X_1^2 + A_6 X_2^2 \\
& + A_7 X_3^2 + A_8 X_4^2 + A_9 X_1 X_2 + A_{10} X_1 X_3 + A_{11} X_1 X_4 \\
& + A_{12} X_2 X_3 + A_{13} X_2 X_4 + A_{14} X_3 X_4
\end{aligned}
\tag{6.1}
$$

The linear mathematical relationships between the output responses (i.e. cutting forces, surface roughness, burrs and hole size) and input parameters were acquired using the experimental data results shown in Table 6.3 which was obtained based on C.C.D discussed previously in chapter 3. The coefficients of regression analysis are given in Table 6.3. To validate the accuracy of the regression models, additional holes were drilled using new cutting parameters and the experimental values of the responses were compared with the values obtained from the regression model as shown in Table 6.4.

Table 6.3: Regression coefficients of input parameters on outputs from RSM analysis

	Output parameters										
	F	T	R	ENBH	EXBH	ENBT	EXBT	HST	HSB	CET	CEB
Constant (A$_0$)	176.55	2.46E-01	-9.95E-01	24.272	0.032979	97.514	-0.102505	6.00662	5.94978	-0.00714	0.073946
Linear terms											
Spindle speed (A$_1$)	-5.24E-02	-1.20E-04	4.22E-04	-0.0023	3.04E-07	-0.0063	1.98E-05	5.86E-06	4.59E-06	-3.20E-08	-2.98E-06
Feed rate (A$_2$)	6.80E-01	1.54E-03	3.17E-03	-0.01321	0.000123	-0.03107	0.00029654	-2.01E-05	3.60E-05	2.48E-05	-7.41E-05
Flow rate (A$_3$)	1.28E-01	6.79E-03	1.69E-02	-0.36178	-5.47E-04	-1.27905	0.00427859	-7.59E-04	0.000554	0.000495	-7.30E-04
Air pressure (A$_4$)	2.10E+00	-4.70E-02	2.67E-01	-8.11783	0.026533	-34.1475	0.0742199	-1.94E-04	0.011724	0.003364	-0.01678
Square terms											
Spindle speed*Spindle speed (A$_5$)	4.09E-06	8.79E-09	-1.63E-08	1.99E-07	2.24E-10	6.58E-07	-8.33E-10	-3.90E-10	-2.70E-10	1.96E-11	2.48E-10
Feed rate*Feed rate (A$_6$)	-1.45E-04	-6.46E-07	-7.26E-07	1.89E-05	-1.97E-08	8.18E-05	-1.21E-07	1.62E-08	-7.45E-09	-1.64E-08	3.83E-08
Flow rate*Flow rate (A$_7$)	-2.43E-03	-8.22E-05	-1.67E-04	0.004807	2.65E-06	0.019942	-3.97E-05	8.17E-06	-3.31E-06	-4.44E-06	5.12E-06
Air pressure*Air pressure (A$_8$)	-8.88E-01	1.01E-02	-2.24E-02	2.25673	0.000309	11.3791	-0.0136236	0.00016	-0.00151	-0.00107	0.002363
Interaction terms											
Spindle speed*Feed rate (A$_9$)	-3.71E-05	-5.67E-08	-2.47E-07	3.80E-07	4.63E-11	4.43E-07	-2.83E-09	-3.79E-10	-9.24E-10	-7.62E-10	-1.19E-10
Spindle speed*Flow rate (A$_{10}$)	-2.60E-06	-3.24E-08	-1.20E-08	2.38E-06	-5.10E-08	-1.83E-05	-9.70E-08	-2.13E-09	1.60E-09	8.93E-10	-8.66E-09
Spindle speed*Air pressure (A$_{11}$)	-1.98E-04	1.32E-07	6.41E-06	-1.99E-05	1.01E-07	-5.21E-04	-2.04E-06	-1.42E-07	1.62E-08	1.44E-07	1.20E-07
Feed rate*Flow rate (A$_{12}$)	7.12E-05	-3.63E-07	-2.65E-06	-1.01E-05	6.02E-07	-2.75E-04	-5.51E-07	1.12E-07	-2.39E-07	-1.42E-07	3.30E-07
Feed rate*Air pressure (A$_{13}$)	2.47E-03	-4.74E-06	-2.76E-04	0.000814	-3.91E-05	-0.01593	-1.64E-05	-7.71E-07	-3.19E-06	1.11E-06	4.66E-06
Flow rate*Air pressure (A$_{14}$)	1.82E-02	2.16E-04	-2.53E-04	-0.02148	-5.73E-05	-0.00337	-1.22E-04	1.47E-06	-1.12E-04	-6.71E-06	0.000108

Additional holes were drilled under new cutting parameters to validate the adequacy of the regression models. The first hole was drilled at a spindle speed of n= 6000 rpm, a feed rate off= 300 mm/min, and a flow rate of 20 mL/hr with the air pressure at 1 bar. The second hole was drilled at a spindle speed of n= 9000 rpm, a feed rate of f= 600 mm/min, flow rate of 60 mL/hr and air pressure of 1 bar. The experimental results of cutting forces and hole quality parameters are compared with the predicted ones using the regression equations as shown below in Table 6.4. The experimental results showed good agreement with predicted results using the regression models. Models for thrust force, torque and surface roughness, hole size at top and circularity error at the top were able to predict the values accurately, while other mathematical models such as for hole size at bottom seemed to be unable to predict the values accurately as indicated by large errors. This was partially due to the large deviation in values of the replicates used in the model which generated a high residual error. Some other models such as entry burr thickness circularity error at the bottom showed acceptable results depending on the cutting parameters used.

Table 6.4: Confirmation test to validate the regression model

Term	6000 rpm, 300 mm/min, 20 ml/hr, 1 bar			9000 rpm, 600 mm/min, 60 ml/hr, 1 bar		
	Experimental	Predicted	Error (%)	Experimental	Predicted	Error (%)
Thrust force (N)	148	136.45	8.46	193	193.92	0.1
Torque (N-m)	0.255	0.208	22.71	0.312	0.318	1.88
Surface roughness (μm)	1.83	1.84	0.54	2.018	2.225	9.3
Entry burr height (μm)	4.958	4.775	3.83	3.774	10.25	63.18
Exit burr height (μm)	21.288	30.054	29.16	18.466	45.372	59.3
Entry burr thickness (μm)	104	80.2	29.67	88.5	92.3	4.11
Exit burr thickness (μm)	203.9	154.9	31.63	204.25	193.9	5.3
Hole size at top (μm)	10.1	9.9	2	4.81	4.6	4.56
Hole size at bottom (μm)	3	8.4	64.28	0.233	1.6	85.43
Circularity error at top (μm)	9.1	8.7	4.59	9.71	12	19
Circularity error at bottom (μm)	13.6	24.2	43.8	11.88	13.6	12.64

In comparison with regression models obtained from the full factorial analysis, RSM models showed somewhat better ability to predict the responses despite having higher residual error and lower R^2 values. The RSM models were also able to show the non-linear relationships which exist between the input cutting parameters, which was not possible using full factorial design.

6.2 Evaluation of Drilling Performance of GLARE under cryogenic liquid nitrogen cooling

6.2.1 Results and discussion

Analysis of cutting forces

Figure 6.15 shows the average thrust force and torque when using liquid nitrogen coolant under different spindle speeds and feed rates. The results show that both cutting forces increased with the increase of the feed rate due to increase in chip loading, and decreased with the increase of spindle speed similar to dry and MQL tests. The lowest thrust force and torque were recorded at f= 300 mm/min and n= 9000 rpm and highest at f= 900 mm/min and n= 3000 rpm respectively.
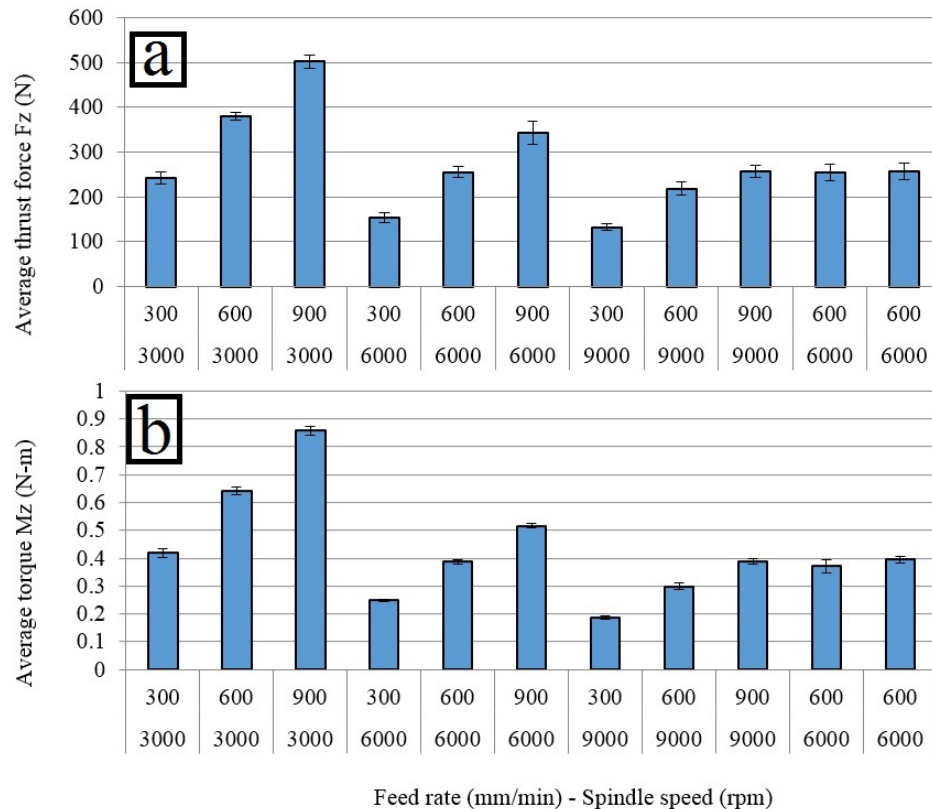
Figure 6.15: The average (a) Thrust force (b) torque in cryogenic drilling trials

ANOVA results in Table 6.5 show that the effect of the feed rate on thrust force was more significant (50.48 %) than the spindle speed (43.59 %) while the spindle speed had a more significant effect on torque (55.94 %) than the feed rate (39.42 %). The linear interaction of both cutting parameters reduced both cutting forces but had a slight influence on them (1.66 % and 4.31 % on thrust force and torque respectively).

Table 6.5: Percentage contribution of input parameters on observed outputs using ANOVA

Output	Inputs			
	Spindle speed	Feed rate	Spindle speed x Feed rate	Error
Thrust force	43.59	50.48	4.27	1.66
Torque	55.94	39.42	4.31	0.33
Surface roughness	21.34	42.06	-	25.62
Entry burr height	22.43	12.51	62.88	2.18
Exit burr height	-	53.27	-	30.09
Entry burr thickness	-	29.99	-	39.88
Exit burr thickness	-	34.86	25.25	35.56
Hole size at top	42.22	-	-	34.81
Hole size at bottom	37.19	-	-	43.47
Circularity error at top	-	-	-	69.32
Circularity at bottom	-	26.6	-	59.15

Analysis of the average surface roughness

Figure 6.16 shows the average surface roughness under different cutting parameters using liquid nitrogen coolant.
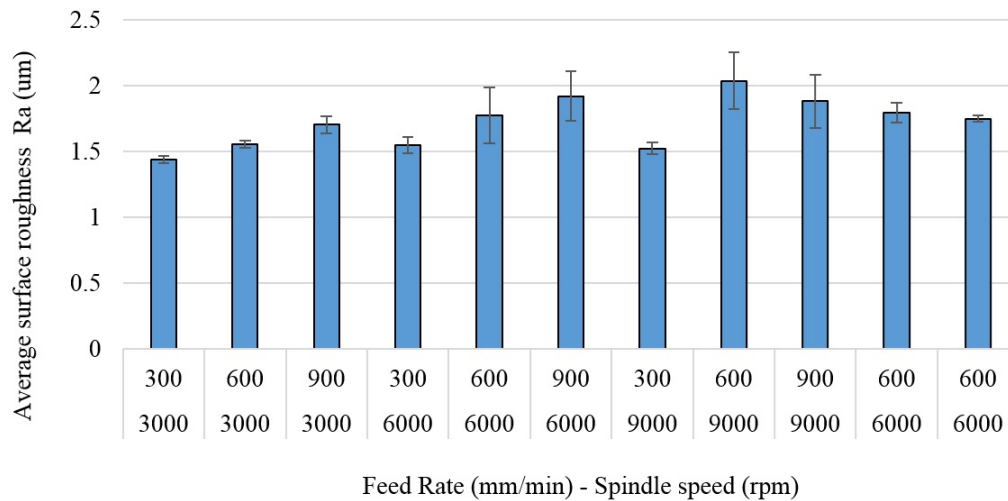
Figure 6.16: Average surface roughness in cryogenic drilling trials

The results show that the surface roughness increased with the increase of the feed rate and spindle speed. The surface roughness ranged from 1.438 to 2.037 µm. The influence of the feed rate was more significant than the spindle speed. It was also observed that using cryogenic liquid nitrogen was more efficient in reducing the surface roughness when drilling at high spindle speeds. Higher temperatures are expected to develop when drilling with these cutting parameters. The application of liquid nitrogen assists in cooling the workpiece and the cutting tool, which is reflected by reducing surface roughness. The ANOVA analysis

(see Table 6.5) shows that the feed rate had a significant contribution (55.94 %) which was twice that of the spindle speed (21.34 %), while their interaction was insignificant, The error in the model was significantly large (25.62 %) which indicates that the model requires the use of non-linear analysis or higher order interactions.

Analysis of burr formation in cryogenic drilling trials

Figure 6.17 shows the average entry and exit burr height and burr root thickness under different cutting parameters using liquid nitrogen coolant.
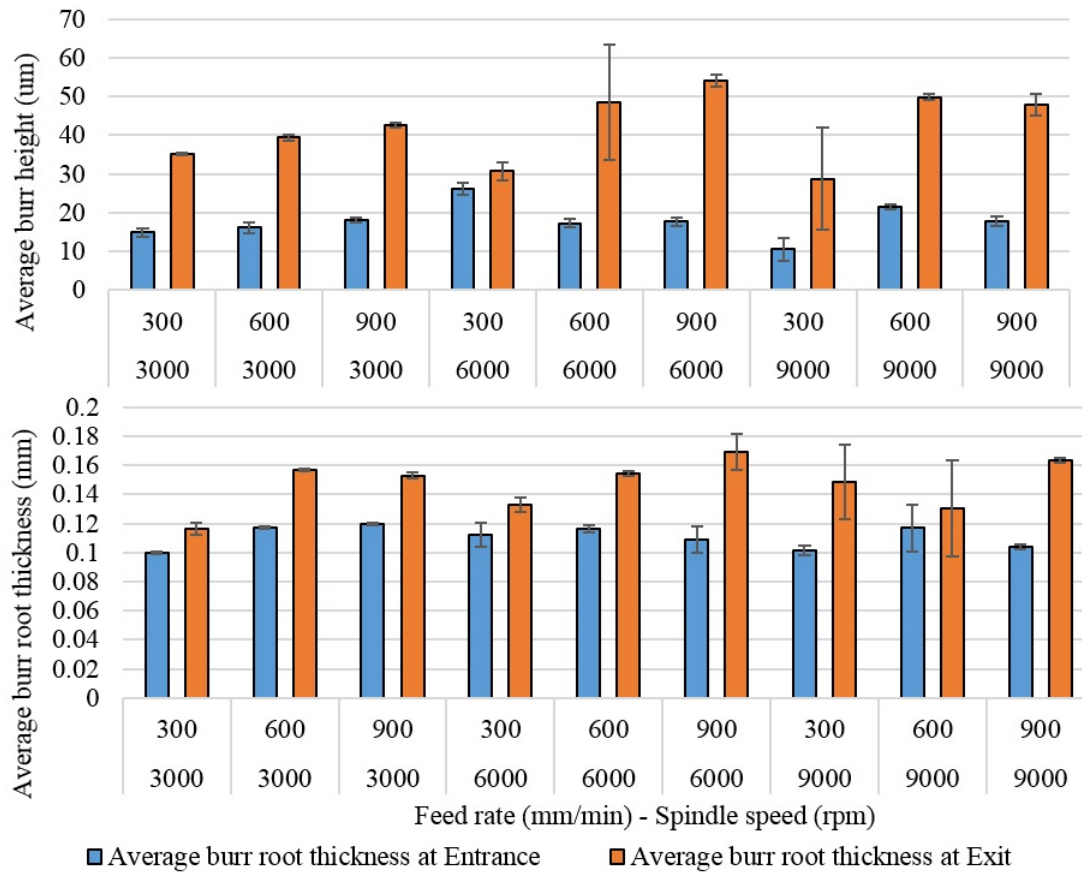
Figure 6.17: The average (a) burr height (b) burr root thickness at entry and exit in cryogenic drilling trials

Similarly to dry and MQL trials, the exit burrs were greater than entry burrs. The entry burr height and root thickness increased with the increase of the feed rate at f= 300 mm/min and decreased with it at f= 600 mm/min. Exit burr height increased with the increase of the feed rate at all cutting conditions and decreased with the increase of spindle speeds at f= 300 mm/min and increased with it at f= 600 mm/min. The entry burr height ranged between 10.5 to 26.3 µm and between 28.78 to 54 µm at exit. The exit burr root the thickness increased with the increase of the feed rate at n= 3000 and 6000 rpm. It also increased with

the increase of spindle speed at f= 300 mm/min and decreased with it at f= 600 mm/min. The entry burr root thickness ranged between 0.01 to 0.11 mm and between 0.11 to 0.17 mm at exit.

The ANOVA statistical analysis provided in Table 6.5 shows that the interaction between the feed rate and spindle speed -at 62.88 %- had the highest percentage contribution on the entry burr height while the spindle speed and feed rate had the contribution of 22.43 % and 12.51 % respectively. For exit burr height and entry burr thickness, only the feed rate seemed to contribute with 53.27 % and 22.99 % respectively. The interaction of the feed rate and spindle speed was a significant contribution to exit burr thickness with 25.5 % while the feed rate had a contribution of 34.86 %. Similarly to surface roughness ANOVA analysis, the error in the entry burr height, entry and exit burr thickness models was significantly large (30-40 %) which indicates that the model requires the use of non-linear analysis or higher order interactions.

Analysis of hole size and circularity error

Figure 6.18 shows the average hole size and circularity at top and bottom locations under different cutting parameters using liquid nitrogen coolant. Results indicate that the hole size is likely to shrink with depth as the hole size at the bottom was smaller than that measured at the top. The hole size at the top increased with the increase of the feed rate and spindle speed. At the bottom, the hole size decreased with the increase of the feed rate and increased with the increase of the spindle speed. ANOVA results indicate that the influence of the spindle speed was greater than the feed rate at both locations. The contribution of the spindle speed ranged from 37.19-45.22 % while the influence of feed rate was insignificant at the entrance and exit. The interaction of the feed rate and the spindle speed was insignificant for hole size and circularity at both locations. The deviation of the hole size between top and bottom locations was very small. All holes produced were oversized which could indicate that using liquid nitrogen can prevent hole shrinkage below the nominal size.

The hole size deviation at the top ranged from 15.8 to 24.7 μm and between 7 to 22.6 μm at the bottom, the largest increase in hole size at the top was when drilling at n= 9000 rpm and f= 900 mm/min and lowest when drilling at =3000 rpm and f= 300. In addition, the largest increase in hole size at bottom occurred when drilling at n= 9000 rpm and f= 600 mm/min and the lowest when drilling at =3000 rpm and f= 900 mm/min. The hole circularity at the top and the bottom decreased with the increase of the feed rate and increased with the increase of the spindle speed when drilling at n= 3000 and 6000 rpm, and yet it increased thereafter at both locations. ANOVA results indicated that both cutting parameters and their interaction had minor contributions on hole circularity at entrance.
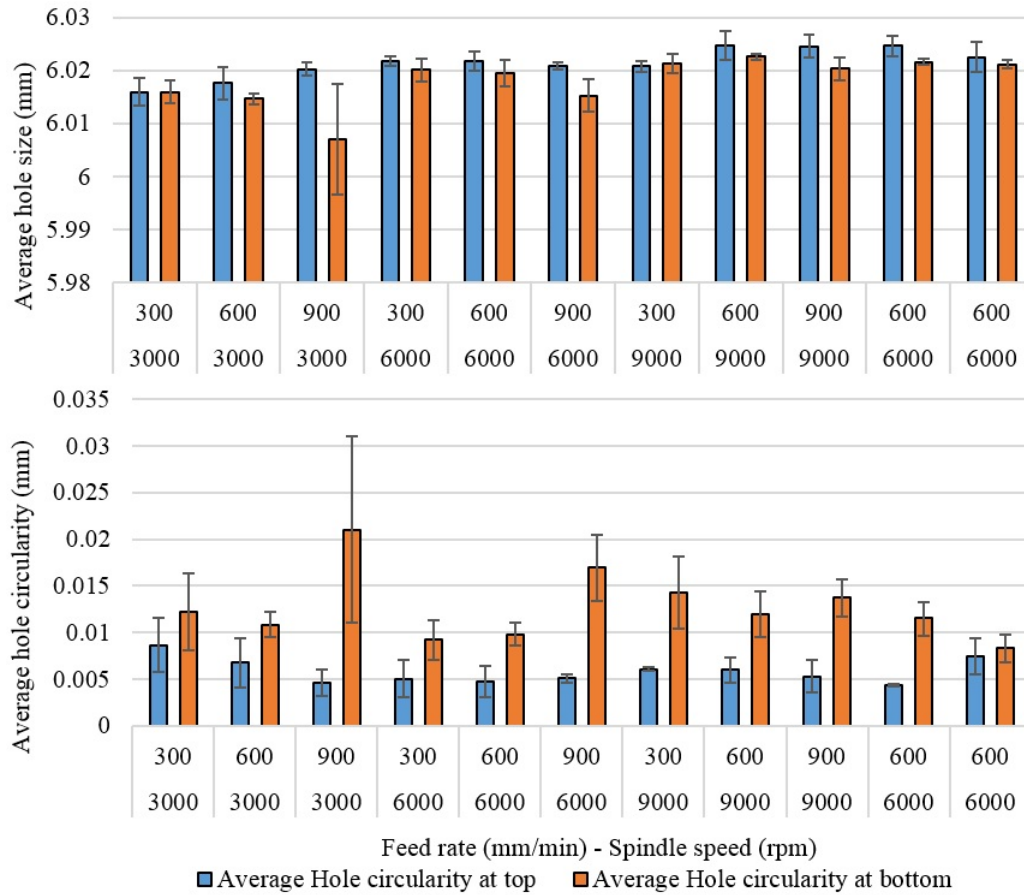
Figure 6.18: The average (a) hole size (b) hole circularity error at entry and exit in
cryogenic drilling trials

Only the feed rate had a significant contribution of 25.6 % at the bottom location. Hole
circularity at the bottom was higher than at the top which indicates that circularity is likely
to increase with drilling depth. Hole circularity error at the top ranged from 4.3 to 8.3 µm
and between 8.3 to 21 µm at the bottom. The largest increase in circularity error at the top
was when drilling at n= 3000 rpm and f= 300 mm/min and lowest when drilling at =6000
rpm and f= 600. In addition, the largest increase in circularity error at bottom occurred
when drilling at n= 3000 rpm and f= 900 mm/min and the lowest when drilling at =6000
rpm and f= 600 mm/min.

Post-machining microhardness near the hole edge of the upper and lower aluminium sheets

Figure 6.19 shows the post machining microhardness measured near the hole edges in the
upper and lower aluminium sheets under cryogenic drilling trials. Results show that the
hardness increased considerably from its typical value of 137 HV and ranged between 146

(6.5 %) and 152 (11 %). The hardness increased with the increase of the feed rate at entrance. This could be due to the rapid increase in cutting temperatures with an increase in feed rate countered by the rapid cooling from liquid nitrogen which increases the hardness of the surface. Generally, the hardness at entrance tended to decrease with the increase of spindle speed at feed rates of f= 300 and 600 mm/min. As spindle speed increases, there is less time for the heat generated to be dissipated, hence temperature increases and less strain hardening takes place despite the continuous cooling by liquid nitrogen. There was no clear relationship between cutting parameters and hardness at exit. The hardness decreased when increasing the feed rate from f= 300 mm/min to 900 mm/min at n= 6000 rpm spindle speed, while it increased with the feed rate increase when drilling at n= 9000 rpm. In machining, the increase in part hardness results in an increase in yield strength of the material and therefore, higher cutting forces are required to machine it.
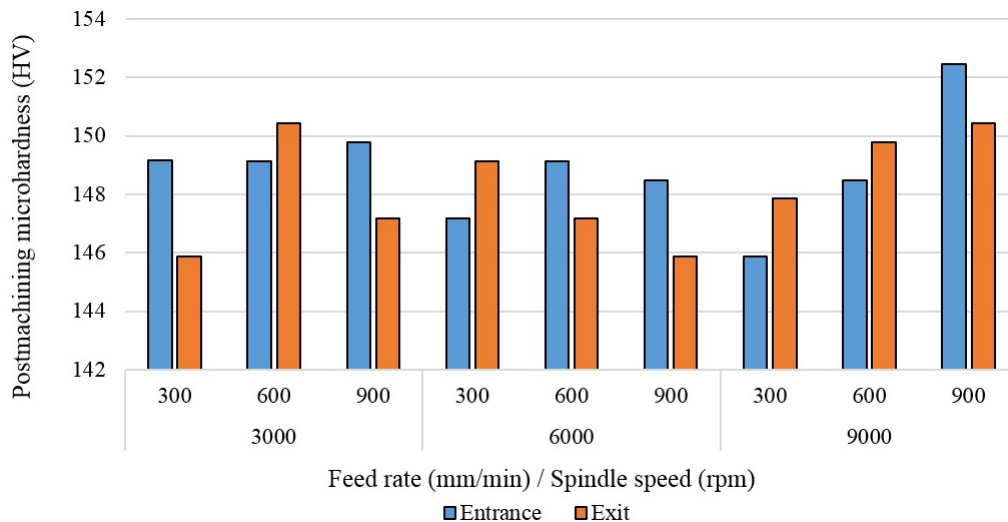
Figure 6.19: Post-machining microhardness at entry and exit in cryogenic drilling trials

Scanning electron microscopy SEM of holes drilled under cryogenic cooling

The status of the boreholes surface was analysed by SEM to detect any defects or damage in the metal sheets and glass fibre layers similar to dry and MQL trials. Images showed that debris and chips were less likely to adhere to the borehole surface under cryogenic cooling regardless of the cutting conditions used as shown in Figure 6.20. It was also observed that limited waste adhered to the borehole surface under all cutting speeds and feeds, which could be related to the cryogenic liquid nitrogen ability to dissipate heat from the machining zone up to a level that prevents adhesion of chips and epoxy to the inner surface. Similar to dry and MQL tests, SEM images showed that similar forms of damage occurred on machined surfaces under cryogenic drilling. Smearing, interlayer burrs and metal chipping

were observed on aluminium sheets while some regions of glass fibre layers were stressed into the laminate as shown in Figure 6.20e. A thin layer of spattered material is deposited from the melt and debris produced during the drilling process which cannot escape through the drill flutes and are eventually stressed into the laminate layers
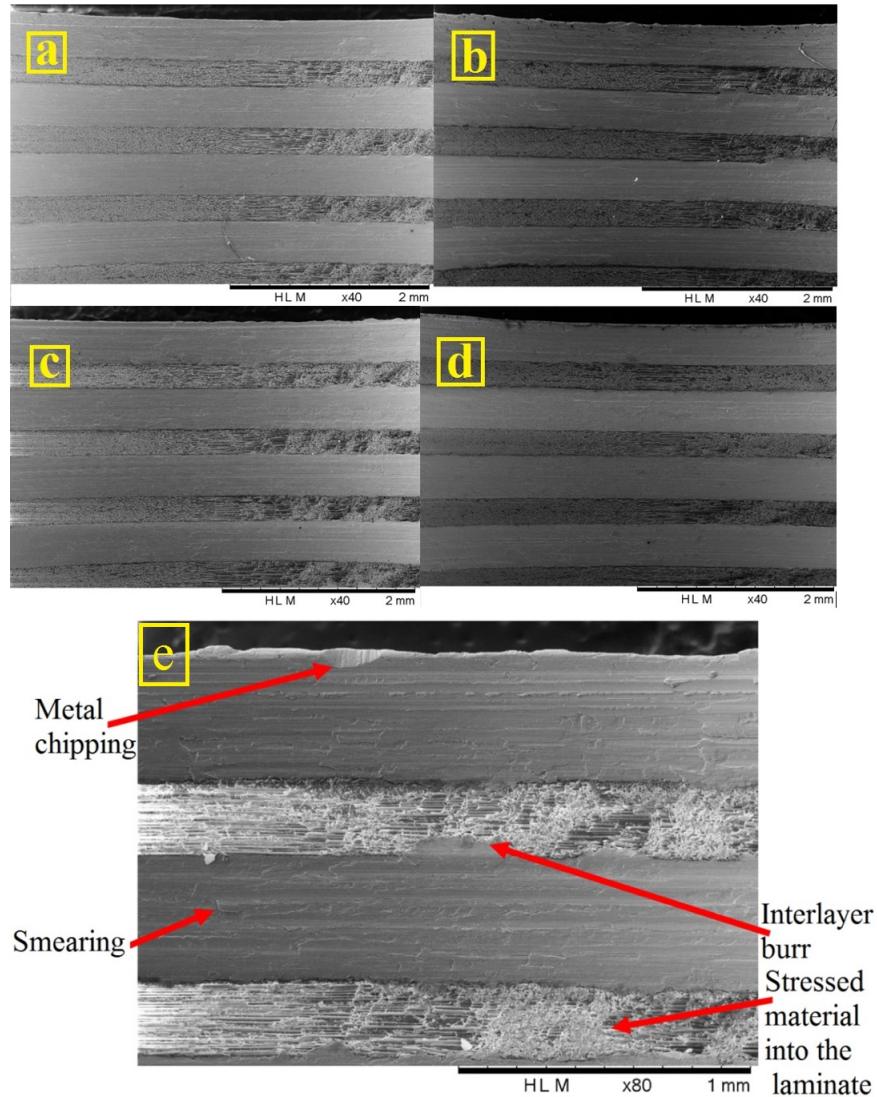
Figure 6.20: SEM images of upper hole section under cryogenic cooling (a) 3000 rpm and 300 mm/min (b) 3000 rpm and 900 mm/min (c) 6000 rpm and 600 mm/min (d) 9000 rpm and 300 mm/min (e) upper hole section under cryogenic cooling 6000 rpm and 900 mm/min

Delamination analysis of hole drilled under cryogenic cooling

Figure 6.21show CT scan images of holes drilled under cryogenic cooling. No cracks, minor surface delamination or separation was observed under all cutting conditions, However,

erosion in the lamina - similar to dry and MQL- was found to occur only at $\pm45\hat{}\circ$ relative to 0° fibre orientation which could be due chip collision with glass fibre layers while exiting the workpiece through the flutes, leading to fibre pull outs in small chunks. Inspecting other locations around the hole edge did not reveal any signs of erosion. The surface delamination factor was negligible and therefore was not reported in here. The maximum erosion depth in glass fibre layers was larger than that found under dry conditions -around 190 μm - and also tended to increase with the increase of the feed rate. The larger erosion under cryogenic cooling could be due to the increase in matrix brittleness from the cryogen coolant which makes it easier for the glass fibre layers to break when in contact with evacuated chip or cutting tool.
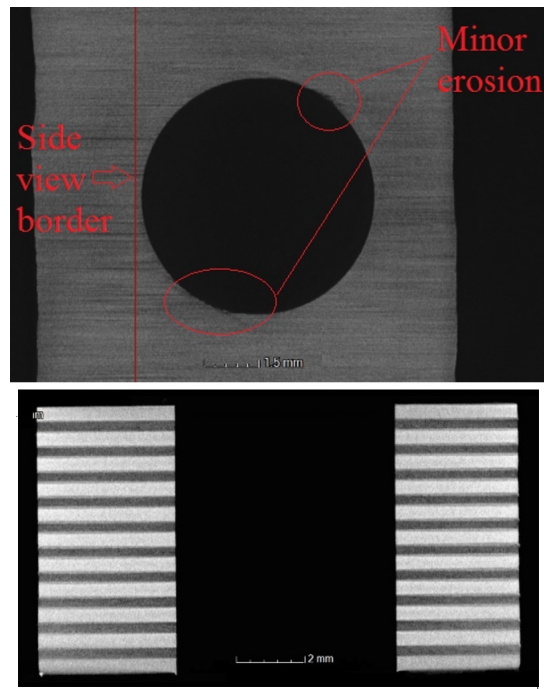
Figure 6.21: CT images of hole drilled under cryogenic cooling at 6000 rpm and 600 mm/min

Hole quality inspection under optical microscopy using cryogenic cooling

Figure 6.22show the entry and exit hole status when drilling GLARE 2B 11/10 using cryogenic liquid nitrogen. Under the investigated cutting parameters, no visible damage was observed on the hole edge and through its thickness. No signs of spalling, fibre fraying or fuzzing or edge chipping fracture were found in all inspected holes. The hole quality at the entry side was in better condition than at the exit side especially in terms of burr formation and edge shape. Similar to MQL, the presence of aluminium sheets which essentially function as backup/support material to glass fibre layers stacked in between was thought to

minimise their susceptibility to drilling-induced damage. In addition, it was observed that the hole edges at exit side did not show signs of coating loss of the bond primer which gives aluminium sheets the yellowish colour with the exception of holes drilled at feed rates of f= 600 mm/min and f= 3000 rpm, and f= 900 mm/min and n= 9000 rpm which could be attributed to the continuous cooling of the workpiece by liquid nitrogen which limits the softening of aluminium sheets to a level were the coating loss occurs.
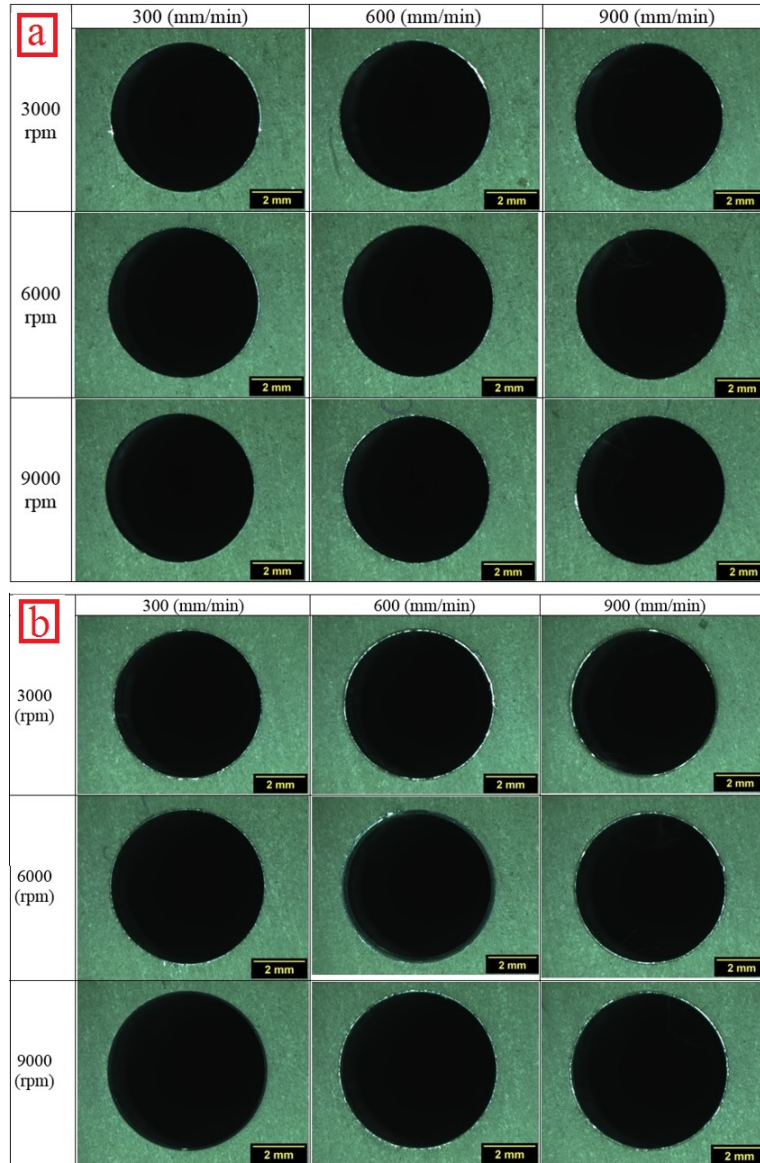
Figure 6.22: Optical microscopy images hole under cryogenic cooling (a) entry (b) exit

6.3 Concluding Remarks

The literature review presented in chapter 2 shows that previous work on machining metals and composites using different cooling strategies such as conventional flooding, minimum quantity lubrication, cryogenic machining were mainly used with hard to cut metals such as titanium and steel, and to a less extent in the recent decade on composites. The literature review also showed that the limited research conducted on the machinability aspects of fibre metal laminates was directed to explore dry drilling and milling operations, with some reported literature on semi-dry milling. semi-dry cooling strategies were encouraging in milling operations since they gave a better surface finish than dry machining at room temperature, especially when machining thick laminates. The literature also showed a research gap where there were no reported studies on the implementation of MQL and LN2 in drilling GLARE fibre metal laminates. Therefore in this thesis, a better understanding towards the feasibility of shifting from conventional dry machining to minimum quantity lubrication (MQL) and cryogenic liquid nitrogen cooling (LN2) was established to highlight the benefits of such coolants.

The machining performance of MQL and LN2 cooling strategies were encouraging to test with GLARE since in most previously reported studies gave a better hole quality than that from dry drilling. The current research aims to fill this gap by incorporating MQL and LN2 cooling methods in the drilling of GLARE fibre metal laminates as a potential environmentally friendly cooling strategies. The thesis also aims to demonstrate an in-depth comparison between those two cooling technologies and dry drilling of GLARE to facilitate the sustainable advantages and disadvantages of machining using those coolants on cutting forces and hole surface finish. The scope of this thesis is limited to the experimental study of twist drilling operation which has been achieved through the implementation of design of experiment methodology using full and fractional factorial designs and response surface methodology. The experimental drilling tests input parameters (spindle speed and feed rate) -in addition to (coolant flow rate and coolant air pressure for MQL trials)- and their levels have been considered by covering a wide range of cutting parameters similar to the previous chapters on dry drilling of Al2024-3, GLARE 2B and GLARE 3 laminates.

In this chapter, experimental studies were conducted for the first time to analyse the impact of using cryogenic liquid nitrogen and minimum quantity lubrication coolants and cutting parameters on cutting forces and hole quality when drilling unidirectional GLARE 2B 11/10 fibre metal laminates. The study also compares the efficiency of the two coolants against dry drilling condition. The machined hole quality was analysed by evaluating surface roughness, burr height and root thickness, the nominal hole size and circularity error, delamination and drilling-induced damage using optical microscopy, CT and SEM scanning techniques. The following results can be concluded:

6.3.1   Conclusions from MQL machining

- In MQL, the feed rate was the most significant contributor to increased thrust force (50.46 %), while the spindle speed was the most significant contributor in reducing thrust force (40.40 %). Also, the interaction of the spindle speed and the feed rate, appeared to influence the thrust force by 6.52 % while the coolant flow rate and air pressure had a no influence on cutting forces.

- In MQL, the spindle speed was the most significant contributor to reduced torque (51.57 %), while the feed rate was the most significant contributor in increasing torque (33.41 %). Also, the interaction of the spindle speed and the feed rate appeared to influence the torque by 5.41 %.

- In MQL, the spindle speed was the most significant contributor to increased surface roughness (37.7 %), followed by the interaction of spindle speed with feed rate (22.18 %) while the feed rate had a minor effect on increased surface roughness (1.22 %). Also, the interaction of the feed rate and air pressure appeared to influence the surface roughness by 3.08 %.

- In MQL, the quadratic interaction of the spindle speed was the most significant contributor to increased entry and exit burr height (37.16 % and 52.75 %) respectively, followed by the feed rate of (35.9 % and 12.49 %) while the coolant flow rate and air pressure had a minor effect on burr height of less than 5 %. Also, the interaction of the feed rate and air pressure appeared to influence the exit burr height by 3.91 %.

- The average burr height of holes under MQL was generally less than 20 μm at entry and less than 72 μm at the exit, while the average burr thickness of holes was generally less than 130 μm at entry and less than 240 μm at the exit. The average deviation from hole size under MQL was between +13.5 and −21 μm, while the average circularity error did not exceed 14μm at the top and 33 μm at the bottom.

- Using higher flow rates could sometimes deteriorate the surface finish, producing higher surface roughness and increased cutting forces. For example, drilling at a spindle speed of 3000 rpm and feed rate of 900 mm/min using higher flow rates of 60 mL/hr and air pressure of 3 bars increased surface roughness by up to 21 % compared to that obtained using flow rates of 20 mL/hr and air pressure of 1 bar.

- In MQL, the feed rate was the major significant contributor to increased entry and exit burr thickness (30.42 % and 21.33 %) respectively, followed by the interaction of the feed rate with air pressure (20.26 %) and flow rate (10.30 %) for entry burr thickness. Also, the spindle speed and the interaction of feed rate with flow rate had a minor effect on increased entry burr thickness (2.08 % and 1.92 %) respectively.

- In MQL, the spindle speed was the only significant contributor to change in hole size (5.25-6.67 %) while the feed rate and the interaction of the feed rate with flow rate had a minor effect on increased circularity error (3.06 % and 2.95 %) respectively.

- In MQL drilling trials, oversized holes were produced at the top location at all times, while undersized holes were produced at the bottom location. Hole circularity error at the top location was greater than at the bottom location, with the feed rate being most dominant among other factors.

- RSM modelling of MQL drilling tests and developed nonlinear regression models showed the ability to predict cutting forces, surface roughness, hole size and circularity at top accurately within the range of tested cutting parameters, while burr formation and exit hole size and circularity error were poorly estimated which could be due to the lack of fit and error within the model.

6.3.2   Conclusions from cryogenic machining

- In cryogenic machining, the effect of the feed rate on thrust force was more significant (50.48 %) than the spindle speed (43.59 %), while the spindle speed had a more pronounced effect on torque (55.94 %) than the feed rate (39.42 %). The interaction of spindle speed with feed rate was around 4.3 % for both cutting forces.

- In cryogenic machining, the average surface roughness ranged from 1.438 to 2.037 µm. The effect of the feed rate on the increased roughness was more significant (42.06 %) than the spindle speed (21.34 %) while the interaction of spindle speed with feed rate was insignificant.

- In cryogenic machining, the average entry burr height ranged from 10.5 to 26.3 µm and from 28.78 to 54 µm at the exit. The interaction of the feed rate with the spindle speed was most significant on entry burr height (68.88 %) followed by the spindle speed and feed rate by 22.43 % and 12.51 % respectively, while the feed rate was the only significant contributing factor on exit burr height with 53.27 %. Additionally, the average entry burr thickness ranged from 10 to 110 µm and from 110 to 170 µm at the exit. The feed rate was only significant input on burr thickness at both sides (30-35 %).

- In cryogenic machining, the hole size deviation at top ranged from 15.8 to 27.7 µm and between 7 to 22.6 µm at the bottom. It increased with spindle speed at both top and bottom locations during cryogenic drilling trials. Using cryogenic coolant, the only contribution was from the spindle speed (37-45 %) at both locations. The hole size increased with the feed rate at the top and decreased at the bottom,

- In cryogenic machining, the hole circularity error at top ranged from 4.3 to 8.3 μm and between 8.3 to 21 μm at the bottom, and error at the top location was greater than at the bottom location, with the feed rate being most dominant among other factors while hole circularity decreased with the feed rate.

- Using liquid nitrogen as a coolant increased the post machining hardness of the upper and lower aluminium sheets of the workpiece from 6.5-9.5 %.

Chapter 7

COMPARISON OF THE PERFORMANCE OF DRY DRILLING OF GLARE TO AL2024-T3, MQL AND CRYOGENIC COOLING of GLARE

I n this chapter, the drilling performance of GLARE 2B 11/10-0.4 when machined under the dry condition as reported in chapter 5 is compared to the dry drilling of monolithic alumni alloy Al2024-T3 reported in chapter 4 and discussed. In addition, a comparison of the drilling performance of GLARE 2B 11/10 when machined with minimum quantity lubrication and cryogenic cooling as reported in chapter 6 will be made against dry drilling tests reported in chapter 5. The performance is evaluated based on the effect of varying the cutting parameters (spindle speed and feed rate) in order to develop the basic understanding of the advantages and disadvantages of semi-dry cooling and cryogenic cooling during conventional drilling of GLARE fibre metal laminates. The evaluated parameters are the same as those reported in the previous chapters. The evaluation includes the assessment of cutting forces and hole quality parameters. In addition, the hardness of the upper and lower surfaces of aluminium sheets will be investigated.

7.1 Comparisons of drilling characteristics between GLARE 2B 11/10 and Al2024-T3 alloy

One of the main aims for drilling Al2024-T3 in this research was to investigate the effect of applying the same cutting parameters used in the dry drilling of GLARE laminates on hole quality and cutting forces in the alloy and compare the results with the ones obtained from a similar thickness of GLARE. In this section, a comparison and analysis between the results obtained from drilling Al2024-T3 alloy and GLARE 2B 11/10 are carried out since they both have equal thickness. The comparison looks into cutting force profiles and data from the inspected hole quality parameters which is discussed below with some details.

7.1.1 Cutting forces analysis

From the results in section 4.2, it was found that cutting forces when drilling Al2024-T3 alloy are greater than those in GLARE for the same thickness and cutting parameters. In addition, the thrust force is almost proportional to the feed rate and spindle speed for both materials. Similar trends using comparable drill diameter were found when drilling composite aluminium stacks reported by other researchers [65, 68, 188, 189, 336, 360, 365–367]. The difference in cutting forces in monolithic aluminium is because GLARE and Al2024-T3 have dissimilar mechanical properties although GLARE is largely made of Al202-T3 sheets. In addition, the higher cutting forces in Al2024-T3 is due to the tendency for aluminium swarf to adhere onto drill edges and cutting lips [189], which was evident from the larger areas of adhered aluminium observed on the cutting tools used for drilling monolithic aluminium than on those used for drilling GLARE as previously shown in Figure 7.1. Moreover, as reported from the literature and as far as the cutting force are concerned, it has been shown that the feed rate is an important parameter which influences the cutting forces during drilling of GLARE and Al2024-T3 aluminium alloy, as it can directly influence the area of undeformed chip thickness [368].

The case is specifically for GFRP composites since changing the feed rate can influence the number of fibre layers to be cut, which can considerably influence the magnitude of cutting forces experienced by the cutting tool during drilling. The chip formation modes discussed previously in the literature for orthogonal cutting and for oblique cutting mechanisms such as drilling and milling indicates that the fracture in glass and epoxy matrix layers in GLARE during the machining process occurs due to its brittle nature, which reduces the tool/chip contact on the flank and rake faces of the tool [368]. This in return tends to reduce the friction between the cutting tool and the workpiece material at each glass fibre layer through GLARE laminates, which results in lower cutting forces as compared to the homogeneous and ductile material, such as Al2024-T3 of the same thickness [368]. Increasing the spindle

speed at a constant feed rate decreased the thrust force when drilling Al2024. This finding contradicts findings previously reported by other researchers [68, 336]. The previous researchers investigated the drilling of composite metal stacks using low spindle speeds of less than n= 3000 rpm and similar feed rates used in this study. However, it was observed that increasing the spindle speed when drilling at higher feed rates does reduce the thrust force [336].
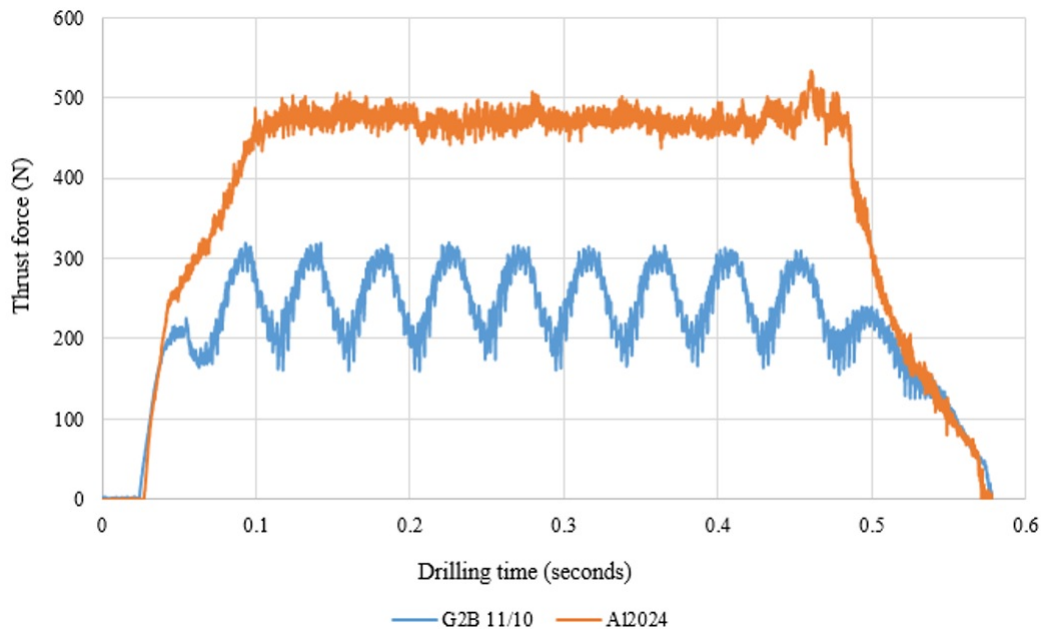
Figure 7.1: Thrust force profiles for hole drilled in GLARE 2B 11/10 and Al2024-T3 at 9000 rpm and 900 mm/min

The time-force curves of thrust force and torque during drilling GLARE and Al2024-T3 increase sharply when the drill engages with aluminium sheets and thrust force for both materials is approximately identical to each other as it can be seen from Figure 7.2. The thrust force and torque in Al2024-T3 continues to rise until reaching a steady state followed by a sharp drop trend indicating the exit of the cutting tool from the workpiece. While for GLARE, the thrust force fluctuates when the drill cuts through the alternating layers of aluminium and glass fibre at the steady state region. Both the thrust force and the torque increased as the laminate thickness increases due to the increase of the working part of the cutting edge. This agrees with the results found in drilling GLARE reported by other researchers [193].
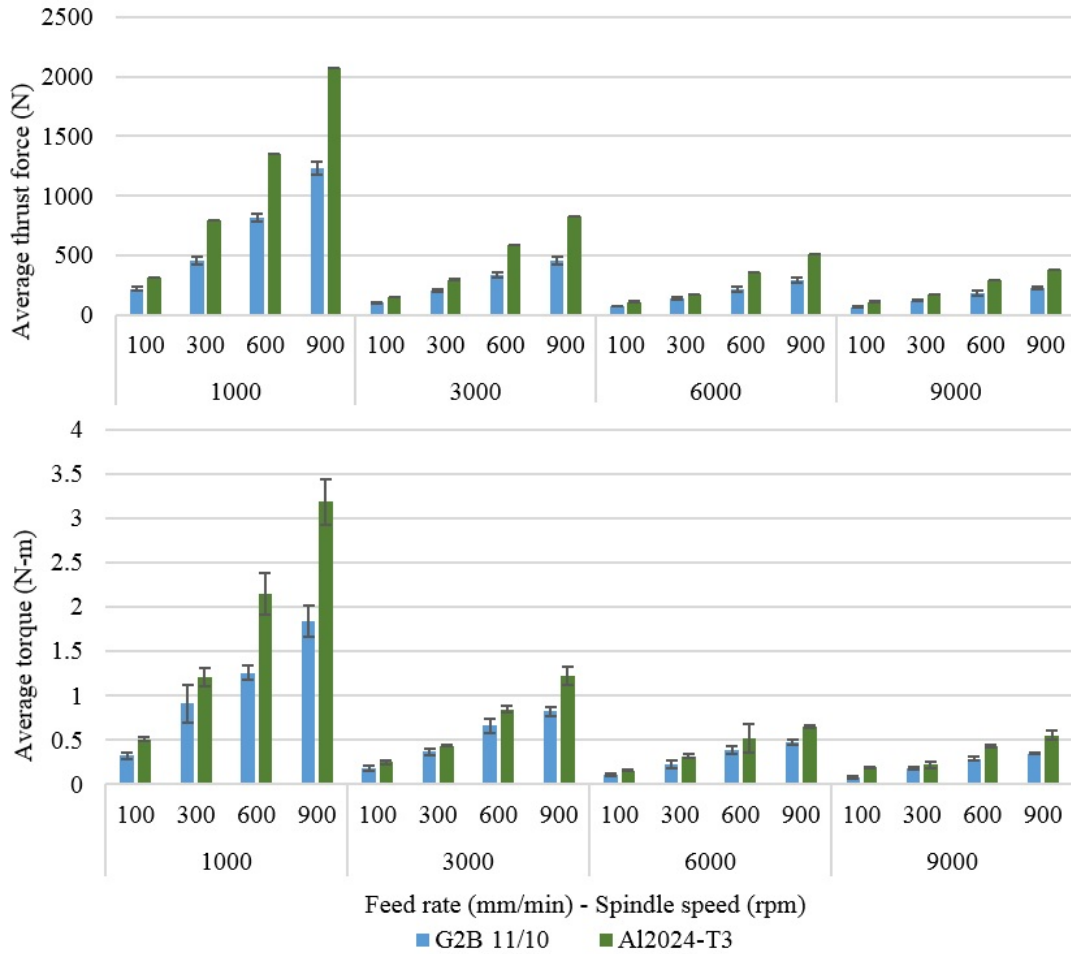
Figure 7.2: Comparison of (a) thrust force ad (b) torque in GLARE 2B 11/10 and Al2024-T3

7.1.2   Hole quality parameters

From the results of hole quality parameters in section 4.2 and comparison graphs provided in appendix B, it was found that for the same cutting parameters, the hole surface roughness in GLARE is always greater than those in Al2024-T3 alloy for the same thickness. This is mainly due to the presence of glass fibre layers in GLARE which considerably have higher surface roughness than aluminium which affects the final (combined) value of surface roughness using the 2D profilometer. As discussed previously, the 3D surface roughness inspection of some of the aluminium sheets in machined GLARE laminates revealed that surface roughness did not exceed 1 micron in most cases which is similar to surface roughness results obtained from drilling monolithic aluminium alloy. It was also observed that the surface roughness of GLARE and monolithic aluminium alloy become similar at higher spindle speeds of n= 9000 rpm which could be due to increased cutting temperatures and

increased deformations.

Regarding burr formation in both materials, it can be seen that the entry burr height in Al2024-T3 was slightly higher than that in GLARE laminate. This could be due to larger amount of chip evacuation during the drilling process and higher temperatures developed when drilling Al2024-T3, which increase plastic deformation and leads to a rise in entry burrs. The exit burr in GLARE tended to be higher than those in Al2024-T3. This could be mainly due to the increased bending in the last aluminium sheet in GLARE due to its inhomogeneous structure and relatively smaller thickness compared to the monolithic aluminium alloy. This makes it easier for the drill to push out aluminium burrs to a greater extent from the hole edges. The variation in exit burr height tended to increase with the increase of spindle speed. Similar results were obtained for exit and entry burr thickness. The entry and exit hole sizes in GLARE were generally undersized and were more affected by cutting parameters than in the aluminium alloy. Undersized holes are common when drilling composites due to the relaxation of the lamina while oversized holes are common when drilling ductile metals due to plastic deformation. The feed rate seemed to have a stronger impact on circularity error in GLARE which could be due to the hybrid nature of the material. However, in both materials, the deviation in hole size did not exceed the $\pm 40\,\mu m$ maximum allowable limit for holes drilled in aerospace structures. the chip formation from Al2024-T3 and GLARE laminates was quiet different. Most of the chip formed in Al2024-T3 trials was very short and discontinuous while the formed chips in GLARE were long and curled with more types at different cutting parameters. This could be due to the small thickness of aluminium sheets in GLARE relative to the monolithic Al2024-T3 workpiece and the presence of glass fibre layers which alters the chip cutting mechanism and the formed chips.

7.2 Comparison and discussion of results from Dry, MQL and cryogenic drilling trials

To consider the effect of MQL and cryogenic cooling on drilling GLARE, results from cutting forces and hole quality parameters discussed previously were plotted at various cutting parameters and are compared and discussed in the following subsections.

7.2.1 Cutting forces comparison

Figure 7.3 shows a comparison of the thrust force and torque under dry, MQL and cryogenic conditions in GLARE 2B 11/10. The application of liquid nitrogen produced higher average thrust and maximum force compared to dry and MQL drilling tests. The increase in average thrust force ranged from 10 % to 21 % compared to dry drilling.
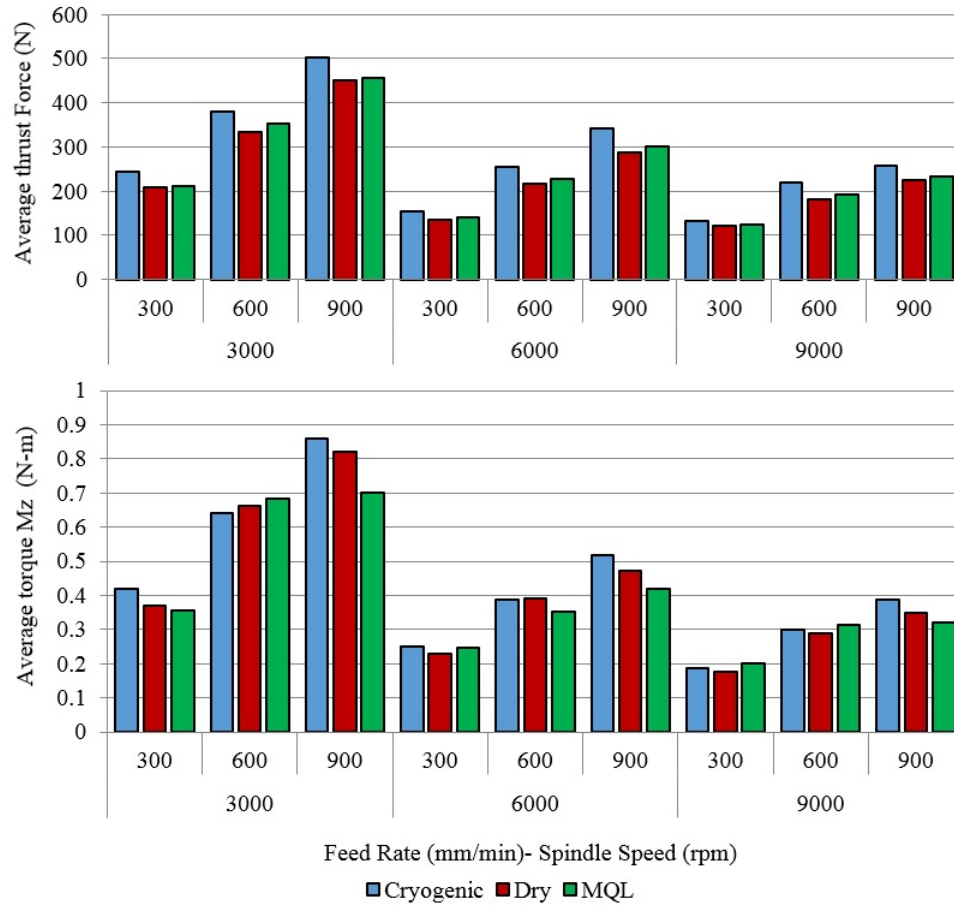
Figure 7.3: Average (a) thrust force (b) torque comparison under dry, MQL and cryogenic conditions

The significant rise in cutting forces when using liquid nitrogen can directly influence the delamination damage in glass fibre layers. The rise in cutting force when using cryogenic cooling could be due to the extremely low temperatures of liquid nitrogen on the cutting tool and the workpiece during the drilling process, which could lead to changes in the mechanical properties of GLARE constituents in the cutting zone. This was confirmed by inspecting the microhardness of the upper and lower aluminium sheets which showed that it increased when applying liquid nitrogen. The increase in workpiece microhardness may have adversely affected the cutting forces. The results obtained from coolants and dry drilling of GLARE laminates agrees with the previously established relationship between cryogenic cooling and cutting forces components in machining of metals and composites, which states that applying cryogenic coolants such as LN2 and CO2 generally increases the cutting forces in machining process in comparison with dry and other cooling methods [369–371]. Cutting forces results using MQL showed a negligible increase in thrust force compared to dry conditions. Cryogenic cooling generates around 40-60 N of thrust force more than dry and MQL conditions at a spindle speed of n= 3000 and 6000 rpm and around 10-30

N of thrust force at n= 9000 which indicates that cryogenic cooling becomes more efficient when drilling GLARE at higher spindle speeds and lower feed rates.

As feed rate was increased from f= 300 mm/min to 900 mm/min, the difference between thrust forces in dry and cryogenic was reduced from 17.4 % to 11.5 % at constant spindle speed of 3000 rpm, while the difference increased from 12.1 % to 18.9 % at n= 6000 rpm and from 9.8 % to 14.2 % at 9000 rpm. Similar for MQL, as feed rate was increased from f= 300 mm/min to 900 mm/min, the difference between thrust forces in dry and MQL was reduced from 2.4 % to 1.2 % at constant spindle speed of n= 3000 rpm, while the difference increased from 2.63 % to 4 % at 6000 rpm and from 3 % to 3.64 % at n= 9000 rpm. It was also observed that the increase in thrust force due to liquid nitrogen cooling compared to dry drilling decreased with the increase of spindle speed, for example when drilling at n= 3000 rpm and f= 900 mm/min the difference in thrust force between dry and cryogenic tests was around 50 N and around 24 N when drilling at n= 9000 rpm and f= 900 mm/min which could indicate that the efficiency of cryogenic liquid nitrogen to remove heat reduces at higher spindle speeds.

Figure 7.4 shows a comparison of thrust force plots under MQL, cryogenic and dry conditions for a drilled hole at n= 3000 rpm and at f =900 mm/min. The use of liquid nitrogen can be seen to increase the cutting forces constantly during the drilling process especially at the upper section of the workpiece which was in direct contact with liquid nitrogen. These observations on cutting forces profiles indicate that the impact of applying cryogenic cooling was more dominant than MQL and dry, especially at the entry stage of the cutting tool into the workpiece, which thereafter, the effect of cryogenic cooling was reduced with deeper drill penetration into the workpiece until finally becoming almost less effective when reaching the last layer of the workpiece. Therefore, it can be stated that the application of cryogenic cooling of the tool-workpiece during drilling did not improve the drilling performance with respect to generated thrust force in GLARE laminates, though the application of cryogenic cooling has been previously reported to provide such benefits in metal machining [282, 372, 373].

Using MQL coolant reduced the torque by up to 17 % compared to dry drilling trials, especially when drilling at high feed rates. This could be due to the lubrication effect of MQL which helps to lubricate the drill while cutting through GLARE. The lubrication of the cutting tool reduces the friction forces caused by the continuous rubbing of the drill against the walls of the holes. Also, the air pressure ejected on the workpiece could have helped to dissipate the heat from the cutting zone region as well as the heat generated by hot chips. Cryogenic cooling generates around 0.03-0.045 N-m more torque than in dry machining and around 0.065 -0.158 more than under MQL conditions at a feed rate of f= 900 mm/min and equal or less at f= 600 mm/min which indicates that cryogenic cooling becomes more

efficient on torque when drilling GLARE at low feed rates and spindle speeds. As feed rate was increased from f= 300 mm/min to 900 mm/min, the difference between torque in dry and cryogenic conditions was reduced from 13.4 % to 4.5 % at constant spindle speed of n= 3000 rpm, while the difference increased from 8.3 % to 9.32 % at n= 6000 rpm and from 4.85 % to 8.36 % at n= 9000 rpm. Similar for MQL, as feed rate was increased from f= 300 mm/min to 900 mm/min, the difference between torques in dry and MQL increased from 3.65 % to 17.3 % at constant spindle speed of n= 3000 rpm, while the difference increased from 7.66 % to 14.6 % at n= 6000 rpm and from 12.3 % to 8.72 % at 9000 rpm.
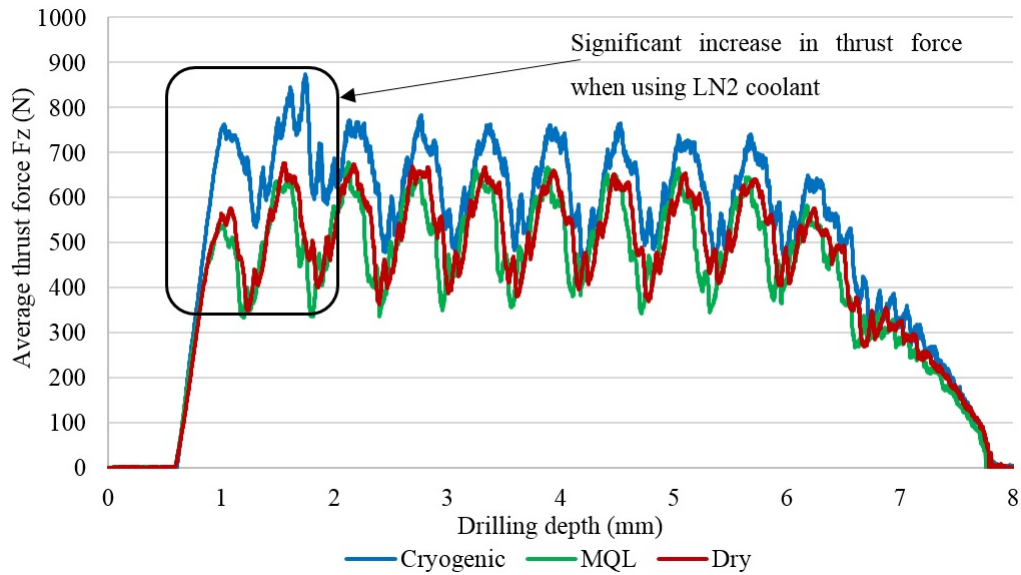
Figure 7.4: Average thrust force comparison under dry, MQL and cryogenic conditions at n= 3000 rpm and at f= 900 mm/min.

Based on the results from cutting forces, the microhardness around drilled hole edges was inspected. Figure 7.5 shows the average Vickers microhardness of the upper and lower aluminium sheets measured near the edge of drilled holes versus cutting parameters and different coolant conditions. The post-machining microhardness of the sample drilled under dry and MQL conditions increased about 1.5-5 % and ranged between 139-144 HV. For LN2, the increase in microhardness was higher than that in MQL and dry conditions under same cutting parameters which could be the reason for the greater developed cutting forces. The increase ranged between 6.5 9.5 % 146-150 HV. Additionally, there was no significant difference observed in microhardness between the upper and lower aluminium sheets under all conditions. The results clearly indicate that cryogenic cooling using liquid nitrogen allows the material to reach a higher surface hardness which could be attributed to the impact of extremely low temperatures of liquid nitrogen during the drilling process [373]. The cooling effect of liquid nitrogen would reduce the thermal softening of GLARE constituents by

reducing the machined surface temperature when applied directly to the workpiece/cutting tool. Rotella et al. [372, 373] previously reported that applying cryogenic coolant during machining process can help maintain small grain size after dynamic recrystallization which gives higher surface hardness. The increase in hardness of the workpiece subjected to liquid nitrogen is reflected in the reduction of surface roughness as it will be shown in the following section. This could be due to the increase in the toughness of Al2024 sheets and glass fibre layers due to microstructural alterations when subjected to the extremely low temperatures of LN2. Also, it is well known that the final mechanical properties can be influenced by cooling rates when the material is rapidly cooled to very low temperatures. Hickey [374] previously reported that a gradual increase in the strength properties of Al2024-T3 in sheet form was observed when cooling from room temperature of 10 °C down to -196 °C.
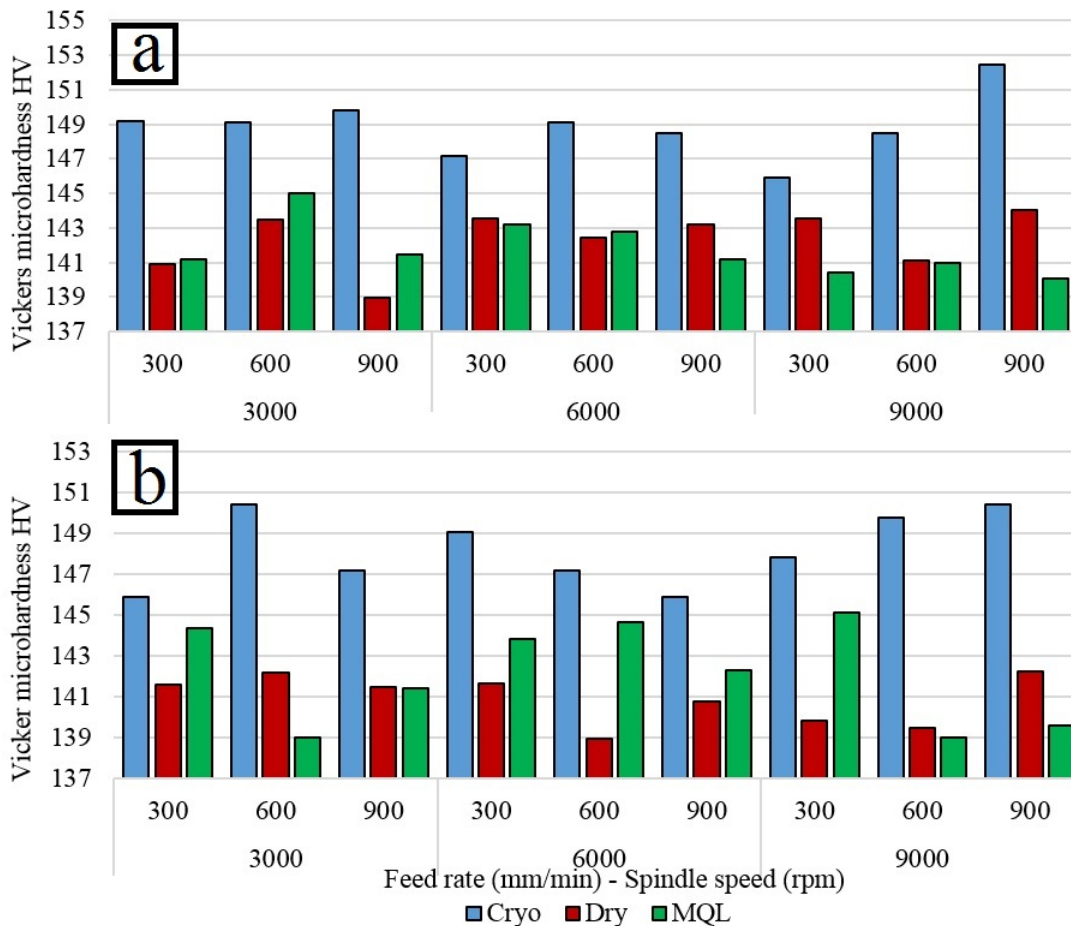
Figure 7.5: Vickers microhardness versus cutting parameters under different cooling conditions at hole (a) entry (b) exit

7.2.2 Surface roughness comparison

Figure 7.6 shows a comparison of the average surface roughness R_a under different cutting parameters using cryogenic, MQL and dry conditions. Using MQL and LN2 coolants improved surface roughness compared to a dry condition. Their application can be seen to be more efficient in reducing surface roughness when drilling at high spindle speeds of n= 9000 rpm compared to dry cutting. The improvement in hole surface roughness using MQL over dry condition ranged from 4 % to 43.1 %. The improvement in hole surface roughness using LN2 over dry condition ranged from 6.3 % to 44.6 %. Previous results on machining Al-7075 alloys showed that surface roughness is reduced when using MQL over dry and air cooling, which was attributed to the reduction in machining temperatures and improved tool life [375]. LN2 outperformed MQL, which could be due to improved penetration of the chip-tool interface observed when using cryogenic coolants in their gaseous form, which reduces the formation of the built-up edge on the cutting tool [376].

When using liquid nitrogen, it was also observed that the influence of spindle speed on surface roughness becomes less significant than feed rate, while for MQL and dry conditions the impact of spindle speed is more significant than the feed rate. This could be because MQL is considered as a lubricating method rather than a cooling method [377], which limits its effectiveness when machining at high spindle speeds and low feed rates. In the case of cryogenic machining, the extremely low temperatures of LN2 restrict the increase in cutting temperatures associated with high spindle speeds. Shane et al. [378] reported that the performance of liquid nitrogen coolant increased with higher cutting speeds when machining titanium alloy Ti-6Al-4V due to the reduction in machining temperatures, which also prevented chips from welding to the cutting tool. Therefore, it could be concluded that the performance of liquid nitrogen is more effective in reducing surface roughness when drilling at low feed rates and high spindle speeds.

In some cases, the use of liquid nitrogen did not show any appreciable reduction in surface roughness compared to dry drilling. For example, when drilling at n= 3000 and feed rate of f= 300 mm/min the surface roughness was greater when using LN2 than in dry and MQL which may be caused by the fact that the liquid nitrogen was deleiverd externally to the cutting tool and the upper surface of the workpiece. Therefore, it had little influence after the cutting tool was engaged with the workpiece and any further cooling might have adversely affected the surface roughness especially when drilling at low feed rates. Generally, the composite structures used in the aerospace structures are relatively thin hence the requirement is for short holes as it is the case in GLARE laminates. Typical demands include surface requirements in machined composites within R_a 4.8 microns when machined alone or Ra of less than 3.2 microns when machined in a composite metal stack. Moreover, it is usually demanded that the metal part of the stack to have surface roughness less than

1.6 microns in the metal part of the hole in the stack [379].
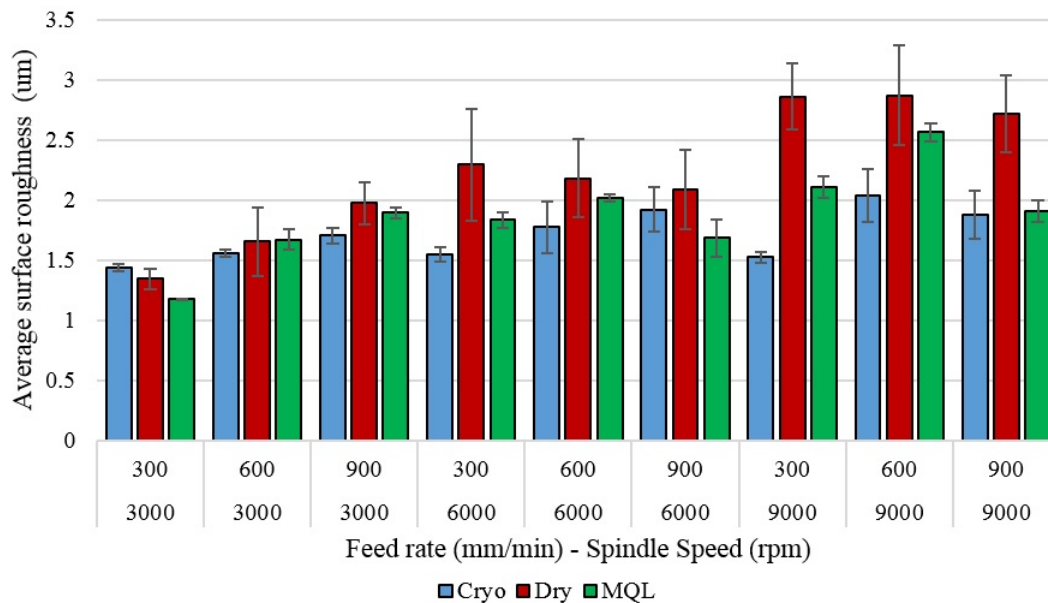
Figure 7.6: Average surface roughness at different cutting parameters under cryogenic, MQL and dry drilling conditions

The results of surface roughness as shown previously in Figure 7.6 were generally below 2 microns under all cutting conditions and cooling conditions, which indicates that achieving hole quality of GLARE in terms of surface roughness is possible and is well below the recommended limits, while the use of coolants proves to be an excellent choice in bringing down surface roughness levels compared to dry drilling. Further analysis was carried out to evaluate the impact of using MQL and cryogenic coolants on the surface integrity of the internal walls of drilled holes. Figure 7.7 shows the surface topography of the inner surface of three holes drilled at f =300 mm/min and n =9000 rpm using 3D optical microscopy scan. The results revealed that using cryogenic coolants improved the overall surface roughness of internal hole walls when comparison to dry and MQL coolants. For example, inspecting the last glass fibre layer at the described cutting conditions revealed that it had a surface roughness ranging between 0.964 and 4.501 μm under dry conditions, between 1.265 and 4.648 μm using an MQL coolant, and between 0.62 and 2.992 μm using a cryogenic coolant. Some adhesions from the dust and chips formed during the drilling process were observed on the internal walls of the holes drilled into the last aluminium sheet under dry condition. It was also observed that a better-machined surface finish was achieved in the glass fibre plies; these plies were relatively less deformed than in MQL and dry conditions. This could be attributed to the fact that the use of liquid nitrogen can reduce the compressive stresses developed in the laminate due to differences in the thermal expansions of the resin and the

fibre, as well as of the prepreg and the aluminium sheets. In addition, the epoxy matrix becomes stiffer at cryogenic temperatures which increases the rigidity of the fibres and reduces their deflection, leading to fibres being cut by shear fracture rather than bending and tearing [250].
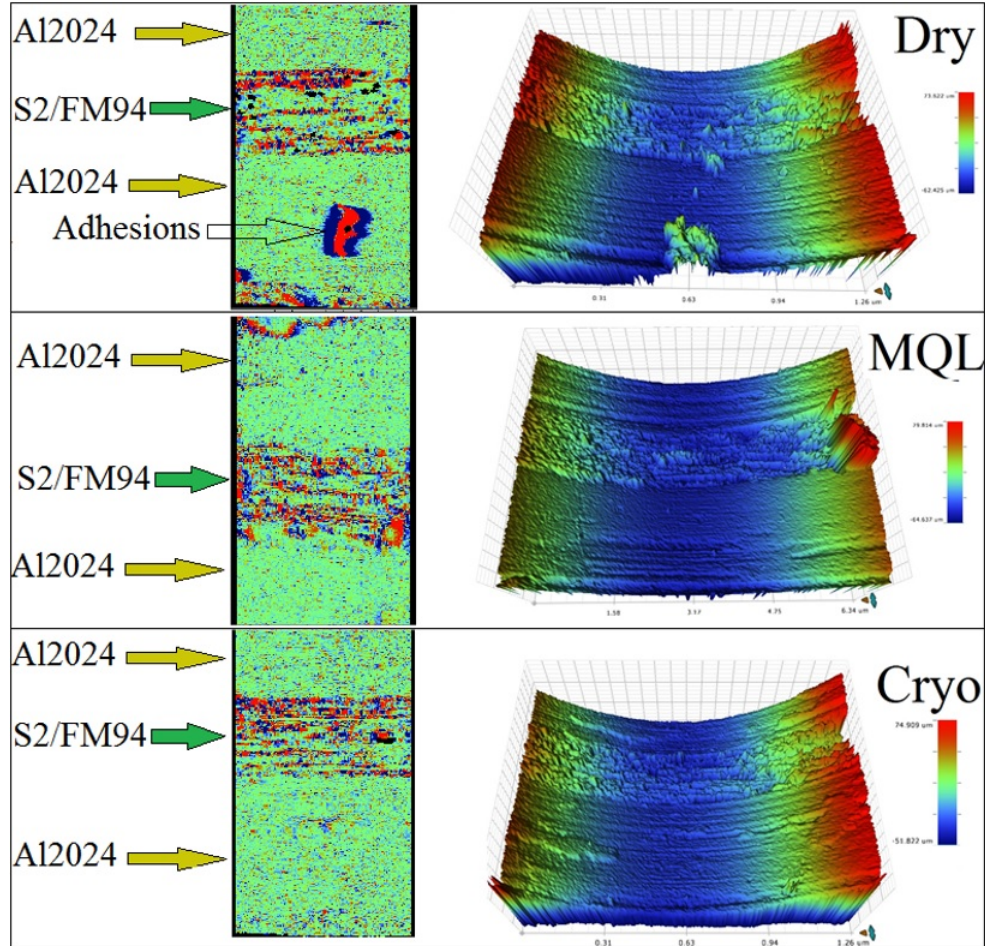
Figure 7.7: Surface topography of the last three layers of GLARE using 3D optical microscopy scan at f= 300 mm/min and n= 9000 rpm

To conclude, the range of surface roughness under tested cutting parameters was between 1-3 µm. The surface roughness is lowest when using cryogenic liquid nitrogen followed by MQL and highest in dry tests under same cutting parameters. As reported previously from the literature, there are no available data on the acceptable surface roughness for GLARE or composite metal stack materials recommended by the aerospace industry for machining/drilling process. However, Sandvik [52] reported common hole quality requirements by aerospace industry of less than 3.2 µm in CFRP and less than 1.6 µm in Al or Ti. The surface roughness in aluminium sheets was below 1 µm on average. For glass fibre layers, the surface roughness varied from 1 to 5 µm on average at measured locations. The results

clearly indicate that the surface roughness of aluminium sheets satisfy the recommended values by the aerospace industry. For glass fibre layers, despite exceeding the recommended roughness values, it was observed that the measured maximum surface roughness occurs only in a narrow region at the edges of the glass fibre layer (between aluminium sheets and glass fibre layer or between glass fibre layers with different fibre orientation) as shown in Figure 7.8, While it was always below the recommended maximum roughness in the remaining regions of glass fibre layer surface. This could be attributed to the difference in cutting mechanisms of glass fibre layers with respect to fibre orientation, and the formation of interlayer burrs which damages the adjacent region in glass fibre layers leading to higher surface roughness. In addition, this could be due to the sudden change in surface texture height when moving from aluminium surface to glass fibre layer surface or when the fibres alternate from $0°$ to $90°$. Indeed, Takeyyama [338] previously reported that the roughness of the machined surface with reference to the fibre angle showed that surface roughness increases steeply at fibre angles greater than $60°$ due to the generation of larger compressive strains within the work material resulting in larger surface roughness. The surface roughness values of glass fibre layers are generally within the range of previously reported studies of surface roughness in drilled GFRP and CFRP/metal stacks [65, 79, 189, 339–341].
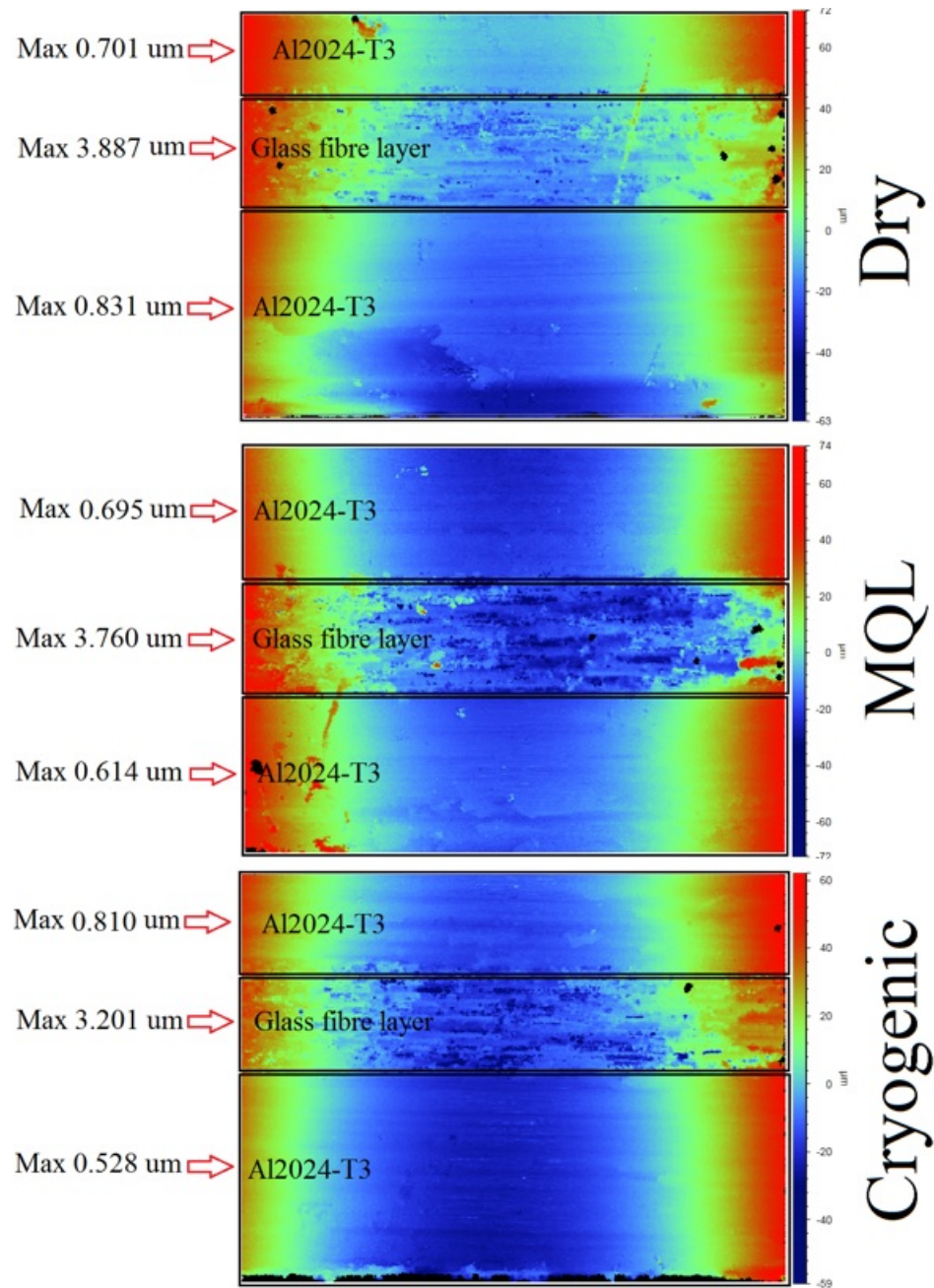
Figure 7.8: Surface topography of the last three layers of GLARE 2B 11/10 using 3D optical microscopy scan at f= 900 mm/min and n= 9000 rpm

7.2.3   Burr formation comparison

Figure 7.9 shows a comparison of entry and exit burr height under cryogenic, MQL and dry cutting conditions. Results show that using cryogenic and MQL coolants can significantly reduce the exit burr height and root thickness when compared to dry cutting. Murthy et al. [301] previously reported that using MQL cooling can reduce the temperatures at the chip formation area that have an influence on burr formations, leading to a reduction in exit burr heights when compared to dry cutting. However, it was observed that the entrance burr height increased significantly when using either coolant. Drilling with the assistance of liquid nitrogen increased burr height by up to 228 %. Alternatively, using MQL increased burr height up to 175 % compared to dry drilling. The rise in entrance burr height when using both coolants could be due to the excessive cooling and increase in drilling thrust force, as was the case in a previous study on drilling GLARE.
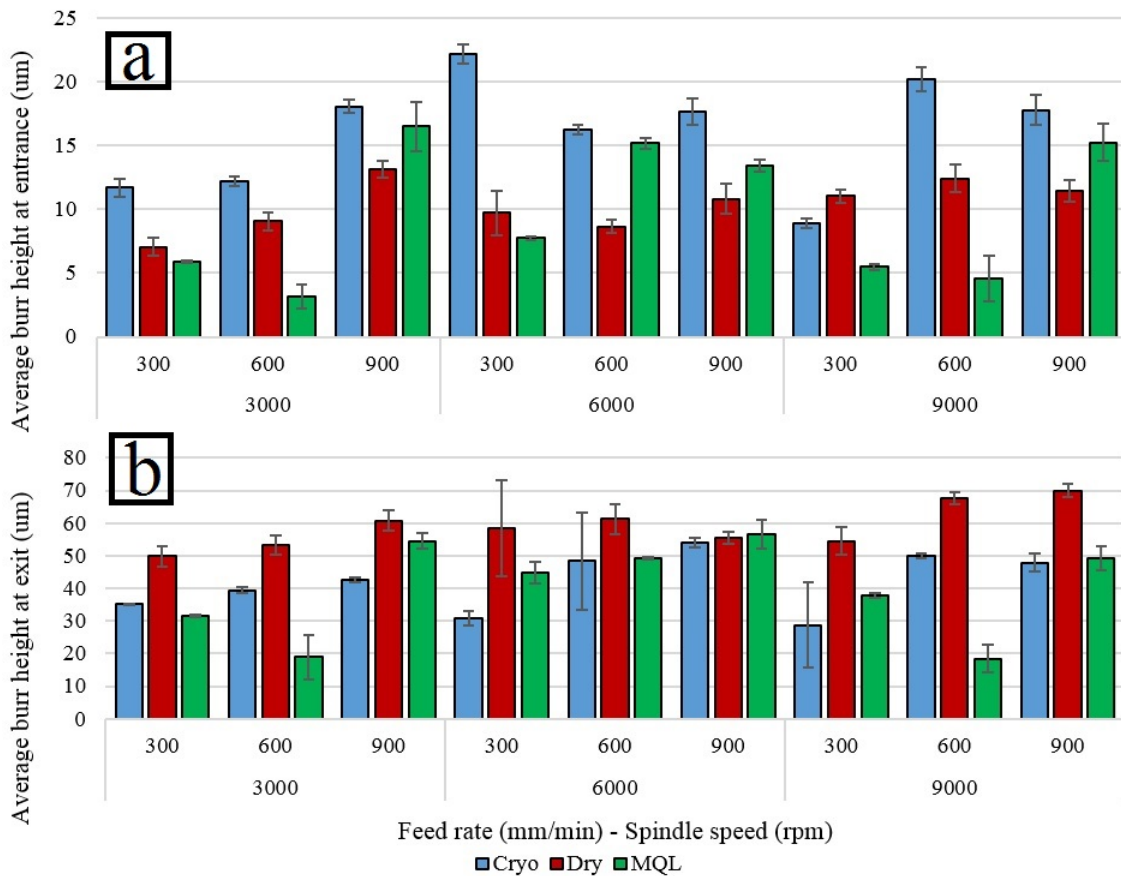
Figure 7.9: Comparison of the (a) entrance (b) exit burr height for Dry, Cryogenic and MQL drilling trials

There are several definitions of what would be an acceptable burr height for a hole drilled in metals. Gillespie [344] states that for common industry applications, a maximum acceptable

burr height in the machined workpiece can be either 5 % to 10 % of the metal thickness, or ideally, burrs that are equal or less than 30 µm tall are considered acceptable even if they are more than 10 % of the metal thickness. This means that an acceptable burr height in drilled holes in GLARE should not exceed 20.32 µm (5 %) or 40.64 µm (10 %). Therefore, entry burr heights produced from all cutting conditions are acceptable and no further process to remove them is required. However, looking at the exit burr heights, only holes drilled using MQL and cryogenic coolants at spindle speeds of n= 3000 rpm and feed rates of f= 300 mm/min can be considered acceptable based on the requirements described above.

The reduction in burr height and root thickness using coolants could be due to the fact that burr formation is highly dependent on the amount of plastic deformation represented by the ductility and elongation of the material [380]. Additionally, the burr formation is highly dependent on the mechanical properties of the workpiece material, such as its yield and ultimate strength [306]. These ultimate and yield strengths can be affected by material temperature. Moreover, the drilling process can considerably increase the temperature of aluminium sheet. This temperature increase causes a reduction in yield strength and an increase in elongation which results in increasing exit burrs. Also, as previous studies reported, the strength of Al2024 alloy increased and elongation decreased under cryogenic temperatures. For example, tensile and yield strength increased by almost 13.5 % and 38.5 %, respectively, when going from room temperature (25 °C) to liquid nitrogen temperatures (-196 °C) [374]. Therefore, the thermal effects induced by using liquid nitrogen coolant may increase the brittleness of the material. This brittleness reduces the exit burr size (height and root thickness) as burrs separate more easily from the hole edge rather than forming on it.

The influence of coolants on burr height was more significant when drilling at high spindle speeds and low feed rates. Such influence resulted as higher machining temperatures developed under this specified cutting condition. As a result, the use of coolants helped reduce the temperatures considerably. In addition, Seyed et al. [381] previously reported that the use of high spindle speeds and feed rates may increase the temperature and strain rate of the machined metal enlarging the exit burr size. When using cryogenic liquid nitrogen, the average exit burr height was reduced by up to 47 %. Similarly, MQL reduced the average height by up to 36.4 %. Using cryogenic and MQL coolants seemed to reduce entrance burr root thickness as shown in Figure 7.10.
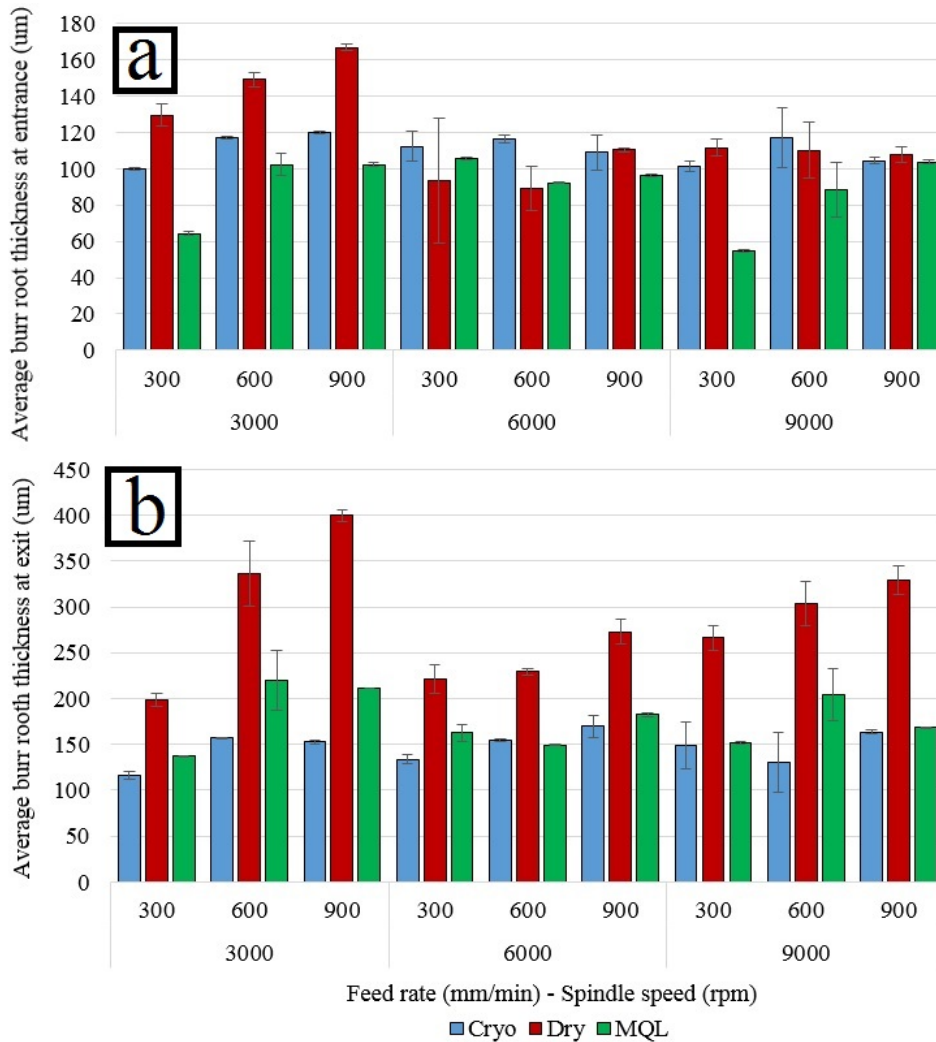
Figure 7.10: Comparison of the (a) entrance (b) exit burr root thickness for Dry, Cryogenic and MQL drilling trials

Generally, MQL is more efficient in reducing burr root thickness than cryogenic coolant. This result could be due an increased lubrication effect of MQL over liquid nitrogen. The reduction for MQL reached as high as 50 % compared to dry drilling while cryogenic reached as high as 28 %. Overall, using MQL and cryogenic coolants considerably reduced exit burr root thickness. The reduction was significant, especially when drilling at high feed rates or high spindle speeds. Figure 7.11 shows a comparison of burr formations taken at 90° on the hole edge of MQL, cryogenic and dry drilling conditions and different cutting parameters.
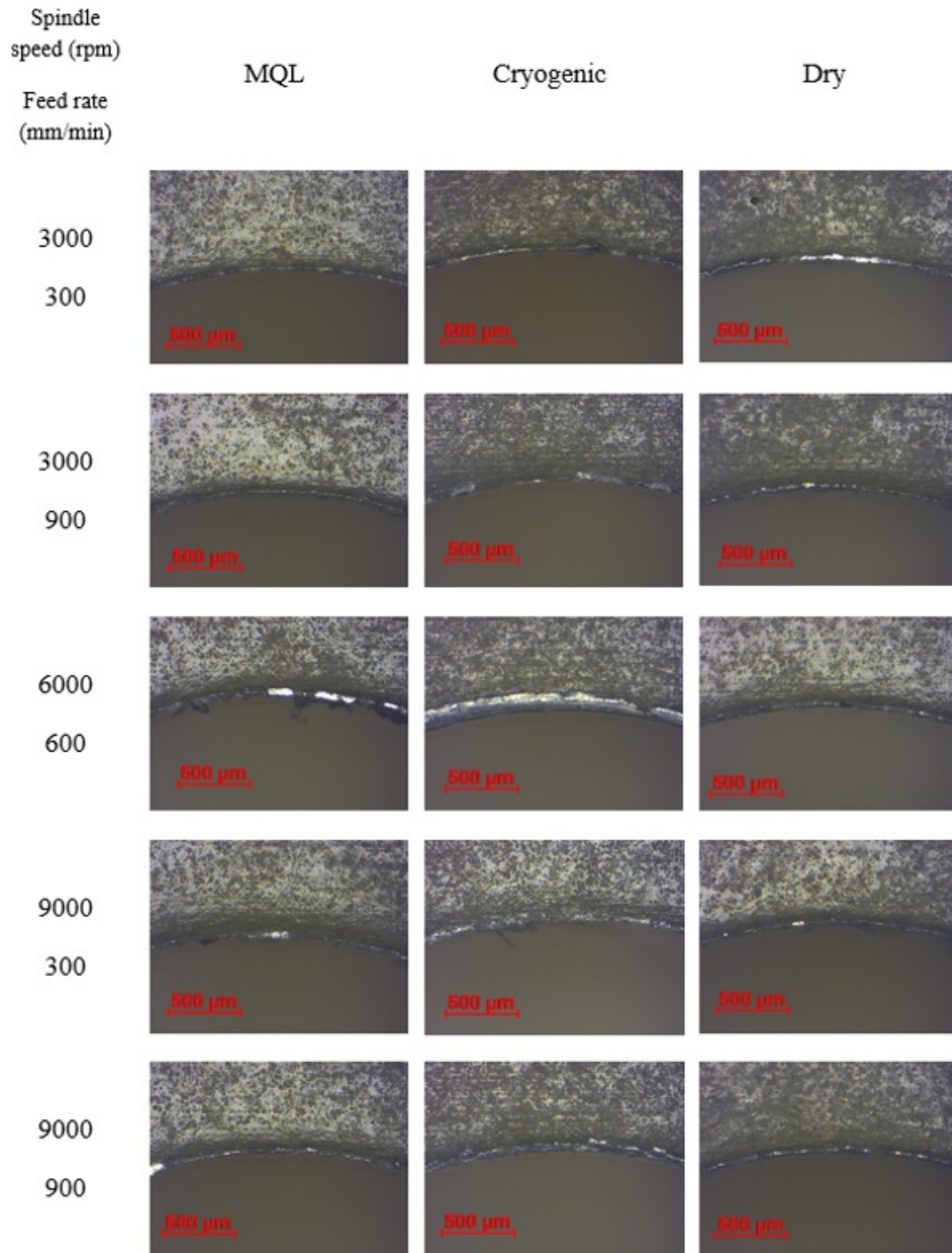
Figure 7.11: Exit burr formation around hole edge under MQL, cryogenic and dry conditions

7.2.4 Hole size and circularity comparison

Figure 7.12 shows a comparison of the average hole size at the top and bottom locations under different cutting parameters and cooling conditions. It is well known that the hole size in composites increases during the drilling process and decreases after a cooling phase [382].
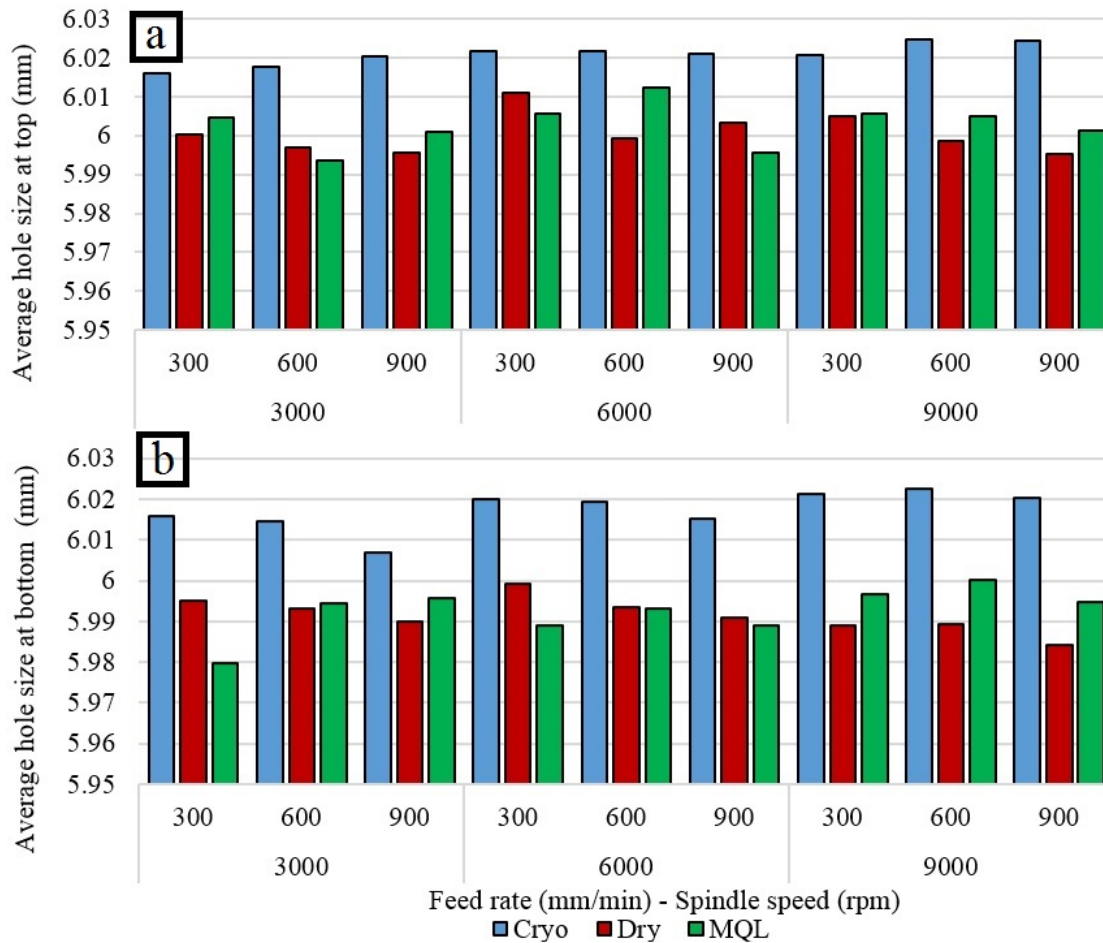
Figure 7.12: Comparison of the hole size at (a) top (b) bottom for Dry, cryogenic and MQL drilling trials

Using cryogenic coolant produced oversized holes for all cutting parameters at both locations. This result could be attributed to the fact that applying liquid nitrogen coolant can slow down the thermal expansion of GLARE constituents. As previously reported, the use of liquid nitrogen increased the epoxy matrix stiffness when drilling Kevlar composites and increased the rigidity of the fibres which caused a reduction in the deflection of the fibres [254], and prevented the lamina from shrinking after expansion. No general trend could be established on hole size using MQL as oversized and undersized holes were produced at both locations depending on the applied cutting parameters. This could be due to the limited ability of MQL coolant to reach through the inner layers of the material as

depth increases and the reduced cooling capacity in comparison with cryogenic coolant at higher cutting speeds. For dry conditions, undersized holes were produced for most cutting parameters in both locations. The difference in hole size deviation between top and bottom locations was much smaller when using cryogenic liquid nitrogen. Using MQL and dry conditions produced holes sizes near the nominal diameter of 6 mm at both top and bottom locations.

The results clearly indicate that the use of liquid nitrogen coolant prevents glass fibre layers from shrinking by reducing their thermal expansion. It is well known that hole shrinkage will occur in glass fibre reinforced epoxy resin materials after drilling due to relaxation of laminate [69]. In contrast, oversized holes are likely to occur when drilling soft aluminium alloys. However, the shrinkage does not take place when using liquid nitrogen as low temperatures induced by a low boiling temperature slow down the expansion rate of the metal sheets and relaxation of the laminate. This outcome could be also attributed to the lubrication effect of liquid nitrogen. Dhananchezian et al. [371] previously reported that applying liquid nitrogen on the tool rake face provided better lubrication and reduced the adhesions between the tool and chip when machining Al-6061 aluminium alloy. It was observed that the hole size at the top increased with feed rate and spindle speed when using cryogenic liquid nitrogen and decreased with feed rate increase when drilling under MQL and dry conditions. This effect could indicate that the type of coolant used can affect the hole size during the drilling process as the coolant directly influences the mechanical and thermal loads the workpiece is subjected to. This example was evident in the previous section which showed that cutting forces increased when using cryogenic liquid nitrogen coolant over MQL and dry conditions.

In conclusion, the strongest rivet joints installed on drilled GLARE fuselage structures are going to be the ones where the holes are as close to the hole nominal diameter as possible. Significantly undersized holes would require an additional reaming operation to bring them to the right size while significantly oversized holes would not take up the load until the other tighter holes have already begun to distort. The variation of hole size in all drilling trials and cooling conditions did not exceed -13 to 22.5 µm which is within the range of allowable hole clearance H9 as stated in hole size tolerances standard ISO 286. In addition, interference fit fasteners usually installed in aerospace structures have the ability to expand during installation which provides a compressive stress on the material bordering the hole and rivets. The installed rivet will expand sideways to fill the hole. On the other side, SANDVIK reports that hole tolerances in composites and composite metal stacks vary between ±20 to 40 µm with hole tolerances tighter than ±25 µm usually requiring a reaming pass [379], which means that under the cutting parameters used for drilling GLARE all holes are considered acceptable and do not require any further process. In addition,

as mentioned previously in chapter 3, the standard for drilled hole tolerance in aerospace metals is H7 (-12 microns based on ISO 286 hole tolerance). However, aerospace industrial manufacturers such as Boeing usually relaxes the tolerance to H8 (18 µm) or H9 (20 µm) to meet the allowable hole tolerances. Nevertheless, oversized holes in blind fasteners create performance issues with the fastener which could require removal of the fastener and reworking of the hole/structure which is considered time-consuming and potentially catastrophic for the structure.

Hole circularity comparison at top and bottom locations shown in Figure 7.13 reveals that using cryogenic liquid nitrogen reduced circularity by more than 70 % compared to MQL and dry conditions. The deviation in hole circularity error obtained using LN2 at the top location were aroundranged between 4.57 and 8.63 µm. and The smallest least deviationss were obtained when drilling at n= 6000 and 9000 rpm regardless of the feed rate used. , While while at bottom wherethey were slightly higher at bottom location and ranged between 9.21 to and 21.031 µm. This results suggests that in addition to cutting parameters (feed rate and spindle speed) the coolant applied during the machining process plays a significant role on hole circularity. It was also observed that hole circularity at the top decreased with feed rate and spindle speed when using LN2 coolant, while circularity increased considerably with the increase of the spindle speed and the feed rate under dry conditions. Using MQL did not show any appreciable improvement on hole circularity at the bottom except when applied at spindle speeds of n= 9000 rpm which could be attributed to MQL ability to remove cutting temperatures at higher cutting speeds. In fact, for some cutting parameters, the use of MQL coolant increased hole circularity by more than 47 % compared to dry conditions which could be due to excessive cooling.
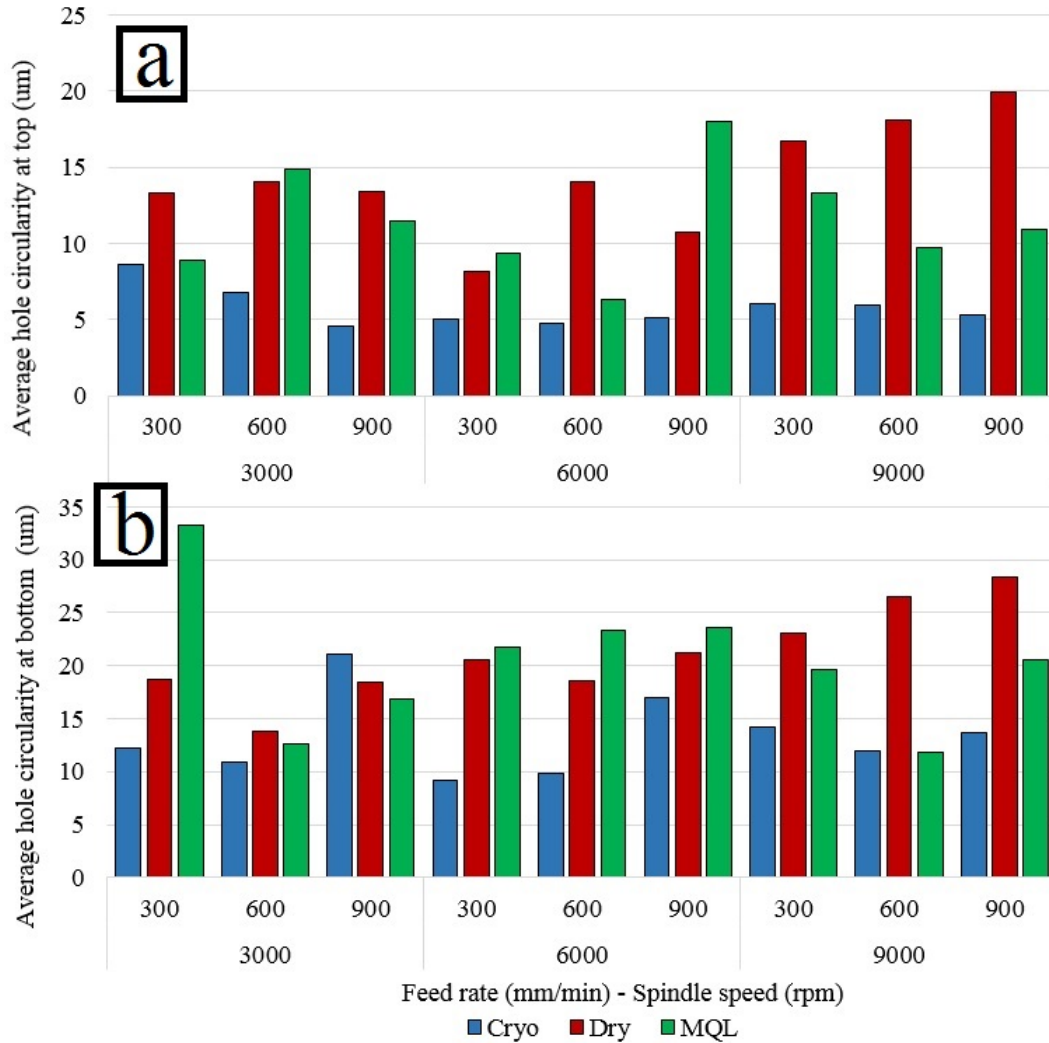
Figure 7.13: Comparison of the hole circularity at (a) top (b) bottom for Dry, cryogenic and MQL drilling trials

Due to the limited literature on machining GLARE in particular and use of coolant in machining composite metal stacks in general. Comparison were carried against other metals such as titanium. The results reported in the current research disagree with a previously reported study which indicated that hole circularity increased when using LN2 in drilling titanium compared to dry and wet conditions, especially with the increase of the feed rate [369]. This might related to the difference in material properties of GLARE and titanium in terms of material hardness and ductility.

7.2.5 Post-machining cutting tool condition

Microscopic investigations of the cutting tools showed that the use of cryogenic and MQL coolants can significantly reduce the adhesions of chips on the cutting tool compared to dry

drilling. The condition of the cutting tool in cryogenic and MQL trials was better than that observed in the dry tests, as shown in Figure 7.14 . Adhesions were seen to form all over the tool surfaces -around the chisel edge, the web thickness and the flank facets of the drill bits used in dry trials which is attributed to the tendency of aluminium alloys and their chips to adhere to the cutting tool and their low melting point [383] , while minor areas of adhesions from aluminium chips were formed around the chisel edge of the drills used in MQL and cryogenic tests. The cooling effect of liquid nitrogen in cryogenic machining and the mist lubricant in MQL have eliminated the production of built-up edge effectively and limited the deterioration of cutting tool to a limited region around the chisel edge. Despite that the cutting forces increased considerably using cryogenic cooling and increased slightly using MQL. However, the application of those coolants limits the adhesions on the aluminium sheets in GLARE and therefore, reducing the frictional force inherent in the cutting process.
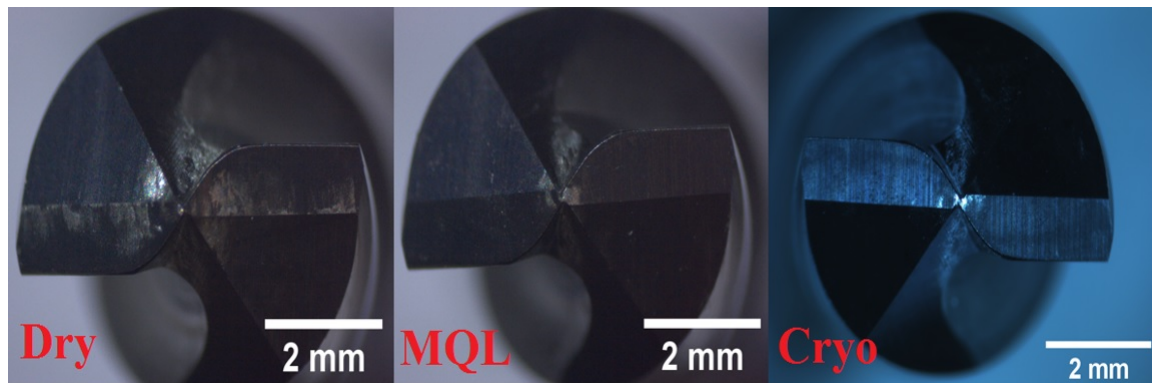
Figure 7.14: Cutting tool condition after drilling trials

The relatively better tool condition using MQL and cryogenic coolants can be related to improved chip breakability. This is due to the increased hardening of sliding chips which tends to reduce their stickiness on the cutting tool facets rather than accumulating on them [384]. Another study reported that cryogenic cooling can help retain the hardness of the cutting tool especially at high cutting speeds which reduced the adhesions compared to dry drilling [369].Hardness of the tool can be retained by improved heat conduction in cryogenic LN2 conditions. However, an interesting study reported that delivering the cryogenic liquid nitrogen through the cutting tool causes adhesions due to the limited lubrication of the cryogenic coolant [385]. This was not observed in the current study which could be due to the fact that the cryogenic was delivered externally.

7.2.6   Temperature measurements comparisons

Temperature measurements were carried out for selected cutting parameters in MQL trials to compare the effect of the coolant on cutting temperatures. The aim was to carry out temperature measurement trials for cryogenic cooling but due to the lack of material and funding, the tests were limited to MQL only. Figure 7.15 shows a comparison of hole temperature at exit between dry and MQL tests. The MQL drilling tests were carried out using 20 mL/hr flow rate coolant and air pressure of 3 bars since they proved to give the best results among all other tested flow rates and air pressures. Results showed that the application of MQL coolant can reduce machining temperatures when drilling at high feed rates of f= 900 mm/min, which could be due to the lubrication effect, which reduces friction around hole walls during drill-workpiece contact. Drilling at feed rates of f= 300 mm/min and spindle speeds of n= 6000 rpm gave similar results to those obtained under dry cutting, which could be due to the evaporation of lubricant before having sufficient time to lubricate the cutting tool and workpiece. Under the same feed rate but at higher spindle speeds of n= 9000 rpm, the application of MQL reduced the temperature by approximately 22 °C , and increased it by approximately 10 ∘C when drilling at feed rate of f= 600 mm/min which indicates that the combination of spindle speed and feed rate plays a significant role in developed temperature. Under spindle speeds of n= 6000 and 9000 rpm, increasing the feed rate tended to decrease the cutting temperature which indicates that MQL becomes more effective when the drilling time is reduced. This could be due to the small amounts of lubricant used in MQL which tend to evaporate before having enough time to lubricate the cutting tool-workpiece properly. Increasing the spindle speed increased the cutting temperatures which is due to increased rubbing between the cutting tool and the workpiece surface, while increasing the feed rate decreased the cutting temperatures which is due to reduced tool-workpiece contact time.

Previous studies indicated that MQL could reduce the maximum workpeice temperatures by 15 to 125 % compared to machining at room temperature for different types of metals such steel and magnesium alloys [230, 241, 294]. The significant temperature reduction was related to the cooling and improved chip breakability [384, 386]. The variation in MQL cooling efficiency in reducing machining temperatures could be due to the setup of process parameters such as the spindle speed, feed rate, cutting tool coating and geometry or the methods used for temperature measurement. Previous studies also reported that using MQL and cryogenic coolants can reduce the tool wear compared to dry machining, and that their effectiveness increases with the increase of the cutting speed [293, 297]. However their effectivness was also reported to vary depending on the properties of the machined material such as its abrasiveness and hardness [386].
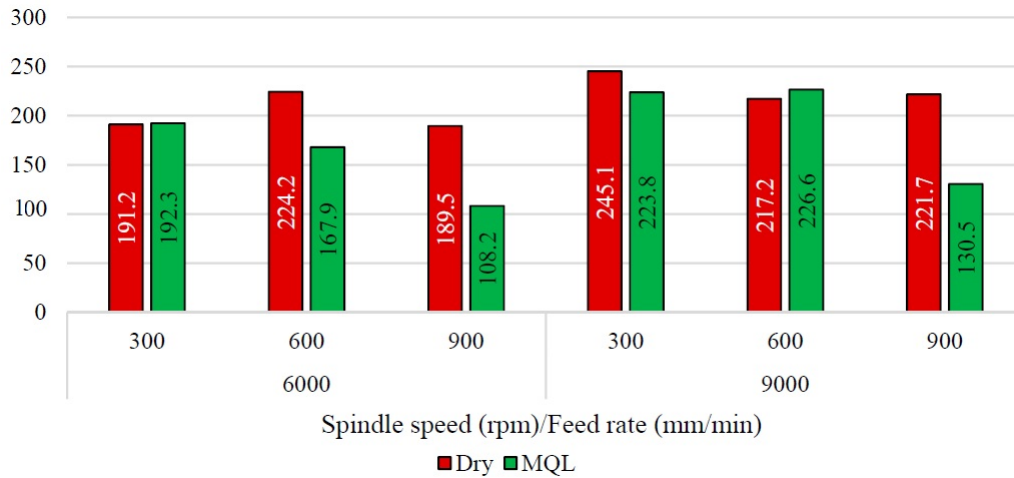
Figure 7.15: Comparison of the exit temperature of holes drilling under MQL and dry conditions

7.3   Concluding Remarks

As discussed in Chapter 2, the application of cryogenic and MQL coolants proved to be a powerful method for improving the surface integrity of the machined part and enhancing tool life when machining metals and composites. The majority of previous literature indicates that the cryogenic and MQL coolants were incorporated with hard to cut metals such as steel and titanium and to less extent on composites. The literature on machining fibre metal laminates using semi-dry cooling was mentioned briefly in milling operations. However, from the few reported studies on machining fibre metal laminates, none of them investigated the use of MQL and cryogenic cooling methods on machining fibre metal laminates in a systematic and complete study. This chapter aims to show the beneficial effects of using minimum quantity lubrication and cryogenic liquid nitrogen cooling in drilling GLARE fibre metal laminates in comparison with drilling GLARE at room temperature. This will help the manufacturing industry to adopt those environmentally friendly cooling technologies by providing an alternative to dry machining and the use of conventional cooling to use higher metal removal rate, equal or better-machined part quality and extended tool life. The following can be concluded from drilling GLARE 2B laminates at room temperature and using MQL and cryogenic liquid nitrogen coolants:

- The influence of spindle speed on cutting forces was more dominant than the feed rate for all GLARE grades and Al2024-T3 alloy. This was evident by the ANOVA analysis which showed that the spindle speed contribution on cutting forces was more than 50 %.

- The reduction in cutting forces with increasing spindle speed was due to faster material

removal rate (smaller chip thickness/load) while the increase of cutting forces with increasing feed rate was due to increased thickness of cut material per unit of time (chip thickness/load).

- The use of liquid nitrogen increased thrust force between 10-21 % and torque by 4-23 % compared to that obtained under dry and MQL conditions.

- A 17 % drop in torque was achieved when using MQL compared to dry conditions while there was a negligible increase in thrust force.

- The use of MQL and LN2 coolants improved surface roughness over dry conditions by up to 44 %, the performance of LN2 on surface roughness was better than MQL, especially when drilling at low feed rates and high spindle speeds. This could be attributed to the reduction of cutting temperature and increased the hardness of aluminium sheets which improves chip breakability.

- The average surface roughness under tested cutting parameters was between 1-3 μm and is minimal when using cryogenic liquid nitrogen followed by MQL and highest in dry tests under same cutting parameters.

- Compared to dry drilling conditions, using liquid nitrogen and MQL coolants showed the ability to reduce the exit burr formation in drilling GLARE by up to 47 % and 36.4 %, respectively.

- The effect of feed rate on height and thickness of the exit burr is significant regardless of coolant used.

- The entrance burr height was greater using coolants compared to dry conditions.

- MQL and dry conditions produced holes sizes near the nominal diameter of the drill at both locations.

- Hole circularity was reduced by more than 70 % using cryogenic liquid nitrogen compared to MQL and dry conditions.

- Powdery (dust) chips are formed from drilling glass fibre layers in GLARE laminates under all cutting conditions and cooling methods due to their low ductility and non-homogeneous properties

- Built up edge and adhesions on the cutting tools were found to be marginally lower when using MQL and cryogenic liquid nitrogen cooling compared to dry drilling. The adhesion of the work material to the tool was observed to be having the highest rate during dry drilling. The use of MQL and cryogenic coolants reduced aluminium adhesion and built-up edge formation on the cutting tools considerably.

- The stacking nature of GLARE laminates which puts each glass fibre layer between two aluminium sheets was thought to provide a form of backup support against delamination damage which significantly reduce peel-up and push-out delamination at hole entry and exit respectively.

- Fibre breakage, fibre pull-out edge and chipping (erosion) were the most dominant damage forms in glass fibre layers.

- The surface delamination factor in glass fibre layers was minimal. It did not exceed 2 % under all cutting conditions.

- The application of MQL could significantly reduce machining temperatures compared to dry cutting when drilling at spindle speeds of n= 6000 rpm and feed rates of f= 600 and 900 mm/min, and n = 9000 rpm and feed rates of f= 900 mm/min which indicates that MQL can be more effective at higher feed rates due to short drilling time period which prevents the evaporation of MQL coolant and provide sufficient lubrication at the tool-workpiece cutting zone.

- As a result, it could be concluded that cryogenic cooling and MQL are an effective method to dry drilling of GLARE fibre metal laminates. Application of liquid nitrogen cooling and MQL in the drilling of GLARE can provide environmentally friendly machining and improve the surface finish of machined part.

Chapter 8

CONCLUSIONS AND RECOMMENDATIONS FOR FUTURE WORK

8.1 Conclusions

The machining of fibre metal laminates was the main objective of this research. The fibre metal laminates considered were made of aluminium sheets and glass fibre layers bonded together using an adhesive epoxy which is commercially known as GLARE. Two grades of GLARE that have different fibre orientation were used in the study in addition to its metallic constituent the Al2024-T3 alloy. Among the several machining processes, drilling was selected for the current research study. The cutting tools used were coated carbide twist drills which were commercially feasible and satisfy the requirements of machining both aluminium and GLARE laminates. The drilling tests were carried out at room temperature and using minimum quantity lubrication and cryogenic liquid nitrogen cooling. The research investigated the influence of a wide range of cutting parameters (spindle speed and feed rate) on cutting forces, hole quality indices and damage around the hole caused by the machining process.

As discussed in Chapter 2, despite the reported literature and knowledge in machining of metals, composites and composite metal stacks, there has been a little work reported on the machinability of fibre metal laminates such as GLARE due to its limited applications in the aerospace sector. Only a limited number of researchers has reported experimental results on limited aspects of GLARE drilling indices. The previous work on drilling GLARE have been approached only by few researchers which looked into the results of machining quality and performance of thin GLARE laminates such as GLARE 3, 5 and 6. The literature review on the machining of fibre metal laminates indicates that a complete drilling machinability

evaluation for GLARE using DOE techniques has not yet been fully investigated. Moreover, the machinability of thick laminates have not been yet investigated since the thickness of GLARE samples tested in all previous studies were less than 2 mm. The current research aimed to fill the gap in machining GLARE by exploring the machinability of GLARE 2B fibre metal laminates using various thicknesses. Moreover, the drilling of GLARE 3 fibre metal laminates was also carried out to evaluate the effect of fibre orientation on hole quality and cutting forces in comparison with GLARE 2B of the same thickness. Apart from that, the quality of machined borehole surface in terms of surface roughness and drilling-induced damage in glass fibre layers and aluminium sheets were not disclosed in previous studies. This is due to complexity in inspecting those indices which require state of the art scanning techniques. Therefore, the primary objective of the current research was to determine the impact of machining parameters on the developed cutting forces and a number of hole quality parameters through the implementation of design of experiment methodologies. The employed design of experiment techniques were based on full factorial and response surface methodology designs which incorporates cutting parameters such as(spindle speed and feed rate) on many levels to cover a wide range of the cutting parameter values.

The literature review presented in chapter 2 also showed that previous work on machining metals and composites using different cooling strategies such as conventional flooding, minimum quantity lubrication, cryogenic machining and high-pressure cooling were mainly used with hard to cut metals such as titanium and steel, and to a less extent in the recent decade on composites. The literature review also showed that the limited research conducted on the machinability aspects of fibre metal laminates was directed to explore dry drilling and milling operations, with some reported literature on semi-dry milling. Semi-dry cooling strategies were encouraging in milling operations since they gave a better surface finish than dry machining at room temperature, especially when machining thick laminates. The literature also showed a research gap where there were no reported studies on the implementation of any kind of coolants including MQL and LN2 on drilling GLARE due to the small thickness of the laminates used in previous machining studies. Therefore in this thesis, a better understanding towards the feasibility of shifting from conventional dry machining to minimum quantity lubrication (MQL) and cryogenic liquid nitrogen cooling (LN2) was also established to highlight the benefits of such coolants. The machining performance of MQL and LN2 cooling strategies were encouraging to test with GLARE since in most previously reported studies gave a better hole quality than that from dry drilling. The current research aims to fill this gap by incorporating MQL and LN2 cooling methods in the drilling of GLARE fibre metal laminates as a potential environmentally friendly cooling strategies. The thesis also aims to demonstrate an in-depth comparison between those two cooling technologies and dry drilling of GLARE to facilitate the sustainable advantages and

disadvantages of machining using those coolants on cutting forces and hole surface finish. The scope of this thesis is limited to the experimental study of twist drilling operation which has been achieved through the implementation of design of experiment methodology using full and fractional factorial designs and response surface methodology. The experimental drilling tests were carefully designed trials of different experimental factors (spindle speed and feed rate) -in addition to (coolant flow rate and coolant air pressure for MQL trials)- and their levels have been considered by covering a wide range of cutting parameters similar to the previous chapters on dry drilling of Al2024-3, GLARE 2B and GLARE 3 laminates. The research on drilling of Al2024-T3 was mainly motivated by the major study in the current research on drilling GLARE fibre metal laminates. The aim is to draw some of the similarities and differences in their machinability since Al2024-T3 makes up the metallic part of the laminate. The study was also motivated by the fact that in most of the earlier scientific research, the cutting speeds used were below n= 5000 rpm and using fewer combinations of cutting parameters. Moreover, only a handful of studies used coated 6 mm drill diameter in their Al2024-T3 drilling experiments and none for GLARE. The following can be concluded:

- When Al2024-T3 is machined at low spindle speed and feed rate, the cutting forces and surface finish/damage are low. Increasing the spindle speed or the feed rate results in an increase in the cutting forces and surface roughness. Increasing the spindle speed increase the potential for a built-up edge on the cutting tool while increasing the feed rate increases the chance of internal surface damage. Under tested cutting parameters, the burr height and thickness were small and the holes do not require any additional deburring process. Moreover, it is most likely that the holes will be oversized and increase with depth. Under the tested cutting parameters. Under tested cutting parameters, the optimum spindle speed and feed rate which gives best hole quality parameters is when drilling at n = 3000 rpm and f = 300 mm/min. At those cutting parameters, the chip formed was small and broken and easy to evacuate. In addition, the internal hole surface quality inspection using SEM and 3D surface scanning showed the absence of damage and minimal feed marks on the borehole surface.

- On the basis of hole quality achieved in GLARE laminates, drilling at a spindle speed of 6000 rpm or less and feed rates of 300 mm/min and less, showed minimum hole damage, better surface finish and reduced burr formations. The application of MQL and cryogenic coolants improved the hole quality in terms of surface roughness, exit burr formations and built up the edge on cutting tool, but was found to increase thrust force and entry burr height. Drilling of GLARE laminates is more challenging that Al2024-T3 alloy due to the brittle nature of glass fibre layers and the difficulty in detecting drilling-induced damage such as delamination. Measurements of cutting forces

reveal that they can directly influence the hole quality. The lower are the cutting forces, the better is the hole quality. The investigation in this research indicated that hole quality improved in terms of reduced surface roughness, reduced exit burr formations and prevention of waste formation can be achieved by optimising the cutting parameters (spindle speed and feed rate) and the use of coolants.

- The evaluation of machined surface quality by roughness measurement was not previously investigated by the few reported studies on drilling GLARE. This is due to the small thickness of laminates, which made surface roughness difficult to measure. Moreover, the alternating metal composite structure of GLARE laminates makes it very difficult to evaluate the surface roughness of aluminium sheets and glass fibre layers individually using 2D mechanical surface profilometers. The presence of two distinguishable zones in GLARE laminates gives relatively very different values of surface roughness, one with high surface roughness from glass fibre layers and one with low surface roughness from aluminium sheets. Moreover, the fibre orientation plays a significant role in the local and overall surface roughness of the laminate. Therefore, a state of the art three-dimensional optical microscopy device was used to determine the surface roughness of individual layers in GLARE, and to depict the influence of fibre orientation on hole quality and surface finish which have not been reported in previous GLARE machining studies.

- From the analysis the surface roughness of Al2024-T3 alloy, it was found that machining at low spindle speed and feed rate gives lower/smaller surface finish/damage. Increasing the spindle speed or the feed rate results in an increase in the surface roughness while increasing the feed rate increased the chance of internal surface damage. The average surface roughness ranged from 1.1 to 3 µm(with the exception of holes drilled at n= 1000 rpm and f= 600 and 900 mm/min) which was similar to previously reported studies on machining Al2024-T3 alloy. For dry drilling of GLARE laminates, The average surface roughness ranged from 1 to 3 µm (with the exception of holes drilled at n= 1000 rpm and f= 600 and 900 mm/min). Increasing the spindle speed and the feed rate increased the surface roughness. GLARE grades with a cross-ply configuration such as GLARE 3 produced holes with relatively higher surface roughness compared to unidirectional ones such as GLARE 2B while the hole depth did not seem to have an impact on surface roughness. Machining GLARE using MQL and cryogenic coolants showed that the interaction of the feed rate and air pressure appeared to have a minimal influence on the surface roughness. The application of MQL and cryogenic coolants improved surface roughness of the machined hole. For example, in cryogenic machining, the average surface roughness increased with the feed rate and spindle speed increase but was reduced considerably compared to dry and MQL

conditions at spindle speeds of n= 9000 rpm. The overall average surface roughness in GLARE 2B and Al2024-T3 alloy were similar using same cutting parameters with slightly higher in GLARE 2B due to the presence of glass fibre layers.

- A design of experiment (DOE) methodology was employed throughout the experimental work to determine the effects of machining parameters (spindle speed and feed rate) on key machinability hole quality outputs to determine the suitable machining parameters. The DOE can be also used as an aid for future studies to avoid damage and to further optimise the process parameters. From these experiments, the empirical relationships between cutting parameters and hole quality outputs were analysed using linear and nonlinear models. Both cutting parameters were identified as the key parameters in influencing the hole quality outputs.

- In MQL, the coolant flow rate and air pressure had a very limited influence on cutting forces, while the coolant flow rate and air pressure had a minor effect on burr height. Using liquid nitrogen as a coolant increased the post machining hardness of the upper and lower aluminium sheets of the workpiece from 6.5-9.5 % and increased cutting forces considerably compared to dry and MQL. MQL and dry conditions produced holes sizes near the nominal diameter of the drill at both locations while hole circularity was reduced by more than 70 % using cryogenic liquid nitrogen compared to MQL and dry conditions.

- A limited number of tests were conducted for workpiece temperature measurement due to the limitation of time and resources. However, these tests give a good idea of the effect of cutting parameters, fibre orientation and MQL cooling on the generated cutting temperatures during the drilling of GLARE. The infrared thermos vision techniques used in the current study suggests the possibility of using those methods to measure the temperatures fields in the machining processes which can serve as a good foundation for future research work involving machining fibre metal laminates and as a tool for temperature monitoring. The emissivity of GLARE found in the current study can be used as an input for future studies which requires measuring the machining temperature of GLARE laminates using infrared techniques.

- The application of MQL could significantly reduce machining temperatures compared to dry when drilling at spindle speeds of n= 6000 rpm and feed rates of f= 600 and 900 mm/min, and n = 9000 rpm and feed rates of f= 900 mm/min which indicates that MQL can be more effective at higher feed rates due to short drilling time period which prevents the evaporation of MQL coolant and provide sufficient lubrication at the tool-workpiece cutting zone. As a result, it could be concluded that cryogenic cooling and MQL are an effective method to dry drilling of GLARE fibre metal laminates.

Application of liquid nitrogen cooling and MQL in the drilling of GLARE can provide environmentally friendly machining and improve the surface finish of machined part.

- The quantification of surface delamination was achieved by the utilisation of computational vision techniques, based on an existing image processing software. The computerised tomography scanning enabled viewing glass fibre layers in GLARE laminates in binary form. Another image processing software allowed the measurement of delamination factor by calculating the delaminated area around the hole. Based on the information collected on cutting force, hole quality parameters and analysis techniques from CT, SEM, 3D surface roughness and optical scans, an optimum range of parameters was determined, based on previously reported tolerances of machining metals, composites and composite metal stack for aerospace applications.

- Computerised tomography CT scan of drilled holes in GLARE laminates is a good technique for delamination detection. The structured nature of GLARE laminates makes it difficult to inspect glass fibre layers directly as they are surrounded by aluminium sheets from both sides. The utilisation of CT scan allows the visualisation of glass fibre layers to observe the size and depth of the damage which occur under different GLARE grades, cutting parameters, thicknesses and cooling conditions. Despite that the delamination factor in glass fibre layers in GLARE was found to be negligible, the criteria itself is useful as it can be applied to images of the drilled hole obtained by CT scanning technique. The criteria can give useful information on the damage level around the hole and can be used as a powerful tool to relate the severity of damage to cutting parameters, fibre orientation or workpiece thickness.

- The damage in borehole surface is related to the workpiece thickness and fibre orientation. Interlaminar failure during drilling is more likely to occur in GLARE 3 than in GLARE 2B because laminates with cross-ply configuration are mechanically weaker than unidirectional ones which mean that the influence of the feed rate is greater in GLARE 3 than on GLARE 2B. Analysis of borehole surface shows signs of fibre pulls out, shearing of the fibre-epoxy matrix and interlayer burr formation in limited regions at $\pm$ 45° with respect to the 0° fibre orientation.

- The limited cutting data reported by previous studies on drilling GLARE made the establishment of a starting point to the development of cutting parameter analysis and optimisation more difficult. The range of tested cutting parameters was based on previous studies on drilling GLARE, composite metals stacks and aluminium alloys.

8.2   Recommendations for Future Work

The comprehensive investigations and findings on the twist drilling of GLARE fibre metal laminates and Al2024-T3 alloy have been demonstrated in this thesis. Based on this research, potential areas of future work are given below for improving their machinability are outlined as follows:

- This research focused on the application of drilling GLARE fibre metal laminates using 6 mm TiAlN coated carbide drills. Although using this cutting tool showed good hole quality results in terms of surface roughness, burr formation, hole size and minimal delamination. A comparison against other cutting tool coatings, types and geometries would be significant to determine the best cutting tool which gives an overall optimum hole quality. Suggested areas of research include studying the effect of point angle and coating type of the cutting tool.

- Airbus is interested into finding the optimum cutting parameters for drilling holes in GLARE wing structures using 4.8 mm cutting tools.

- Airbus is interested in finding the optimum cutting parameters for drilling very thick GLARE laminates.

- In this research, only two grades of GLARE were investigated. Further research is recommended to inspect the machinability of the remaining grades to obtain a broader knowledge and comparison among all GLARE grades for optimum machining parameters.

- A very interesting area of research is to investigate the impact of applying minimum quantity lubrication and cryogenic cooling using liquid nitrogen and carbon dioxide internally through the cutting tools and compare its effectiveness with the current external cooling methods applied in this research. âĂć

- The current work on temperature measurements in drilling GLARE was carried out under dry and MQL conditions, the measurement of induced cutting temperature when using cryogenic liquid nitrogen is recommended to evaluate the performance of those coolants with dry drilling.

- Although not discussed in the current thesis, a decent amount of research was carried out by using finite element modelling (FEM) to simulate the drilling process of Al2024-T3 alloy and GLARE fibre metal laminates and reasonable prediction of cutting forces was achieved. This area has not been investigated previously and it is highly recommended to perform a complete research on finite element modelling of the machining

process of fibre metal laminates to help understand the cutting mechanisms involved and to accurately predict cutting forces, delamination and developed temperatures.

Bibliography

[1] A Vlot and J W Gunnink. *Fibre metal laminates: an introduction.* Springer, 2001.

[2] A Vlot, L B Vogelesang, and T J De Vries. Towards application of fibre metal laminates in large aircraft. *Aircraft Engineering and Aerospace Technology*, 71(6):558–570, 1999.

[3] Ian Thirsk. *De Havilland Mosquito: an illustrated history*, volume 2. MBI Publishing Company, 2006.

[4] T Sinmazçelik, E Avcu, M Ö Bora, and O Çoban. A review: Fibre metal laminates, background, bonding types and applied test methods. *Materials & design*, 32(7):3671–3685, 2011.

[5] J W Gunnink, A Vlot, R C Alderliesten, W van der Hoeven, A de Boer, J Sinke, M S Ypma, T J de Vries, and T Wittenberg. Towards technology readiness of fibre metal laminates. In *International Congress of Aeronautical Sciences, 22 nd, Harrogate, United Kingdom*, 2000.

[6] Hyoungseock Seo. *Damage Tolerance and Durability of GLARE Laminates.* ProQuest, 2008.

[7] M Sadighi, T Pärnänen, R C Alderliesten, M Sayeaftabi, and R Benedictus. Experimental and numerical investigation of metal type and thickness effects on the impact resistance of fiber metal laminates. *Applied composite materials*, 19(3-4):545–559, 2012.

[8] J Pora. Composite materials in the airbus A380âĂŞfrom history to future. *Proceedings of ICCM13, Plenary lecture, CD-ROM*, 2001.

[9] T C Wittenberg, T J van Baten, and A de Boer. Design of fiber metal laminate shear panels for ultra-high capacity aircraft. *Aircraft Design*, 4(2âĂŞ3):99–113, 2001.

[10] Yongxiang Hu, Xingwei Zheng, Dongyu Wang, Zhengyu Zhang, Yufei Xie, and Zhenqiang Yao. Application of laser peen forming to bend fibre metal laminates by high dynamic loading. *Journal of Materials Processing Technology*, 226:32–39, 2015.

[11] Tjerk Johan De Vries. *Blunt and sharp notch behaviour of Glare laminates.* TU Delft, Delft University of Technology.

[12] Mohit Garg, Michael Falugi, Frank Abdi, and Galib Abumeri. Predicting bearing strength of fiber metal laminates via progressive failure analysis. In *52nd AIAA/ASME/ASCE/AHS/ASC Structures, Structural Dynamics and Materials Conference 19th AIAA/ASME/AHS Adaptive Structures Conference 13t*, page 2055.

[13] A Seyed Yaghoubi and B Liaw. Damage Assessments of Ballistic Impact Behaviors of GLARE 5 (3/2) Beams with Various Stacking Sequences. In *Dynamic Behavior of Materials, Volume 1*, pages 503–512. Springer, 2013.

[14] Michiel Hagenbeek. *Characterisation of fibre metal laminates under thermomechanical loadings.* TU Delft, Delft University of Technology, 2005.

[15] Thomas Beumler. *Flying Glare.* TU Delft, Delft University of Technology, 2004.

[16] John Graham-Cumming. *The Geek Atlas: 128 places where science and technology come alive.* ” O’Reilly Media, Inc.”, 2009.

[17] FAA Federal Aviation Adminstration. Airbus a380 composite profile.

[18] Reyndert Christiaan Alderliesten. *Fatigue crack propagation and delamination growth in Glare.* DUP Science, 2005.

[19] Edson Cocchieri Botelho, Rogério Almeida Silva, Luiz Cláudio Pardini, and Mirabel Cerqueira Rezende. A review on the development and properties of continuous fiber/epoxy/aluminum hybrid composites for aircraft structures. *Materials Research*, 9(3):247–256, 2006.

[20] S U Khan, R C Alderliesten, and R Benedictus. Crack Growth in Fibre Metal Laminates Under Variable Amplitude Loading. In M J Bos, editor, *ICAF 2009, Bridging the Gap between Theory and Operational Practice*, chapter 45, pages 839–858. Springer Netherlands, 2009.

[21] Aluminum Association. International alloy designations and chemical composition limits for wrought aluminum and wrought aluminum alloys. *The Aluminum Association, Arlington, Virginia*, 2006.

[22] Robert John Hussey and Josephine Wilson. *Light Alloys: Directory and Databook.* Springer Science & Business Media, 2013.

[23] Philip A Schweitzer. *Metallic materials: physical, mechanical, and corrosion properties*, volume 19. CRC Press, 2003.

[24] D R Hartman, Mark E Greenwood, and David M Miller. High strength glass fibers. *Moving Forward With 50 Years of Leadership in Advanced Materials.*, 39:521–533, 1994.

[25] Sanjay Mazumdar. *Composites manufacturing: materials, product, and process engineering.* CrC press, 2001.

[26] J A Sanchez, I Pombo, R Alberdi, B Izquierdo, N Ortega, S Plaza, and J Martinez-Toledano. Machining evaluation of a hybrid MQL-CO 2 grinding technology. *Journal of Cleaner Production*, 18(18):1840–1849, 2010.

[27] A Asundi and A Y N Choi. Fiber metal laminates: an advanced material for future aircraft. *Journal of Materials Processing Technology*, 63(1):384–394, 1997.

[28] Riccardo RODI and R Benedictus. *The Residual Strength Failure Sequence in Fibre Metal Laminates.* PhD thesis, 2012.

[29] Jamal Y Sheikh-Ahmad. *Machining of polymer composites.* Springer, 2009.

[30] David A Stephenson and John S Agapiou. *Metal cutting theory and practice*, volume 68. CRC press, 2005.

[31] H Hocheng, H Y Puw, and Y Huang. Preliminary study on milling of unidirectional carbon fibre-reinforced plastics. *Composites Manufacturing*, 4(2):103–108, 1993.

[32] Mikell P Groover. *Fundamentals of modern manufacturing: materials processes, and systems.* Wiley. com, 2007.

[33] Thomas Childs. *Metal machining: theory and applications.* Butterworth-Heinemann, 2000.

[34] Milton Clayton Shaw. *Metal cutting principles*, volume 2. Oxford university press New York, 2005.

[35] J Paulo Davim. *Modern mechanical engineering.* Springer, 2014.

[36] Fritz Klocke. Manufacturing Processes, 1, 1, 2011.

[37] Hans Kurt Toenshoff and Berend Denkena. *Basics of cutting and abrasive processes.* Springer, 2013.

[38] Winston A Knight and Geoffrey Boothroyd. *Fundamentals of metal machining and machine tools*, volume 69. CRC Press, 2005.

[39] G Venu Gopala Rao, Puneet Mahajan, and Naresh Bhatnagar. Machining of UD-GFRP composites chip formation mechanism. *Composites Science and Technology*, 67(11):2271–2281, 2007.

[40] Azwan Iskandar. Chip formation studies in machining fibre reinforced polymer composites. 2013.

[41] A Koplev, Aa Lystrup, and T Vorm. The cutting process, chips, and cutting forces in machining CFRP. *Composites*, 14(4):371–376, 1983.

[42] D H Wang, M Ramulu, and D Arola. Orthogonal cutting mechanisms of graphite/epoxy composite. Part I: unidirectional laminate. *International Journal of Machine Tools and Manufacture*, 35(12):1623–1638, 1995.

[43] D Arola, M Ramulu, and D H Wang. Chip formation in orthogonal trimming of graphite/epoxy composite. *Composites Part A: Applied Science and Manufacturing*, 27(2):121–133, 1996.

[44] Kevin A Calzada, Shiv G Kapoor, Richard E DeVor, Johnson Samuel, and Anil K Srivastava. Modeling and interpretation of fiber orientation-based failure mechanisms in machining of carbon fiber-reinforced polymer composites. *Journal of Manufacturing Processes*, 14(2):141–149, 2012.

[45] Gurusiddeshwar Gudimani. *Oblique machining of uni directional carbon fiber reinforced polymer composites.* PhD thesis, 2011.

[46] Pipat Bhudwannachai. *Performance evaluation and analysis of the use of CO2 cooling for conventional drilling of carbon fibre reinforced plastics.* PhD thesis, 2014.

[47] K Kerrigan. *Characterisation of an Integrated Telemetric Temperature Sensor for CFRP Milling Applications.* 2013.

[48] Vijayan Krishnaraj, Redouane Zitoune, and J Paulo Davim. *Drilling of polymer-matrix composites.* Springer, 2013.

[49] Erik Oberg. *Machinery's Handbook 29th Edition-Full Book.* Industrial Press, 2012.

[50] Yusuf Altintas. *Manufacturing automation: metal cutting mechanics, machine tool vibrations, and CNC design.* Cambridge university press, 2012.

[51] Hans Vandervelde. Drilling processes. *BOARD AUTHORITY*, 3(2):38–44, 2001.

[52] SANDVIK Coromant. Machining carbon fibre materials, 2010.

[53] P J Blau, R L Martin, and LAURA Riester. A comparison of several surface finish measurement methods as applied to ground ceramic and metal surfaces. Technical report, 1996.

[54] Palanisamy Shanmughasundaram and Ramanathan Subramanian. Study of parametric optimization of burr formation in step drilling of eutectic AlâĂŞSi alloyâĂŞGr composites. *Journal of Materials Research and Technology*, 3(2):150–157, 2014.

[55] P Stringer, G Byrne, and E Ahearne. Tool design for burr removal in drilling operations.

[56] J Y Mann and I S Milligan. *Aircraft Fatigue: Design, Operational and Economic Aspects.* Elsevier Science, 2013.

[57] D Dornfeld. Strategies for preventing and minimizing burr formation. 2004.

[58] L K Gillespie. Deburring precision miniature parts. *Precision Engineering*, 1(4):189–198, 1979.

[59] I H Choi and J D Kim. Electrochemical deburring system using electroplated CBN wheels. *International Journal of Machine Tools and Manufacture*, 38(1):29–40, 1998.

[60] Liang Jie. The formation and effect of interlayer gap in dry drilling of stacked metal materials. *The International Journal of Advanced Manufacturing Technology*, 69(5-8):1263–1272, 2013.

[61] Ozden Isbilir and Elaheh Ghassemieh. Finite element analysis of drilling of titanium alloy. *Procedia Engineering*, 10:1877–1882, 2011.

[62] Bc. LUKÁŠ PILNÝ and CSc prof. Ing. MIROSLAV PÍŠKA. *High speed drilling of aluminium plates.* PhD thesis, 2011.

[63] A M Abdelhafeez, S L Soo, D K Aspinwall, A Dowson, and D Arnold. Burr Formation and Hole Quality when Drilling Titanium and Aluminium Alloys. *Procedia CIRP*, 37:230–235, 2015.

[64] Omanath A Pawar, Yogesh S Gaikhe, Asim Tewari, Ramesh Sundaram, and Suhas S Joshi. Analysis of hole quality in drilling GLARE fiber metal laminates. *Composite Structures*, 123:350–365, 2015.

[65] I S Shyha, S L Soo, D K Aspinwall, S Bradley, R Perry, P Harden, and S Dawson. Hole quality assessment following drilling of metallic-composite stacks. *International Journal of Machine Tools and Manufacture*, 51(7):569–578, 2011.

[66] Laroux Gillespie. *Countersinking handbook.* Industrial Press Inc., 2008.

[67] E Brinksmeier and R Janssen. Drilling of Multi-Layer Composite Materials consisting of Carbon Fiber Reinforced Plastics (CFRP), Titanium and Aluminum Alloys. *CIRP Annals - Manufacturing Technology*, 51(1):87–90, 2002.

[68] R Zitoune, V Krishnaraj, and F Collombet. Study of drilling of composite material and aluminium stack. *Composite Structures*, 92(5):1246–1255, 2010.

[69] J Paolo Davim. *Machining composites materials.* John Wiley & Sons, 2013.

[70] Abhijeet Amritkar, Chandra Prakash, and Atul P Kulkarni. Development of temperature measurement setup for machining. *World Journal of Science and Technology*, 2(4):15–19, 2012.

[71] EngineersEdge. Machinist Drilling Mechanical Tolerance Capabilities Chart-ANSI size Drills, ISO Metric Drill Sizes.

[72] ASME Standard. Dimensioning and tolerancing. *ASME Y14. 5M-1994, American Society of Mechanical Engineers, New York*, 1994.

[73] Nick Van Gestel. Determining Measurement Uncertainties of Feature Measurements on CMMs (Bepalen van meetonzekerheden bij het meten van vormelementen met CMMs). *status: published*, 2011.

[74] Peter Hoffman, Eric Hopewell, Brian Janes, and Kent Sharp Jr. *Precision machining technology.* Cengage Learning, 2011.

[75] M Nouari, G List, F Girot, and D Coupard. Experimental analysis and optimisation of tool wear in dry machining of aluminium alloys. *Wear*, 255(7):1359–1368, 2003.

[76] M Kurt, Y Kaynak, and E Bagci. Evaluation of drilled hole quality in Al 2024 alloy. *The International Journal of Advanced Manufacturing Technology*, 37(11):1051–1060, 2008.

[77] Mustafa Kurt, Eyup Bagci, and Yusuf Kaynak. Application of Taguchi methods in the optimization of cutting parameters for surface finish and hole diameter accuracy in dry drilling processes. *The International Journal of Advanced Manufacturing Technology*, 40(5-6):458–469, 2009.

[78] M S Sureshkumar, D Lakshmanan, and A Murugarajan. Experimental investigation and mathematical modelling of drilling on GFRP composites. *Materials Research Innovations*, 18(S1):S1–94–S1–97, 2014.

[79] Vinod Kumar Vankanti and Venkateswarlu Ganta. Optimization of process parameters in drilling of GFRP composite using Taguchi method. *Journal of Materials Research and Technology*, 3(1):35–41, 2014.

[80] V Krishnaraj, A Prabukarthi, A Ramanathan, N Elanghovan, M Senthil Kumar, R Zitoune, and J P Davim. Optimization of machining parameters at high speed drilling of carbon fiber reinforced plastic (CFRP) laminates. *Composites Part B: Engineering*, 2012.

[81] B M Umesh Gowda, H V Ravindra, H R Gurupavan, G Ugrasen, and G V Naveen Prakash. Optimization of Process Parameters in Drilling Al-Si3N4 Metal Matrix Composites Material Using Taguchi Technique. *Procedia Materials Science*, 5:2207–2214, 2014.

[82] Reddy Sreenivasulu. Optimization of Burr size, Surface Roughness and Circularity Deviation during Drilling of Al 6061 using Taguchi Design Method and Artificial Neural Network. *Independent Journal of Management & Production*, 6(1):93–108, 2015.

[83] Materials European Conference on Composite, M G Bader, Materials Institute of, Division Composites, and Materials European Association for Composite. ECCM-7 Seventh European Conference on Composite Materials : realising their commercial potential. Woodhead.

[84] A Mouritz. *Introduction to aerospace materials*. Elsevier, 2012.

[85] J Y Mann, A S Machin, W F Lupson, and R A Pell. The use of interference-fit bolts or bushes and hole cold expansion for increasing the fatigue life of thick-section aluminium alloy bolted joints. Technical report, 1983.

[86] Flake C Campbell Jr. *Manufacturing technology for aerospace structural materials*. Elsevier, 2011.

[87] W König and P Grass. Quality definition and assessment in drilling of fibre reinforced thermosets. *CIRP Annals-Manufacturing Technology*, 38(1):119–124, 1989.

[88] Frédéric Lachaud, Robert Piquet, Francis Collombet, and Laurent Surcin. Drilling of composite structures. *Composite Structures*, 52(3âĂŞ4):511–516, 2001.

[89] U.D.O. Defense. *Composite Materials Handbook-MIL 17, Volume 2: Polymer Matrix Composites: Materials Properties*. CRC Press, 2000.

[90] M Fernandes and C Cook. Drilling of carbon composites using a one shot drill bit. Part I: Five stage representation of drilling and factors affecting maximum force and torque. *International Journal of Machine Tools and Manufacture*, 46(1):70–75, 2006.

[91] Kimberley Dransfield, Caroline Baillie, and Yiu-Wing Mai. Improving the delamination resistance of CFRP by stitchingâĂŤa review. *Composites Science and Technology*, 50(3):305–317, 1994.

[92] Izhak Sheinman and George A Kardomateas. Energy release rate and stress intensity factors for delaminated composite laminates. *International Journal of solids and structures*, 34(4):451–459, 1997.

[93] H Ho-Cheng and C K H Dharan. Delamination during drilling in composite laminates. *Journal of Engineering for Industry(Transactions of the ASME)*, 112(3):236–239, 1990.

[94] A M Abrao, P E Faria, J C Campos Rubio, P Reis, and J Paulo Davim. Drilling of fiber reinforced plastics: A review. *Journal of Materials Processing Technology*, 186(1):1–7, 2007.

[95] S M Wu T. L. Wong and G M Croy. An analysis of delamination in drilling composite materials, 1982.

[96] Erol Kilickap. Analysis and modelling of delamination factor in drilling glass fiber reinforced plastic using response surface methodology. *Journal of composite materials*, 2010.

[97] U A Khashaba, M A Seif, and M A Elhamid. Drilling analysis of chopped composites. *Composites Part A: Applied Science and Manufacturing*, 38(1):61–70, 2007.

[98] R Stone and K Krishnamurthy. A neural network thrust force controller to minimize delamination during drilling of graphite-epoxy laminates. *International Journal of Machine Tools and Manufacture*, 36(9):985–1003, 1996.

[99] Zhang Linbo, Wang Lijiang, and Wang Xin. Study on vibration drilling of fiber reinforced plastics with hybrid variation parameters method. *Composites Part A: Applied Science and Manufacturing*, 34(3):237–244, 2003.

[100] Laurence Frost Tim Hepher. Airbus A380 wing checks extended to entire fleet, 2012.

[101] Viktor P Astakhov. *Drills: science and technology of advanced operations*. CRC Press, 2014.

[102] A T Marques, L M Durão, A G Magalhães, J F Silva, and J.M.R.S. Tavares. Delamination analysis of carbon fibre reinforced laminates: evaluation of a special step drill. *Composites Science and Technology*, 69(14):2376–2382, 2009.

[103] Tin-Lup Wong. *An analysis of delamination in drilling composite materials*. University of Wisconsin–Madison, 1981.

[104] E Capello. Workpiece damping and its effect on delamination damage in drilling thin composite laminates. *Journal of Materials Processing Technology*, 148(2):186–195, 2004.

[105] O Isbilir and E Ghassemieh. Delamination and wear in drilling of carbon-fiber reinforced plastic composites using multilayer TiAlN/TiN PVD-coated tungsten carbide tools. *Journal of Reinforced Plastics and Composites*, 31(10):717–727, 2012.

[106] G Dini. OnâĂŘLine Prediction of Delamination in Drilling of GFRP by Using a Neural Network Approach. 2003.

[107] J P Davim, J C Rubio, and A M Abrao. A novel approach based on digital image analysis to evaluate the delamination factor after drilling composite laminates. *Composites Science and Technology*, 67(9):1939–1945, 2007.

[108] P K Mallick. *Composites engineering handbook*, volume 11. CRC, 1997.

[109] Mohd Sapuan Salit, Mohammad Jawaid, Nukman Bin Yusoff, and Muhammad Enamul Hoque. Manufacturing of Natural Fibre Reinforced Polymer Composites. *Springer. DOI*, 10:973–978, 2015.

[110] A Brent Strong. *Fundamentals of composites manufacturing: materials, methods and applications*. Society of Manufacturing Engineers, 2008.

[111] D D L Chung. *Composite Materials: Science and Applications*. Springer London, 2010.

[112] Stuart S J Moy. *FRP composites: life extension and strengthening of metallic structures*, volume 2. Thomas Telford, 2001.

[113] T V Rajamurugan, K Shanmugam, and K Palanikumar. Mathematical Model for Predicting

Thrust Force in Drilling of GFRP Composites by Multifaceted Drill. *Indian Journal of Science and Technology*, 6(10):5316–5324, 2013.

[114] Eshetu D Eneyew and Mamidala Ramulu. Experimental study of surface quality and damage when drilling unidirectional CFRP composites. *Journal of Materials Research and Technology*, 3(4):354–362, 2014.

[115] Chongyang Gao, Jianzhang Xiao, Jiuhua Xu, and Yinglin Ke. Factor analysis of machining parameters of fiber-reinforced polymer composites based on finite element simulation with experimental investigation. *The International Journal of Advanced Manufacturing Technology*, pages 1–13, 2015.

[116] Seyedbehzad Ghafarizadeh, Gilbert Lebrun, and Jean-François Chatelain. Experimental investigation of the cutting temperature and surface quality during milling of unidirectional carbon fiber reinforced plastic. *Journal of composite materials*, page 0021998315587131, 2015.

[117] X M Wang and L C Zhang. An experimental investigation into the orthogonal cutting of unidirectional fibre reinforced plastics. *International Journal of Machine Tools and Manufacture*, 43(10):1015–1022, 2003.

[118] S.Balasivanandha Prabu S.Madhavan. An Experimental Study of Influence of Drill Geometry on Drilling of Carbon Fibre Reinforced Plastic Composites. *International Journal of Engineering Research and Development*, 3(1):36–44.

[119] Luís Miguel Pereira Durão. *Machining of hybrid composites*. PhD thesis, 2005.

[120] K Palanikumar. Modeling and analysis for surface roughness in machining glass fibre reinforced plastics using response surface methodology. *Materials & design*, 28(10):2611–2618, 2007.

[121] H Gao, Y J Bao, and Z M Feng. A study of drilling uni-directional carbon/epoxy composites. *International Journal of Abrasive Technology*, 4(1):1–13, 2011.

[122] D Abdul Budan, S Basavarajappa, M Prasanna Kumar, and Ajith G Joshi. Influence of fibre volume reinforcement in drilling GFRP laminates. *Journal of Engineering Science and Technology*, 6(6):733–744, 2011.

[123] R Zitoune, F Collombet, F Lachaud, R Piquet, and P Pasquet. ExperimentâĂŞcalculation comparison of the cutting conditions representative of the long fiber composite drilling phase. *Composites Science and Technology*, 65(3):455–466, 2005.

[124] J L Merino-Pérez, R Royer, S Ayvar-Soberanis, E Merson, and A Hodzic. On the temperatures developed in CFRP drilling using uncoated WC-Co tools Part I: Workpiece constituents, cutting speed and heat dissipation. *Composite Structures*, 123:161–168, 2015.

[125] J Paulo Davim. *Machining: fundamentals and recent advances*. Springer Science & Business Media, 2008.

[126] ZAPFAR M KHAN and B Mills. *A study of the drilling of advanced carbon fibre composites*. PhD thesis, University of Salford, 1991.

[127] Srichand Hinduja and Lin Li. *Proceedings of the 36th International MATADOR Conference*. Springer Science & Business Media, 2010.

[128] J Paulo Davim. *Modern machining technology: A practical guide*. Elsevier, 2011.

[129] Helmi A Youssef and Hassan El-Hofy. *Machining technology: machine tools and operations*. CRC Press, 2008.

[130] Hassan Abdel-Gawad El-Hofy. *Fundamentals of machining processes: conventional and non-conventional processes*. CRC press, 2013.

[131] E P DeGarmo, J T Black, and R A Kohser. *Materials and Processes in Manufacturing*. Wiley, 2003.

[132] Norberto Feito, José Díaz-Álvarez, Antonio Díaz-Álvarez, José Luis Cantero, and María Henar Miguélez. Experimental Analysis of the Influence of Drill Point Angle and Wear on the Drilling of Woven CFRPs. *Materials*, 7(6):4258–4271, 2014.

[133] Uwe Heisel and Tobias Pfeifroth. Influence of point angle on drill hole quality and machining forces when drilling CFRP. *Procedia CIRP*, 1:471–476, 2012.

[134] Alper Uysal. Investigation of the effects of cutting parameters on surface roughness in drilling of polymer composite materials. *Int. J. Arts Sci*, 3:27–32, 2009.

[135] E Kilickap. Optimization of cutting parameters on delamination based on Taguchi method during drilling of GFRP composite. *Expert Systems with Applications*, 37(8):6116–6122, 2010.

[136] A Ramanjaneya Reddy, K Siva Bhushan Reddy, P Hussain, B Sidda Reddy, and S Sudhakar Babu. An experimental study using design of experiment method to compare the performance of solid carbide and HSSs drills in drilling of GFRP composite material. *Int. J. Mech. Eng. & Rob. Res*, 2(4), 2013.

[137] I El-Sonbaty, U A Khashaba, and T Machaly. Factors affecting the machinability of GFR/epoxy composites. *Composite Structures*, 63(3âĂŞ4):329–338, 2004.

[138] S Panneer Selvan, M Balamurugan, and B E Balamurugan. Study on Drilling Delamination in Glass Fiber Reinforced Plastic Composites. 2015.

[139] Eda Okutan, Sedat Karabay, Tamer SÄśnmazçelik, and Egemen Avcu. A Study on Derivation of Parametric Cutting Force Equations In Drilling of GFRP Composites. *Strojniški vestnik-*

Journal of Mechanical Engineering, 59(2):97–105, 2013.

[140] N S Mohan, Manjunath Shettar, and Pavan Hiremath. Influence of Drilling Conditions of Glass Fiber-Reinforced Plastic [GFRP] Composite Materials. 2015.

[141] R Joseph and J R Davis. Aluminium and Aluminium Alloys. *ASM International, Materials Park, OH*, 1993.

[142] D M Haan, S A Batzer, W W Olson, and J W Sutherland. An experimental study of cutting fluid effects in drilling. *Journal of Materials Processing Technology*, 71(2):305–313, 1997.

[143] Durval U Braga, Anselmo E Diniz, Gilberto W A Miranda, and Nivaldo L Coppini. Using a minimum quantity of lubricant (MQL) and a diamond coated tool in the drilling of aluminumâĂŞsilicon alloys. *Journal of Materials Processing Technology*, 122(1):127–138, 2002.

[144] M Nouari, G List, F Girot, and D Géhin. Effect of machining parameters and coating on wear mechanisms in dry drilling of aluminium alloys. *International Journal of Machine Tools and Manufacture*, 45(12âĂŞ13):1436–1442, 2005.

[145] S Alizadeh Ashrafi, S Sharif, A Akhavan Farid, and M Y Yahya. Performance evaluation of carbide tools in drilling CFRP-Al stacks. *Journal of composite materials*, 48(17):2071–2084, 2014.

[146] Vijayan Krishnaraj, Redouane Zitoune, and Francis Collombet. Comprehensive review on drilling of multi material stacks. *Journal of Machining and Forming Technologies*, 2(3-4):1–32, 2010.

[147] Ranga Komanduri, Bi Zhang, and Chandra M Vissa. Machining of fiber reinforced composites. In *Processing and Manufacturing of Composite Materials*, volume 1, pages 1–36, 1991.

[148] S Gordon and M T Hillery. A review of the cutting of composite materials. *Proceedings of the Institution of Mechanical Engineers, Part L: Journal of Materials Design and Applications*, 217(1):35–45, 2003.

[149] VINOD KUMAR SAINI, Zahid A Khan, and Arshad Noor Siddiquee. Developments in Conventional Machining of Aluminum Matrix Composite Material: A Review. *International Journal of Advanced Design and Manufacturing Technology*, 7(3):73–81, 2014.

[150] Demeng Che, Ishan Saxena, Peidong Han, Ping Guo, and Kornel F Ehmann. Machining of carbon fiber reinforced plastics/polymers: A literature review. *Journal of manufacturing science and engineering*, 136(3):34001, 2014.

[151] Subodh Das and Weimin Yin. Trends in the global aluminum fabrication industry. *JOM*, 59(2):83–87, 2007.

[152] Ali Akhavan Farid, Safian Sharif, and Mohd Hasbullah Idris. Chip morphology study in high speed drilling of AlâĂŞSi alloy. *The International Journal of Advanced Manufacturing Technology*, 57(5-8):555–564, 2011.

[153] Subodh K Das and Weimin Yin. The worldwide aluminum economy: The current state of the industry. *Jom*, 59(11):57–63, 2007.

[154] Aluminium.matter.org.uk. aluMATTER — Aluminium — Cutting — Machinability: Summary of the Advantages of Aluminium, 2015.

[155] P S Sreejith and B K A Ngoi. Dry machining: Machining of the future. *Journal of Materials Processing Technology*, 101(1âĂŞ3):287–291, 2000.

[156] W Carter Ralph, W Steven Johnson, Paul Toivonen, Andrew Makeev, and J C Newman Jr. Effect of various aircraft production drilling procedures on hole quality. *International Journal of Fatigue*, 28(8):943–950, 2006.

[157] Ron Cobden and Banbury Alcan. TALAT Lecture 1501: Properties, Characteristics and Alloys of Aluminium. 2010.

[158] Ugur Köklü. Influence of the process parameters and the mechanical properties of aluminum alloys on the burr height and the surface roughness in dry drilling. *Materiali in tehnologije*, 46(2):103–108, 2012.

[159] Houcine Milouki Mohamed Elajrami and Farouk. B Boukhoulda. Effect of Drilling Parameters on Hole Quality. *International Journal of Mining, Metallurgy & Mechanical Engineering*, 1(4):254–257, 2013.

[160] Ali Davoudinejad, Sina Alizadeh Ashrafi, Raja Ishak Raja Hamzah, and Abdolkarim Niazi. Experimental Analysis of Wear Mechanism and Tool Life in Dry Drilling of Al2024. In *Advanced Materials Research*, volume 566, pages 217–221. Trans Tech Publ, 2012.

[161] S Amini, H Paktinat, A Barani, and A Fadaei Tehran. Vibration drilling of Al2024-T6. *Materials and Manufacturing Processes*, 28(4):476–480, 2013.

[162] A Barani, S Amini, H Paktinat, and A Fadaei Tehrani. Built-up edge investigation in vibration drilling of Al2024-T6. *Ultrasonics*, 54(5):1300–1310, 2014.

[163] Sung-Lim Ko and Jing-Koo Lee. Analysis of burr formation in drilling with a new-concept drill. *Journal of Materials Processing Technology*, 113(1âĂŞ3):392–398, 2001.

[164] C Dandekar, E Orady, and P K Mallick. Drilling characteristics of an e-glass fabric-reinforced polypropylene composite and an aluminum alloy: a comparative study. *Journal of manufac-*

turing science and engineering, 129(6):1080–1087, 2007.

[165] S A Batzer, D M Haan, P D Rao, W W Olson, and J W Sutherland. Chip morphology and hole surface texture in the drilling of cast aluminum alloys. *Journal of Materials Processing Technology*, 79(1):72–78, 1998.

[166] Chuck Kazmierski. Growth Opportunities in Global Composites Industry, 2012âĂŞ2017. *Composites*, 2012.

[167] Boeing Commercial Airplanes. Current Market Outlook: 2015-2034. *Seattle, USA*, 2015.

[168] Krishan K Chawla. *Composite materials: science and engineering*. Springer Science & Business Media, 2012.

[169] Justin Hale. Boeing 787 from the ground up. *Aero*, 4:17–24, 2006.

[170] Brian Smith. The Boeing 777. *Advanced Materials and Processes*, 161(9):41–44, 2003.

[171] Ajoy Kumar Kundu. *Aircraft design*, volume 27. Cambridge University Press, 2010.

[172] Bruno Béral. Airbus composites technologies & structures. In *Colloque CompositeâĂŤ-Toulouse. Toulouse, France*, 2007.

[173] V Tagliaferri, G Caprino, and A Diterlizzi. Effect of drilling parameters on the finish and mechanical properties of GFRP composites. *International Journal of Machine Tools and Manufacture*, 30(1):77–84, 1990.

[174] V N Gaitonde, S R Karnik, J C Rubio, A E Correia, A M Abrão, and J P Davim. Analysis of parametric influence on delamination in high-speed drilling of carbon fiber reinforced plastic composites. *Journal of Materials Processing Technology*, 203(1-3):431–438, 2008.

[175] J P Davim and P Reis. Drilling carbon fiber reinforced plastics manufactured by autoclaveâĂŤ-experimental and statistical study. *Materials & design*, 24(5):315–324, 2003.

[176] C C Tsao. Investigation into the effects of drilling parameters on delamination by various step-core drills. *Journal of Materials Processing Technology*, 206(1):405–411, 2008.

[177] H Hocheng and C C Tsao. Comprehensive analysis of delamination in drilling of composite materials with various drill bits. *Journal of Materials Processing Technology*, 140(1):335–339, 2003.

[178] R Piquet, B Ferret, F Lachaud, and P Swider. Experimental analysis of drilling damage in thin carbon/epoxy plate using special drills. *Composites Part A: Applied Science and Manufacturing*, 31(10):1107–1115, 2000.

[179] C C Tsao and H Hocheng. Taguchi analysis of delamination associated with various drill bits in drilling of composite material. *International Journal of Machine Tools and Manufacture*, 44(10):1085–1090, 2004.

[180] N S Mohan, A Ramachandra, and S M Kulkarni. Influence of process parameters on cutting force and torque during drilling of glassâĂŞfiber polyester reinforced composites. *Composite Structures*, 71(3âĂŞ4):407–413, 2005.

[181] M S Won and C K H Dharan. Chisel edge and pilot hole effects in drilling composite laminates. *Journal of manufacturing science and engineering*, 124(2):242–247, 2002.

[182] J Paulo Davim and Pedro Reis. Study of delamination in drilling carbon fiber reinforced plastics (CFRP) using design experiments. *Composite Structures*, 59(4):481–487, 2003.

[183] L M Durão, A G Magalhães, J.M.R.S. Tavares, and A T Marques. Analyzing objects in images for estimating the delamination influence on load carrying capacity of composite laminates. *ELCVIA: electronic letters on computer vision and image analysis*, 7(2):11–21, 2008.

[184] M Ramulu, T Branson, and D Kim. A study on the drilling of composite and titanium stacks. *Composite Structures*, 54(1):67–77, 2001.

[185] D Kim and M Ramulu. Drilling process optimization for graphite/bismaleimideâĂŞtitanium alloy stacks. *Composite Structures*, 63(1):101–114, 2004.

[186] R Garrick. Drilling Advanced Aircraft Structures with PCD (Poly-Crystalline Diamond) Drills. *Life (holes drilled)*, 1500(1000):45, 2007.

[187] K H Park, A Beal, D Kim, P Kwon, and J Lantrip. Tool wear in drilling of composite/titanium stacks using carbide and polycrystalline diamond tools. *Wear*, 2011.

[188] Redouane Zitoune, Vijayan Krishnaraj, Belkacem Sofiane Almabouacif, Francis Collombet, Michal Sima, and Alain Jolin. Influence of machining parameters and new nano-coated tool on drilling performance of CFRP/Aluminium sandwich. *Composites Part B: Engineering*, 43(3):1480–1488, 2012.

[189] I Shyha, S L Soo, D K Aspinwall, S Bradley, S Dawson, and C J Pretorius. Drilling of Titanium/CFRP/Aluminium Stacks. *Key Engineering Materials*, 447:624–633, 2010.

[190] K. Giasin, S. Ayvar-Soberanis, and A. Hodzic. An experimental study on drilling of unidirectional GLARE fibre metal laminates. *Composite Structures*, 133:794–808, 2015.

[191] J Sinke. Manufacturing of GLARE parts and structures. *Applied composite materials*, 10(4-5):293–305, 2003.

[192] AGY. 401 S-2 Glass® Chopped Strands, 2013.

[193] J.F.W.Coesel and R.Van Pragg. *Drilling Of Fibre-Metal Laminates*. PhD thesis, 1994.

[194] Piotr Tyczynski, Jan Lemanczyk, and Robert Ostrowski. Drilling of CFRP, GFRP, glare type composites. *Aircraft Engineering and Aerospace Technology*, 86(4):312–322, 2014.

[195] B S Nagendra Parashar and R K Mittal. *Elements of manufacturing processes.* PHI Learning Pvt. Ltd., 2002.

[196] Cebeli Ozek and Zulkuf Demir. Investigate the Friction Drilling of Aluminium Alloys According to the Thermal Conductivity. *Tem Journal Technology Education Management Informatics*, 2:93–101, 2013.

[197] J Paulo Davim. *Tribology in Manufacturing Technology.* Springer, 2012.

[198] J Fleischer, R Pabst, and S Kelemen. Heat Flow Simulation for Dry Machining of Power Train Castings. *CIRP Annals - Manufacturing Technology*, 56(1):117–122, 2007.

[199] Sanjay Rawat and Helmi Attia. Wear mechanisms and tool life management of WCâĂŞCo drills during dry high speed drilling of woven carbon fibre composites. *Wear*, 267(5âĂŞ8):1022–1030, 2009.

[200] J Dörr, Th Mertens, G Engering, and M Lahres. âĂŸIn-situ'temperature measurement to determine the machining potential of different tool coatings. *Surface and Coatings Technology*, 174:389–392, 2003.

[201] Masahiko Sato, Tomoyuki Aoki, Hisataka Tanaka, and Satoshi Takeda. Variation of temperature at the bottom surface of a hole during drilling and its effect on tool wear. *International Journal of Machine Tools and Manufacture*, 2013.

[202] Joung-Man Park, Dong-Jun Kwon, Zuo-Jia Wang, Ga-Young Gu, and K Lawrence Devries. A new strategy of carbon fiber reinforced plastic drilling evaluation using thermal measurement. *Journal of composite materials*, 47(16):2005–2011, 2013.

[203] A Taskesen and K Kutukde. Non-contact measurement and multi-objective analysis of drilling temperature when drilling B 4 C reinforced aluminum composites. *Transactions of Nonferrous Metals Society of China*, 25(1):271–283, 2015.

[204] T Brockhoff and A Walter. Fluid minimization in cutting and grinding. *Abrasives Magazine*, pages 38–42, 1998.

[205] Vasim Shaikh. *Effects of Minimum Quantity Lubrication in Drilling 1018 Steel.* PhD thesis, 2008.

[206] Steven Y Liang and a Ronan. Minimum quantity lubrication in finish hard turning, 2003.

[207] Gurpreet Singh, Sehijpal Singh, Manjot Singh, and Ajay Kumar. Experimental Investigations Of Vegetable & Mineral Oil Performance During Machining Of En-31 Steel With Minimum Quantity Lubrication. *International Journal of Research in Engineering and Technology*, 2(6):1030–1037, 2013.

[208] Heinz Tschätsch. *Applied machining technology.* Springer Science & Business Media, 2010.

[209] Graham T Smith. *Cutting tool technology: industrial handbook.* Springer Science & Business Media, 2008.

[210] M Rahman, A Senthil Kumar, and M S Ling. Effect of chilled air on machining performance in end milling. *The International Journal of Advanced Manufacturing Technology*, 21(10-11):787–795, 2003.

[211] Yakup Yildiz and Muammer Nalbant. A review of cryogenic cooling in machining processes. *International Journal of Machine Tools and Manufacture*, 48(9):947–964, 2008.

[212] O ÇakÄŗr, A Yardimeden, T Ozben, and E Kilickap. Selection of cutting fluids in machining processes. *Journal of Achievements in materials and Manufacturing engineering*, 25(2), 2007.

[213] C C Tsao, K L Kuo, and I C Hsu. Evaluation of a novel approach to a delamination factor after drilling composite laminates using a coreâĂŞsaw drill. *The International Journal of Advanced Manufacturing Technology*, 59(5):617–622, 2012.

[214] J Campos Rubio, A M Abrao, P E Faria, A Esteves Correia, and J Paulo Davim. Effects of high speed in the drilling of glass fibre reinforced plastic: Evaluation of the delamination factor. *International Journal of Machine Tools and Manufacture*, 48(6):715–720, 2008.

[215] E Kilickap. Determination of optimum parameters on delamination in drilling of GFRP composites by Taguchi method. *Indian Journal of Engineering & Materials Sciences*, 17:265–274, 2010.

[216] W C Chen. Some experimental investigations in the drilling of carbon fiber-reinforced plastic (CFRP) composite laminates. *International Journal of Machine Tools and Manufacture*, 37(8):1097–1108, 1997.

[217] C C Tsao and H Hocheng. The effect of chisel length and associated pilot hole on delamination when drilling composite materials. *International Journal of Machine Tools and Manufacture*, 43(11):1087–1092, 2003.

[218] E U Enemuoh, A S El-Gizawy, and A Chukwujekwu Okafor. An approach for development of damage-free drilling of carbon fiber reinforced thermosets. *International Journal of Machine Tools and Manufacture*, 41(12):1795–1814, 2001.

[219] C C Tsao. Experimental study of drilling composite materials with step-core drill. *Materials & design*, 29(9):1740–1744, 2008.

[220] M B Lazar and P Xirouchakis. Experimental analysis of drilling fiber reinforced composites. *International Journal of Machine Tools and Manufacture*, 51(12):937–946, 2011.

[221] Uday Shanker Dixit, D K Sarma, and J Paulo Davim. *Environmentally friendly machining.* Springer Science & Business Media, 2012.

[222] Nilesh C Ghuge, V K Dhatrak, and A M Mahalle. Minimum Quantity Lubrication.

[223] M M A Khan, M A H Mithu, and N R Dhar. Effects of minimum quantity lubrication on turning AISI 9310 alloy steel using vegetable oil-based cutting fluid. *Journal of Materials Processing Technology*, 209(15):5573–5583, 2009.

[224] Nikhil Ranjan Dhar, Sumaiya Islam, and Mohammad Kamruzzaman. Effect of minimum quantity lubrication (MQL) on tool wear, surface roughness and dimensional deviation in turning AISI-4340 steel. *Gazi University Journal of Science*, 20(2):23–32, 2010.

[225] J P Davim. *Sustainable Manufacturing.* Wiley, 2013.

[226] F Klocke and A Kuchle. *Manufacturing Processes 1: Cutting.* Springer Berlin Heidelberg, 2011.

[227] S M Ali, N R Dhar, and S K Dey. Effect of minimum quantity lubrication (MQL) on cutting performance in turning medium carbon steel by uncoated carbide insert at different speed-feed combinations. *Advances in Production Engineering & Management*, 6(3):185–196, 2011.

[228] N R Dhar, M Kamruzzaman, and Mahiuddin Ahmed. Effect of minimum quantity lubrication (MQL) on tool wear and surface roughness in turning AISI-4340 steel. *Journal of Materials Processing Technology*, 172(2):299–304, 2006.

[229] Leonardo Roberto da Silva, Eduardo Carlos Bianchi, Ronaldo Yoshinobu Fusse, Rodrigo Eduardo Catai, Thiago Valle França, and Paulo Roberto Aguiar. Analysis of surface integrity for minimum quantity lubricantâĂŤMQL in grinding. *International Journal of Machine Tools and Manufacture*, 47(2):412–418, 2007.

[230] N R Dhar, M T Ahmed, and S Islam. An experimental investigation on effect of minimum quantity lubrication in machining AISI 1040 steel. *International Journal of Machine Tools and Manufacture*, 47(5):748–753, 2007.

[231] S Zhang, J F Li, and Y W Wang. Tool life and cutting forces in end milling Inconel 718 under dry and minimum quantity cooling lubrication cutting conditions. *Journal of Cleaner Production*, 32:81–87, 2012.

[232] L R Silva, E C Bianchi, R E Catai, R Y Fusse, T V Franca, and P R Aguiar. Study on the behavior of the minimum quantity lubricant-MQL technique under different lubricating and cooling conditions when grinding ABNT 4340 steel. *Journal of the Brazilian Society of Mechanical Sciences and Engineering*, 27(2):192–199, 2005.

[233] T Tawakoli, M J Hadad, and M H Sadeghi. Influence of oil mist parameters on minimum quantity lubricationâĂŞMQL grinding process. *International Journal of Machine Tools and Manufacture*, 50(6):521–531, 2010.

[234] Y S Liao and H M Lin. Mechanism of minimum quantity lubrication in high-speed milling of hardened steel. *International Journal of Machine Tools and Manufacture*, 47(11):1660–1666, 2007.

[235] Y S Liao, H M Lin, and Y C Chen. Feasibility study of the minimum quantity lubrication in high-speed end milling of NAK80 hardened steel by coated carbide tool. *International Journal of Machine Tools and Manufacture*, 47(11):1667–1676, 2007.

[236] A R Machado and J Wallbank. The effect of extremely low lubricant volumes in machining. *Wear*, 210(1):76–82, 1997.

[237] N R Dhar, M W Islam, S Islam, and M A H Mithu. The influence of minimum quantity of lubrication (MQL) on cutting temperature, chip and dimensional accuracy in turning AISI-1040 steel. *Journal of Materials Processing Technology*, 171(1):93–99, 2006.

[238] T Tawakoli, M J Hadad, M H Sadeghi, A Daneshi, S Stöckert, and A Rasifard. An experimental investigation of the effects of workpiece and grinding parameters on minimum quantity lubricationâĂŤMQL grinding. *International Journal of Machine Tools and Manufacture*, 49(12):924–932, 2009.

[239] J F Kelly and M G Cotterell. Minimal lubrication machining of aluminium alloys. *Journal of Materials Processing Technology*, 120(1):327–334, 2002.

[240] Alexander Bardetsky, Helmi Attia, and Mohamed Elbestawi. Evaluation of Tool Wear Suppressive Ability of Lubricants Usein in Minimum Quantity Lubrication Application in High Speed Machining of Cast Aluminum Alloys. In *ASME 2005 International Mechanical Engineering Congress and Exposition*, pages 23–29. American Society of Mechanical Engineers, 2005.

[241] Sukanta Bhowmick, Michael J Lukitsch, and Ahmet T Alpas. Dry and minimum quantity lubrication drilling of cast magnesium alloy (AM60). *International Journal of Machine Tools and Manufacture*, 50(5):444–457, 2010.

[242] S Bhowmick and A T Alpas. The performance of hydrogenated and non-hydrogenated diamond-like carbon tool coatings during the dry drilling of 319 Al. *International Journal of Machine Tools and Manufacture*, 48(7):802–814, 2008.

[243] Sukanta Bhowmick and Ahmet T Alpas. Minimum quantity lubrication drilling of aluminiumâĂŞsilicon alloys in water using diamond-like carbon coated drills. *International Journal of Machine Tools and Manufacture*, 48(12âĂŞ13):1429–1443, 2008.

[244] M S Najiha, M M Rahman, and K Kadirgama. Performance of water-based TiO2 nanofluid during the minimum quantity lubrication machining of aluminium alloy, AA6061-T6. *Journal of Cleaner Production*.

[245] G Fox-Rabinovich, J M Dasch, T Wagg, K Yamamoto, S Veldhuis, G K Dosbaeva, and M Tauhiduzzaman. Cutting performance of different coatings during minimum quantity lubrication drilling of aluminum silicon B319 cast alloy. *Surface and Coatings Technology*, 205(16):4107–4116, 2011.

[246] J P Davim, P S Sreejith, R Gomes, and C Peixoto. Experimental studies on drilling of aluminium (AA1050) under dry, minimum quantity of lubricant, and flood-lubricated conditions. *Proceedings of the Institution of Mechanical Engineers, Part B: Journal of Engineering Manufacture*, 220(10):1605–1611, 2006.

[247] Young-Kug Hwang, Choon-Man Lee, and Soo-Hyeon Park. Evaluation of machinability according to the changes in machine tools and cooling lubrication environments and optimization of cutting conditions using Taguchi method. *International Journal of Precision Engineering and Manufacturing*, 10(3):65–73, 2009.

[248] Franci Pušavec, Antun Stoić, and Janez Kopač. The role of cryogenics in machining processes. *Tehnički vjesnik*, 16(4):3–10, 2009.

[249] B Dilip Jerold and M Pradeep Kumar. The Influence of Cryogenic Coolants in Machining of TiâĂŞ6AlâĂŞ4V. *Journal of manufacturing science and engineering*, 135(3):31005, 2013.

[250] H Hocheng. *Machining technology for composite materials : principles and practice*. Woodhead Pub., Cambridge, UK; Philadelphia, PA, 2012.

[251] Simranpreet Singh Gill, Harpreet Singh, Rupinder Singh, and Jagdev Singh. Cryoprocessing of cutting tool materialsâĂŤa review. *The International Journal of Advanced Manufacturing Technology*, 48(1-4):175–192, 2010.

[252] K L Wiggins and S Malkin. Cryogenic enhancement of machinability of bone. pages 169–170, 1974.

[253] D Bhattacharyya, M N Allen, and S J Mander. Cryogenic machining of Kevlar composites. *MATERIAL AND MANUFACTURING PROCESS*, 8(6):631–651, 1993.

[254] D Bhattacharyya and D P W Horrigan. A study of hole drilling in Kevlar composites. *Composites Science and Technology*, 58(2):267–283, 1998.

[255] S Chatterjee. Performance characteristics of cryogenically treated high speed steel drills. *International journal of production research*, 30(4):773–786, 1992.

[256] Flávio J da Silva, Sinésio D Franco, Álisson R Machado, Emmanuel O Ezugwu, and Antônio M Souza Jr. Performance of cryogenically treated HSS tools. *Wear*, 261(5âĂŞ6):674–685, 2006.

[257] A Y L Yong, K H W Seah, and M Rahman. Performance of cryogenically treated tungsten carbide tools in milling operations. *The International Journal of Advanced Manufacturing Technology*, 32(7-8):638–643, 2007.

[258] A Y L Yong, K H W Seah, and M Rahman. Performance evaluation of cryogenically treated tungsten carbide tools in turning. *International Journal of Machine Tools and Manufacture*, 46(15):2051–2056, 2006.

[259] Hui-Bo He, Wen-Qiang Han, Hua-Ying Li, Dong-Yang Li, Jun Yang, Tao Gu, and Tao Deng. Effect of deep cryogenic treatment on machinability and wear mechanism of TiAlN coated tools during dry turning. *International Journal of Precision Engineering and Manufacturing*, 15(4):655–660, 2014.

[260] R Thornton, T Slatter, and R Lewis. Effects of deep cryogenic treatment on the wear development of H13A tungsten carbide inserts when machining AISI 1045 steel. *Production Engineering*, 8(3):355–364, 2014.

[261] Nursel Altan Özbek, Adem Çiçek, Mahmut Gülesin, and Onur Özbek. Effect of cutting conditions on wear performance of cryogenically treated tungsten carbide inserts in dry turning of stainless steel. *Tribology International*, 94:223–233, 2016.

[262] Y Ding and S Y Hong. Improvement of Chip Breaking in Machining Low Carbon Steel by Cryogenically Precooling the Workpiece. *Journal of manufacturing science and engineering*, 120(1):76–83, 1998.

[263] Shane Y Hong and Zhibo Zhao. Thermal aspects, material considerations and cooling strategies in cryogenic machining. *Clean Products and Processes*, 1(2):107–116, 1999.

[264] Shane Y Hong and Mark Broomer. Economical and ecological cryogenic machining of AISI 304 austenitic stainless steel. *Clean Products and Processes*, 2(3):157–166, 2000.

[265] Shanmugam Murugappan, Sanjivi Arul, and Surendran K Narayanan. An Experimental Study on Turning of AL6063 under Cryogenic Pre Cooled Condition. *Procedia CIRP*, 35:61–66, 2015.

[266] S Sun, M Brandt, and M S Dargusch. Machining TiâĂŞ6AlâĂŞ4V alloy with cryogenic com-

pressed air cooling. *International Journal of Machine Tools and Manufacture*, 50(11):933–942, 2010.

[267] Z Y Wang, K P Rajurkar, J Fan, and G Petrescu. Cryogenic Machining of Tantalum. *Journal of Manufacturing Processes*, 4(2):122–127, 2002.

[268] Z Y Wang and K P Rajurkar. Cryogenic machining of hard-to-cut materials. *Wear*, 239(2):168–175, 2000.

[269] Z Y Wang and K P Rajurkar. Wear of CBN tool in turning of silicon nitride with cryogenic cooling. *International Journal of Machine Tools and Manufacture*, 37(3):319–326, 1997.

[270] K A Venugopal, R Tawade, P G Prashanth, S Paul, and A B Chattopadhyay. Turning of titanium alloy with TiB2-coated carbides under cryogenic cooling. *Proceedings of the Institution of Mechanical Engineers, Part B: Journal of Engineering Manufacture*, 217(12):1697–1707, 2003.

[271] K A Venugopal, S Paul, and A B Chattopadhyay. Tool wear in cryogenic turning of Ti-6Al-4V alloy. *Cryogenics*, 47(1):12–18, 2007.

[272] K A Venugopal, S Paul, and A B Chattopadhyay. Growth of tool wear in turning of Ti-6Al-4V alloy under cryogenic cooling. *Wear*, 262(9âĂŞ10):1071–1078, 2007.

[273] Mirghani I Ahmed, Ahmad F Ismail, Y A Abakr, and A K M Amin. Effectiveness of cryogenic machining with modified tool holder. *Journal of Materials Processing Technology*, 185(1):91–96, 2007.

[274] Zbigniew Zurecki, J H Frey, and R Ghosh. Finish-turning of hardened powder-metallurgy steel using cryogenic cooling. *Advances in Powder Metallurgy and Particulate Materials*, (7):7–185, 2003.

[275] T Xia, Y Kaynak, C Arvin, and I S Jawahir. Cryogenic cooling-induced process performance and surface integrity in drilling CFRP composite material. *The International Journal of Advanced Manufacturing Technology*, pages 1–12, 2015.

[276] S Paul and A B Chattopadhyay. Effects of cryogenic cooling by liquid nitrogen jet on forces, temperature and surface residual stresses in grinding steels. *Cryogenics*, 35(8):515–523, 1995.

[277] S Paul and A B Chattopadhyay. The effect of cryogenic cooling on grinding forces. *International Journal of Machine Tools and Manufacture*, 36(1):63–72, 1996.

[278] S Paul, P P Bandyopadhyay, and A B Chattopadhyay. Effects of cryo-cooling in grinding steels. *Journal of Materials Processing Technology*, 37(1):791–800, 1993.

[279] S Paul and A B Chattopadhyay. A study of effects of cryo-cooling in grinding. *International Journal of Machine Tools and Manufacture*, 35(1):109–117, 1995.

[280] B Dilip Jerold and M Pradeep Kumar. Experimental investigation of turning AISI 1045 steel using cryogenic carbon dioxide as the cutting fluid. *Journal of Manufacturing Processes*, 13(2):113–119, 2011.

[281] N R Dhar and M Kamruzzaman. Cutting temperature, tool wear, surface roughness and dimensional deviation in turning AISI-4037 steel under cryogenic condition. *International Journal of Machine Tools and Manufacture*, 47(5):754–759, 2007.

[282] K V B S Kalyan Kumar and S K Choudhury. Investigation of tool wear and cutting force in cryogenic machining using design of experiments. *Journal of Materials Processing Technology*, 203(1âĂŞ3):95–101, 2008.

[283] A B Chattopadhyay, A Bose, and A K Chattopdhyay. Improvements in grinding steels by cryogenic cooling. *Precision Engineering*, 7(2):93–98, 1985.

[284] V Firouzdor, E Nejati, and F Khomamizadeh. Effect of deep cryogenic treatment on wear resistance and tool life of M2 HSS drill. *Journal of Materials Processing Technology*, 206(1):467–472, 2008.

[285] D Kim and M Ramulu. Cryogenically treated carbide tool performance in drilling thermoplastic composites. *Transactions of the North American Manufacturing Research Institute of SME*, 32:79–85, 2004.

[286] Harold A Stewart. Cryogenic treatment of tungsten carbide reduces tool wear when machining medium density fiberboard. *Forest products journal*, 54(2):53–56, 2004.

[287] Stuart Barnes, Pipat Bhudwannachai, and Aishah Najiah Dahnel. Drilling performance of carbon fiber reinforced epoxy composite when machined dry, with conventional cutting fluid and with a cryogenically cooled tool. 2013.

[288] Turgay KÄśvak and Ulvi Åđeker. Effect of cryogenic treatment applied to M42 HSS drills on the machinability of Ti-6Al-4V alloy. *Materiali in tehnologije*, 49(6):949–956, 2015.

[289] B R Ramji, H N Narasimha Murthy, M Krishna, and M J Raghu. Performance Study of Cryogenically Treated HSS Drills in Drillilg Gray Cast Iron Using Orthogonal Array Technique. *Research Journal of Applied Sciences, Engineering and Technology*, 2(5):487–491, 2010.

[290] Maria Fátima Vaz, Helena Canhão, and João Eurico Fonseca. Bone: A Composite Natural Material.

[291] Judith Gisip, Rado Gazo, and Harold A Stewart. Effects of cryogenic treatment and refrigerated air on tool wear when machining medium density fiberboard. *Journal of Materials Processing Technology*, 209(11):5117–5122, 2009.

[292] Vijayender Singh, S Ghosh, and P Venkateswara Rao. Grindability Improvement of Composite Ceramic with Cryogenic Coolant. In *Proceedings of the World Congress on Engineering*, volume 2, 2010.

[293] Chetan, S Ghosh, and P V Rao. Environment Friendly Machining of NiâĂŞCrâĂŞCo Based Super Alloy using Different Sustainable Techniques. *Materials and Manufacturing Processes*, pages 1–8, 2015.

[294] Yusuf Kaynak. Evaluation of machining performance in cryogenic machining of Inconel 718 and comparison with dry and MQL machining. *The International Journal of Advanced Manufacturing Technology*, 72(5-8):919–933, 2014.

[295] Y Sun, B Huang, D A Puleo, and I S Jawahir. Enhanced Machinability of Ti-5553 Alloy from Cryogenic Machining: Comparison with MQL and Flood-cooled Machining and Modeling. *Procedia CIRP*, 31:477–482, 2015.

[296] G Rotella, O W Dillon Jr, D Umbrello, Luca Settineri, and I S Jawahir. The effects of cooling conditions on surface integrity in machining of Ti6Al4V alloy. *The International Journal of Advanced Manufacturing Technology*, 71(1-4):47–55, 2014.

[297] Y Kaynak, S W Robertson, H E Karaca, and I S Jawahir. Progressive tool-wear in machining of room-temperature austenitic NiTi alloys: The influence of cooling/lubricating, melting, and heat treatment conditions. *Journal of Materials Processing Technology*, 215:95–104, 2015.

[298] D U Braga, A E Diniz, G W A Miranda, and N L Coppini. Minimum lubrication in Al-Si drilling. *Journal of the Brazilian Society of Mechanical Sciences and Engineering*, 25:63–68, 2003.

[299] P S Sreejith. Machining of 6061 aluminium alloy with MQL, dry and flooded lubricant conditions. *Materials Letters*, 62(2):276–278, 2008.

[300] Arup Kumar Nandi and J Paulo Davim. A study of drilling performances with minimum quantity of lubricant using fuzzy logic rules. *Mechatronics*, 19(2):218–232, 2009.

[301] Krishnan S Murthy and Irusa G Rajendran. Prediction and analysis of multiple quality characteristics in drilling under minimum quantity lubrication. *Proceedings of the Institution of Mechanical Engineers, Part B: Journal of Engineering Manufacture*, 226(6):1061–1070, 2012.

[302] National Institute of Standards, Technology, Carrol Croarkin, Paul Tobias, and Chelli Zey. *Engineering statistics handbook*. The Institute, 2001.

[303] K. Giasin, S. Ayvar-Soberanis, and A. Hodzic. The effects of minimum quantity lubrication and cryogenic liquid nitrogen cooling on drilled hole quality in GLARE fibre metal laminates. *Materials and Design*, 89:996–1006, 2016.

[304] K Giasin, S Ayvar-Soberanis, and A Hodzic. Evaluation of cryogenic cooling and minimum quantity lubrication effects on machining GLARE laminates using design of experiments. *Journal of Cleaner Production*, 135:533–548, 2016.

[305] R Heinemann, S Hinduja, G Barrow, and G Petuelli. Effect of MQL on the tool life of small twist drills in deep-hole drilling. *International Journal of Machine Tools and Manufacture*, 46(1):1–6, 2006.

[306] L Ken Lauderbaugh. Analysis of the effects of process parameters on exit burrs in drilling using a combined simulation and experimental approach. *Journal of Materials Processing Technology*, 209(4):1909–1919, 2009.

[307] Eugene Feldshtein. The influence of machining conditions on burr shapes when drilling reach-through holes in difficult-to-cut materials. *Advances in Manufacturing Science and Technology*, 35(4):75–83, 2011.

[308] S Kalidas, R E DeVor, and S G Kapoor. Experimental investigation of the effect of drill coatings on hole quality under dry and wet drilling conditions. *Surface and Coatings Technology*, 148(2):117–128, 2001.

[309] Iqbal Shareef, Manikandan Natarajan, and Oyelayo O Ajayi. Dry machinability of aluminum alloys. In *World Tribology Congress III*, pages 831–832. American Society of Mechanical Engineers, 2005.

[310] Khaled Giasin, Alma Hodzic, Vaibhav Phadnis, and Sabino Ayvar-Soberanis. Assessment of cutting forces and hole quality in drilling Al2024 aluminium alloy: experimental and finite element study. *The International Journal of Advanced Manufacturing Technology*, pages 1–21, 2016.

[311] Khaled Giasin, Sabino Ayvar-Soberanis, Toby French, and Vaibhav Phadnis. 3d finite element modelling of cutting forces in drilling fibre metal laminates and experimental hole quality analysis. *Applied Composite Materials*, pages 1–25, 2016.

[312] H Hocheng and C C Tsao. Effects of special drill bits on drilling-induced delamination of composite materials. *International Journal of Machine Tools and Manufacture*, 46(12âĂŞ13):1403–1416, 2006.

[313] C C Tsao and H Hocheng. Computerized tomography and C-Scan for measuring delamination in the drilling of composite materials using various drills. *International Journal of Machine Tools and Manufacture*, 45(11):1282–1287, 2005.

[314] B Ramesh, A Elayaperumal, S Satishkumar, Anish Kumar, T Jayakumar, and D Dinakaran. Influence of cooling on the performance of the drilling process of glass fibre reinforced epoxy composites. *Archives of Civil and Mechanical Engineering*, 16(1):135–146, 2016.

[315] Mitutoyo. Surftest SV-600, 1999.

[316] Friedrich Schäfer, Fritz Breuninger, Harro Sauer, Bernhard Schuh, Wolfgang Seyderhelm, Hans-Jochen Winter, Hans-Jürgen Warnecke, and Hans U Brauner. *Entgraten: Theorie, Verfahren, Anlagen.* Krausskopf, 1975.

[317] Shusheng Bi and Jie Liang. Experimental studies and optimization of process parameters for burrs in dry drilling of stacked metal materials. *The International Journal of Advanced Manufacturing Technology*, 53(9):867–876, 2011.

[318] Bianca M Colosimo and Nicola Senin. *Geometric Tolerances.* Springer, 2010.

[319] Suleiman Mahmoud Obeidat. *Adaptive methods for form error determination in discrete point metrology.* ProQuest, 2008.

[320] David Dornfeld and Dae-Eun Lee. *Machine design for precision manufacturing.* Springer, 2008.

[321] Khaled Giasin and Sabino Ayvar-Soberanis. Evaluation of workpiece temperature during drilling of glare fiber metal laminates using infrared techniques: Effect of cutting parameters, fiber orientation and spray mist application. *Materials*, 9(8):622, 2016.

[322] R L Champoux, J H Underwood, and J A Kapp. *Analytical and Experimental Methods for Residual Stress Effects in Fatigue.* Number no. 1004. ASTM, 1988.

[323] R Zitoune, V Krishnaraj, F Collombet, and S Le Roux. Experimental and numerical analysis on drilling of carbon fibre reinforced plastic and aluminium stacks. *Composite Structures*, 146:148–158, 2016.

[324] M Hazarika and U S Dixit. *Setup Planning for Machining.* Springer International Publishing, 2014.

[325] M.J. Jackson. *Surface Engineering: Proceedings of the 5th International Surface Engineering Congress - May 15-17, 2006, Washington State Convention Center, Seattle, Washington, USA.* A S M International, 2006.

[326] Mridul Singal. *Fundamentals of machining and machine tools.* IK International Pvt Ltd, 2008.

[327] MQ Jiang and LH Dai. Formation mechanism of lamellar chips during machining of bulk metallic glass. *Acta Materialia*, 57(9):2730–2738, 2009.

[328] W Bouzid Saı, N Ben Salah, and JL Lebrun. Influence of machining by finishing milling on surface characteristics. *International Journal of Machine Tools and Manufacture*, 41(3):443–450, 2001.

[329] M J Li, S L Soo, D K Aspinwall, D Pearson, and W Leahy. Influence of Lay-up Configuration and Feed Rate on Surface Integrity when Drilling Carbon Fibre Reinforced Plastic (CFRP) Composites. *Procedia CIRP*, 13:399–404, 2014.

[330] F Lachaud, R Piquet, and L Michel. Delamination in mode I and II of carbon fibre composite materials: fibre orientation influence. In *Proc. 12th International Conference on Composite Materials, Paris, July*, 1999.

[331] M Henerichs, R Voß, H Tanaka, F Kuster, and K Wegener. Analysis of Material Weakening in CFRP after a Drilling Operation. *Procedia CIRP*, 24:44–48, 2014.

[332] Gabriel Castro. *Drilling Carbon Fiber Reinforced Plastic and Titanium Stacks.* PhD thesis, 2010.

[333] D G Thakur. Precision Drilling of Glass Fiber Reinforced Composite (GFRP) with Modified HSS Drill Geometry. *Advanced Materials Manufacturing & Characterization*, 4(1), 2014.

[334] T S Srivatsan. Composite Materials: Fatigue and Fracture Edited by Roderick H. Martin. *MATERIAL AND MANUFACTURING PROCESS*, 12(1):155–157, 1997.

[335] Serope Kalpakjian, Steven R Schmid, and Chi-Wah Kok. *Manufacturing processes for engineering materials.* Pearson-Prentice Hall, 2008.

[336] Lin Zhang, Zi Liu, Wei Tian, and Wenhe Liao. Experimental studies on the performance of different structure tools in drilling CFRP/Al alloy stacks. *The International Journal of Advanced Manufacturing Technology*, pages 1–11, 2015.

[337] Alokesh Pramanik and Guy Littlefair. Developments in Machining of Stacked Materials Made of CFRP and Titanium/Aluminum Alloys. *Machining Science and Technology*, 18(4):485–508, 2014.

[338] H Takeyama and N Iijima. Machinability of Glassfiber Reinforced Plastics and Application of Ultrasonic Machining. *CIRP Annals - Manufacturing Technology*, 37(1):93–96, 1988.

[339] Vijayan Krishnaraj, Redouane Zitoune, and Francis Collombet. Study of drilling of multi-material (CFRP/Al) using Taguchi and statistical techniques. *Usak University Journal of Material Sciences*, 1(2):95–109, 2012.

[340] V Krishnaraj, S Vijayarangan, and G Suresh. An investigation on high speed drilling of glass fiber reinforced plastic (GFRP). *Indian Journal of Engineering & Materials Sciences*, 12(3):189–195, 2005.

[341] B Latha and V S Senthilkumar. Fuzzy Rule Based Modeling of Drilling Parameters for De-

lamination in Drilling GFRP Composites. *Journal of Reinforced Plastics and Composites*, 28(8):951–964, 2009.

[342] Nripen Mondal, Biswajit Sing Sardar, Ranendra Nath Halder, and Santanu Das. Observation of Drilling Burr and Finding out the Condition for Minimum Burr Formation. *International Journal of Manufacturing Engineering*, 97:230–240, 2014.

[343] Sanjib Kundu, Santanu Das, and Partha Pratim Saha. Optimization of drilling parameters to minimize burr by providing back-up support on aluminium alloy. *Procedia Engineering*, 97:230–240, 2014.

[344] LaRoux K Gillespie. *Deburring and edge finishing handbook.* Society of Manufacturing Engineers, 1999.

[345] Cody Hellstern. *Investigation of interlayer burr formation in the drilling of stacked aluminum sheets.* PhD thesis, 2009.

[346] A Velayudham, R Krishnamurthy, and T Soundarapandian. Evaluation of drilling characteristics of high volume fraction fibre glass reinforced polymeric composite. *International Journal of Machine Tools and Manufacture*, 45(4):399–406, 2005.

[347] L Vijayaraghavan. Machining Of Composites An Overview. *Journal on Design and Manufacturing Technologies*, 1(1), 2007.

[348] Ekkard Brinksmeier. Machinability of Carbon-Fiber-Reinforced and GLARE Materials. *CIRP Encyclopedia of Production Engineering*, pages 782–787, 2014.

[349] V Songmene, A Djebara, I Zaghbani, J Kouam, and R Khettabi. *Machining and machinability of aluminum alloys.* INTECH Open Access Publisher, 2011.

[350] R van Praag and J Sinke. Manufacturing fibre-metal laminates: Part 2: The forming properties. Technical report, 1994.

[351] S Abrate and D A Walton. Machining of composite materials. Part I: Traditional methods. *Composites Manufacturing*, 3(2):75–83, 1992.

[352] C C Tsao and H Hocheng. Effects of exit back-up on delamination in drilling composite materials using a saw drill and a core drill. *International Journal of Machine Tools and Manufacture*, 45(11):1261–1270, 2005.

[353] Pankaj K Mallick. *Composites engineering handbook.* CRC Press, 1997.

[354] Vijay Kumar Thakur. *Green composites from natural resources.* CRC Press, 2013.

[355] Bogdan P Nedić and Milan D Erić. Cutting temperature measurement and material machinability. *Thermal Science*, 18(suppl. 1):259–268, 2014.

[356] E Brinksmeier, S Fangmann, and R Rentsch. Drilling of composites and resulting surface integrity. *CIRP Annals - Manufacturing Technology*, 60(1):57–60, 2011.

[357] V Kolesnyk, J Zajac, S Radchenko, and M Adamian. The effect of cutting temperature on hole quality when drilling CFRP/metal stack. 4:138–141, 2015.

[358] K Jessy, D Dinakaran, and V Seshagiri Rao. Influence of different cooling methods on drill temperature in drilling GFRP. *The International Journal of Advanced Manufacturing Technology*, 76(1-4):609–621, 2015.

[359] Eyup BaĞci and Babur Ozcelik. Investigation of the effect of drilling conditions on the twist drill temperature during step-by-step and continuous dry drilling. *Materials & Design*, 27(6):446–454, 2006.

[360] Chang-Ying Wang, Yu-Han Chen, Qing-Long An, Xiao-Jiang Cai, Wei-Wei Ming, and Ming Chen. Drilling temperature and hole quality in drilling of CFRP/aluminum stacks using diamond coated drill. *International Journal of Precision Engineering and Manufacturing*, 16(8):1689–1697, 2015.

[361] G Le Coz, M Marinescu, A Devillez, D Dudzinski, and L Velnom. Measuring temperature of rotating cutting tools: Application to MQL drilling and dry milling of aerospace alloys. *Applied Thermal Engineering*, 36:434–441, 2012.

[362] A Rivero, G Aramendi, S Herranz, and L N Lopez de Lacalle. An experimental investigation of the effect of coatings and cutting parameters on the dry drilling performance of aluminium alloys. *The International Journal of Advanced Manufacturing Technology*, 28(1-2):1–11, 2006.

[363] O C Mendes, R F Avila, A M Abrao, Pedro Reis, and J Paulo Davim. The performance of cutting fluids when machining aluminium alloys. *Industrial Lubrication and Tribology*, 58(5):260–268, 2006.

[364] Ginger Gardiner. Machining update: One-shot dry drilling of stacked materials, 2014.

[365] Maxime Montoya, Madalina Calamaz, Daniel Gehin, and Franck Girot. Evaluation of the performance of coated and uncoated carbide tools in drilling thick CFRP/aluminium alloy stacks. *The International Journal of Advanced Manufacturing Technology*, 68(9-12):2111–2120, 2013.

[366] Zhenchao Qi, Kaifu Zhang, Yuan Li, Shunuan Liu, and Hui Cheng. Critical thrust force predicting modeling for delamination-free drilling of metal-FRP stacks. *Composite Structures*, 107:604–609, 2014.

[367] C L Kuo, S L Soo, D K Aspinwall, W Thomas, S Bradley, D Pearson, R M'Saoubi, and

W Leahy. The Effect of Cutting Speed and Feed Rate on Hole Surface Integrity in Single-shot Drilling of Metallic-Composite Stacks. *Procedia CIRP*, 13:405–410, 2014.

[368] Azwan Iskandar Azmi. *Machinability study of fibre-reinforced polymer matrix composites*. PhD thesis, 2012.

[369] L Shakeel Ahmed, N Govindaraju, and M Pradeep Kumar. Experimental Investigations on Cryogenic Cooling in the Drilling of Titanium Alloy. *Materials and Manufacturing Processes*, (just-accepted), 2015.

[370] T Xia, Y Kaynak, C Arvin, and I S Jawahir. Cryogenic cooling-induced process performance and surface integrity in drilling CFRP composite material. *The International Journal of Advanced Manufacturing Technology*, 82(1-4):605–616, 2016.

[371] M Pradeep kumar M.Dhananchezian A. Rajadurai. Experimental Investigation of Cryogenic Cooling by Liquid Nitrogen in the Orthogonal Machining Process. *International Journal of Recent Trends in Engineering*,, 1(5), 2009.

[372] Giovanna Rotella, T Lu, Luca Settineri, O W Dillon Jr, and I S Jawahir. Dry and cryogenic machining: comparison from the sustainability perspective. In *Sustainable Manufacturing*, pages 95–100. Springer, 2012.

[373] G Rotella and D Umbrello. Numerical simulation of surface modification in dry and cryogenic machining of AA7075 alloy. *Procedia CIRP*, 13:327–332, 2014.

[374] Charles F Hickey Jr. Mechanical properties of titanium and aluminum alloys at cryogenic temperatures. Technical report, 1962.

[375] Erol Kilickap, Mesut Huseyinoglu, and Cihan Ozel. Empirical study regarding the effects of minimum quantity lubricant utilization on performance characteristics in the drilling of Al 7075. *Journal of the Brazilian Society of Mechanical Sciences and Engineering*, 33(1):52–57, 2011.

[376] B Dilip Jerold and M Pradeep Kumar. Experimental comparison of carbon-dioxide and liquid nitrogen cryogenic coolants in turning of AISI 1045 steel. *Cryogenics*, 52(10):569–574, 2012.

[377] J Paulo Davim. *Green manufacturing processes and systems*. Springer, 2013.

[378] Shane Y Hong, Irel Markus, and Woo-cheol Jeong. New cooling approach and tool life improvement in cryogenic machining of titanium alloy Ti-6Al-4V. *International Journal of Machine Tools and Manufacture*, 41(15):2245–2260, 2001.

[379] SANDVIK. Improved hand-held hole making in composites. Technical report, http://www.sandvik.coromant.com, 2011.

[380] VPLIV PARAMETROV PROCESA I N MEHANSKIH LASTNOSTI and HRAPAVOST POVRŠINE P R I SUHEM VRTANJU. Influence of the process parameters and the mechanical properties of aluminum alloys on the burr height and the surface roughness in dry drilling. *Materiali in tehnologije*, 46(2):103–108, 2012.

[381] Yasser Zedan Seyed Ali Niknam Victor Songmene. Machining Burrs Formation & Deburring of Aluminium Alloys, 2014.

[382] Tian Xia. Investigation of Drilling Performance in Cryogenic Drilling on CFRP Composite Laminates. 2014.

[383] Vimal Dhokia, A Shokrani, D Correa Paulino, and S T Newman. Effect of cryogenic cooling on the surface quality and tool wear in end milling 6061-T6 Aluminium. In *22nd International Conference on Flexible Automation and Intelligent Manufacturing (FAIM 2012)*, volume 10, pages 1–7. University of Bath, 2012.

[384] B Tasdelen, T Wikblom, and S Ekered. Studies on minimum quantity lubrication (MQL) and air cooling at drilling. *Journal of Materials Processing Technology*, 200(1âĂŞ3):339–346, 2008.

[385] Kyung-Hee Park, Gi-Dong Yang, M A Suhaimi, Dong Yoon Lee, Tae-Gon Kim, Dong-Won Kim, and Seok-Woo Lee. The effect of cryogenic cooling and minimum quantity lubrication on end milling of titanium alloy Ti-6Al-4V. *Journal of mechanical science and technology*, 29(12):5121–5126, 2015.

[386] D Biermann, H Abrahams, and M Metzger. Experimental investigation of tool wear and chip formation in cryogenic machining of titanium alloys. *Advances in Manufacturing*, 3(4):292–299, 2015.

[387] Thomas B Barker. *Quality by experimental design*, volume 183. CRC Press, 2005.

[388] Inc Minitab. MINITAB release 17: statistical software for windows. *Minitab Inc, USA*, 2014.

[389] David Lane. Online Statistics Education. In *International Encyclopedia of Statistical Science*, pages 1018–1020. Springer, 2011.

[390] J P Davim. *Design of Experiments in Production Engineering*. Springer International Publishing, 2015.

Publications

Refereed Journal Publications

1. K Giasin, S Ayvar-Soberanis, A Hodzic, An experimental study on drilling of unidirectional GLARE fibre metal laminates , Composite Structures 133, 794-808, 2015

2. K Giasin, S Ayvar-Soberanis, A Hodzic, The effects of minimum quantity lubrication and cryogenic liquid nitrogen cooling on drilled hole quality in GLARE fibre metal laminates, Materials and Design 89, 996-1006, 2016

3. K Giasin, A Hodzic, V Phadnis, S Ayvar-Soberanis, Assessment of cutting forces and hole quality in drilling Al2024 aluminium alloy: experimental and finite element study The International Journal of Advanced Manufacturing Technology, 1-21, 2016

4. K Giasin, Tobby French, S Ayvar-Soberanis, V Phadnis, 3D Finite Element Modelling of Cutting Forces in Drilling Fibre Metal Laminates and Experimental Hole Quality Analysis, Applied composite materials 2016.

5. K Giasin, S Ayvar-Soberanis, A Hodzic, Evaluation of cryogenic cooling and minimum quantity lubrication effects on machining GLARE laminates using design of experiments, Journal of Cleaner production 2016, 135, 533-548.

6. Khaled Giasin, and Sabino Ayvar-Soberanis. "Evaluation of Workpiece Temperature during Drilling of GLARE fibre Metal Laminates Using Infrared Techniques: Effect of Cutting Parameters, fibre Orientation and Spray Mist Application." Materials 9.8 (2016): 622.

Submitted Journal Publications

1. K Giasin, S Ayvar-Soberanis, An Investigation of Burrs, Chip formation, Hole Size, Circularity and Delamination during Drilling Operation of GLARE using ANOVA, Composite structures.

2. Khaled Giasin, Sabino Ayvar-Soberanis, Delamination analysis during machining of fibre metal laminates under minimum quantity lubrication and cryogenic cooling environments, Composites A.

Conferences

1. Khaled Giasin , Sabino Ayvar-Soberanis, Alma Hodzic , Improving performance of machined glare laminates for aerospace applications ECCM-16 Conference; Seville, June 22-26, 2014

Curriculum Vitae

Khaled Giasin (Yasin) was born in Irbid-Jordan on the 8th of August 1986. In August 2004, after successfully passing the Jordanian Tawjihi scientific stream year with a score of 89.8 % at Al-Etihad secondary schools, he began a five-year bachelor degree course in Mechanical/Mechatronics Engineering at Jordan University of Science and Technology and graduated a semester earlier with a score of 68.9 % (Good). After graduation, he worked for short period of time as a sales engineering trainee in JOVECO promoting the company products of lighting fixtures, overhead cranes and uninterrupted power supply systems. On September 2009, he started his Master studies at the University of Liverpool and graduated with Merit in October 2010. Later on, he achieved a spectacular opportunity to undertake a one-year full-time master degree in international business engineering offered by Leonardo (previously known as Finmeccanica) at their headquarter in Rome-Italy from September 2011 to December 2011, but he decided to go back and pursue his doctoral studies in the U.K after completing the first semester of the course. In February 2012, he started a Ph.D. research under the supervision of Dr Eli Ghassemieh on machining hybrid composite-metals for a period of eleven months after which he then started working under the supervision of Professor Alma Hodzic for a period of two and a half years and later with Dr Christophe Pinna in the Composite Systems Innovation Centre in the Department of Mechanical Engineering on the machinability of fibre metal laminates. His Ph.D. was sponsored by the department of Mechanical engineering at the university of Sheffield and support from the Advanced Manufacturing Research Centre with Boeing AMRC in Sheffield. His research involved investigating the machinability of fibre metal laminates commercially know as GLARE using conventional drilling and the application of minimum quantity lubrication and cryogenic cooling using liquid nitrogen. The research was carried out through experimental studies to evaluate the machined hole quality and predict the cutting forces while drilling GLARE.

Appendices

Appendix A

Statistical experimental design techniques

An experiment can be defined as a structured set of coherent tests that are analysed as a whole to obtain an understanding of the process [387]. Statistical design of experiments (DOE) is a numerical method aiming to maximise the amount of information and to determine the relationship which exists between controlled factors affecting a process, and the output of that process [302]. DOE is often used in applications which require a large number of trials to reduce the process costs by running a fewer number of trials and speeding up the process. For example, when a machining trial is controlled by two or more input factors, the input factors can influence the output response individually or by interacting with another factor. Experimental design can be used to give an idea about the effect of each factor and the interaction of these factors with each other. In any design of experiment test, there are three elements involved which are: the factors to be tested, the levels of that factor and the experiment conditions such as the number or runs, repetitions, randomization, etc. as shown in Figure A.1. For any design of the experiment, a series of steps is undertaken to determine the best route to carry out the experimental design as shown in the flow chart in Figure A.2. The steps from 1 to 4 are performed during the planning stage of the experiment. Part of the planning stage studies previous work done on similar problems in order to determine the input parameters and outputs of the study. The steps from 5-8 are carried out during the screening process stage which aims to determine the most influential factors from a list of many potential ones [302], usually in screening stage the designs are limited such that they can only estimate the effects of each factor and their linear interactions, but canâĂŹt estimate individual pure quadratic effects, however it can detect them effectively [388]. The steps from 8 to 10 are conducted during the optimisation process stage (commonly known as response surface designs) which aims to better understand and optimise the response of the study. Response surface designs are used to refine the models after determining the
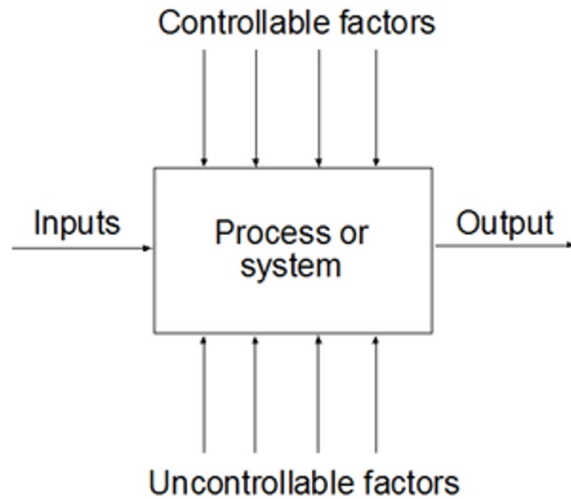
Figure A.1: Schematic for a typical process with controlled inputs, outputs, uncontrolled factors [302]

important factors from the screening trials, they can also detect higher order interactions between input factors and minimise/maximise the outputs.
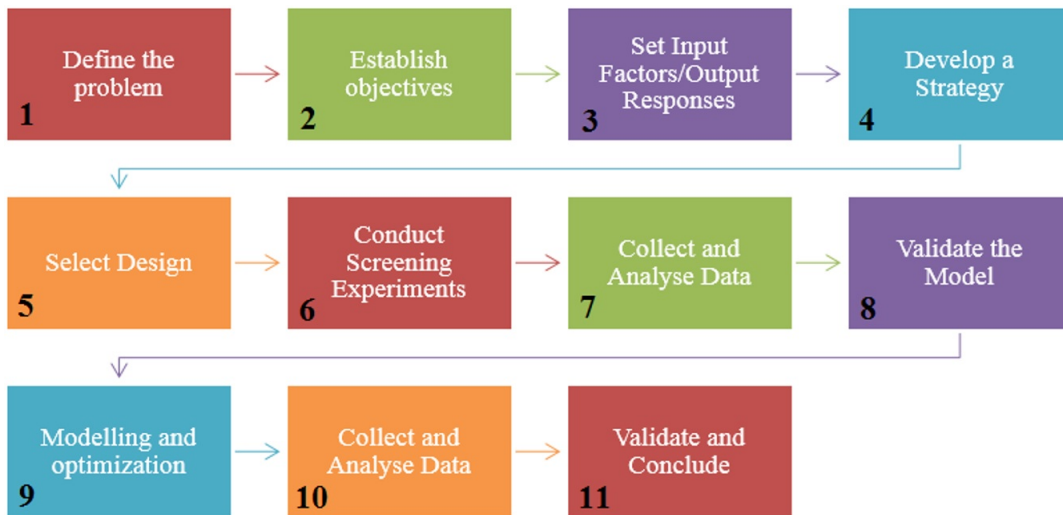

Figure A.2: Design of experiments flowchart

There are three major types of experimental design which are frequently used to determine the important factors in engineering problems which are shown in Figure A.3. Full and fractional factorial designs are good for screening purposes and identifying the linear interactions between the inputs. Response surface designs (RSM) are for more robust and usually used for improving the optimal process settings.
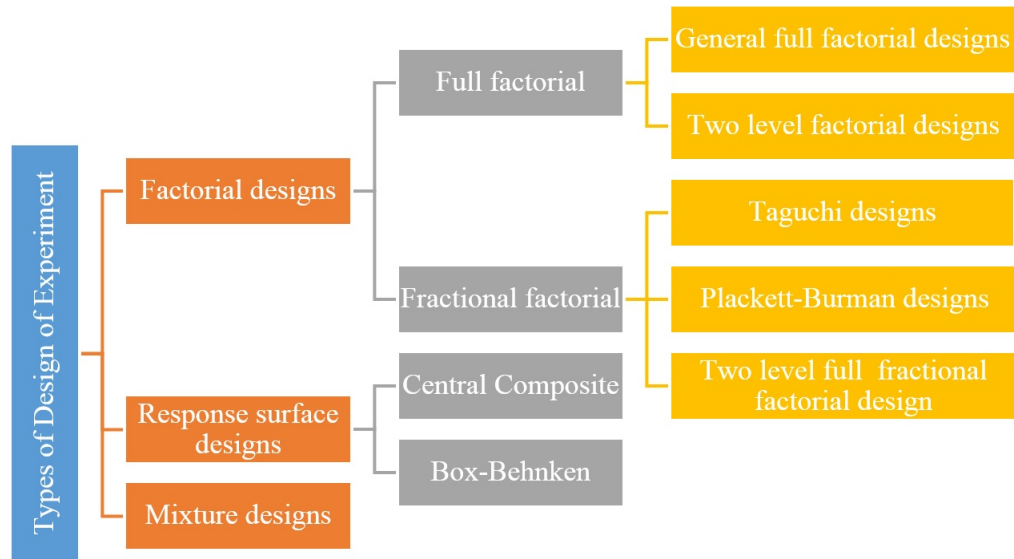
Figure A.3: Types of design of experiment

A.0.1   Analysis of Variance (ANOVA)

Analysis of variance also known as ANOVA is a statistical- oriented decision-making method to test the hypothesis that the means of two or more populations are equal [388]. ANOVA is used to test generally rather than specific differences among means at the different factor levels [389, 390]. ANOVA results are usually summarised in a table as shown in Table A.1. The first row in the table contains information about the degrees of freedom (DF) which refer to terms in the sum of squares (SS) that can be assigned arbitrarily [390]. The degrees of freedom for ANOVA analyses for a specific set equals n-1, where n is the number of observations in the set. The second row represents the sum of squares (SS) which measures the variation from the mean [388]. SS is calculated by summing the squares of the differences from the mean considering the sum of squares from factors and randomness or error. The mean sum of squares (MS) is the sum of squares (SS) divided by the number of degrees of freedom. F is the variance ratio which equals the mean sum of squares (MS) divided by the means square error. F is compared 5 % and 1 % F (from standard F tables) to analyse the main effect or interactive effect has a significant effect on selected response with 95 % confidence level [388]. Therefore, a factor is said to have a significant effect on a response if F value is less than the calculated F value. The P value is used to determine if the results are statically significant. P-value ranges from 0 to 1. P-value measures the probability of evidence against the null hypothesis [388]. The lower the P value the more significant the test statistic is. A value of 0.05 is often used to determine whether an input, its square term or an interaction of two or more inputs are significant to the output factor. The percentage of contribution is the ratio of the sum of square for each source input over the total sum of

squares for all sources in percentile form. The percentage contribution shows the relative amount of variance a particular source contributes to the process (considering only those with a P-value < 0.05). In RMS, the response parameters (Y) are given by a second order

Table A.1: An example of a typical ANOVA table.

Source	DF	SS	MS	F	P	% Contribution
Input A	3	4.12261	1.3742	323.75	0	60.60
Input B	3	2.32839	0.77613	182.85	0	34.22
Input A x Input B	9	1.01697	0.113	26.62	0	4.98
Error	32	0.13583	0.00424			0.18
Total	47	7.6038				100

response equation which is expressed as a function of the spindle speed (n), the feed rate (f), their linear interaction ($n \times f$) and their quadratics n^2, f^2. The relationship between the output and input parameters can be related as shown in the following equation:

$$Response(Y) = A_0 + A_1.n + A_2.f + A_3.f.n + A_4.n^2 + A_5.f^2 \qquad (A.1)$$

Where:

- Y is the response output.

- n, f are spindle speed and feed rate respectively.

- A$_0$ to A$_5$ are regression coefficients associated with the model.

The lack of fit tests checks whether the model fits the data well and is only available when carrying out a test with replicated values of the model effects. The test calculates an estimation of pure error using the replicated data in an experiment. For example, checking for the assumption of linearity in the model, such that a small P value of lack of fit is an indication of a lack of fit (i.e the means are not linear in the model). However, having a lack of fit does not show what would be the right relationship in the model. For example, a transform function such as logarithmic transform function might be needed, or it could be the need of adding additional explanatory terms to the model which have not been included previously in the analysis. The R^2 determines how much of the variance in the output variable Y is explained by the regression model. A linear model with R^2 of 0.89 suggests that 89 % of the variation in output variable can be explained with the linear equation. The same also applies to multiple regression models but on a linear and polynomial level. R-squared, is a unit-less statistical measure known as the coefficient of determination value.

R-squared ranges between 0.0 and 1.0 and is calculated by dividing the sum of squares (SS) explained by a regression model and the total sum of squares around the mean. Further experimental data analysis is carried out on GLARE 2B 11/10 to investigate the influence of input parameters (spindle speed, feed rate) on the output responses (cutting forces, surface roughness, etc..). The drilling tests data are based on factorial central composite design consisting from three-factor-three-level system. Multiple regression analysis using response surface methodology is employed to build the mathematical relationships between the input factors and the output responses. The developed models are also verified using the analysis of variance ANOVA. The main, linear and quadratic interactions effect of the input variables which are used to predict the output responses are investigated. Finally, the multiple regression models are tested for their accuracy of predicting the output responses using new drilling parameters.

Appendix B

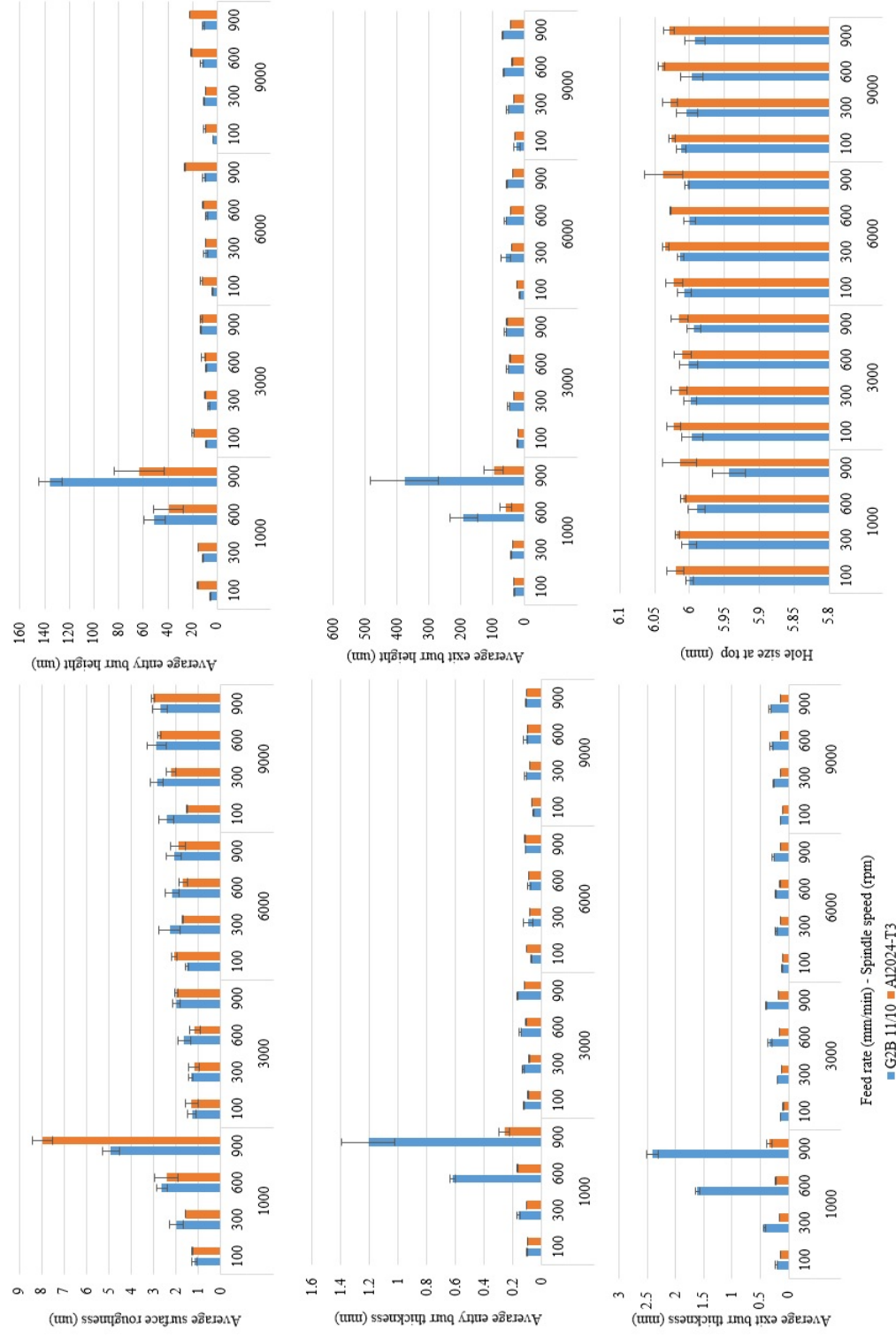# Comparison graphs of GLARE 2B 11/10 and Al2024-T3 alloy

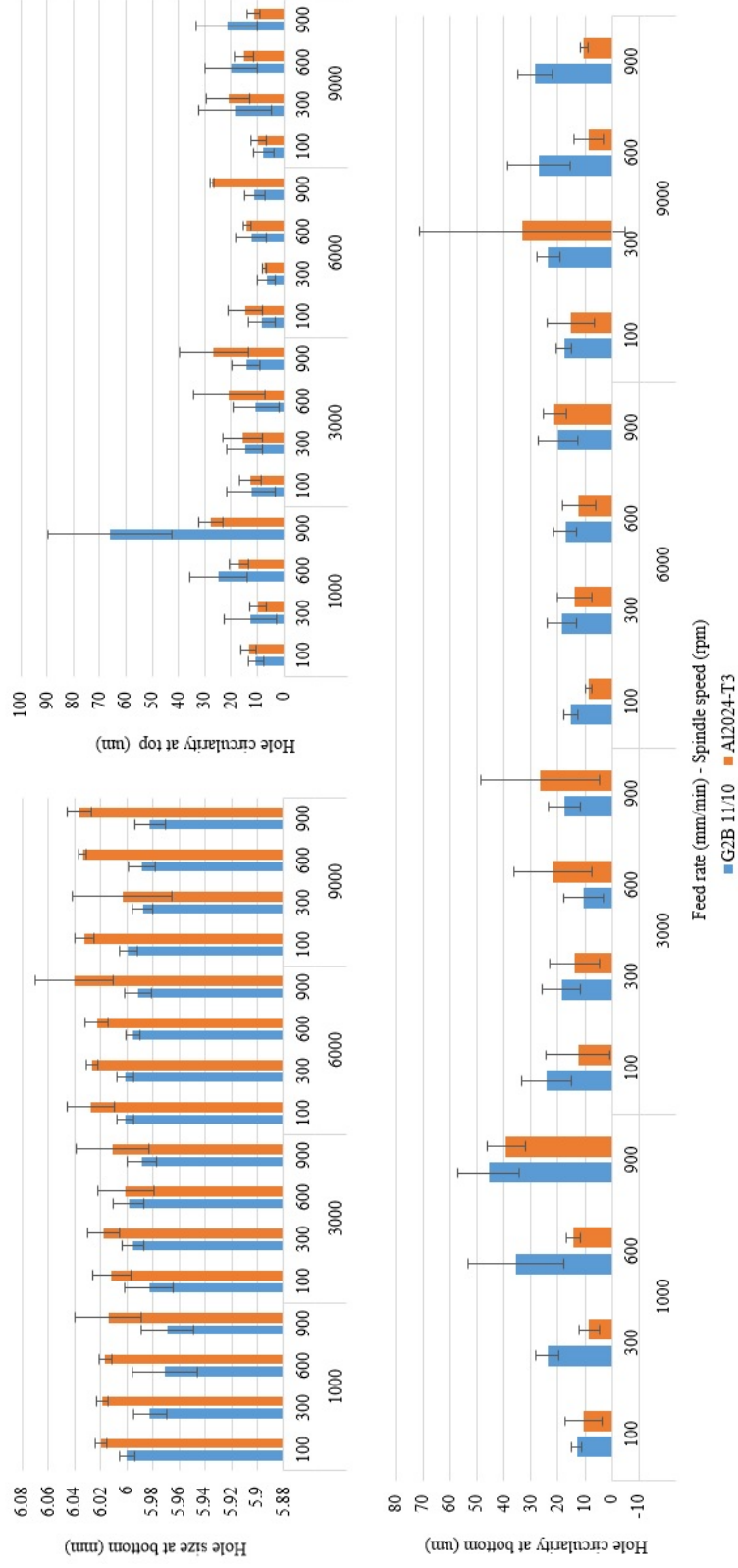Figure B.1: Determination of GLARE emissivity in the third test

Figure B.2: Determination of GLARE emissivity in the third test